THE EFFECT OF STRESSED CELL-DERIVED EXOSOMES ON METASTATIC ACTIVITY OF OVARIAN AND BREAST CANCER CELL LINES *IN VITRO*

Thesis is submitted in partial fulfilment of the requirements of the award of Doctor of Philosophy

LAURA ANN MULCAHY

Degree awarded by Oxford Brookes University

Department of Biological and Medical Sciences

Oxford, United Kingdom

May 2016

Abstract

Metastasis is one of the main causes of cancer related death worldwide; hence elucidation of this mechanism, at least in part, will support development of effective therapies to improve the morbidity and mortality of people with cancer. Cells continually expel a large number and variety of extracellular vesicles. Of these secreted vesicles, exosomes have been studied extensively over the past decade. Exosomes are between 30–100 nm in diameter and contain protein and nucleic acids. They have only very recently become appreciated as communication mediators that transport signals between cells.

It was hypothesised that exosomes secreted by more metastatic cells may have the ability to increase the motility of less metastatic cells, and vice versa. The motile capacity of nine ovarian cancer cell lines was established using the scratch wound healing assay. Following this, exosome swapping experiments were performed between more and less metastatic cells. It was shown that exosomes were unable to influence the motility of recipient cells, irrespective of the metastatic phenotype of their cells of origin.

It was also hypothesised that exosomes derived from stressed cells increase the invasive capacity of recipient cells. Exosomes were extracted from heat shocked or cisplatin treated cells and were introduced to naïve cells. The invasive capacity of recipient cells was tested following administration of stressed cell-derived exosomes. It was discovered that cell invasiveness increased following uptake of either heat shock or cisplatin exosomes. Additionally, both heat shock and cisplatin exosomes were found to be statistically significantly smaller in diameter than those extracted from control cells, when measured using transmission electron microscopy.

This has implications for patients with cancer because tumour cells that resist, but become stressed during administration of cisplatin therapy, could be expelling exosomes that increase the invasiveness of neighbouring cancer cells, and the cells of the surrounding healthy stroma.

Acknowledgements

Table of contents

List of figures

List of tables

Publications

Mulcahy, L.A., Pink, R.C., Carter, D.R.F. (2014) 'Routes and mechanisms of extracellular vesicle uptake', *Journal of Extracellular Vesicles*, 3, pp. 24641.

Jacobs, L. A., Bewicke-Copley, F., Poolman, M. G., Pink, R. C., **Mulcahy, L. A.**, Baker, I., Beaman, E. M., Brooks, T., Caley, D. P., Cowling, W., Currie, J. M., Horsburgh, J., Kenehan, L., Keyes, E., Leite, D., Massa, D., McDermott-Rouse, A., Samuel, P., Wood, H., Kadhim, M. and Carter, D. R. (2013) 'Meta-analysis using a novel database, miRStress, reveals miRNAs that are frequently associated with the radiation and hypoxia stress-responses', *PLoS One*, 8(11), pp. e80844.

Mulcahy, L.A. and Carter, D. R. (2013) 'RNAi2013: RNAi at Oxford', *J RNAi Gene Silencing*, 9, pp. 486-489.

See Appendix A (**8.1**) for copies of these publications.

Abbreviations

BCA	bicinchoninic acid
BSA	bovine serum albumin
DMEM	Dulbecco's modified eagle's medium
dNTP	deoxyribonucleotide triphosphate
DPX	di-N-butyle phthalate in xylene
DSB	double-strand break
DTT	dithiothreitol
ECM	extracellular matrix
EDTA	ethylenediaminetetraacetic acid
EFM	exosome-free media
EGFR	epidermal growth factor receptor
EMT	epithelial-mesenchymal transition
ERK	extracellular signal-regulated kinases
ESCRT	endosomal sorting complexes required for transport
EV	extracellular vesicle
FBS	foetal bovine serum
GO	gene ontology
HIF1α	hypoxia-inducible factor 1-alpha
HRP	horseradish peroxidase
Hrs	hepatocyte growth factor-associated tyrosine kinase
HSP60	heat shock protein 60 kDa
HSP70	heat shock protein 70 kDa
HSP90	heat shock protein 90 kDa

HSP90α	heat shock protein 90 kDa alpha form
ILV	intraluminal vesicles
ITGA3	integrin alpha 3
ITGB1	integrin beta 1
JNK	c-Jun N-terminal kinases
MAPK	mitogen-activated protein kinase
MET	mesenchymal-epithelial transition
MFG-E8	milk-fat globule-epidermal growth factor 8
MHC-II	major histocompatibility complex class 2
MMP	matrix metalloproteinase
MVB	multivesicular body
NTA	nanoparticle tracking analysis
PBS	phosphate buffered saline
PI-3K	phosphoinositide 3-kinase
PVDF	polyvinylidene difluoride
qPCR	quantitative polymerase chain reaction
RIPA	radioimmunoprecipitation assay
RPMI	Roswell Park Memorial Institute
SDS	sodium dodecyl sulphate
SDS-PAGE	sodium dodecyl sulphate-polyacrylamide gel electrophoresis
SFM	serum-free medium
SNARE	soluble N-ethylmaleimide sensitive fusion protein attachment receptor protein
TBST	tris buffered saline with 0.05% Tween 20
TEM	transmission electron microscopy

TSG101	tumour susceptibility gene 101
UF-LC	ultrafiltration liquid chromatography
UTR	un-translated region
VPS4	vacuolar protein sorting 4
VWR	Van Waters and Nat Rogers
WB	western blotting

Glossary

A-2780	ovarian cancer cell line
CD	cluster of differentiation protein
CP-70	ovarian cancer cell line
DNA	deoxyribose nucleic acid
$\times g$	relative centrifugal force (G-force)
IC_{50}	concentration at which an inhibitor decreases cellular response or binding) by 50%
IGROV-1	ovarian cancer cell line
MCF-7	breast cancer cell line
MCP-1	ovarian cancer cell line
mg	milligram
miR	micro ribonucleic acid
miRNA	micro ribonucleic acid
mL	millilitre
mM	millimoles
mRNA	messenger ribonucleic acid
MTT	3-(4,5-dimethylthiazol-2-yl)-2,5-diphenyltetrazolium bromide
n	sample size
nm	nanometers
OVCAR-3	ovarian cancer cell line
OVCAR-4	ovarian cancer cell line
OVCAR-5	ovarian cancer cell line
OVCAR-8	ovarian cancer cell line
p	p value

PKH26	red fluorescent lipophilic cell membrane dye
PKH67	green fluorescent lipophilic cell membrane dye
RNA	ribonucleic acid
rpm	revolutions per minute
R^2	coefficient of determination
siRNA	small interfering RNA
SKOV-3	ovarian cancer cell line
µg	micrograms
µl	microlitres
µM	micromoles
w/v	weight per total volume
yl	yottalitres
%	percentage

Chapter 1

Introduction

1. <u>Introduction</u>

1.1. Cancer

Cancer is a growth or tumour that is caused by uncontrollable proliferation of abnormal cells in the body (Weinberg, 1996). Almost all mammalian cells have anti-cancer defence machinery that is responsible for regulating their proliferation, differentiation, and death (Hanahan and Weinberg, 2000). These protective mechanisms are generally very effective in preventing development of cancer (Hanahan and Weinberg, 2000). However, when these mechanisms are overcome, malignant cells are able to flourish. Transformation of normal human cells into malignant cancers is a multistep process facilitated by mutations that occur in essential genes responsible for normal cell proliferation and homeostasis (Foulds, 1954; Nowell, 1976). As a result the cell acquires a combination of: (1) oncogenes with dominant gain of function and (2) tumour suppressor genes with recessive loss of function.

1.1.1. The six hallmarks of cancer

Cancer research has revealed six common molecular, biochemical, and cellular characteristics (or acquired capabilities) shared by all types of human cancer. These essential alterations in cell physiology collectively dictate malignant growth and represent successful breach of cellular anti-cancer defence mechanisms. The six hallmark capabilities are: (1) initiation of replicative immortality; (2) induction of angiogenesis; (3) evasion of growth suppressors; (4) activation of invasion and metastasis; (5) sustained proliferative signalling; and (6) resistance to programmed cell death (apoptosis) (**Figure 1.1**) (Hanahan and Weinberg, 2000). A cell must acquire all six of these capabilities in order to develop malignancy. More recently, additional hallmarks have been proposed including: deregulating cellular energetics, and avoiding immune destruction. Additionally, the enabling characteristics: genome instability, and mutation and tumour promoting inflammation have also been identified (Hanahan and Weinberg, 2011).
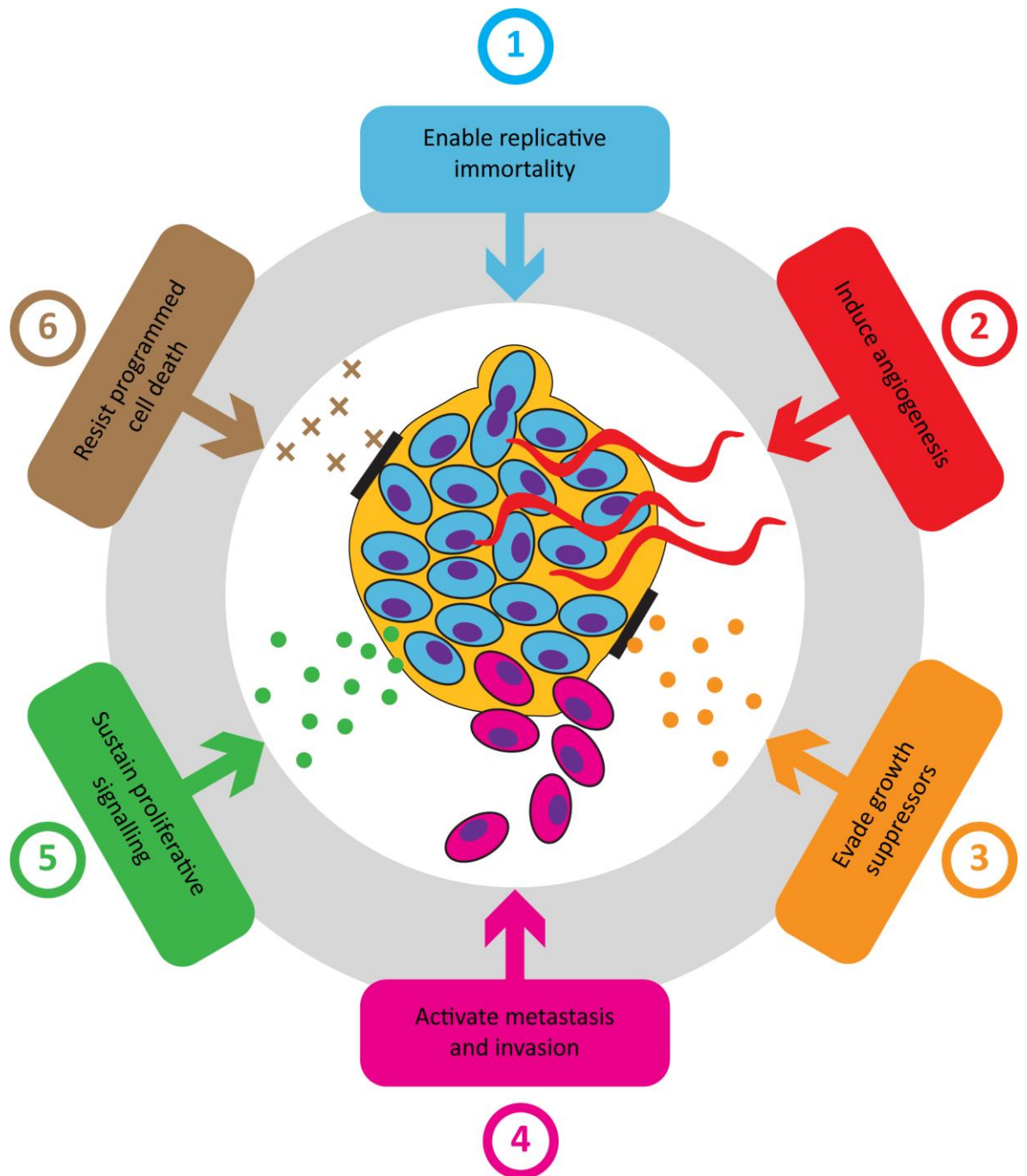
Figure 1.1: The six hallmarks of cancer. (1) initiation of replicative immortality; (2) induction of angiogenesis; (3) evasion of growth suppressors; (4) activation of invasion and metastasis; (5) sustained proliferative signalling; and (6) resistance to programmed cell death (apoptosis). Adapted from Hanahan and Weinberg, 2000.

Each of these protective mechanisms are controlled by several proteins, the functionality of at least one protein essential to each pathway must be inhibited, or significantly reduced, in order to overcome the cancer defence strategy. This occurs through mutations in the DNA sequence of the genes associated with the essential proteins (Hanahan and Weinberg, 2000). The mechanisms by which mutations occur, and the affected genes, do not need to be identical between different tumours in order for cancer to prevail. Additionally, the sequence in which the hallmark

capabilities are acquired varies across different cancer types and subtypes (Hanahan and Weinberg, 2000). Moreover, in some tumours, a single genetic mutation may result in the acquisition of several hallmark capabilities simultaneously, which reduces the number of mutational events needed for successful tumourigenesis. For example, loss of function of the p53 tumour suppressor can enable both angiogenesis, resistance to apoptosis, and genomic instability (Fridman and Lowe, 2003). In other instances, a hallmark capability may only develop following occurrence of two or more distinct genetic mutations, which lengthens the tumourigenesis process (Hanahan and Weinberg, 2000).

1.1.2. Ovarian cancer

Ovarian cancer refers to growth of an invasive tumour that arose from cells of the ovary. Over 90% of diagnosed ovarian cancers are of epithelial origin (Cancer Research UK, 2014b). In 2012, 152,000 women were killed by ovarian cancer; approximately 4200 of these fatal cases occurred in the UK (Cancer Research UK, 2014b). Ovarian cancer, despite being only the fifth most prevalent malignancy in women, is accountable for more deaths than all other gynaecological cancers combined (National Institute for Health and Care Excellence, 2010). Symptoms manifest once the disease has become well-established, therefore the prognosis is poor (Schwartz *et al.*, 2002). Little is known on how progression occurs from a primary tumour to an invasive and metastatic disease (Brooks *et al.*, 2010; Lancaster *et al.*, 2006). Only 35% of patients survive for 10 years following diagnosis (Cancer Research UK, 2014b).

1.1.3. Breast cancer

Breast cancer is the term used to describe growth of a malignant mass of cells inside the breast tissue. The vast majority of breast cancers are carcinomas meaning that the cancer began in the epithelial layer. Breast cancer is the most common malignancy of women in the Western world (Cancer Research UK, 2014a; Scully *et al.*, 2012; Torre *et al.*, 2015; Weigelt *et al.*, 2005). In 2012, 522,000 women worldwide died of breast cancer; 11,600 of these were British (Cancer Research UK, 2014a). Seventy-five percent of deaths caused by breast cancer that occurred in British women were in individuals who were over the age of 60 (Cancer Research UK, 2014a); it is now recommended by the NHS Breast Screening Programme that all women aged between 47 and 73 should have a mammographic screen every three years. Because of increases in breast cancer awareness, and frequency in screening, unlike ovarian cancer breast cancer is usually diagnosed at a much earlier stage. As a result of early diagnosis, implementation of systemic adjuvant

therapy is much more successful, and has decreased metastasis and mortality rates (Scully *et al.*, 2012; Weigelt *et al.*, 2005). In contrast to ovarian cancer, 78% of patients survive for 10 years following diagnosis (Cancer Research UK, 2014a).

1.2. Metastasis

In terms of tumour survival and progression, an important factor is the ability of the tumour to invade and metastasize. This is usually the final hallmark acquired by a primary tumour (Hanahan and Weinberg, 2000). Typically, for both ovarian and breast cancers, current treatment involves removal surgery and chemotherapy. The majority of patients respond well initially, but eventually, in most cases, a chemoresistant and metastatic malignancy recurs, sometimes following multiple rounds of treatment (Appleton *et al.*, 2007). This is usually the final stage of tumour progression, with few treatment options remaining. Metastasis is responsible for approximately 90% of cancer related deaths (Steeg, 2006), and is the main cause of death in both ovarian and breast cancer.

Metastasis is the process whereby rare subpopulations of cells within the primary tumour attain advantageous genetic alterations, which enable these cells to leave the primary site and metastasize to form new solid tumours at distant locations where there are reduced nutrient and space constraints (Fidler and Kripke, 1977; Fidler, 2003; Weigelt *et al.*, 2005).

1.2.1.   The metastatic cascade

Neoplastic cells must successfully complete a cascade of events in order for a tumour to become established at a secondary site (Brooks *et al.*, 2010). Millions of cells are shed from a tumour every day, but very few successfully complete all steps of the metastatic cascade (Bockhorn *et al.*, 2007; Butler and Gullino, 1975; Liotta *et al.*, 1976). It is thought that shear stress experienced in the circulation and destruction by immune cells, are the two major factors that prevent all but the most capable cells from establishing secondary colonies (Bockhorn *et al.*, 2007). There are an extensive number of molecular mechanisms that contribute to the metastatic cascade and it is very complex, however the events involved can be summarised into seven key physiological steps (**Figure 1.2**) (Brooks *et al.*, 2010; Polyak and Weinberg, 2009):

 (1) **Angiogenesis** – the development of new blood vessels inside the tumour for supply of nutrients.

(2) **Detachment** of tumour cells from their neighbours and subsequent escape from the primary tumour mass.

(3) **Invasion** of, and **migration** through, the tumour basement membrane and surrounding extracellular matrix (ECM). Subsequently, malignant cells burrow through the basement membrane of blood vessels (or lymphatics).

(4) **Intravasation** of the tumour cells into the blood vessel (or lymphatic). Malignant cells travel to distant anatomical sites assisted by the circulation.

(5) **Adhesion** of a single circulating tumour cell to the endothelial vessel lining at the capillary bed of the target organ at a remote location.

(6) **Extravasation** of the metastatic cells where they invade through vascular endothelial cells and surrounding basement membrane, and colonise in the target organ tissue.

(7) **Establishment** of a secondary colony of tumour cells at the target organ site (Brooks *et al.*, 2010).

The process described above is typical of haematogenous or lymphatic metastasis whereby tumour cells are assisted by either the circulation or lymphatics, respectively. Breast cancer metastasis follows the haematogenous route described (Weigelt *et al.*, 2005). Ovarian cancer, however, appears to colonise other tissues through a slightly different mechanism (Lengyel, 2010) (section **1.2.3**).
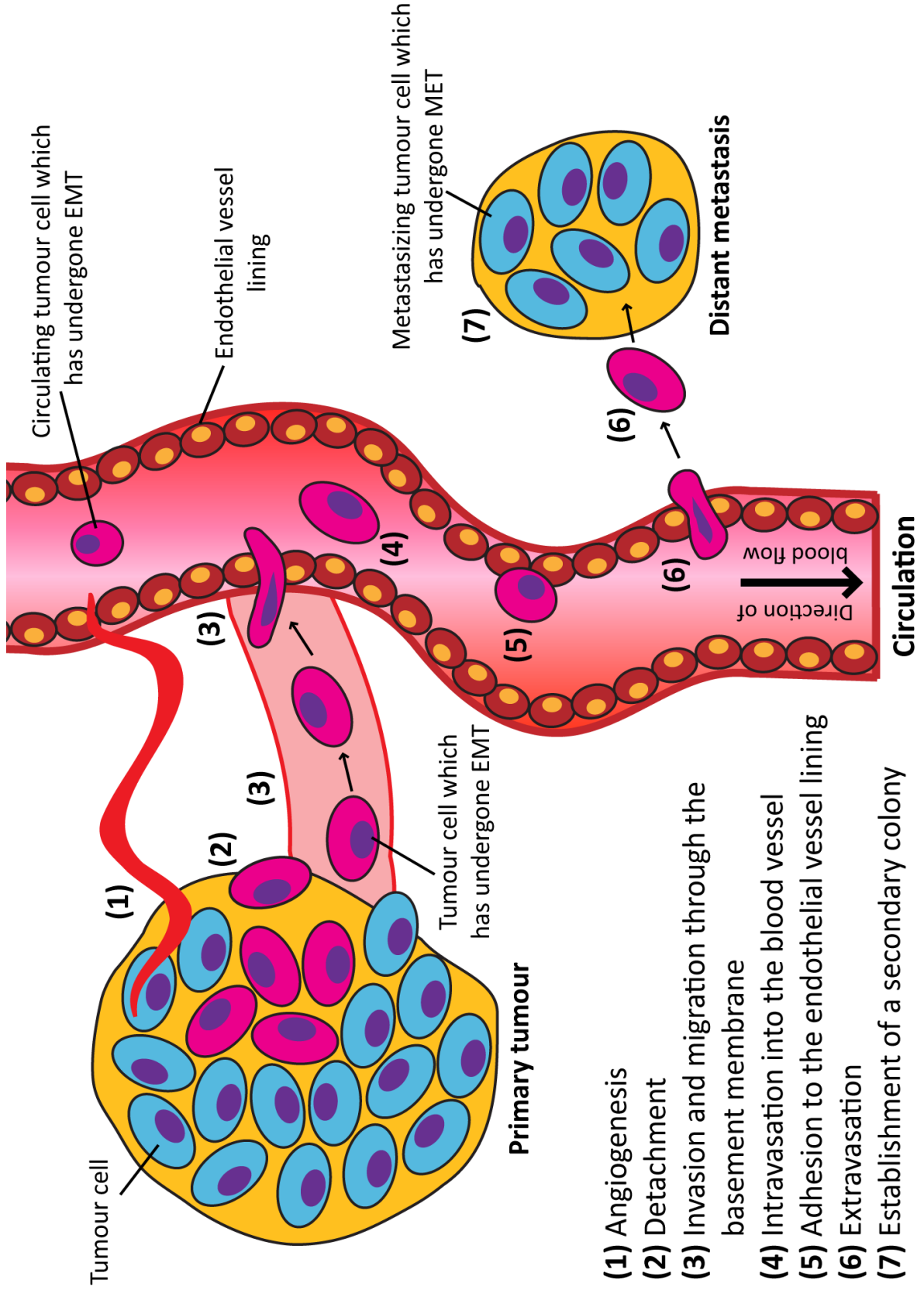
Figure 1.2: The metastatic cascade. (1) Angiogenesis where new blood vessels develop inside the tumour. (2) Detachment of tumour cells from their neighbours. (3) Invasion of, and migration through, the tumour basement membrane. (4) Intravasation of the tumour cells into the blood vessel. (5) Adhesion of a single circulating tumour cell to the endothelial vessel lining of the target organ at a remote location. (6) Extravasation of the metastatic cells where they invade through vascular endothelial cells and colonise in the target organ tissue. (7) Establishment of a secondary colony of tumour cells.

Circulating tumour cell which has undergone EMT

Endothelial vessel lining

Metastasizing tumour cell which has undergone MET

Distant metastasis

Primary tumour

Tumour cell

Tumour cell which has undergone EMT

Direction of blood flow

Circulation

(1) Angiogenesis
(2) Detachment
(3) Invasion and migration through the basement membrane
(4) Intravasation into the blood vessel
(5) Adhesion to the endothelial vessel lining
(6) Extravasation
(7) Establishment of a secondary colony

1.2.2. Phenotypic plasticity

Epithelial-mesenchymal transition (EMT) and mesenchymal-epithelial transition (MET) are important processes in the mechanisms of metastasis. Without these processes cells would not be able to detach from tissues at the primary site and reattach to tissues at secondary locations (**Figure 1.2**) (Franzen *et al.*, 2015; Tsai and Yang, 2013).

1.2.2.1.   Epithelial-mesenchymal transition

EMT is the transition from a stationary epithelial-like cell to one that has the ability to detach from the tissue mass and migrate, characteristics that are usually associated with cells of mesenchymal lineage (Charpentier and Martin, 2013). Cellular migration is not only essential for normal development but is a vital trait developed by aggressive and advanced tumours that metastasize to new sites (Liu *et al.*, 2012). E-cadherin (an epithelial marker) expression becomes reduced with synergistic increase in N-cadherin expression during EMT. Vimentin is a marker of cells with a mesenchymal phenotype expressed in cells that have successfully undergone EMT (Kalluri and Weinberg, 2009).

1.2.2.2.   Mesenchymal-epithelial transition

On arrival at the secondary site there is a recapitulation of the events that were required for primary tumour growth. Cells undergo MET where they become able to re-attach to the tissue matrix and proliferation increases, consequently a tumour is created at a new site (Chaffer *et al.*, 2007). During the MET process cancer cells lose their invasive capacity and acquire self-renewal competence (Liao *et al.*, 2014).

1.2.3. Ovarian cancer metastasis

Ovarian cancer metastasis demonstrates the 'seed and soil hypothesis' proposed by Paget in 1889 (Ramakrishna and Rostomily, 2013). The 'soil' for ovarian carcinoma 'seeds' is either the omentum, a highly vascular protective fat pad; or the peritoneum, a serous membrane that consists of a single layer of mesothelial cells supported by a thin layer of ECM; both of which cover all organs of the abdomen and act as a protective layer (Lengyel, 2010). The ovarian cancer 'seed and soil' concept was supported by a study performed in patients living with severe ascites caused by inoperable cancer. To relieve abdominal pain and distension, peritoneovenous shunts were used to drain excess fluid from the peritoneum and transfer it, via the jugular vein, to the

systemic circulation for disposal. Despite continuous shunting for up to two years, and hence infusion of billions of cancer cells into the venous system, patients did not develop aggressive metastases outside the abdominal region (Tarin *et al.*, 1984).

Despite ovarian carcinomatosis to the omentum/peritoneum being well documented, the specific cascade responsible is not well understood. Of paramount importance is the ability of ovarian cancer cells to invade the innermost layer of the peritoneum known as the mesothelium, a monolayer of mesothelial cells that protect abdominal organs (**Figure 1.3**) (Heath *et al.*, 2004). Once this barrier has been breached, tumour cells can adhere, infiltrate, and proliferate within the submesothelial ECM (Kenny *et al.*, 2009). Patients with extensive intra-abdominal cancer metastasis have a particularly poor prognosis (Kenny *et al.*, 2007; Kenny *et al.*, 2009; Kenny *et al.*, 2011).
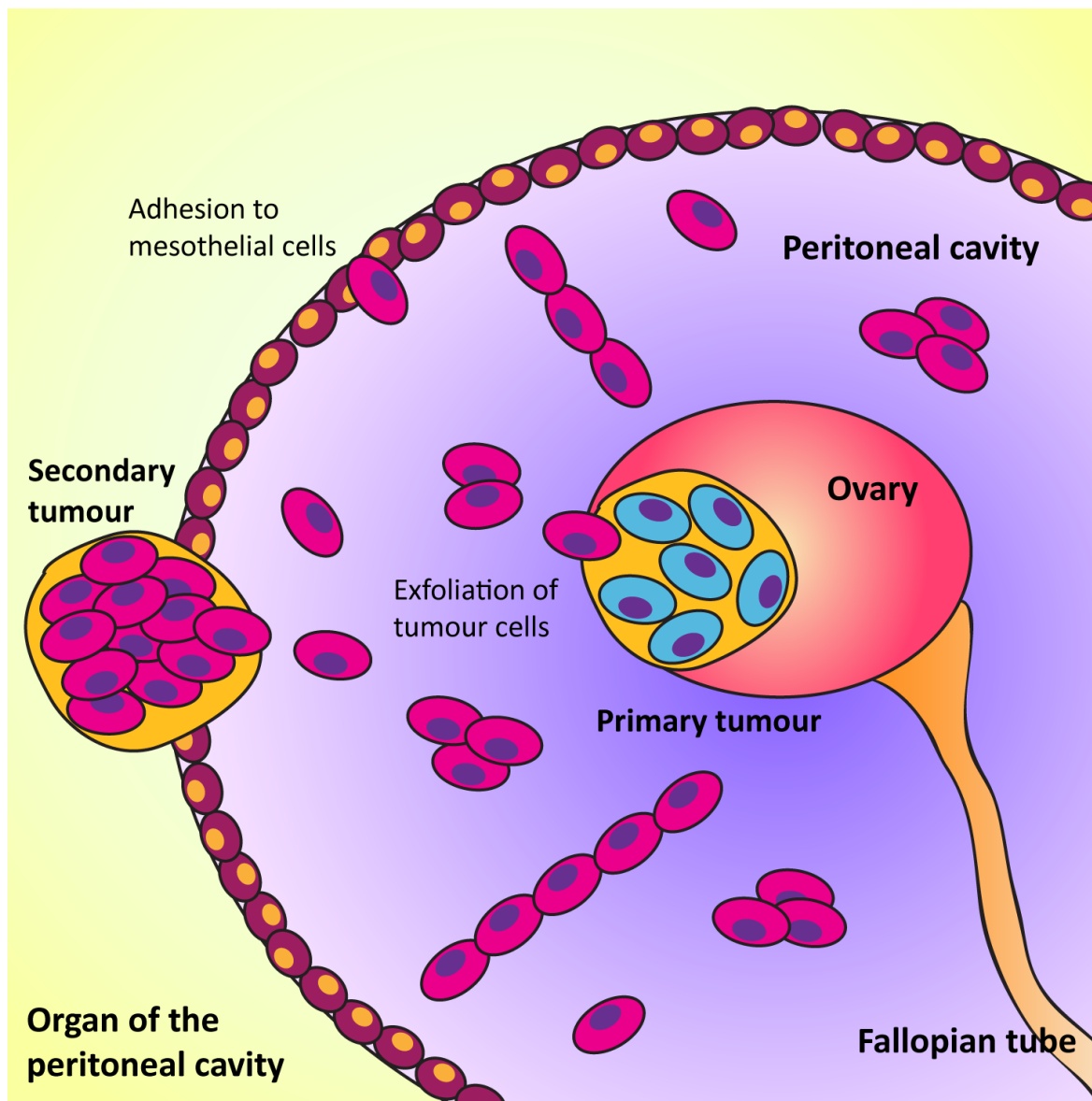
Figure 1.3: Ovarian cancer transcoleomic metastasis. Ovarian cancer cells are notorious for thriving in the peritoneal cavity however they rarely metastasize beyond this region. This is because of the mechanism of ovarian cancer metastasis that is distinctive from typical haematogenous pathways. Instead, exfoliated single ovarian carcinoma cells, or chains, or spheroids are transported to the secondary site (omentum or peritoneum) in the peritoneal fluid, assisted by natural physiological movement. For this reason, ovarian cancer typically metastasizes transperitoneally, most commonly to the omentum or the peritoneum but also to organs found in the peritoneal cavity for example the liver. Adapted from Singh and colleagues, 2008.

1.2.3.1.   Extracellular matrix

The ECM is a dynamic matrix of molecules secreted by cells, which form a scaffold that provides structural and biochemical support to neighbouring cells (Badylak *et al.*, 2015; Bonnans *et al.*, 2014; Michel *et al.*, 2010). The ECM includes the interstitial matrix and the basement membrane (Badylak *et al.*, 2015; Brownlee, 2002). Interstitial matrix is the gel of polysaccharides and fibrous

proteins that fill the space between cells. Basement membranes are composed of sheet-like layers of ECM on which epithelial cells are grounded and supported (Brownlee, 2002).

The ECM has many functions, such as providing cellular support, assisting cell adhesion, separating tissues from one another, and modulating intercellular communication (Abedin and King, 2010). ECM formation is essential in many mechanisms including: growth, wound healing, and fibrosis (Maquart and Monboisse, 2014). ECM degradation is a key step in the metastatic cascade (**Figure 1.2** and **Figure 4.1**). The elasticity of the ECM modulates cell migration (Lo *et al.*, 2000), gene expression (Wang *et al.*, 2007), and cell differentiation (Engler *et al.*, 2006). Cells constantly assess their ECM elasticty/rigidity, and regulate this depending on desired cell activity. For example, cell migration is guided by rigidity gradients of ECM, where cells preferentially migrate towards more rigid surfaces (this process is called durotaxis) (Choquet *et al.*, 1997; Lo *et al.*, 2000). Additionally, ECM elasticity regulates gene expression that can impact cell differentiation and cancer progression (Adams and Watt, 1993; Provenzano *et al.*, 2009).

ECM constituents are synthesised intracellularly and secreted into the local intercellular environment by exocytosis. Once secreted, the new ECM components combine with the existing matrix (Badylak *et al.*, 2015). The ECM is composed of an interlocking mesh of fibrous proteins and proteoglycans. Proteoglycan components include: heparan sulphate, chondroitin sulphate, and keratan sulphate (Iozzo, 1998). ECM-associated heparin sulphate binds to a number of protein ligands and regulates several biological activities including tumour metastasis (Kim *et al.*, 2011). Hyaluronic acid is a non-proteoglycan polysaccharide component of ECM responsible for the regulation of numerous processes including tumour development (Peach *et al.*, 1993). Collagen, elastin fibres, fibronectin, and laminin are other common components of ECM (Bonnans *et al.*, 2014; Brownlee, 2002; Di Lullo *et al.*, 2002).

1.2.4. The role of the tumour microenvironment in metastatic disease

The best strategy to reduce morbidity and mortality caused by cancer is to prevent development of disseminated disease (Eccles and Welch, 2007). Despite significant developments and successes in cancer research, current treatments do not target metastatic disease (Eustace *et al.*, 2004; McCready *et al.*, 2010). Tumours are not just a mass of abnormal cells but complex pathogenic organs, which attract and corrupt many other types of cell. The interactions between transformed cancer cells and healthy cells of the surrounding stroma create the tumour microenvironment (Balkwill *et al.*, 2012). Recent data suggests that the tumour microenvironment plays a vital role in both initiation and progression of cancer (Marcucci *et al.*, 2013). Before cancer cells can establish a tumour at a distant site, the secondary organ must be prepared so it can provide an ideal

environment to accommodate metastasising cancer cells (Ramakrishna and Rostomily, 2013). Organs that are suitable for remote tumour implantation may be primed ahead of the arrival of metastasizing cells to promote grafting and prosper (Bidard *et al.*, 2008). The mechanism responsible for tumour cell-tumour microenvironment communication is not fully understood. The healthy cells of the tumour microenvironment have a dynamic relationship with the tumour (Balkwill *et al.*, 2012). They support carcinogenesis by coordinating a complex network of cytokines, chemokines, growth factors, inflammatory proteins, matrix remodelling enzymes, and RNA molecules that disrupt the physical and chemical properties of the surrounding tissue enabling tumour growth and spread (Hanahan and Coussens, 2012). Most recently, the impact of extracellular vesicles (EVs) in tumour cell-tumour microenvironment communication has become appreciated (section **1.6.3**) (Hosseini-Beheshti *et al.*, 2012; Paltridge *et al.*, 2013; Svensson *et al.*, 2013).

1.2.5. Cancer cell interactions with healthy stroma

In addition to cytokine stimulation (Esquivel-Velázquez *et al.*, 2015), an alternative way that cancer cells interact with the normal stroma is through secretion of hyaluronan. Hyaluronan concentration increases in cancer cells and causes disruption to normal cell-cell and cell-ECM interactions by interfering with cell-cell adhesions (Kamińska *et al.*, 2015). This leads to aberrant epithelial morphogenesis that is associated with pre-malignant changes, including intraluminal invasion and deregulated epithelialisation (Bose and Masellis, 2005; Twarock *et al.*, 2009). It is not clear whether cancer cells directly or indirectly secrete hyaluronan, however conditioned media collected from cancer cells was shown to increase the proliferation of non-cancerous cells. This effect was caused by soluble factors in the conditioned media secreted by the tumour cells. It is possible that EVs may mediate this activity by transporting hyaluronan from cancer cells to cells of the surrounding healthy stroma (Pistone Creydt *et al.*, 2013).

1.3. Extracellular vesicles

Cells continually expel a large number and variety of EVs. Analysis of the contents, size and membrane composition of EVs suggests that they are a highly heterogeneous and dynamic population of vesicles. Data suggest that their composition is dependent upon the cell of origin, cellular state, and environmental conditions (Yáñez-Mó *et al.*, 2015). At present, three main subgroups of EVs have been defined (Gould and Raposo, 2013): (1) apoptotic bodies/plasma membrane blebs, (2) microvesicles (microparticles/ectosomes), and (3) exosomes (**Figure 1.5**) (Yáñez-Mó *et al.*, 2015). The main distinguishing factor between these different classes of EV is

their biogenesis mechanisms. Apoptotic bodies are released as a result of plasma membrane blebbing during apoptosis, they are 1–5 µm (1000–5000 nm) in diameter (Hristov *et al.*, 2004). Microvesicles range in size between 100–1000 nm (Raposo and Stoorvogel, 2013) and pinch off directly from the plasma membrane (Gould and Raposo, 2013). Exosomes are intraluminal vesicles (ILVs) that originate from membrane enclosed sub-compartments of cells (multivesicular bodies [MVBs]). Exosomes are secreted into the extracellular environment upon fusion of MVBs with the plasma membrane (Théry *et al.*, 2002; Yáñez-Mó *et al.*, 2015).

It is difficult to distinguish between these subgroups of EVs as many of the protein markers are expressed across all types of EVs. Some specific characteristics have been identified for these sub-classifications of EVs, however there is currently a lack of widely accepted markers that distinguish these populations (Kalra *et al.*, 2013; Tauro *et al.*, 2012). This may be due, in part, to the lack of standardisation of both EV extraction and characterisation procedures. In particular, EV isolation procedures, at present, are generally unable to separate specific types of EV, instead a mixture of different EV types are yielded (Gould and Raposo, 2013; Yáñez-Mó *et al.*, 2015). Therefore, the best practice following EV extraction is to characterise EVs using multiple techniques (Yáñez-Mó *et al.*, 2015) (section **3.3.1**).

1.4. Exosomes

Over the past decade, exosomes have been extensively studied (Vader *et al.*, 2014), and an appreciation of their role in cell-cell communication has been gained (Denzer *et al.*, 2000; Raposo *et al.*, 1996; Vlassov *et al.*, 2012). The term 'exosome' was first used by Trams *et al.* in 1981 to describe vesicles 40–1000 nm in diameter that exfoliated from ectoenzyme-active cells (Trams *et al.*, 1981). Later that decade, this nomenclature was adopted for vesicles that were 40–100 nm in diameter and originated in the endosome (Pan *et al.*, 1985). In the same study electron microscopic analysis was performed where the secretion of vesicles approximately 50 nm in diameter by sheep erythrocytes was observed. These vesicles contained the transferrin receptor, no longer needed by the maturing erythrocytes; hence it was thought that the role of exosomes was limited to the removal of proteins. This study also identified the initial stages of biogenesis in endosomes where, what are now referred to as MVBs, are created (Pan *et al.*, 1985). Exosomes were first isolated by Johnstone and colleagues in 1987 who also identified that they contained numerous active enzymes (Johnstone *et al.*, 1987).

In 2007, Valadi and colleagues discovered that exosomes were able to deliver murine mRNA and miRNA to human mast cells, determined by the expression of mouse proteins in human recipient

cells (Valadi *et al.*, 2007). Realisation that exosomes may elicit epigenetic effects through transfer of selected molecules between cells has revolutionised the outlook within the exosome research field regarding potential mechanisms of exosome signalling (Stoorvogel, 2012). This study alone triggered great interest, and therefore increased exploration into exosome molecular biology (Lässer *et al.*, 2011). As a result, the exosome has become the most well-defined member of the EV family and exosome research continues to increase exponentially (Marcus and Leonard, 2013).

Exosomes are small vesicles released by a variety of cell types into the extracellular environment (Février and Raposo, 2004; Théry *et al.*, 2002; Vlassov *et al.*, 2012). Exosomes can be distinguished from apoptotic bodies and microvesicles by size. Exosomes are approximately 30–160 nm (Ludwig and Giebel, 2012; Théry *et al.*, 2002; Théry, 2011), with the exosomal lumen predicted to be 20–150 nm across, making the volume of an exosome approximately 4.2–380 yL (yottalitres [10^{-24} L]). Using this value it is estimated that an exosome can hold ≤100 proteins and ≤10,000 nucleotides (Vlassov *et al.*, 2012). Exosomes are spherical but have a cup-shaped morphology when visualised by electron microscopy; this is caused by the effects of dehydration (Pan *et al.*, 1985). They are pelleted at 100,000–120,000 × *g* (Eldh *et al.*, 2012; Johnstone *et al.*, 1987) and float at a density between 1.13 and 1.19 g/mL on a sucrose gradient (Mathivanan *et al.*, 2012; Raposo *et al.*, 1996). This distinguishes them from larger EVs, Golgi bodies, and vesicles of the endoplasmic reticulum (Raposo *et al.*, 1996; van Niel *et al.*, 2006).

Exosomes are biologically active vesicles that have paracrine, endocrine, and autocrine effects (Skog *et al.*, 2008; Valadi *et al.*, 2007). Their protein (Johnstone *et al.*, 1987), mRNA, and miRNA (Palma *et al.*, 2012; Valadi *et al.*, 2007) cargo are enclosed by a lipid-rich bilayer, of similar, yet distinctive consistency to the cellular plasma membrane (**Figure 1.4**). mRNAs are RNA molecules representative of cellular DNA that hold the specific genetic code involved in gene expression. miRNAs are non-coding RNA molecules that have silencing and post-transcriptional regulation of gene expression capabilities. The biological content of exosomes is influenced by both the cell of origin and the intended recipient cell. The RNAs isolated with exosomes have been shown to be enriched relative to the RNA profiles of the cells of origin suggesting that RNA molecules are specifically selected for packaging into exosomes (Nolte-'t Hoen *et al.*, 2012a; Ratajczak *et al.*, 2006; Skog *et al.*, 2008; Valadi *et al.*, 2007). Exosomes have been shown to transfer the protein and RNA they contain to recipient cells; examples of transported material include surface receptors, bioactive lipids, and signalling molecules (Ratajczak *et al.*, 2006; Silva *et al.*, 2012).
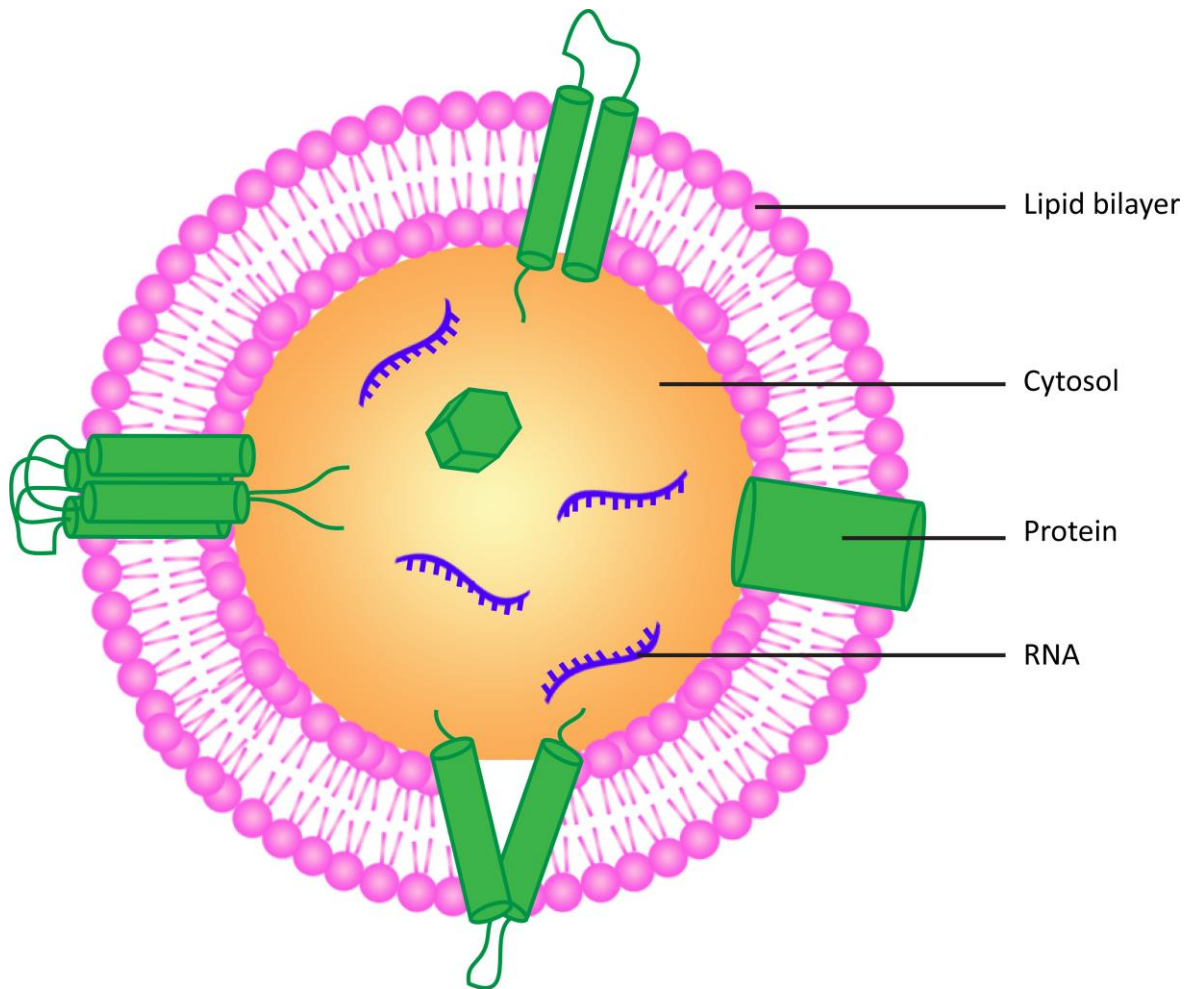
Figure 1.4: Illustration of an exosome. The size of the membrane and cargo are approximately proportional (green shapes represent proteins, blue ribbons represent RNAs).

The horizontal transfer of RNA is now appreciated as a form of intercellular communication, whereby donor cells can regulate gene expression of recipient cells (Chen *et al.*, 2012). Exosomes can reprogram surrounding cells by altering their translational profile, for example, mRNA transferred by exosomes can be translated into protein inside the recipient cell (Valadi *et al.*, 2007), inducing potent epigenetic changes (Baj-Krzyworzeka *et al.*, 2006; Deregibus *et al.*, 2007; Ratajczak *et al.*, 2006; Valadi *et al.*, 2007). Additionally, exosome-delivered miRNAs have been shown to interfere with translation by pairing to the un-translated regions (UTRs) of target mRNAs in the recipient cell (Bartel, 2004; Bartel, 2009). Exosome-delivered miRNAs were functional in recipient cells as gene expression was inhibited (Antonyak *et al.*, 2011; Baj-Krzyworzeka *et al.*, 2006; Hong *et al.*, 2009; Sheldon *et al.*, 2010; Skog *et al.*, 2008; Valadi *et al.*, 2007; Zhuang *et al.*, 2012). It is important to consider, however, that an alternative exosome-independent RNAi pathway exists involving miRNAs in blood plasma that are associated with argonaute proteins. The association with argonaute proteins appears to protect miRNA in the extracellular environment and enable them to execute RNAi in recipient cells (Turchinovich *et al.*, 2011). More

recently, a diverse range of small RNA sequences that can mediate transmission of functional gene silencing have been identified inside exosomes suggesting that exosomal RNA content is not limited only to mRNA and miRNAs (Bellingham *et al.*, 2012; Pan *et al.*, 2012).

Exosomes are released by all types of cells in culture and are also present in body fluids. The durability of exosomes in culture enables collection of a high number of exosomes through differential/sequential centrifugation of culture medium (Sahoo *et al.*, 2011). It is difficult to know whether the concentration of membrane vesicles observed *in vitro* correspond to those secreted *in vivo* and whether they function in the same way *in vitro* as *in vivo* (Théry, 2011).

The exosomal microenvironment remains tightly controlled and provides a platform that accommodates complex interactions between numerous molecules. These molecules remain safe from, but still able to interact with, the extracellular environment (Anderson *et al.*, 2010; Chaput and Théry, 2011; Valadi *et al.*, 2007). Hence, exosomes are excellent signal transporters (Taylor and Gercel-Taylor, 2008) capable of carrying small soluble molecules such as cytokines, growth factors, transcription factors, and RNAs, which would otherwise be hydrolytically or enzymatically degraded if they subsisted as free molecules in the extracellular milieu (Chaput and Théry, 2011). Exosomes have the ability to transfer messages to both neighbouring and distant cells, a process facilitated by the circulation, and other biological fluids (Al-Nedawi *et al.*, 2008; Raposo *et al.*, 1996; Skog *et al.*, 2008; Valadi *et al.*, 2007). Consequently they have become recognised as potential mediators of disease, amongst many other applications (Alvarez-Erviti *et al.*, 2011; Ohno *et al.*, 2013; O'Loughlin *et al.*, 2012; Raposo *et al.*, 1996; Zitvogel *et al.*, 1998). In addition, exosomes have excellent potential as gene therapy nanovehicles since they are non-immunogenic, have exceptional potency, biodistribution and biocompatibility, and can cross the blood brain barrier (Zhuang *et al.*, 2011). siRNAs have been successfully introduced to exosomes and delivered to recipient cells causing selective gene silencing (Wahlgren *et al.*, 2012). There is a promising possibility that exosomes could be packed with cancer therapeutics and targeted to specific recipient cancer cells (Fan *et al.*, 2013; Lakhal and Wood, 2011). Exosome-based gene therapy awaits accurate understanding of the mechanism of exosomes' target selection (Seow and Wood, 2009).

1.4.1. Exosome biogenesis and secretion

Exosome biogenesis and secretion is a highly controlled process (Stoorvogel *et al.*, 2002; Théry *et al.*, 1999). The release process involves four stages: initiation, endocytosis, formation of MVBs, and exosome secretion (**Figure 1.5**) (Kharaziha *et al.*, 2012). The signalling pathway that triggers

the initiation stage is unknown, however following initiation, membrane proteins are sorted into endosomes depending on whether they need to be degraded (e.g. epidermal growth factor receptor [EGFR]) or recycled (e.g. transferrin receptor, low-density lipoprotein receptor) (Fader and Colombo, 2009; Razi and Futter, 2006). The mechanisms involved in protein sorting into ILVs are not yet fully understood. However, there is evidence to suggest that ubiquitin and endosomal sorting complexes required for transport (ESCRT) machinery are involved in this process (Lakkaraju and Rodriguez-Boulan, 2008; Stoeck *et al.*, 2006), along with lipids (including ceramide) and tetraspanin proteins (Kowal *et al.*, 2014). It is well established that tumour susceptibility gene 101 (TSG101) facilitates trafficking of ubiquitinated receptors from early endosomes to late endosomes through interactions with the early endosome associated protein hepatocyte growth factor-associated tyrosine kinase (Hrs) (Bache *et al.*, 2003; Lu *et al.*, 2003; Pornillos *et al.*, 2003) and the late endosomal protein Alix (von Schwedler *et al.*, 2003). Its detection in exosomes suggests that TSG101 is involved in exosome biogenesis. Additional ESCRT proteins, for example, vacuolar protein sorting 4 (VPS4), also direct the formation of and cargo selection for MVBs (Henne *et al.*, 2011; Hurley and Stenmark, 2011). MVBs are then formed by internalisation of the delimiting endosomal membrane through clathrin-coated pit assembly (Sorkin and von Zastrow, 2009). Selected endosomal membrane proteins and soluble factors are sequestered in the membrane and cytosol of ILVs (Sorkin and von Zastrow, 2009). The ~100 nm internal vesicles are referred to as ILVs whilst contained inside the MVBs and are only referred to as exosomes following secretion (Février and Raposo, 2004). Vesicle accumulation is mediated by Hrs (Razi and Futter, 2006). After sufficient vesicle accumulation, MVBs endure one of three fates: (1) they are directed to fuse with the lysosome for degradation (Futter *et al.*, 1996); (2) are trafficked to the trans-Golgi network or plasma membrane for recycling (Johnstone *et al.*, 1991); (3) the MVB limiting membrane fuses with the plasma membrane, releasing ILVs (exosomes) into the extracellular milieu (Babst, 2005; Bedoui *et al.*, 2009; Johnstone *et al.*, 1991). The RAB proteins RAB11, RAB27, and RAB35 have been shown to participate in transfer of MVBs to the plasma membrane and subsequent exosome secretion (Kowal *et al.*, 2014). It is predicted that soluble N-ethylmaleimide sensitive fusion protein attachment receptor protein (SNAREs) also participate in fusion of MVBs with the plasma membrane. Different types of EVs bud directly from the plasma membrane, these are typically referred to as microvesicles or microparticles (Kowal *et al.*, 2014).

Exosomes are the only identified vesicles to be derived from intracellular membranes (Raposo and Stoorvogel, 2013). Since multiple stimuli and different cellular microenvironments have been shown to induce exosome release (including hypoxia [Park *et al.*, 2010], cytokine interaction [Skokos *et al.*, 2001], and viral infection [Barreto *et al.*, 2010]), it is presumed that MVBs (derived from the same cell type) synthesised in different conditions hold vesicles with distinct

compositions that reflect their environment during production. Neural progenitor cell-derived exosomes have been shown to carry a specific selection of viral miRNAs relative to intracellular levels (Meckes *et al.*, 2010).

Figure 1.5: Exosome biogenesis and secretion. The release process involves four stages: initiation, endocytosis, formation of MVBs, and exosome secretion. Ubiquitin, ESCRT machinery ceramide, and tetraspanins are involved in formation of MVBs and protein sorting into ILVs. TSG101, Hrs, Alix, and VPS4 are known proteins responsible for the selection of specific cargo for loading into exosomes. MVBs are formed by inward budding of the delimiting endosomal membrane facilitated by clathrin-coated pit assembly. Selected endosomal membrane proteins and soluble factors are sequestered in the membrane and cytosol of ILVs. Vesicle accumulation is mediated by Hrs and once a sufficient number of vesicles have accumulated, MVBs endure one of three fates: (1) they fuse with the lysosome for degradation; (2) are trafficked to the trans-Golgi network or plasma membrane for recycling; (3) fusion of the MVB limiting membrane with the plasma membrane occurs, releasing ILVs (exosomes) into the extracellular milieu. RABs have been shown to participate in transfer of MVBs to the plasma membrane and subsequent exosome secretion. Furthermore it is predicted that SNAREs participate in fusion of MVBs with the plasma membrane. In addition to exosomes, different types of EV bud directly from the plasma membrane, these are usually referred to as microvesicles.
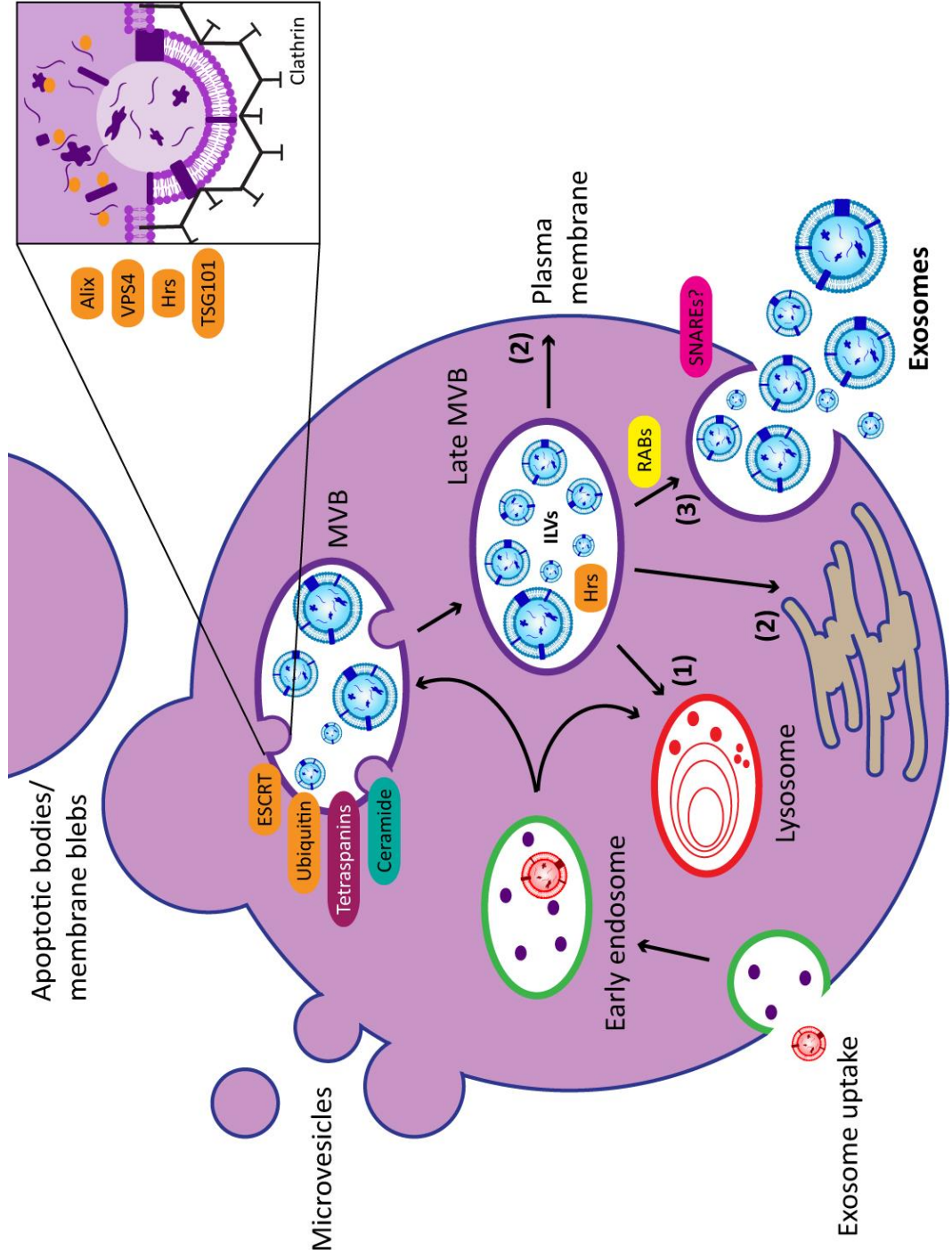
1.4.2. Exosome uptake

Because of the multiple functions of exosomes in humans, particularly their role in metastasis during cancer development (section **1.6**), it is essential that the process responsible for exosome signal transmission is elucidated. Many mechanisms have been proposed including: endocytosis of exosomes (Escrevente *et al.*, 2011; Montecalvo *et al.*, 2012; Morelli *et al.*, 2004); exosome-cell fusion, where exosome contents are released into the cytoplasm of the recipient cell, and the exosomal membrane merges with the plasma membrane (Parolini *et al.*, 2009); and direct activation of cellular surface-expressed ligands (Christianson *et al.*, 2013; Morelli *et al.*, 2004; Raposo *et al.*, 1996; Svensson *et al.*, 2013; Tumne *et al.*, 2009), see **Figure 1.6**. For a more in depth assessment of exosome uptake mechanisms refer to the author's recent review article (Mulcahy *et al.*, 2014) (**Appendix A, 8.1.1**).

Figure 1.6: Pathways shown to participate in EV uptake by target cells. EVs transport signals between cells. EVs have been shown to be internalised by cells through phagocytosis, clathrin- and caveolin-mediated endocytosis. There is also evidence to support their interaction with lipid rafts resulting in EV uptake. Lipid rafts are involved in both clathrin- and caveolin-mediated endocytosis. EVs can be internalised by macropinocytosis where membrane protrusions or blebs extend from the cell, fold backwards around the EVs and enclose them into the lumen of a macropinosome; alternatively EVs are macropinocytosed after becoming caught in membrane ruffles. EVs may also deliver their protein, mRNA, and miRNA cargo by fusion with the plasma membrane. Alternatively, intraluminal EVs may fuse with the endosomal limiting membrane following endocytosis to enable their extracellular vesicular contents to elicit a phenotypic response. (Taken directly from Mulcahy *et al.,* 2014).

COPYRIGHTED IMAGE REMOVED FROM ELECTRONIC VERSION

1.4.3. Exosome markers

Exosomes contain specific protein markers including tetraspanins, chaperone proteins, ESCRT machinery components, and plasma membrane components (Kharaziha *et al.*, 2012; Théry *et al.*, 1999).

1.4.3.1. Tetraspanins

Tetraspanins are membrane bound proteins with four transmembrane domains known to function principally as scaffolding proteins responsible for anchoring multiple proteins to a region of the plasma membrane (Hemler, 2005; Maecker *et al.*, 1997). Humans have 33 tetraspanins (Rubinstein, 2011). They are present on the cellular plasma membrane and some, most commonly CD9, CD63, and CD81, are present on the exosomal membrane. CD63 and CD81 have ESCRT machinery binding capabilities (Gan and Gould, 2011), and CD9 and CD81 play key roles in cell penetration, invasion, and fusion events (Hemler, 2003). These proteins are also MVB/late endosome markers that are efficiently sorted into ILVs; hence they are also regarded as exosome markers (Booth *et al.*, 2006; Escola *et al.*, 1998; Heijnen *et al.*, 1999; Koumangoye *et al.*, 2011; Mathivanan and Simpson, 2009; Rana and Zöller, 2011; Théry *et al.*, 1999). In addition, tetraspanins are more concentrated in exosomal membranes compared with both endosomal and cellular membranes; CD63 is found at approximately 7-fold greater concentration in the ILV membrane in comparison with the endosomal limiting membrane (Escola *et al.*, 1998).

1.4.3.2. Chaperone proteins

Heat shock protein 70 kDa (HSP70), HSP90 and HSP60 are heat shock cognate proteins that are ubiquitously expressed in human cells (Tavaria *et al.*, 1995). HSP70 has numerous cellular functions one of which involves specific selection and escort of proteins to the lysosome or late endosomal surface for subsequent microautophagy during chaperone-mediated autophagy (Sahu *et al.*, 2011; Salvador *et al.*, 2000). It is therefore reasonable to suggest that exosome synthesis and protein content determination occurs via a similar mechanism to chaperone-mediated autophagy, which could explain the high HSP70 concentration (and high concentrations of other heat shock proteins) detected in exosomes. It is now well-established that HSP70 plays a key role in exosome formation and/or release inside cells (Théry, 2011).

1.4.3.3.   ESCRT machinery components

Because of their endosomal origin the majority of exosomes hold proteins that play a role in membrane transport and fusion (Escrevente *et al.*, 2011). The ESCRT is essential in ILV formation and content selection (Williams and Urbé, 2007) for this reason, exosomes are enriched in ESCRT constituents, namely TSG101 and Alix (**Figure 1.5**).

1.4.3.4.   Plasma membrane components

The exosomal membrane is comparable, yet distinct from, the plasma membrane of the cells in which they were synthesised (Mathivanan *et al.*, 2010). The exosomal membrane is far more rigid compared with the fluid cellular membrane because of a decreased phosphatidylcholine content and enrichment in lipid-raft components including sphingomyelin, cholesterol, and ceramide (Eldh *et al.*, 2012; Laulagnier *et al.*, 2004; Mitchell *et al.*, 2009; Trajkovic *et al.*, 2008). Ceramide is speculated to mediate membrane invagination of ILVs, hence it is enriched in the exosomal membrane. Exosomes also carry the distinctive lipid-raft markers: caveolins, flotillins (Logozzi *et al.*, 2009; Staubach *et al.*, 2009), and clathrin, because of the process through which they are synthesised in endosomes (**Figure 1.5**) (Février and Raposo, 2004). Cholesterol concentration is elevated in the exosomal membrane compared with the typical cholesterol concentration of the plasma membrane (Zakharova *et al.*, 2007). The presence of resident lipid-raft components in the exosomal membrane suggests that multiple pathways contribute to MVB formation and consequential exosome secretion, possibly because of specific cellular stimulation or dependent on the cargo to be loaded into the exosome (Meckes and Raab-Traub, 2011).

1.5. Role of exosomes in tumour development

Exosomes are released into the organ microenvironment or directly spilled into the blood stream by both normal cells and tumour cells (Koga *et al.*, 2005; Llorente *et al.*, 2004; Théry *et al.*, 2002; Wolfers *et al.*, 2001). There are many differences between exosomes derived from tumour cells and normal cells, at both the molecular and functional levels (McDonald and Baluk, 2002; Morikawa *et al.*, 2002; St Croix *et al.*, 2000). Cancer cell-derived exosomes have been proposed to act as regulators of cancer progression (Merkerova *et al.*, 2008; Rabinowits *et al.*, 2009). They can support progression of cancer by mediating interactions between the tumour and its surrounding stroma (Antonyak *et al.*, 2011; Kahlert *et al.*, 2014; Muralidharan-Chari *et al.*, 2010; Webber *et al.*, 2010), activating proliferative, migratory, and angiogenic pathways (Epple *et al.*, 2012; Hood *et al.*, 2011; Tadokoro *et al.*, 2013); initiating development of pre-metastatic sites (Hoffman, 2013;

Rolfo *et al.*, 2014; Zhang and Grizzle, 2014); and by suppressing the immune-surveillance machinery (Whiteside, 2013). Tumour cells may be able to escape apoptosis by liberation of selected apoptosis-inducing proteins via exosomes (Jang *et al.*, 2013).

It has been hypothesised that cancer cells send specific signals via exosomes by dictating their content. Additionally they only accept signals from exosomes holding beneficial information in order to aid tumour growth (Liu *et al.*, 2006; Qu *et al.*, 2009; Zhang *et al.*, 2013). Furthermore, they are predicted to assist tumour progression through their elevated RNA content, enabling increased intracellular communication through transfer of oncoproteins, oncogenes, and onco-miRNA (Al-Nedawi *et al.*, 2008; Andre *et al.*, 2002; Chairoungdua *et al.*, 2010; Higginbotham *et al.*, 2011; Keller *et al.*, 2009; Miyanishi *et al.*, 2007; Taylor and Gercel-Taylor, 2008; Valadi *et al.*, 2007; Verweij *et al.*, 2011), it is also possible that exosomes released from the surrounding tissues may alter cancer cell gene expression, which repress tumour progression (Renzulli *et al.*, 2010).

1.5.1.   Elevated levels of exosomes in patients living with cancer

In comparison with the normal population, exosomes are found in greater abundance in the biological fluids of patients living with cancer (Silva *et al.*, 2012; Taylor and Gercel-Taylor, 2008). Additionally, exosome concentration in serum increases with tumour stage in ovarian cancer (Taylor and Gercel-Taylor, 2008), and other cancers (Logozzi *et al.*, 2009; Rabinowits *et al.*, 2009; Tavoosidana *et al.*, 2011). Therefore exosome blood plasma concentrations correlate with shorter patient survival; consequently exosomes are potential diagnostic and prognostic biomarkers (Al-Nedawi *et al.*, 2008; Silva *et al.*, 2012; Taylor and Gercel-Taylor, 2008; Zhou *et al.*, 2006). It has been hypothesised that oncogene activation and tumour suppressor gene deactivation may contribute to this increased exosome secretion (Kharaziha *et al.*, 2012). It has been shown that hypoxic environments cause an increase in exosome secretion (King *et al.*, 2012). Tumour-derived exosomes carry both pro- and anti-tumour microRNAs (Fernández-Medarde and Santos, 2011; Kogure *et al.*, 2011; Ohshima *et al.*, 2010; Roccaro *et al.*, 2013). The net outcome of these contradictory factors *in vivo* has not yet been established. The general opinion within the field supports the hypothesis that tumours actively release exosomes to promote their growth. However this has not been proven, and it is possible that increased levels of tumour-derived exosomes in the biological fluids of people living with cancer could be the result of tumour expansion, instead of an indicator of active participation of these vesicles in tumour progression (Théry, 2011).

1.6. The effect of exosomes on metastasis

EVs have been shown to facilitate cancer progression; more specifically, in many studies exosomes have been linked with increased metastatic activity (Bobrie *et al.*, 2012; Minciacchi *et al.*, 2015; Zomer *et al.*, 2015). Several different mechanisms through which exosomes mediate metastasis have been identified.

1.6.1. Increased cell motility

Increased motility is an important step in the progression of a cancer cell towards metastasis. Cell surface proteoglycans have been shown to be integral in exosome-mediated stimulation of cancer cell migration (Christianson *et al.*, 2013). Additionally, it has been shown that there is a synergistic association between exosome secretion and invadopodia synthesis (section **4.1.1**) in head and neck squamous cell carcinoma cells signifying an essential role for exosomes in supporting cancer cell motility (Hoshino *et al.*, 2013).

1.6.2. Involvement of protein in exosome-mediated metastatic mechanisms

Exosomes isolated from metastatic human isogenic colorectal cancer (Ji *et al.*, 2013) and melanoma (Xiao *et al.*, 2012) cell lines have been found to be enriched in metastatic factors compared with those derived from non-metastatic cell equivalents. Specific proteins have been identified in exosome-mediated pro-metastatic activity, more specifically in ECM degradation and EMT regulation that support metastasis (Banyard and Bielenberg, 2015; Mu *et al.*, 2013). For example, amphiregulin-carrying exosomes, derived from human breast and colorectal cancer cells, had the capacity to increase invasiveness of recipient breast and colon cancer cells (Higginbotham *et al.*, 2011). There is also evidence to suggest that exosome-associated Wnt-5a increases invasion of breast cancer cells (Menck *et al.*, 2013). In addition, exosome-associated Synuclein-γ (Liu *et al.*, 2014a) and prominin-1/CD133 (Rappa *et al.*, 2013) have been linked with increased cell migration and invasiveness.

1.6.2.1. ECM degradation

HSP90α-containing exosomes derived from a breast cancer cell line were shown to activate plasmin, a protease that participates in metastasis. Plasmin contributes to metastasis through interactions with many proteins including ECM proteins, integrins, endocytosis receptors, and growth factors. These interactions promote degradation of ECM during invasion (Andreasen *et al.*,

2000). Matrix metalloproteinases (MMPs) degrade the ECM, and hence advocate cell invasion. Exosome uptake has been associated with increased MMP1 (Atay *et al.*, 2014) and MMP9 (Deng *et al.*, 2012) production in recipient cells.

1.6.2.2.   Exosome-associated EMT regulation

Exosomes have been associated with increased metastasis by promoting EMT. Mesenchymal stem cell-derived exosomes increased the migratory potential of the non-metastatic breast cancer cell line, MCF-7 (Lin *et al.*, 2013). Additionally, the proteome of exosomes released by cells that have undergone induction of an EMT-like state through blockade of E-cadherin and EGFR stimulation was shown to be distinct from control cells. Differences in protein enrichment were identified, many associated with cell movement (Garnier *et al.*, 2013). Also, exosomes derived from metastatic human bladder cancer cells have been shown to be enriched with EMT associated proteins, including vimentin and hepatoma-derived growth factor that were located in the exosomal membrane; and casein kinase IIα and annexin A2 that were located in the exosomal lumen (Jeppesen *et al.*, 2014). Furthermore, hypoxia-inducible factor 1-alpha (HIF1α) was shown to participate in exosome-mediated pro-metastatic effects in recipient human embryonic kidney cells through decreased E-cadherin and increased N-cadherin expression (Aga *et al.*, 2014).

1.6.3. Interactions between metastasis promoting exosomes and surrounding normal stroma

Several studies have reported the pro-tumour effects of exosomes on the surrounding normal stroma. For example, gastrointestinal stromal tumour development has been shown to be promoted by tumour-derived exosome uptake in stromal cells (Atay *et al.*, 2014). The surrounding stroma of breast cancer became more accommodating to the tumour following exosome-mediated delivery of tumour-promoting factors (Dutta *et al.*, 2014). In a different report, exosome-associated changes in breast cancer morphology and phenotype were observed, which resulted in increased cell motility (McCready *et al.*, 2010). Furthermore, fibroblast-secreted exosomes have been shown to interact with neighbouring breast epithelium and promote breast cancer cell protrusive activity and motility. This was supported by co-injection of breast cancer cells with fibroblasts, which significantly increased metastasis in a mouse model (Luga *et al.*, 2012).

In addition to this, invasive capacity of recipient cells has been shown to increase following administration of exosomes derived from a brain metastatic cancer cell line compared with a non-brain metastatic melanoma cell line (Camacho *et al.*, 2013). This was also observed in a renal

cancer cell line (Chen *et al.*, 2014). Evidence suggests that integrin alpha 3 (ITGA3) and integrin beta 1 (ITGB1)/CD29 components of prostate cancer cell-derived exosomes have the capacity to manipulate non-cancerous surrounding prostate epithelium (Bijnsdorp *et al.*, 2013). Additionally, pancreatic and colon carcinoma-derived exosomes presenting HSP70 on their surface have been shown to stimulate a migratory phenotype in natural killer cells (Gastpar *et al.*, 2005). Hao and colleagues (2006) also showed that the tumour antigen Met 72 was transferred from highly metastatic melanoma cells to non-metastatic cells by exosomes (Hao *et al.*, 2006).

1.6.3.1.   Preparation of the metastatic niche

It is now well-recognised that distant sites are pre-conditioned in preparation for the arrival of metastatic cells. These distant microenvironments are known as the 'metastatic niche' (Brooks *et al.*, 2010). Haematopoietic stem cells migrate to these sites, and induce remodelling of the ECM, and alter secreted growth factor combinations resulting in creation of a microenvironment that both attracts circulating metastatic cells and supports secondary tumour establishment (Kaplan *et al.*, 2005; Kaplan *et al.*, 2006). It has been suggested that exosomes may be sent to prepare the metastatic niche in foreign microenvironments (Hendrix and Hume, 2011; Minciacchi *et al.*, 2015; Rana *et al.*, 2013) and promote metastasis through communication with neighbouring normal stromal cells (McCready *et al.*, 2010). In a comprehensive study, melanoma-derived exosomes were shown to effectively prepare the metastatic niche in bone marrow through stimulation of vascular leakiness (Peinado *et al.*, 2012). Additionally, CD105-bearing microvesicles were reported to stimulate lung metastasis through preparation of the pre-metastatic niche in renal cancer (Grange *et al.*, 2011). Also there is evidence to show that melanoma-derived exosomes condition lymph nodes in preparation for metastasis through molecular signals that induce vascular proliferation, ECM deposition, and promote melanoma cell establishment (Hood *et al.*, 2011).

1.6.3.2.   The role of exosomes in Paget's 'soil and seed' hypothesis

There is some evidence to suggest that exosomes participate in Paget's proposed metastatic organotropism (Paget, 1989). Exosomes have been shown to prepare cells of specific organs to facilitate cancer cell metastasis at specialised sites. Exosomes derived from metastatic mouse and human lung, liver, and brain tumour cells were taken up by cells at their preferred destination organ: fibroblasts and epithelial cells in the lung, Kupffer cells in the liver and brain endothelial cells (Hoshino *et al.*, 2015). These tumour-derived exosomes were shown to prepare the pre-metastatic niche; specifically, exosomes from lung tumour cells redirected the metastasis of

bone tumour cells. The exosomal integrins α6β4 and α6β1 were identified as facilitators of lung metastasis, and αvβ5 was associated with liver metastasis. Exosome uptake was reduced by interfering with the binding ability of the exosomal integrins α6β4 and αvβ5 that resulted in decreased lung and liver metastasis, respectively (Hoshino *et al.*, 2015).

Understanding the molecular basis of metastasis is therefore imperative if the effective treatment of cancer is to be prolonged, and if novel treatment strategies are to be identified (Lengyel, 2010; Weigelt *et al.*, 2005). Our current knowledge of the effects of exosomes upon metastasis are summarised in **Figure 1.7**.

Figure 1.7: The effect of exosomes upon metastasis. Exosomes have been shown to promote metastasis through: 1) communication with cells of surrounding normal stroma, and preparation of cells of the pre-metastatic niche at distant sites; 2) Delivery of proteins, and 3) miRNA that deliver invasion-stimulating signals to recipient cells; and 4) by increasing cell motility.
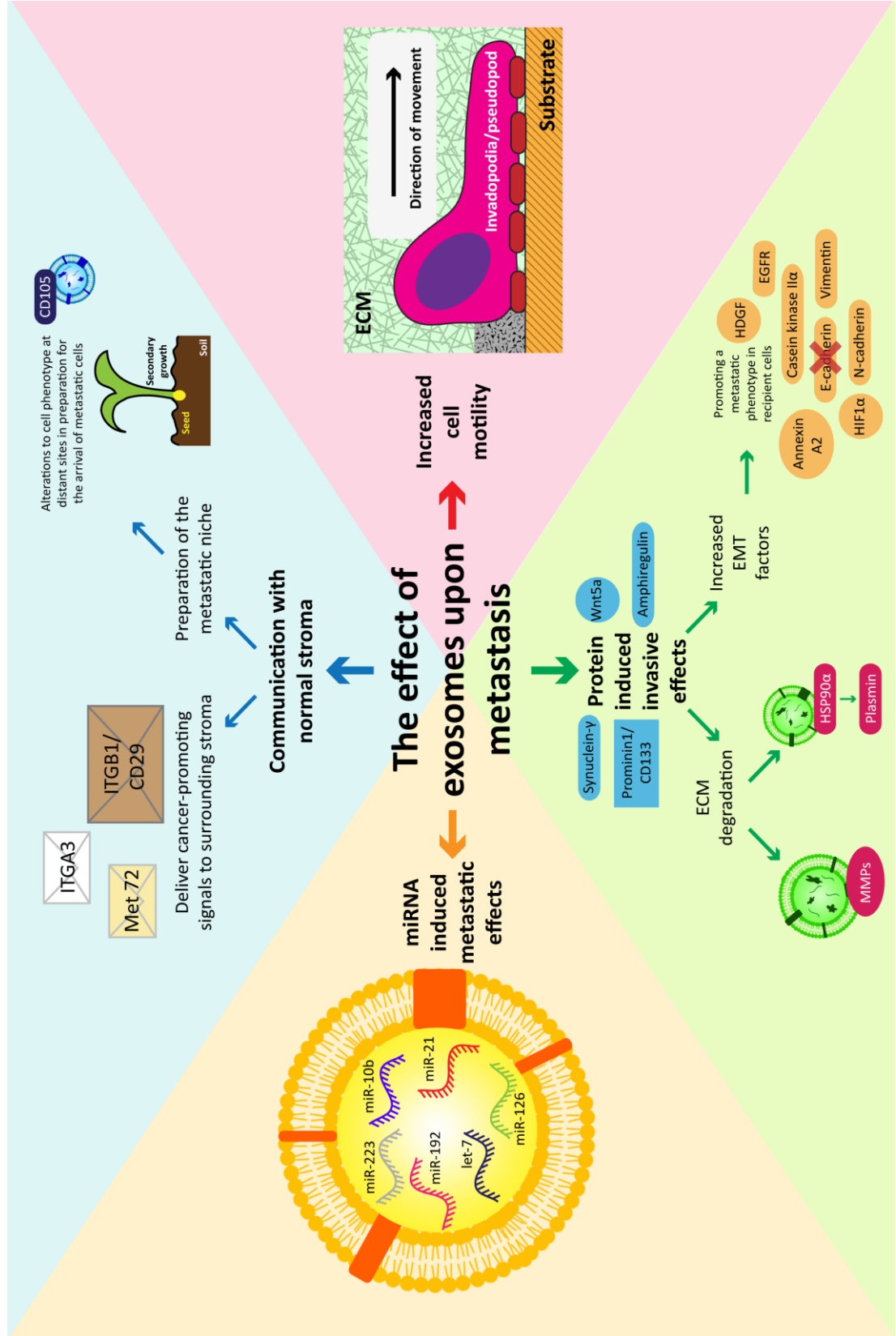
1.6.4. Investigating exosome uptake by human cells

Prior to exploring the project outlined below (section **1.7**) exosome uptake in human cells was investigated. Twelve months was spent optimising labelling of exosomes using: (1) fluorescent lipid dyes, (2) transfecting exosome-producing cells with a plasmid that induced expression of ubiquitous green fluorescent protein, and (3) [^{35}S]-radiolabelling of proteins of exosome donor cells with the expectation that radiolabelled proteins would incorporated into exosomes. The future objectives were to quantify exosomes in terms of either fluorescence intensity or radioactivity. Quantified exosomes would have been administered to human cells, and their uptake would have been measured using a fluorescence plate reader and/or confocal microscope, or a scintillation counter. Following this a number of compounds and antagonistic antibodies could have been tested to see which ones were able to prevent exosome uptake. This could have elucidated, at least in part, the mechanism of exosome uptake by human cells. The direction of this project changed once it became clear that specifically labelling exosomes is very difficult. It became apparent that two large groups (one at Harvard) are working on this mechanism so the project became too high risk considering the funds, equipment, and man-power available at the time.

1.7. Project aims

This project had two aims, (1) to investigate whether exosomes derived from highly motile ovarian cancer cell lines could induce a more motile phenotype in less aggressive ovarian cancer cell lines; (2) to determine the effect of stressed cell-derived exosomes upon metastatic capacity cancer cell lines *in vitro*. The findings of this investigation may indicate the suitability of exosomal communication modulation as a possible future cancer therapeutic. The key objectives of this project were to:

- Characterise exosomes using western blotting (WB), confocal microscopy, transmission electron microscopy (TEM), and nanoparticle tracking analysis (NTA) to identify specific exosome protein components

- Establish the motility of nine ovarian cancer cell lines using the scratch wound healing assay

    - Cell proliferation, invasion and exosome secretion rates were also confirmed

- Confirm the effect of exosomes derived from more motile ovarian cancer cell lines on the motility of less motile cell lines

- Confirm the effect of exosomes derived from stressed cells (stressed by heat shocking or cisplatin treatment) upon invasive capacity of recipient ovarian cancer cell lines

1.8. Novel contribution

Novel work in this project was the demonstration of an increased metastatic phenotype expressed by cells in response to uptake of exosomes derived from cells that had been stressed by either heat shocking or cisplatin treatment. In addition, this project involved the first comparative investigation of motility, proliferation, invasion, and exosome secretion rates of nine ovarian cancer cell lines.

Chapter 2

Methods

2. <u>Methods</u>

2.1. Cell culture

For conventional cell culture, the MCF-7 breast cancer cell line, and IGROV-1 and OVCAR-5 ovarian cancer cell lines were seeded in T75 culture flasks (Thermo Fisher Scientific), these are cell culture flasks that have a surface area of 75 cm^2 on their base (the area in which cells area able to attach and grow), with Dulbecco's modified eagle's medium (DMEM) (Life Technologies) supplemented with 10% foetal bovine serum (FBS) (Life Technologies) and 2.0 mM L-glutamine (Thermo Fisher Scientific). A-2780, MCP-1, CP-70, OVCAR-3, OVCAR-8, and SKOV-3 cell lines were cultured in Roswell Park Memorial Institute (RPMI) media (Life Technologies) supplemented with 10% FBS and 2.0 mM L-glutamine. OVCAR-3 cell culture medium also contained 0.01 mg/mL bovine insulin (SigmaAldrich), and 1.0 mM sodium pyruvate (SigmaAldrich). Cultures were maintained at 37°C in a humidified incubator in an atmosphere of 20% O_2, 5% CO_2, and 75% N_2. The cell lines were maintained within cell concentrations between 2.0×10^5 and 1.0×10^6 cells/mL. MCF-7 cells were a generous gift from Dr Miriam Dwek (University of Westminster). A-2780, CP-70, and MCP-1 cells were kindly donated by Professor Robert Brown (University College London). IGROV-1, SKOV-3, OVCAR-3, OVCAR-4, OVCAR-5, and OVCAR-8 were purchased from National Cancer Institute, Frederick Cancer Division of Cancer Treatment and Diagnosis Tumor/Cell Line Repository (Bethesda, USA). Details of the cell lines used in this project are outlined in **Table 2.1**.

Table 2.1: Origins of ovarian cancer cell lines and their chemotherapeutic resistance status.

Cancer cell line	Tissue	Origin	Resistance	Reference
A-2780	Ovary	Solid ovarian tumour of untreated patient	None (untreated tumour)	(Godwin *et al.*, 1992)
CP-70	Ovary	Sister of A-2780 (solid ovarian tumour of untreated patient)	10-fold more resistant to cisplatin than parent A-2780 cells	(Louie *et al.*, 1985)
IGROV-1	Ovary	Solid ovarian tumour of untreated patient	None (untreated tumour)	(Bénard *et al.*, 1985)
MCF-7	Breast	Metastatic mammary carcinoma	None (untreated tumour)	(Soule *et al.*, 1973)
MCP-1	Ovary	Sister of A-2780 (solid ovarian tumour of untreated patient)	More resistant to cisplatin than parent A-2780 cells but less resistant than CP-70 cells	(Anthoney *et al.*, 1996)
OVCAR-3	Ascites	Malignant ascites	Cyclophosphamide Adriamycin Cisplatin	(Hamilton *et al.*, 1983)
OVCAR-4	Ascites	Malignant ascites	Cyclophosphamide Adriamycin Cisplatin	(Godwin *et al.*, 1992)
OVCAR-5	Ascites	Malignant ascites	Advanced untreated tumour	(Godwin *et al.*, 1992)
OVCAR-8	Associated with ovarian cancer	Unknown	Carboplatin	(Godwin *et al.*, 1992)
SKOV-3	Ascites	Malignant ascites	Diphtheria toxin Adriamycin Cisplatin	(Fogh *et al.*, 1977)

2.1.1. Sub-culturing

Assessment of the degree of confluency of the cells was performed every two to three days using a Nixon TMS inverted microscope, using x100 magnification. When cultures were approximately 70–80% confluent, spent medium was removed and replaced with fresh pre-warmed complete media. When cultures were >70–80% confluent they were sub-cultured in order to maintain cell growth. Spent medium was removed and the cell layer was washed with phosphate buffered saline (PBS) (Thermo Fisher Scientific). 0.05% (w/v) trypsin and 0.53 mM ethylenediaminetetraacetic acid (EDTA) (Thermo Fisher Scientific) in PBS was used to wash the cell layer of A-2780, CP-70, MCP-1, OVCAR-3, OVCAR-4, OVCAR-5, OVCAR-8, and SKOV-3 cells. 0.25% (w/v) trypsin and 2.65 mM EDTA in PBS was used to wash the cell layer of IGROV-1 and MCF-7 cells. 1.0 mL per 25 cm^2 of the flask surface area was used, excess trypsin/EDTA was immediately decanted and the flask was returned to the 37°C incubator for 2–10 minutes. Once detached, the cells were resuspended in fresh pre-warmed complete media; the minimum

volume of media used to resuspend cells was at least equivalent to the volume of trypsin/EDTA used initially. This ensured there was enough serum (FBS) available in the media to effectively inactivate the trypsin/EDTA. At this point the cell concentration could be determined if necessary (section **2.1.2**). The required number of cells were transferred to a new flask containing pre-warmed complete media. The cells were returned to the 37°C incubator.

2.1.2. Cell concentration determination

Adherent cells were brought into suspension using trypsin/EDTA as described in section **2.1.1**. The cell resuspension was concentrated by centrifuging at 300 × *g* (1500 rpm) in the MSE Centaur centrifuge for five minutes and the cell pellet was resuspended in a smaller volume. 15 µL of the cell resuspension was removed and loaded onto a haemocytometer. Cells within the 5 x 5 square were counted under a Nixon TMS inverted microscope, using x100 magnification. A minimum of 100 cells were counted to increase the accuracy of the cell count. At least three counts were recorded. The cell concentration was calculated by taking the average of the three cell counts and multiplying by 10^4 to give the number of cells present in 1.0 mL of the cell suspension.

2.1.3. Clearing foetal bovine serum for exosome-free medium

Exosomes were collected from supernatants of cell culture medium, therefore, for all exosome investigative experimentation, cells were cultured in exosome-free medium (EFM). This required clearing FBS of bovine exosomes. This was achieved by ultracentrifuging FBS at 120,000 × *g* using Beckman Coulter Optima LE-80K ultracentrifuge overnight at 4°C (Eldh *et al.*, 2012). Following clearing, the media was sterilised by passing through a syringe filter with pore size of 0.22 µm (Thermo Fisher Scientific). The cleared FBS replaced the non-cleared FBS in EFM.

2.2. Exosome extraction

2.2.1. Standard exosome extraction

Cells were grown in T175 flasks (Thermo Fisher Scientific), cell culture flasks that have a surface area of 175 cm² on their base (the area in which cells area able to attach and grow), to 70–80% confluence ($\sim 2.0 \times 10^7$). Exosome-containing medium was removed and centrifuged at 300 × *g* for five minutes in the MSE Centaur centrifuge to remove suspended dead cells. The harvested medium was centrifuged at 16,500 × *g* (14,182 rpm in JA-25.50 fixed angle rota) in a Beckman

Avanti J-25I centrifuge for 20 minutes at 4°C to remove cell debris and suspended cellular organelles. Syringe filters with a pore size of 0.22 μm were blocked with 0.1% bovine serum albumin (BSA) (SigmaAldrich) to prevent exosomes sticking to the hydrophilic polyethersulfone membranes inside the filters. Cell conditioned (exosome-containing) medium was then passed through these filters to remove the remaining cell debris and bacteria. The supernatant was ultracentrifuged at 120,000 × g (40,400 rpm in 70Ti fixed angle rota) using a Beckman Coulter Optima LE-80K ultracentrifuge for 90 minutes at 4°C to pellet exosomes. The extracted exosomes were resuspended in PBS, and finally pelleted once more at 120,000 × g (Eldh et $al.$, 2012). The exosome pellet was then resuspended in 50 μL PBS and used in subsequent experiments. When not used immediately after extraction, the exosomes were stored at -80°C.

2.2.2. Stress exosome collection

2.2.2.1. Heat shocked cell-derived exosomes

T175 flasks of cells were seeded. Once 70% cell confluence was reached, complete (serum-containing) medium was removed from the flasks. The cell layers were washed with PBS and were then replenished with EFM (section **2.1.3**). Half of the flasks were heat shocked at 45°C in an atmosphere of 5% CO_2 for 1 hour. The remaining flasks were maintained at 37°C to be used as controls.

2.2.2.2. Cisplatin treated cell-derived exosomes

T175 flasks of cells were seeded. Once 70% cell confluence was reached, half of the flasks were treated with 40 μM cisplatin (SigmaAldrich). Each flask contained 25 mL of complete media therefore 60 μL 16.7 mM cisplatin in PBS was spiked into the media of each flask ([0.040 mM x 25,000 μL] ÷ 16.7 mM). The flasks were swirled to mix the media and then returned to the 37°C, 5% CO_2 incubator. After 2 hours, cisplatin-containing media was removed from treated flasks and spent media was removed from control cells. The cells in all of the flasks were washed with PBS and replenished with EFM (section **2.1.3**). Two hours later, media was removed from all of the flasks to alleviate cisplatin secreted by the treated cells. The cells were replenished with EFM.

2.2.2.3. Stress exosome extraction

Twenty-four hours later exosomes were extracted as described in section **2.2**.

2.3. Exosome characterisation

2.3.1. Western blotting of whole cell and exosome protein extracts

2.3.1.1. Whole cell protein extraction

Cells were scraped from the surface of a culture flask into ice cold PBS and pelleted at 300 × *g*. Cells were scraped rather than trypsinised to prevent degradation of surface proteins that were later probed for. The cells were pelleted at 300 × *g* in the MSE Centaur centrifuge, the pellet was resuspended in ice cold PBS, and further pelleted at 300 × *g*. Cell preparations were then lysed in 1X radioimmunoprecipitation assay (RIPA) buffer (0.1 M Tris-hydrogen chloride, 0.3 M sodium chloride, 0.1% sodium dodecyl sulphate [SDS], 0.5% sodium deoxycholate, 1% Triton X 100) under constant agitation using a Revolver 360° sample mixer (Thermo Fisher Scientific) for 30 minutes at 4°C. Nuclei and cell debris were removed by centrifugation at 14,000 × *g* in a Heraeus biofuge fresco centrifuge.

2.3.1.2. Exosome protein extraction

Exosomes were extracted from 8 x T175 cells that were 70–80% confluent and had been conditioned for 24 hours in EFM, as described in section **2.2**. Exosome pellets from 8 x T175 flasks were resuspended in PBS, pooled into one tube, pelleted at 120,000 × *g* and resuspended in 50 μL 1X RIPA buffer (section **2.2**). The samples were mixed by pipetting and vortex mixing using Van Waters and Nat Rogers (VWR) lab dancer (VWR International Ltd, Lutterworth) for 15 seconds. The sample was then sonicated three times for five minutes in a Decon FS100 frequency sweep sonicating water bath (Decon) filled with ice cold water (in order not to denature the sample proteins). Between sonications the sample was vortex mixed for 15 seconds. Following sonication steps, the exosome samples were spun at 14,000 × *g* for 20 minutes at 4°C in a Heraeus biofuge fresco centrifuge to pellet non-protein debris.

2.3.1.3. Sample protein concentration determination using bicinchoninic acid assay

Following whole cell (section **2.3.1.1**) or exosome protein extraction (section **2.3.1.2**), lysates were quantified using a bicinchoninic acid (BCA) assay kit (Life Technologies), whereby 0–2000 μg/mL BSA (ampule provided in kit) were made using 1X RIPA buffer. Working reagent was made using 50 parts BCA reagent A and one part BCA reagent B. Working reagent was incubated at room temperature for five minutes. 25 μL of whole cell protein or 5.0 μL exosome protein samples were loaded in triplicate into 96-well flat bottom, non-treated, polystyrene plates (Life

Technologies). Working reagent, 200 µL or 40 µL for whole cell and exosome samples, respectively, was loaded and the content of each well was mixed by pipetting. The plate was incubated at 37°C for 30 minutes and allowed to cool for five minutes before the absorbance at 570 nm was determined for each well using a Labtech LT-4000MS Microplate Reader.

2.3.1.4.   Sodium dodecyl sulphate-polyacrylamide gel electrophoresis

The protein samples were solubilised at 100°C for 10 minutes in 5X sodium dodecyl sulphate-polyacrylamide gel electrophoresis (SDS-PAGE) loading dye under reducing conditions (1.0 M Tris-hydrogen chloride, 50% glycerol [SigmaAldrich], 5% SDS, 0.05% bromophenol blue [SigmaAldrich], 1.0 M dithiothreitol [DTT] [SigmaAldrich]). Protein samples were cooled on ice for five minutes prior to loading into the gel. After protein concentration determination (section **2.3.1.3**), 10.0 µg protein from whole cells or solubilised exosomes were loaded into wells of 12% pre-cast acrylamide gels (Bio-Rad) (used because the proteins of interest ranged in sizes from 9–130 kDa). Gels were enclosed in the gel cassette and running buffer (25 mM Trisbase [Thermo Fisher Scientific], 192 mM glycine [SigmaAldrich], 0.1% SDS, pH 8.3) was poured to the correct level in the gel tank. An electric field was applied across the gel at 80 V for the first 10 minutes, then 120 V for 60 minutes, causing the negatively charged proteins to migrate down the gel towards the anode.

2.3.1.5.   Protein transfer

Separated proteins were transferred onto polyvinylidene difluoride (PVDF) membrane (Bio-Rad) by semi-dry blotting for 10 minutes using high molecular weight protocol on a Trans-Blot® Turbo™ Transfer Starter System (Bio-Rad).

2.3.1.6.   Protein detection

The membrane was blocked for 1 hour with 5% dried skimmed milk powder (Marvel) in tris buffered saline with 0.05% Tween 20 (TBST) and cut into sections so that different parts of the membrane could be incubated with different antibodies. The membrane was incubated overnight at 4°C with anti-human primary antibodies (Abcam) diluted in 5% dried skimmed milk powder in TBST. 1:2500 monoclonal mouse anti-human HSP70 (ab5439), 1:1700 monoclonal rabbit anti-human cytochrome C oxidase (ab150422), 1:15,000 monoclonal rabbit anti-human GAPDH (ab128915), 1:1000 monoclonal rabbit anti-human calnexin (ab22595), and 1:1000 monoclonal

rabbit anti-human GM130 (ab31561). The membrane was then incubated for 60 minutes at room temperature with 1:2000 polyclonal goat anti-mouse-DyLight 550 conjugate (84540, Thermo Fisher Scientific) for sections of the membrane that had been incubated with mouse anti-human antibodies, or 1:2000 polyclonal goat anti-rabbit-horseradish peroxidase (HRP) conjugate (170-6515, Bio-Rad) secondary antibody for all sections of the membrane that were incubated with rabbit anti-human primary antibodies. The secondary antibodies were also diluted in 5% dried skimmed milk powder in TBST. After each antibody incubation period the membrane was washed three times for five minutes in TBST to remove background signal. Fluorescence or chemiluminescence was visualised using ChemiDoc MP (Bio-Rad) using the blot: Chemi or blot: Cy3 protocols.

2.3.1.7. Verification of heat shock induced cell stress by western blotting

Cells were heat stressed as described in section **2.2.2.1**. Twenty-four hours later the media was removed for exosome extraction and the cells were harvested for protein, as described in section **2.3.1.1**. Cell lysate protein concentration was quantified, as described in section **2.3.1.3** and western blotting (WB) was performed (section **2.3**).

2.3.2. Transmission electron microscopy of exosome samples

2.3.2.1. Grid preparation

A fraction of each exosome sample was combined with an equal volume of 4% paraformaldehyde (SigmaAldrich) and was preserved on ice for 15 minutes. A droplet of each sample was distributed using a pipette onto Parafilm (Thermo Fisher Scientific). Carbon-formvar coated copper 300 mesh grids (Agar Scientific, Stanstead) were placed dull-side downwards onto each sample droplet and left to incubate at room temperature for 30 minutes. Grids were then washed three times by placing dull-side downwards onto a droplet of 0.22 µm filtered ultrapure water. Between each wash, excess water was removed using filter paper. Finally, each grid was placed onto a 30 µL droplet of 2% uranyl acetate (aqueous) (SigmaAldrich) for two minutes. Excess solution was removed using filter paper and the samples were left to air dry for 60 minutes.

2.3.2.2.   Transmission electron microscopy

Grids were visualised using a Hitachi H7650 Transmission Electron Microscope at 100 kV with x40,000 magnification. Exosome diameter was measured using the measurement function in AMT software (Advanced Microscopy Techniques, Massachusetts, USA).

2.3.3.   Visualisation of exosome and cellular interactions by confocal microscopy

2.3.3.1.   Fluorescent staining exosomes with PKH26

The membrane stain PKH26 was used for confocal visualisation of exosome-cell interactions. Of the lipid stains tested, PKH26 was the most stable and did not photo-bleach easily. Its lipid-dissociation rate was low; therefore PKH26 was ideal for staining exosomes. Following the first $120,000 \times g$ ultracentrifugation step in the exosome extraction protocol (section **2.2**) the resuspended exosome pellet or 2000 ng BSA (used as a positive control) was introduced to 1.0 mL Diluent C (SigmaAldrich). Diluent C is a solution of unknown composition provided by SigmaAldrich as part of the PKH26 staining kit. 1.0 mM PKH26 lipophilic membrane dye (SigmaAldrich) was then diluted to 4.0 µM in 1.0 mL Diluent C and subsequently combined with the exosome-Diluent C mixture (or the BSA positive control) to give a total volume of 2.0 mL (final concentration of PKH26 = 2.0 µM). The mixture was incubated for five minutes at room temperature with periodic mixing with P1000 pipetman. To quench the staining reaction, 2.0 mL of 10.0 mg/mL BSA in PBS was added to the mixture to bind excess dye. Then the final ultracentrifugation step of the exosome extraction protocol was performed. The PKH26-labelled exosomes were transferred to a 300 kDa molecular weight cut-off Vivaspin 6 ultracentrifugal filter (GE Healthcare, Little Chalfont) and centrifuged at $4000 \times g$ in a Beckman Coulter Allegra 25R centrifuge. The sample was washed three times with 5.0 mL of PBS before being transferred to a new 300 kDa ultracentrifugal filter, and washed twice with 5.0 mL complete medium. The 50 µL stained exosome sample was transferred from the concentrate pocket to an Eppendorf tube (Eppendorf, Stevenage) and stored at -80 °C in the dark until use (Lässer *et al.*, 2011).

2.3.3.2.   Confocal microscopic analysis of exosome-cell interactions

A-2780 cells were seeded at 250,000 cells/cover slip in 6-well plates (Thermo Fisher Scientific) and grown for 24 hours to reach 70–80% confluency. At this point, 5.0 µL of PKH26-labelled exosomes (equivalent to 2 million cells worth of exosomes secreted over 24 hours) were introduced to the cells and incubated at 37°C for 60 minutes. Cells were fixed in 4% paraformaldehyde (SigmaAldrich) at 4°C for 30 minutes. Excess paraformaldehyde was quenched with 50 mM glycine

(SigmaAldrich). The fixed cells and exosomes were mounted and simultaneously the nuclei were stained using 15 µL of DAPI supplemented ProLong Fade Gold mounting media (Thermo Fisher Scientific). After overnight incubation at 4°C in the dark, the exosome-cell interaction was visualised using a Zeiss LSM 880 inverted confocal microscope (Zeiss, Cambridge), using x630 magnification. Viable cells were identified by their DAPI stained nuclei using 405 nm laser. PKH26-exosome interaction and trafficking inside A-2780 cells was observed using the 543 nm laser. Brightness and contrast were adjusted to improve visibility of particles. Images and z-stacks were collected using LSM 510 software (Zeiss, Cambridge).

2.3.4.   Exosome size determination and quantification by nanoparticle tracking analysis

One T175 flask of cells was cultured in EFM for 24 hours. Cell conditioned media was removed and exosomes were extracted (section **2.2**). The cells from which exosomes were extracted were counted (section **2.1.2**) to establish the size and number of exosomes released per cell for each cell type. Exosome pellets were resuspended in 50 µL PBS and diluted 1 in 100, leading to particle concentrations of approximately 5.0×10^8/mL (Sokolova *et al.*, 2011). Exosome size and concentration were determined by NTA with a NanoSight LM10 instrument equipped with the NTA 2.0 analytical software (Malvern Instruments Ltd, Malvern). Three biological replicates for each cell line were collected (**Figure 2.1**). Five, 30 second videos of each sample were recorded, and from these the software calculated the mean diameter (nm) and exosome concentrations ($x \times 10^8$). Each sample was measured in duplicate. The standard error of the mean was calculated for all data. Differences in exosome size and concentration between the different cell lines were determined using the two tailed T-test. All values are reported to three significant figures.

Exosomes were cultured in
SFM for 24 hours

Samples analysed by NTA
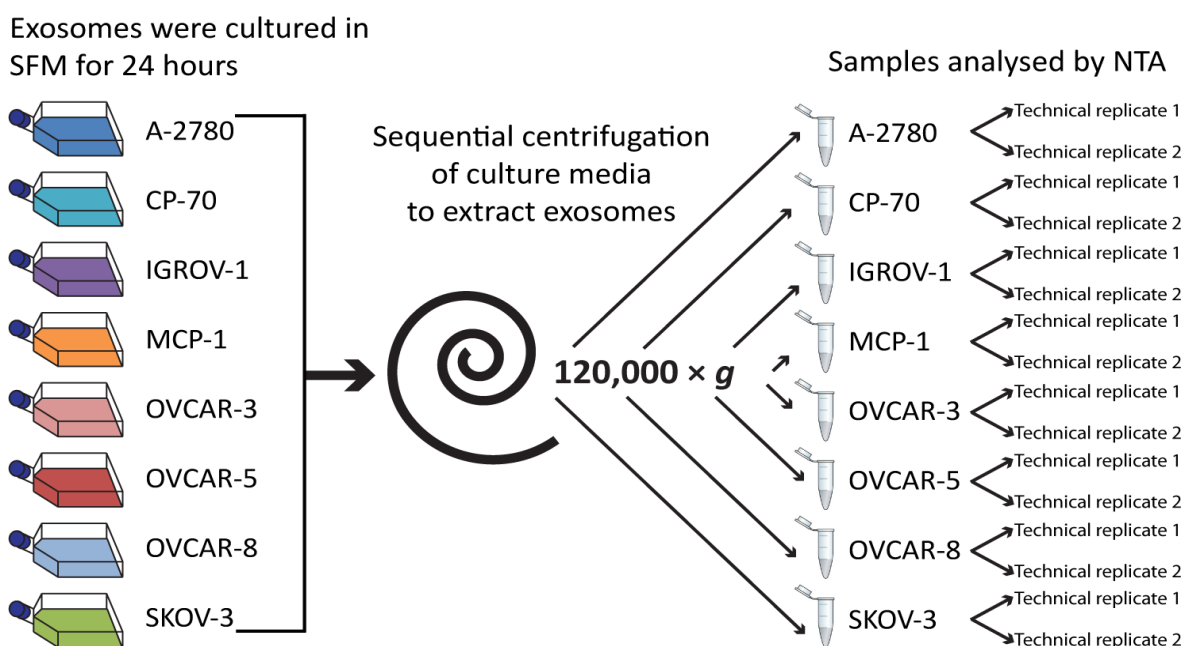
Figure 2.1: The procedure performed to collect a single biological replicate of exosomes from eight ovarian cancer cell lines in order to determine exosome size and the concentration differences by NTA. To determine the size difference by NTA and to quantify exosomes released by eight different ovarian cancer cell lines by NTA, eight T175 flasks of cells (one for each ovarian cancer cell line) were conditioned in media containing 10% exosome-free FBS for 24 hours. Following the conditioning period, media was removed and the exosomes were extracted. Cells were counted using a haemocytometer to allow the concentration of exosomes to be associated with the number of cells from which they were extracted. Exosome pellets were resuspended in PBS and stored at -80°C. A total of 24 samples were collected by repeating this procedure in triplicate on three different days over a seven day period to provide three biological replicates for each of the eight ovarian cancer cell lines. When analysed by NTA, two technical replicates were used to represent each biological replicate.

2.4. Exosome uptake inhibition

The procedure described in section **2.3.3** was used to verify exosome uptake and inhibition of exosome uptake. Uptake was inhibited using heparin or proteinase K, as described below. Following isolation of stress exosomes (section **2.2.2**) they were pooled, then stained with PKH26 (section **2.3.3.1**) and, finally, treated with an exosome uptake inhibitor prior to administration onto cells.

2.4.1.1.   Exosome uptake inhibition with heparin

Prior to addition of exosomes to cells, cells and half of the pooled exosome sample were both pre-treated with 10.0 mg/mL heparin sodium salt from porcine intestinal mucosa (SigmaAldrich) for 30 minutes at 37°C. The other half of the pooled exosome sample (control sample) was treated with PBS for 30 minutes at 37°C.

2.4.1.2.   Exosome uptake inhibition with proteinase K

The exosome sample was split in half. One half of the sample was treated with 1.0 mg/mL proteinase K (Thermo Fisher Scientific), and the other half (control sample) was treated with an equal volume of PBS, both for 30 minutes at 37°C. Proteinase K activity was inhibited immediately following the treatment incubation period by boiling the sample for 10 minutes.

2.4.1.3.   Quantification of exosome uptake

Confocal microscopic analysis was used to visualise exosome-cell interactions and to confirm inhibition of exosome uptake (section **2.3.3.2**). Three slides, seeded at 250,000 A-2780 cells, were prepared for each treatment type. Each slide received PKH26-stained exosomes extracted from 1 x T175 flask of A-2780 cells (equivalent to approximately 10 million cells worth of exosomes). Three z-stacks for a single layer of cells for each slide were acquired at 1.0 μm slice intervals. Volocity 3D Image Analysis software version 6.3 (PerkinElmer, Coventry) was used to quantify exosome uptake by measuring the volume (μm^3) of exosomes (PKH26 signal) inside each cell. The average volume of exosomes per cell was then calculated for each treatment type using 140 cells from each slide using Microsoft Excel 2010.

2.5. Cell motility assay

2.5.1.   Scratch wound healing/cell motility assay

Cells were seeded at an optimal concentration (this varied depending upon cell type, **Table 2.2**) in 24-well tissue culture plates (Corning, Deeside) (**Figure 2.2B**). The plates were marked with three horizontal lines on the bottom to enable alignment of the plate on the microscope to ensure the same area of the well was imaged at each data collection point (**Figure 2.2A**). The cells were maintained at 37°C, 5% CO_2 for 48 hours. During this time the cells proliferated and reached 100% confluence, i.e. a monolayer of cells had formed over the bottom surface of each well. A scratch was made in a straight line down the centre of three wells of each cell type using a P200 pipette tip (**Figure 2.2C**). The media containing floating cells was removed carefully, and the cell monolayer was washed with 1.0 mL pre-warmed media to smooth the edges of the scratch. Each well was replenished with 2.0 mL pre-warmed media. Each point along the scratch (A, B and C) was located using the marks on the bottom of the plate (**Figure 2.2C**), and photographed under a Motic AE31 inverted microscope (Motic, Wetzlar, Germany), using x100 magnification. The cells were incubated at 37°C, 5% CO_2. Photographs were taken every 12 hours, unless stated otherwise, with the last photograph taken 48 hours after the scratch was made.

Table 2.2: Optimum cell seeding concentrations in 24-well plates for scratch assay.

Cell Line	Concentration in 24-well plate (cells/well)
A-2780	1,100,000
CP-70	400,000
IGROV-1	400,000
MCF-7	560,000
MCP-1	1,800,000
OVCAR-3	180,000
OVCAR-4	190,000
OVCAR-5	220,000
OVCAR-8	175,000
SKOV-3	350,000
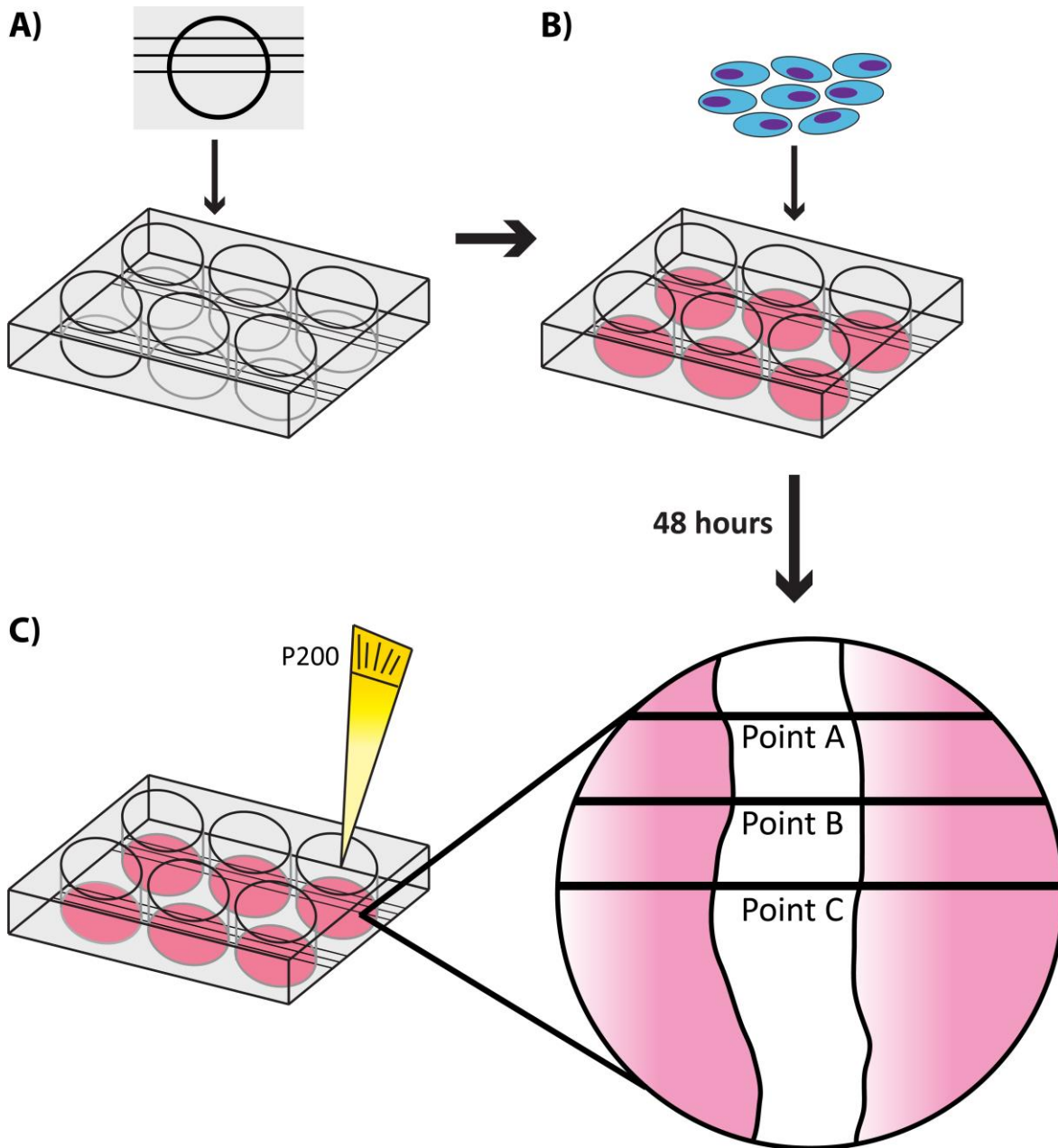
Figure 2.2: Scratch motility assay. A) The base of 24-well plates were marked to enable alignment of the plate on the microscope to ensure the same area of the well was imaged at each data collection point. B) Cells were seeded in plates and grown to 100% confluency over a 48 hour period. C) A scratch was made down the centre of the well using a P200 pipette tip. For data collection, images were taken at points A, B, and C.

2.5.2. Scratch wound healing assay with exosome treatment

Two T175 flasks (Thermo Fisher Scientific) containing cells of each cell line (OVCAR-5 and SKOV-3), at 70–80% confluency, were cultured in 10% cleared FBS (section **2.1.3**) containing media for 24 hours (approximately 6 million cells per flask). Exosomes were then extracted from the culture media following the procedure described in section **2.2**. The exosomes were filtered using 0.22 μm filters previously blocked with 0.1% BSA, mixed with fresh media, and then distributed across three wells of a 24-well plate. This was performed twice, once 24 hours prior to creating the scratch, and once immediately after the scratch was made, then the cells were washed with media. This method is illustrated in **Figure 2.3**.

Figure 2.3: Scratch assay with exosome swapping experimental method. The scratch assay was performed to determine the effect of OVCAR-5 and SKOV-3 cell-derived exosomes on OVCAR-5 cell motility. Twenty-four hours prior to starting the scratch assay exosomes were extracted from approximately 6 million OVCAR-5 or SKOV-3 cells. Exosomes were immediately administered to the cells that were subsequently going to participate in the scratch assay (3 x wells of 24-well plate approximately 220,000 cells per well). Twenty-four hours later the exosome extraction procedure was repeated and fresh exosomes were administered to cells immediately following scratch creation.
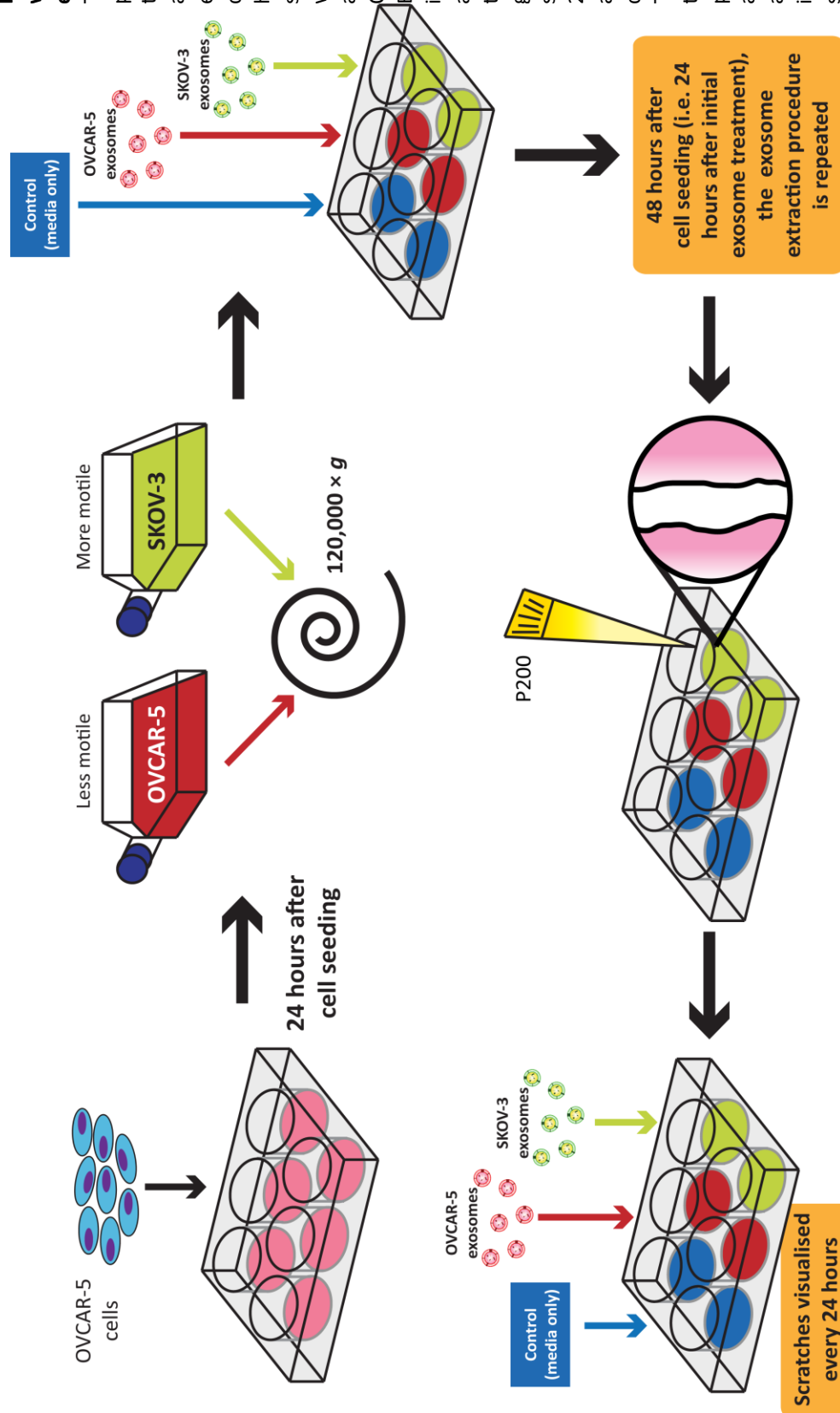
2.5.3. Scratch assay image analysis using ImageJ

ImageJ (National Institutes of Health, Bethesda, USA) was used to determine the scratch size in terms of percentage of the image size. The 'autoAdjust' tool was used to correct the brightness and contrast of the scratch image (**Figure 2.4A**). In order to convert the image into a binary drawing that could be analysed by the ImageJ software, the 'Analysed Image Generating Macro' script file was installed. This macro performed the following steps: inverted the image, created north facing shadows, found edges, sharpened and smoothed the image, and made the final image binary. This process resulted in an image where the cells and the empty scratch area were distinguishable (**Figure 2.4B**). ImageJ automatically fills the largest area white, but in order to analyse the scratch, the scratch area must be black. For scratches that covered >50% of the image area, the image was inverted (**Figure 2.4C**). The freehand selection tool was used to select the scratch area, the particles in this section of the image were analysed using the following settings: size: 12,000; circularity: 0.00–1.00; show: outlines; flag: summarise. This produced a drawing of the scratch outline and a percentage value for the scratch area (**Figure 2.4D**). The percentage value for the scratch area did not represent the area of the scratch in the entire image, only the percentage within the area that was selected. In order to determine the scratch size, the scratch areas were filled black on the drawing of the scratch outline. This image was then converted to binary format. For images where the scratch area was >50%, the image inversion step was repeated. The particles within the entire image were analysed once more (**Figure 2.4E**). The final percentage value given in the summary table represented the percentage area of the scratch within the image area (**Figure 2.4F**). This analysis was performed on each scratch image to determine the speed of scratch closure in terms of percentage area reduction per hour, an example is shown in **Figure 2.5**. Scratch width percentage values were normalised to scratch area at time = 0, i.e. scratch width at t=0 was regarded as 100%.
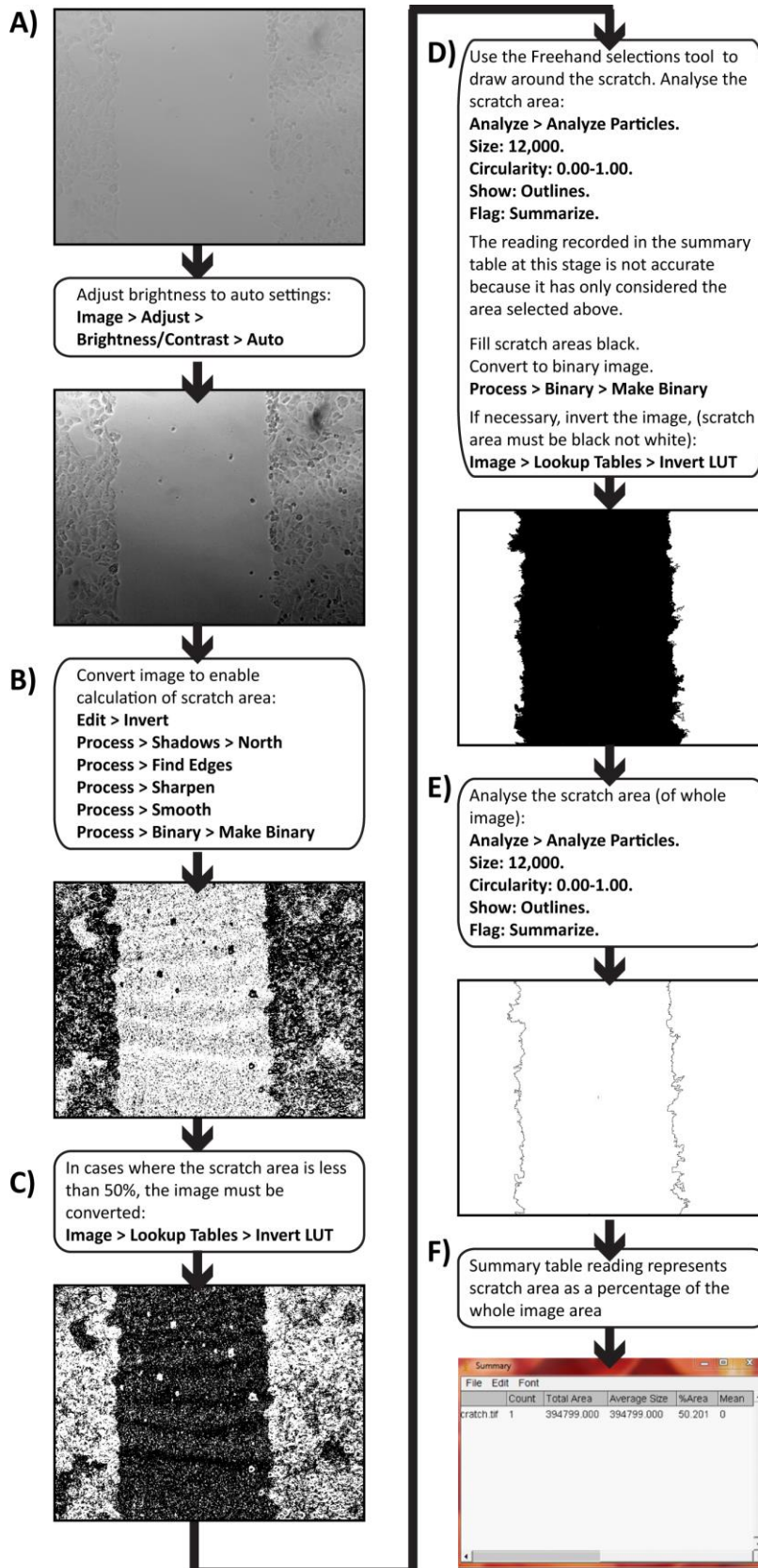
Figure 2.4: Scratch assay analysis using ImageJ. A macro was designed to enable analysis of the captured scratch images using ImageJ. IGROV-1 cells were used as an example. A) Image brightness and contrast was adjusted automatically. B) The image was converted into binary format. C) The image was inverted if necessary. D) Scratch area was selected and isolated using the 'Analyse Particles' tool. E) Scratch size was determined. F) The scratch size in terms of percentage of the image area was summarised.

	Time (hours)		
	0	12	24
A) Original image			
B) ImageJ scratch analysis			
C) Analysed scratch area			
D) Final scratch outline			
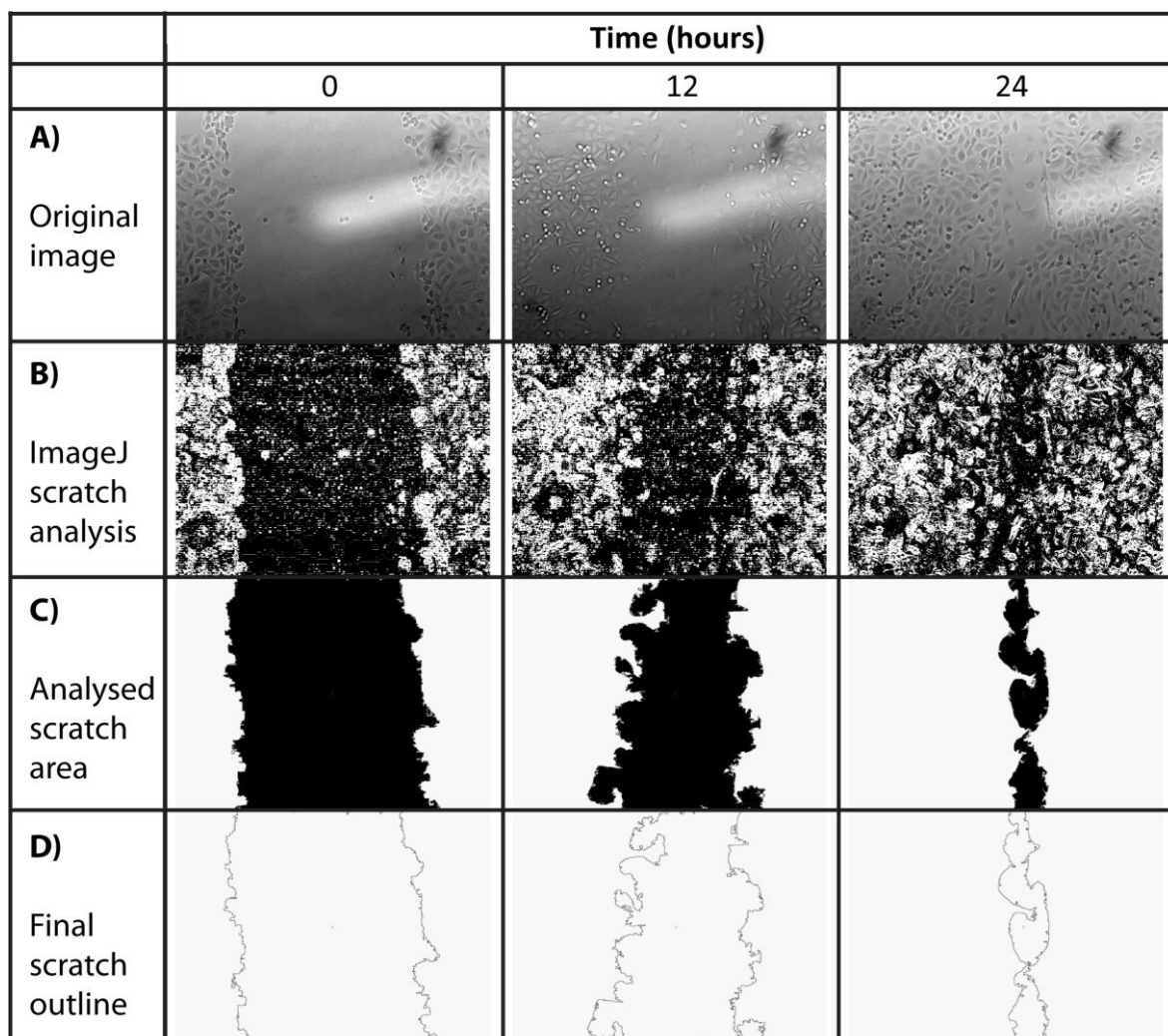
Figure 2.5: Scratch images of OVCAR-5 cells over a 24 hour period were used as an example to show the different images generated by ImageJ during scratch image analysis. The original image (A) was initially converted into a binary format (B). The area of interest was selected (C) enabling outlines of the scratch area (D) and calculation of percentage scratch area to be made.

2.5.4. Scratch assay with stress exosomes

To determine whether cells released signals into the media that had the capacity to increase motility of MCF-7 cells following heat stress, the scratch assay (section **2.5.1**) was used. In this experiment, heat shock media transfer was performed instead of exosome extraction (because of insufficient resources). MCF-7 cells were seeded in four 24-well plates at 560,000 cells/well and were grown to 100% confluence over a period of 48 hours. After 24 hours, complete media on plate A was replaced with EFM and the cells were heat shocked for 1 hour at 45°C. 24 hours later, heat shocked cell conditioned media was aspirated from plate A. The media on cells in plate B was removed and the cells were washed with PBS. Then the heat shocked cell conditioned media from plate A was administered to the naïve MCF-7 cells in plate B. At the same time, plate C was heat shocked for 1 hour at 45°C. 24 hours later, plate D was heat shocked at 45°C for 1 hour. Then

scratches were made down the centre of six wells of each cell type in plate B and six wells of directly heat shocked cells in plate D using a P200 pipette tip (**Figure 2.2C**). The media containing floating cells was removed carefully and the cell monolayer was washed to smooth the edges of the scratch with 1.0 mL pre-warmed EFM. Each well was replenished with 2.0 mL heat shocked cell conditioned media that had been aspirated from plate C. The scratch was visualised and photographed under a Motic AE31 inverted microscope, using x100 magnification. The cells were incubated at 37°C, 5% CO_2. Photographs were taken every 12 hours with the last photograph taken 48 hours after the scratch was made. Scratch images were analysed as described in section **2.5.3**.

2.6. Cell proliferation assay

2.6.1. Measurement of cell proliferation

Ovarian cancer cell lines were seeded at 500,000 cells per flask in 15 T25 flasks (Thermo Fisher Scientific) per cell line. T25 flasks are cell culture flasks that have a surface area of 25 cm^2 on their base (the area in which cells area able to attach and grow). Over the following five days, every 24 hours the total number of cells in three flasks was determined by counting the cells as described in section **2.1.2**. The cell concentration per millilitre was multiplied by the total volume of the cell resuspension to establish the total number of cells in each flask at each data collection point. These values were used to determine the proliferation rates of each cell line.

Doubling time (T_d) was determined using the following formula:

$$T_d = \left(t^{96} - t^0\right) \times \frac{\log 2}{\log\left(\dfrac{q^{96}}{q^0}\right)}$$

time = 0 hours (t^0)

cell number at time = 0 hours (q^0)

time = 96 hours (t^{96})

cell number at time = 96 hours (q^{96})

2.7. Assessment of cellular migratory capacity and invasiveness

2.7.1. Matrigel trans-well cell invasion and migration assays

Cell cultures were starved of serum over a 24 hour period (Guo *et al.*, 2014). Only cultures that were <80% confluent and would not reach 80% confluency over the next 24 hours were used to ensure cells were starved of FBS effectively. Complete medium was removed and the cell layer was washed with PBS. Complete culture medium was replaced with serum-free medium (SFM). The cells were returned to the incubator at 37°C, 5% CO_2 for 24 hours. Cells were harvested using a cell scraper (Thermo Fisher Scientific) instead of trypsin because the trypsin method (section **2.1.1**) requires the use of FBS which would reverse the effects of serum starvation. The cells were centrifuged at 300 × *g* (1500 rpm) in the MSE Centaur centrifuge to pellet them. The cell pellet was resuspended in PBS. The cells were further pelleted at 300 × *g*. Cell concentration was determined as described in section **2.1.2**. The cells were distributed into either uncoated (no Matrigel, 8.0 µm pore membrane only) (BD Biosciences) or Matrigel (artificial ECM secreted by Engelbreth-Holm-Swarm mouse sarcoma cells) coated 8.0 µm pore membrane trans-well inserts (BD Biosciences) at 100,000 cells/well. There were three biological replicates for each cell line (in three separate wells). To act as a chemoattractant, complete medium (10% FBS) was loaded into receiver wells (24-well plate). The cells in the trans-wells were incubated for 24 hours. Following the incubation period, medium from assay/receiver plate and trans-well inserts was aspirated carefully. The upper surface of the control/Matrigel inserts were swabbed with a cotton bud to remove cells that had not invaded the Matrigel/membrane. The inserts and receiver wells were washed with PBS and the cells that had invaded were stained with 1% crystal violet (SigmaAldrich) (1.0 g crystal violet in 25 mL 100% methanol and 75 mL de-ionised water) for 10 minutes. After staining, the inserts were rinsed under running water until the water ran clear. Inserts were dried completely before they were removed from the insert housing using a scalpel (Swann Morton, Sheffield). The membranes were then mounted onto glass slides using di-N-butyle phthalate in xylene (DPX) and glass coverslips. The membranes were visualised under the Zeiss Axioplan inverted microscope using x125 magnification in differential interference contrast. Where possible, all cells that invaded the membrane were counted, where this was not possible (because there were too many cells to count accurately), cells were counted in five representative fields of view. The field of view was 0.005 cm^2 and the membranes had a total area of 0.33 cm^2, therefore the average number of cells in each field of view was used to calculate the total number of invading cells using this calculation: = ([average number of invasive cells in five fields of view] ÷ 0.005cm^2) × 0.33 cm^2. This method is shown in **Figure 2.6**.
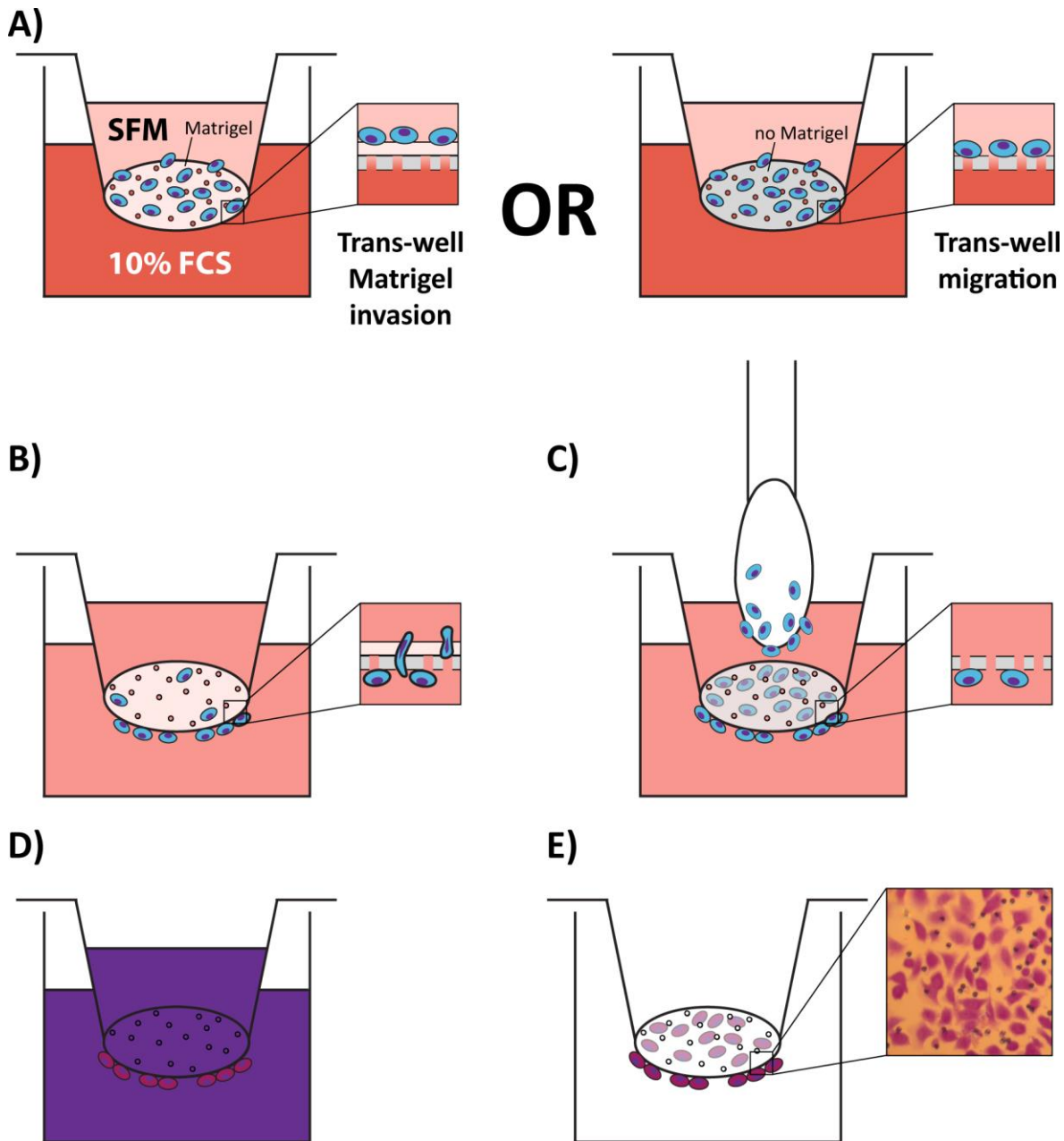
Figure 2.6: Trans-well Matrigel invasion and trans-well migration assays. A) Cells were seeded at 100,000 cells/trans-well in SFM. Inserts had membranes with 8.0 μm pores coated in Matrigel (trans-well invasion assay) or uncoated inserts with no membrane coating (trans-well migration assay). Complete media containing 10% FBS was added to receiver wells. B) Cells were left (at 37°C) to invade the membrane. C) After 24 hours, non-invasive cells were removed from the insert using a cotton bud. D) Remaining cells on the bottom side of the membrane were stained with 1% crystal violet. E) Membranes were washed with water until all the excess crystal violet stain was removed. Subsequently membranes were cut out of the trans-well inserts using a scalpel and mounted on glass slides using DPX and glass coverslips for visualisation.

2.7.1.1.   Matrigel invasion assay with exosome treatment of cells

Control or stressed cell-derived exosomes were extracted from approximately 60 million cells (sections **2.2** and **2.2.2**), resuspended in SFM and administered to cells at the same time as SFM (24 hours prior to harvesting for the Matrigel assay). Exosomes extracted from 6 million cells were administered to approximately 1 million cells. The control and stress exosome extraction procedures were repeated the following day and a second dose of exosomes was added to the cells immediately after they were seeded in the Matrigel trans-well inserts. For all stress exosome invasion experiments, all invasive cells on each membrane were counted. This method is illustrated in **Figure 2.7**.

2.7.1.2.   Matrigel invasion assay with cisplatin exosome treatment and additional DNA-PK inhibition in recipient cells

In addition to cisplatin exosomes, 10.0 µM NU7441, an inhibitor of DNA-PK, was administered to cells (at the same time as cisplatin exosomes were added), both 24 hours prior to and immediately after seeding the cells in the trans-well inserts. This method is illustrated in **Figure 2.7**.
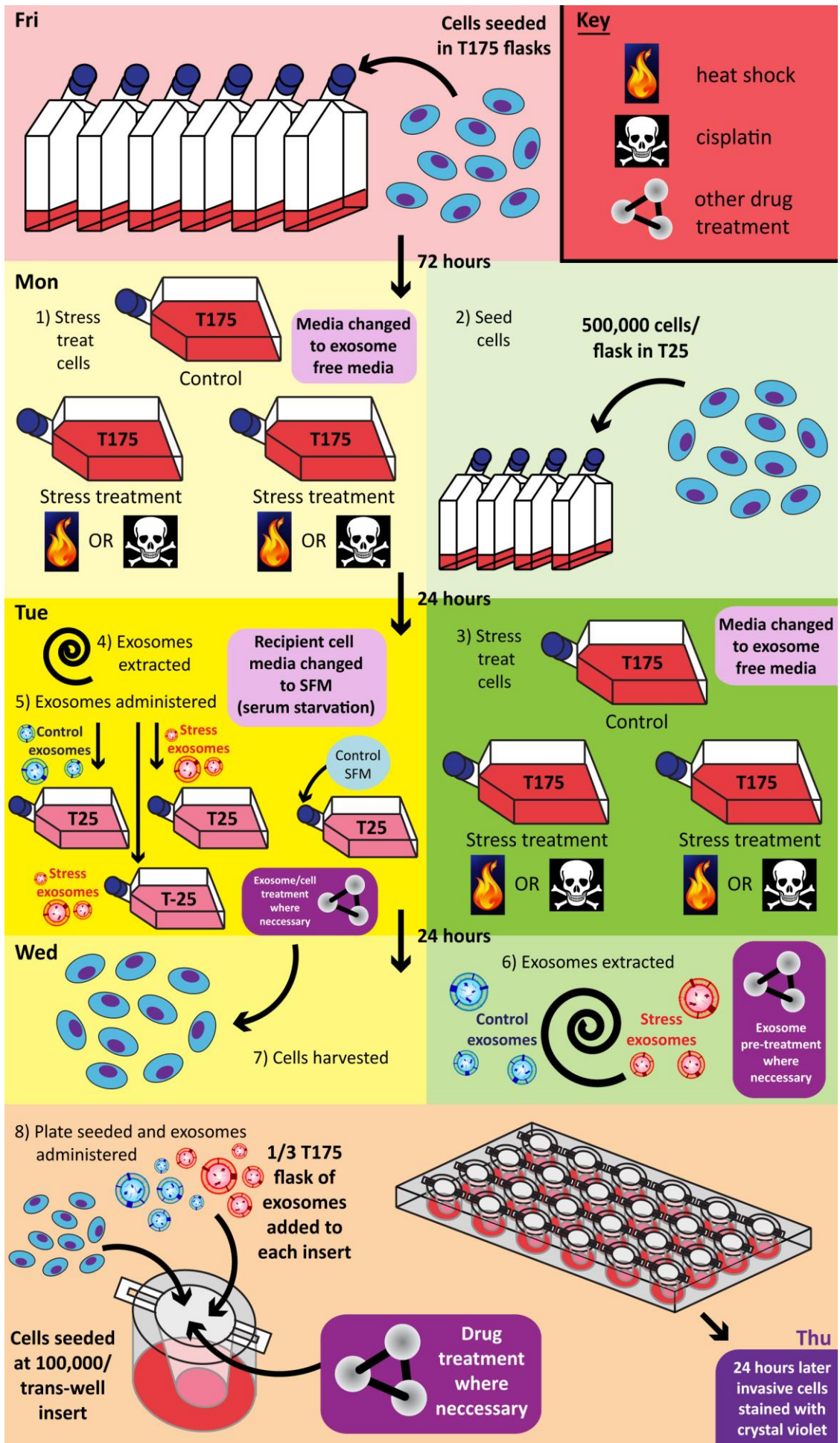
Figure 2.7: Trans-well Matrigel invasion assay with stress exosome treatment of cells. Friday, cells that were to be stressed and from which exosomes were to be extracted were seeded in T175 flasks. Monday, 1) Media was changed to EFM and cells were stressed by either heat shocking or cisplatin treatment. 2) Fresh cells were seeded in T25 flasks at 500,000 cells/flask. Tuesday, 3) A second batch of cells were stressed (step 1 was repeated). 4) Stress and control exosomes were extracted and resuspended in SFM. Drug treatment of exosomes/cells was performed at this point in the procedure, where necessary. 5) FBS-containing medium was removed from cells in T25 flasks and media was replaced with SFM containing stress or control exosomes, or SFM only for control flasks. Exosomes extracted from 6 million cells were administered to approximately 1 million cells. Wednesday, 6) Step 4 was repeated. 7) Serum-starved, stress exosome-treated cells were harvested and cell concentration was determined. 8) Cells were seeded into trans-well inserts in a 24-well plate, exosomes were administered to the appropriate trans-well inserts, exosomes extracted from 6 million cells were administered to 100,000 cells. Complete media was added to the receiver wells to act as a chemoattractant.

2.8. Proteome profiler human phospho-MAPK array

2.8.1. Sample collection

The proteome profiler human phospho-MAPK array (R&D Systems, Abingdon) procedure was performed as outlined in the manufacturer's protocol. Cells were seeded at 1.0×10^7 cells/T175 flask. Cells were stressed using the appropriate method, heat shocking for MCF-7 cells (section **2.2.2.1**) and cisplatin treatment for A-2780 cells (section **2.2.2.2**). Twenty-four hours later, stressed cell-derived exosomes were collected (section **2.2.2**) and administered to cells (1 x T175 flask worth of exosomes/1.0×10^6 cells). Twenty-four hours later, spent media was removed and the cell layer was washed with PBS; the PBS was discarded. Fresh PBS was added and the cells were scraped into suspension. After cell concentration determination (section **2.1.2**) the cells were pelleted at $300 \times g$ for five minutes at room temperature. The supernatant was removed and the appropriate volume of Lysis Buffer 6 was added to each cell sample to give a final concentration of 1.0×10^7 cells/mL. Cells were solubilised initially by pipette mixing, and then by gentle rocking at 4°C for 30 minutes. Protein samples were then centrifuged at $14,000 \times g$ at 4°C for five minutes in a Heraeus biofuge fresco centrifuge. The supernatant was transferred to a fresh tube. Cell lysates were stored at -70°C until use.

2.8.2. Assay procedure

Cell lysates were defrosted and the nitrocellulose membranes were blocked in Array Buffer 5 for 60 minutes at room temperature on a rocking platform shaker. 400 µL of the cell lysate was combined with 1100 µL Array Buffer 1. After thawing, 20 µL of Detection Antibody Cocktail was added to each protein sample and mixed by pipetting. The protein samples were incubated for 60 minutes at room temperature. Array Buffer 5 (blocking buffer) was aspirated from the membranes and the sample/antibody mixtures were added to each membrane and incubated

overnight at 4°C on a rocking platform shaker. Membranes were washed three times for 10 minutes in 1X Wash Buffer. The membranes were incubated with 2.0 mL streptavidin-HRP for 30 minutes at room temperature on a rocking platform shaker. Membranes were washed three times for 10 minutes in 1X Wash Buffer. 1.0 mL Chemi Reagent Mix was distributed evenly over each membrane and imaged using the blot: chemi protocol on the ChemiDoc MP (Bio-Rad). Reference spots were included to demonstrate that the membrane had been incubated successfully with streptavidin-HRP during the assay procedure.

2.8.3.   Data analysis

Spot intensity was measured in Image Lab software version 5.2.1. Average intensity of the pair of duplicate spots was determined for each kinase. Background signal was subtracted using the intensity of a clear area of the membrane (of equal size to each spot).

2.9. Microarray

2.9.1.   Directly heat shocked and control cell preparation for RNA extraction

The cells, that were either control treated (at 37°C) or heat shocked at 45°C to produce heat shock exosomes (section **2.2.2**), were lysed for yielding RNA. This was following removal of cell conditioned media for exosome extraction.

2.9.2.   Heat shock or control exosome treatment of MCF-7 cells prior to RNA extraction

MCF-7 cells were seeded at 125,000 cells/flask in T25 flasks. Control and heat shock exosomes were each extracted from 10 x T175 flasks of control or heat shocked MCF-7 cells (each flask contained approximately 2.0×10^6 cells) and were administered to the T25 flask of cells 24 hours after seeding (sections **2.2** and **2.2.2**). This exosome treatment was repeated 48 hours after initial seeding to replicate the exosome treatments received by cells in the Matrigel trans-well invasion assay (section **2.7.1.1**). Twenty-four hours after receiving the second dose of exosomes, the cells were harvested and RNA was extracted.

2.9.3.   RNA extraction from MCF-7 cells

RNA was extracted from cells using the miRcury RNA cell and plant kit (300110, Exiqon). The cells had been either directly heat shocked, or treated with either control or heat shock exosomes

(section **2.2.2**). For each sample, media was aspirated from the cell monolayer and the cells were washed with PBS, spent PBS was removed. 350 µL of Lysis Solution (provided in the kit) was added directly to the culture plate and the cells were lysed by gently tapping and swirling the culture plate for five minutes or until all cells were immersed in the Lysis Solution. The lysate was then transferred to a clean microcentrifuge tube. To maximise cell lysis, the sample was vortex mixed for 15 seconds, or until the cell pellet had completely dissolved. 200 µL 100% ethanol was added to the lysate, and then the sample was vortex mixed for 10 seconds. An RNA extraction column was assembled with one of the provided collection tubes (one column was required per sample). The sample was transferred onto the column and centrifuged for 1 minute at 3500 × g. To ensure the entire sample had passed through the column, the column was centrifuged for a further minute at 14,000 × g in a Heraeus biofuge fresco centrifuge. The flowthrough was discarded and the column was reassembled with the collection tube. 400 µL Wash Solution was applied to the column and the column was centrifuged for 2 minutes at 14,000 × g. The flowthrough was discarded and the column was reassembled. 0.25 Kunitz unit/µL RNase-free DNase I working solution was prepared by combining 0.5 mL DNase I (AMPD1-1KT, SigmaAldrich) with 1.0 mL reaction buffer. 100 µL DNase I working solution was added to the column. The column assembly was centrifuged for 2 minutes at 200 × g to enable the DNase I to pass through the column. The flowthrough was transferred onto the surface of the column and it was incubated at 25°C for 15 minutes on a heat block. Following the incubation period, the column was washed twice more with 400 µL Wash Solution followed by centrifugation for 1 minute at 14,000 × g. The flowthrough was discarded and the column was reassembled. The column was centrifuged for 2 minutes at 14,000 × g to thoroughly dry the resin. At this point the collection tube was discarded. The column was placed into a clean 1.7 mL elution tube (provided in the kit). 50 µL of Elution Buffer was added to the column, and the column was centrifuged for 2 minutes at 200 × g followed immediately by 1 minute at 14,000 × g. The column was discarded and the purified RNA sample was stored at -80°C until use.

2.9.4.   cDNA synthesis

Extracted RNA was measured for quality and quantity using the RNA protocol on the NanoDrop 1000 (Thermo Fisher Scientific). The High Capacity cDNA Kit (Applied Biosystems) was used to make cDNA. A reaction tube for each sample was made (on ice) by combining 1.0 µg RNA, 1.0 µL 20X reverse transcriptase enzyme mix, 2.0 µL 10X reverse transcriptase buffer, 0.8 µL deoxyribonucleotide triphosphates (dNTPs), 2.0 µL 10X random primers, and a sufficient quantity of nuclease free water to bring the total reaction volume to 20 µL. The tubes were sealed and liquid was pulled to the bottom of the tube by lightly tapping the tubes on the bench. The

reaction tubes were incubated in an MJ mini thermal cycler (Bio-Rad) at 25°C for 10 minutes, followed immediately by a 2 hour incubation period at 37°C, and finally a 5 minute incubation at 85°C. The samples were then maintained at 4°C until they were moved to permanent storage (until use) at -20°.

2.9.5.   Agilent G3 Human Gene Expression 8 x 60K v3 microarray

Experiments were performed as four biological replicates, samples were extracted using a Qiagen RNeasy miniprep kit and the RNA was DNase treated. The extracted RNA was quality verified on a 2100 expert Agilent bioanalyzer, to confirm that all samples had an RNA yield greater than 30 µg and RIN values above 9. Samples were amplified and labelled with Agilent Low Input Quick Amp labelling two colour kit, hybridised to an Agilent G3 8plex x 60k gene Human transcriptome microarray, and washed to supplier's protocol. The array slide was scanned at 3.0 µM and 20 bit Tiff file dynamic range on an Agilent Surescan G2565CA microarray scanner at 100% PMT gain for both red and green lasers, and exported TIFF images. The TIFF images were then aligned to their design files and converted into probe intensity values using the Agilent Feature Extraction Software. Using this software this data was probe and Loess normalised, and then quantile normalised for array variation using DNAstar (ArrayStar Inc.).

2.9.6.   DAVID analysis of genes involved in biological pathways

All genes with statistically significantly differential expression between two samples (control MCF-7 cells, directly heat shocked MCF-7 cells, control exosome recipient MCF-7 cells or heat shock exosome recipient MCF-7 cells), represented by a p value of <0.05, were further analysed using the online functional annotation tool DAVID Bioinformatic Resources 6.7 (National Institute of Allergy and Infectious Diseases, National Institutes of Health, USA). The method described by Huang and colleagues (2009) was used to identify pathways affected by heat shock exosomes (Huang *et al.*, 2009a; Huang *et al.*, 2009b). Briefly, Entrez gene identification numbers of statistically significantly differentially expressed genes were pasted into the 'Enter Gene List' box. 'ENTREZ_GENE_ID' was selected from the 'Select Identifier' options. 'Gene List' was selected as the 'List Type'. In the 'Annotation Summary Results', 'KEGG_PATHWAY' was selected from the 'Pathways' tab. The 'Chart' button was pressed to reveal the pathways affected by up-/down-regulation of the listed genes. The relevant pathway was selected to uncover a diagram of the selected pathway highlighting the statistically significantly differentially expressed genes.

2.10. Statistical methods

2.10.1. Student's one tailed T-test

The one tailed T-test was used to determine the probability of two small sets of quantitative data (collected independently) being significantly increased or decreased compared with one another in terms of the difference between sample means; i.e. the probability that two populations were the same with regards to the variable being tested. This enabled acceptance or rejection of the hypothesis in question.

2.10.2. Student's two tailed T-test

The Student's two tailed T-test was used to determine the probability of two small sets of quantitative data (collected independently) being significantly different from one another in terms of the difference between sample means.

2.10.3. Pearson's correlation coefficient

Pearson's correlation coefficient was calculated to determine the strength of the linear relationship between two variables.

2.10.4. Spearman's rank correlation coefficient

Spearman's rank correlation coefficient is a nonparametric measure of statistical dependence between two variables. It was used to determine the monotonic relationship between two data sets.

2.10.5. Grubbs' test for outliers

The Grubbs' test was used to identify outliers in datasets of >6 data points. The Grubbs' test detects one outlier at a time. Each outlier is removed from the dataset and the test is repeated until no further outliers are detected.

Chapter 3

Exosome characterisation

3.   Exosome characterisation

3.1. Introduction

Characterisation of exosomes from different sources (e.g. cell lines or patients) under different biological conditions (e.g. stress or people with disease) will improve our understanding of their role in health and disease (Théry *et al.*, 2002). Exosomes are currently distinguished from other EVs based primarily on size, but also using other characteristics including protein composition and density (Raposo and Stoorvogel, 2013). Exosomes have been reported to have a diameter of 30–160 nm (Ludwig and Giebel, 2012; Théry *et al.*, 2002; Théry, 2011), this along with enrichment in specific protein markers distinguishes them from Golgi bodies and vesicles derived from the endoplasmic reticulum (Raposo *et al.*, 1996; van Niel *et al.*, 2006). Exosome characterisation is challenging mainly because of their small size and time-consuming extraction procedures (Gould and Raposo, 2013). Several methods and techniques have been optimised over the past decade with exponential increase in the study of exosomes. Common exosome characterisation methods include: western blotting (WB), transmission electron microscopy (TEM), nanoparticle tracking analysis (NTA), and confocal microscopy (Gardiner *et al.*, 2013; Théry *et al.*, 2006). These techniques were used in this chapter to characterise exosomes and examine their purity.

3.1.1.   Western blotting

In order to verify that the exosomal pellet obtained at the end of the exosome extraction procedure contains exosomes, and is not contaminated with apoptotic bodies and other EVs, the sample must be characterised. A highly purified exosome sample should be free from contaminants, such as protein components of the intracellular compartments (e.g. endoplasmic reticulum or mitochondria) that never come into contact with exosomes (Raposo and Stoorvogel, 2013). WB has advantages over other exosome characterisation methods, as organelles and soluble contaminants, which cannot be identified by TEM, NTA, and confocal microscopy, can be detected (Webber and Clayton, 2013).

3.1.2.   Transmission electron microscopy

In addition to WB, exosomes can be visualised using TEM, this technique is often used to examine exosome structure (Webber and Clayton, 2013). Exosomes are prepared as whole mount samples (samples that have been deposited on electron microscopy grids without prior sectioning)

following negative staining with uranyl acetate. On electron micrographs exosomes appear as round dark spheres with diameters <200 nm (Raposo and Stoorvogel, 2013).

3.1.3. Confocal microscopic analysis of exosomes

Confocal microscopy can be used to visualise the interactions between fluorescently labelled exosomes and cells. Cells and exosomes are labelled with fluorescent dyes that are activated at different wavelengths to distinguish interactions between cell material and exosomal material (Escrevente *et al.*, 2011; Franzen *et al.*, 2014; Parolini *et al.*, 2009).

3.1.4. Nanoparticle tracking analysis

To complement WB and TEM, NTA measures the size distribution and concentration of exosome samples (Soo *et al.*, 2012). NTA measures particles in a liquid of 10 nm–1 μm in diameter using the rate of Brownian motion to determine particle size. A laser illuminates the particles in a sample causing dispersal of scattered light. The scattered light is detected and tracked. Brownian motion is affected by the viscosity of the liquid, the temperature, and the size of the particle. By measuring temperature and liquid viscosity NTA is able to establish the size of particles suspended in samples using their refractive index. Particles are automatically tracked, measured and quantified by the NTA instrument. This technology was first used for analysing exosomes by Dragovic and colleagues in 2011 (Dragovic *et al.*, 2011) and has since become a well-established method of exosome characterisation (Gardiner *et al.*, 2013; Raposo and Stoorvogel, 2013).

3.2. Results

3.2.1. Exosomal marker detection by western blotting

In order to distinguish exosome populations from their cellular derivatives, exosome samples required characterisation following extraction. The WB method was developed to identify: HSP70, a protein involved in MVB synthesis that is found enriched on the exosome surface (Mathew *et al.*, 1995) and is also present in the cytosol of cells; cytochrome C oxidase, a mitochondrial marker (also found in apoptotic bodies) (Finucane *et al.*, 1999; Siekevitz and Watson, 1956); the cell organelle markers: calnexin, found in endoplasmic reticulum (Wada *et al.*, 1991), and GM130, a Golgi maker (Nakamura *et al.*, 1995); and GAPDH, used as a control as it is a cytosolic protein expressed at high levels in both cells and exosomes (Seidler, 2013). The exosome marker HSP70 was detected in both cell protein and exosome protein extracts, shown in two WB membranes in **Figure 3.1**. Cytochrome C oxidase was present in the cell sample but not in the exosome sample, suggesting that the exosome sample was not contaminated with either apoptotic bodies or cellular organelles, specifically, mitochondria. To further confirm that no contamination had occurred during the exosome extraction procedure, the cell organelle markers calnexin and GM130 were identified in cell protein lysate only. GAPDH was present in both cellular and exosomal protein samples and was therefore used as a control to check that the WB process had worked effectively. The results suggest that the characterised sample was free of cellular or organelle contamination and contained only EVs.
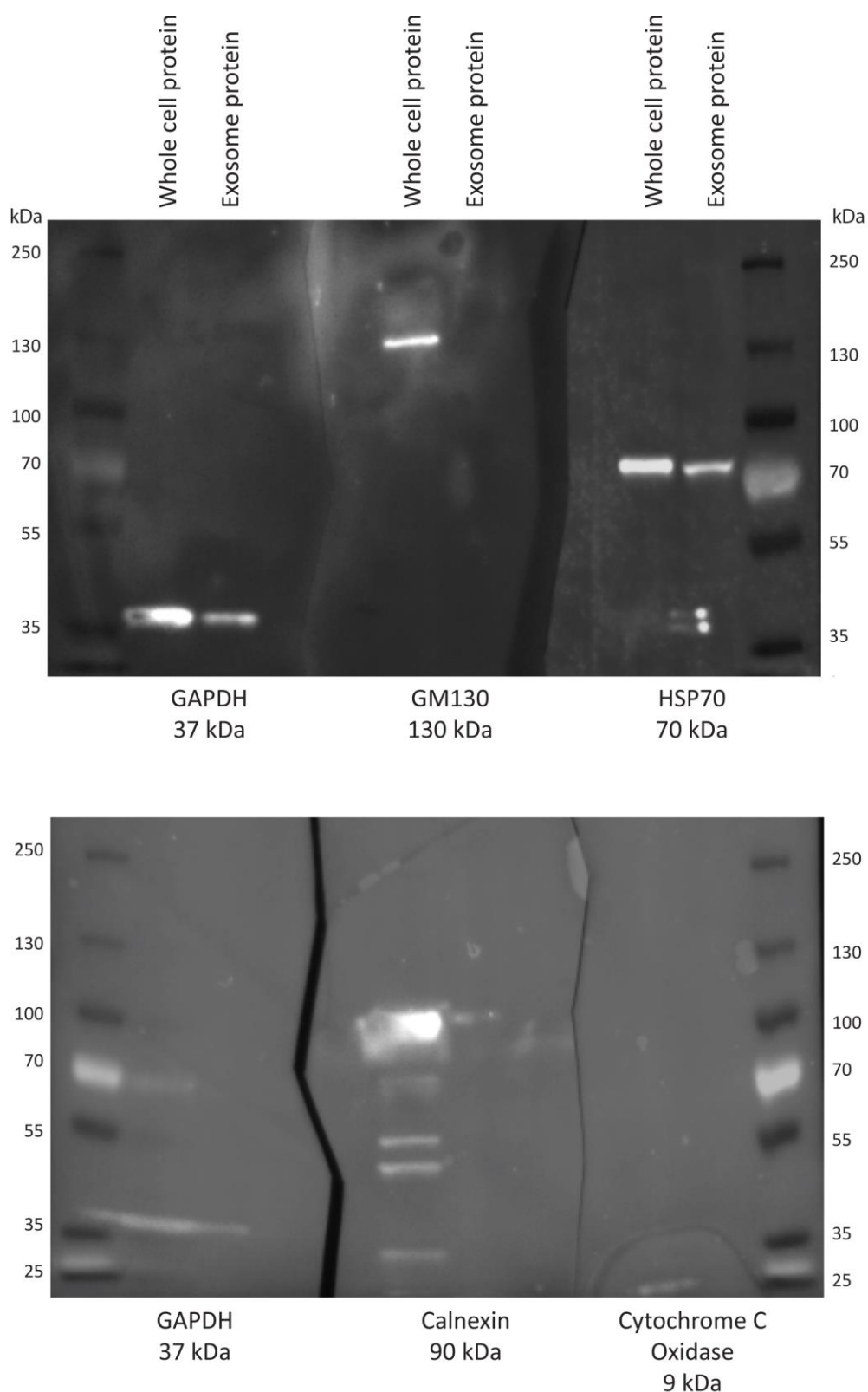
Figure 3.1: Exosome characterisation by western blotting. 10.0 µg MCF-7 cell protein lysate and 10.0 µg MCF-7-derived exosome protein lysate were characterised. Proteins identified were GAPDH, calnexin, and GM130 (cell markers), cytochrome C oxidase (mitochondrial marker also found in apoptotic bodies), and HSP70 (a known exosome component). Presence of GAPDH and HSP70 in the exosome protein lysates suggests that the sample contains exosomes. Absence of GM130 and calnexin in the exosome protein lysate suggests that the exosome sample had not been contaminated with intracellular organelles (Golgi and endoplasmic reticulum, respectively) during the sequential centrifugation extraction process. Absence of cytochrome C oxidase suggests that the sample had not been contaminated with apoptotic bodies or mitochondrial debris.

3.2.2.   Exosome visualisation by transmission electron microscopy

As exosomes are small in size, they are impossible to visualise using a standard light microscope therefore negative staining is used to visualise exosomes using TEM. To ensure that the exosome extraction procedure (section **2.2**) is effective in isolating exosomes, TEM was performed on whole mount exosome samples extracted from MCF-7 cells (**Figure 3.2**). Exosomes within the expected size range were identified (Raposo *et al.*, 1996). Because of failure to recognise that the formvar coated grids needed hydrophilising (with Glow Discharge treatment and subsequent magnesium acetate conditioning to give a negative charge), there is a lot of background staining on the electron micrograph. Hydrophobic surfaces inhibit the spreading of particles in suspension in negative staining solutions. Despite this, exosomes were identified and measured on the carbon coated grid.
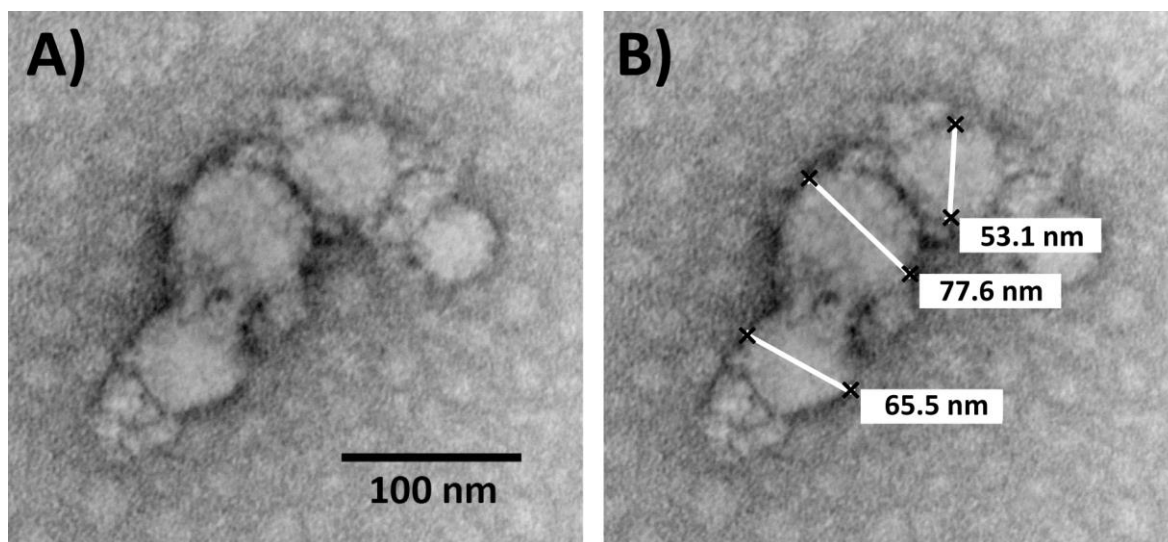
Figure 3.2: Electron micrograph of exosomes extracted from MCF-7 cells. A) Exosomes at x40,000 magnification. B) Same image as A) but with data labels for vesicle diameter. Images taken using a Hitachi H7650 Transmission Electron Microscope at 100 kV.

3.2.3.   Confocal microscopic analysis of exosome-cell interactions

Internalisation and trafficking of exosomes inside A-2780 cells that had their nuclei stained with DAPI was visualised (**Figure 3.3**). The clear co-localisation observed between exosomes and A-2780 cells suggested that the exosomes isolated during the sequential/differential ultracentrifugation extraction method were viable following extraction and storage at -20°C.
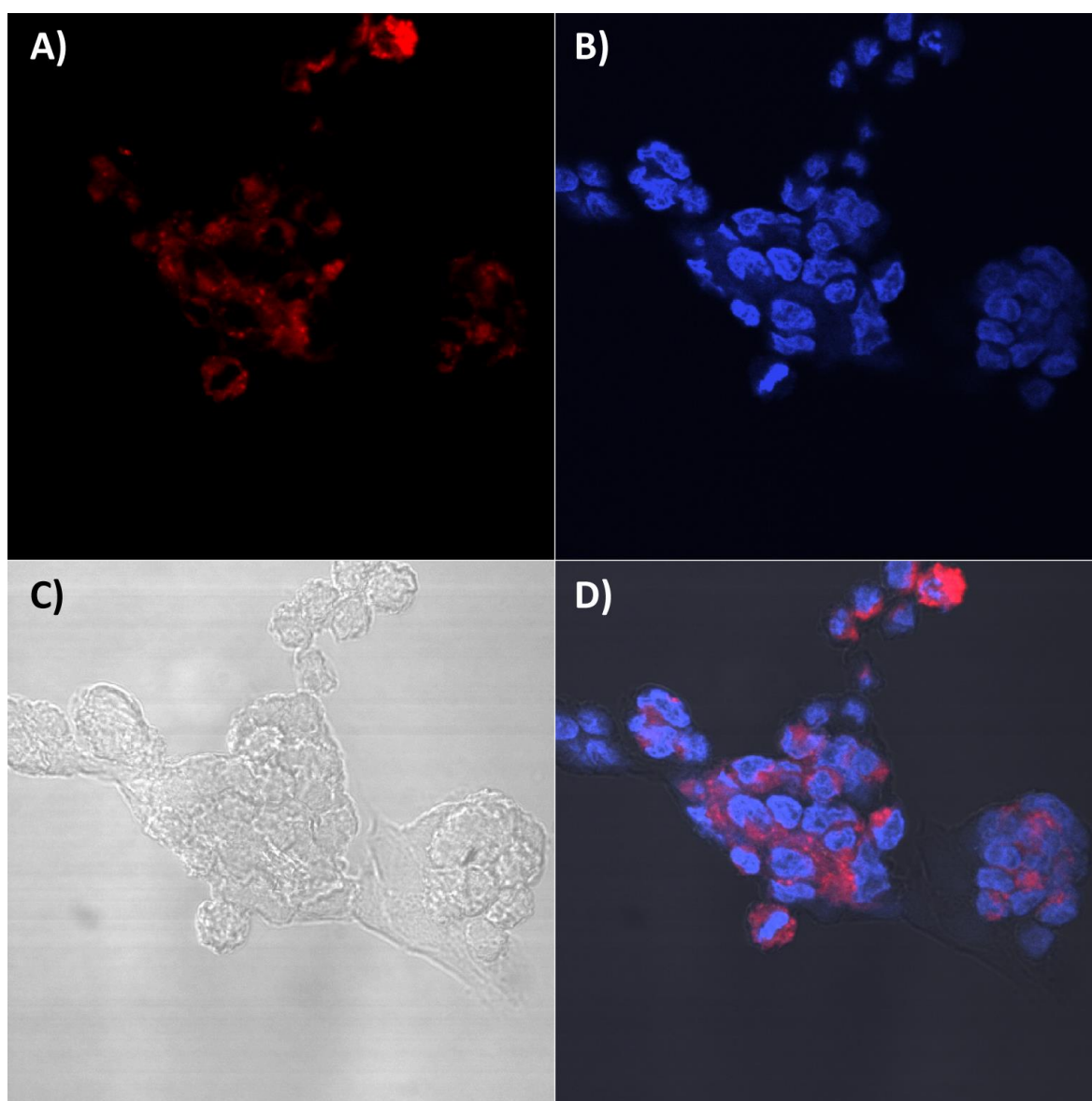
Figure 3.3: Interaction between exosomes and A-2780 cells. PKH26 stained exosomes (red) were identified inside the A-2780 cells with DAPI stained nuclei (blue) after 60 minutes of co-incubation. Following this period they were fixed in 4% paraformaldehyde. Images were acquired using a Zeiss LSM 510 inverted confocal microscope, using x630 magnification. A) Image acquired using the 543 nm laser showing exosomes interacting with cells, most exosomes have been taken up by the cells. B) Image achieved using the 405 nm laser showing the nuclei of A-2780 cells stained with DAPI. C) Phase contrast image of the A-2780 cells. D) Combined image of A), B) and C).

3.2.4. Exosome size determination by nanoparticle tracking analysis

In addition to sample protein identification by WB, and visualisation by TEM, exosomes were also characterised by NTA. The mode average diameters of exosomes released by eight different ovarian cancer cell lines were determined using NTA. The mean average of three biological replicates of exosome diameter for eight ovarian cancer cell lines is shown in **Figure 3.4**, in descending order. The largest exosomes were extracted from MCP-1 cells (average exosome diameter of 149.17 nm) and the smallest from OVCAR-5 (average diameter of 127.10 nm). All exosomes were larger than particles detected in PBS (average diameter of 121.70 nm). There was no significant exosome size difference between the eight different ovarian cancer cell lines. The results suggest that exosomes of a similar size are produced from the eight ovarian cancer cell lines of interest.
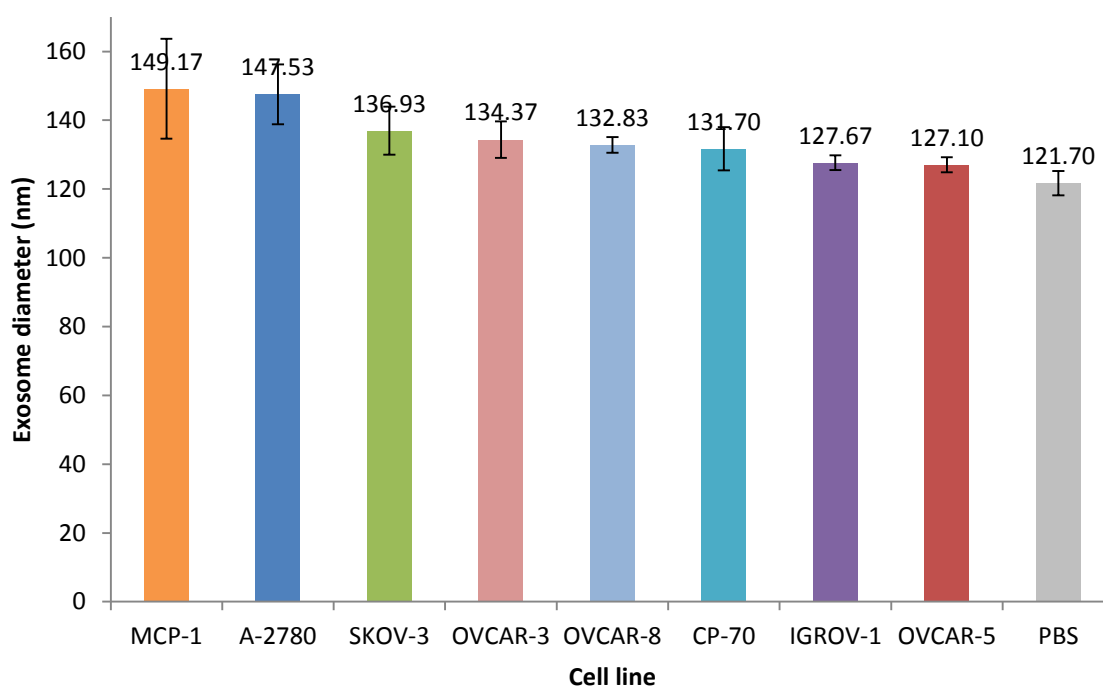
Figure 3.4: Average diameter of exosomes released per cell from eight different ovarian cancer cell lines. The mode average diameter of exosomes released by each cell line over 24 hours was determined by NTA. The exosome samples were resuspended in PBS and diluted 1 in 100, leading to particle concentrations of approximately 5.0×10^8/mL. There were three biological replicates for each cell line. For each biological replicate there were two technical replicates. Five 30 second videos of each technical replicate were recorded and from these exosome diameter (nm) was calculated. The bar graph represents the mode average diameter of exosomes calculated using three biological replicates that were collected on three days over a seven day period for each cell line. The error bars represent standard error of the mean.

3.2.5. Quantification of exosomes released by eight different ovarian cancer cell lines over a 24 hour period by Nanoparticle Tracking Analysis

After numerous attempts to label and subsequently quantify exosomes using fluorescent lipid dyes, cellular transfection of plasmids to induce expression of cytosolic fluorescent protein and protein radiolabelling, a decision was made to revert to NTA, a method used commonly for exosome quantification (Gardiner *et al.*, 2013). To determine the concentration of exosomes released by eight different ovarian cancer cell lines, the exosome samples used to measure exosome size were also analysed for particle concentration by NTA (**Figure 2.1**). The highest concentration of exosomes released per cell were secreted by all eight ovarian cancer cell lines in biological replicate 3; the second most in biological replicate 1 and the least in biological replicate 2. This may be caused by confounding experimental factors. To account for variation, exosome secretion level per cell was normalised to that of OVCAR-3 cells for each biological replicate of the other seven cell lines. OVCAR-3 was chosen as the normalisation reference because, when cell lines were ranked according to the average number of exosomes released per cell, OVCAR-3 was considered mid-range (fifth highest number of exosomes released per cell), and also because OVCAR-3 is the most commonly used cell line in preclinical research. The average number of exosomes present in the media after 24 hours of cell culture for the eight ovarian cancer cell lines of interest (as calculated by NTA) is shown in **Figure 3.5** in descending order. There was no statistically significant difference between any of the eight cell lines; this was probably because of the high variability between biological replicates. However, IGROV-1 cells consistently secreted the highest concentration of exosomes.

A)

B)
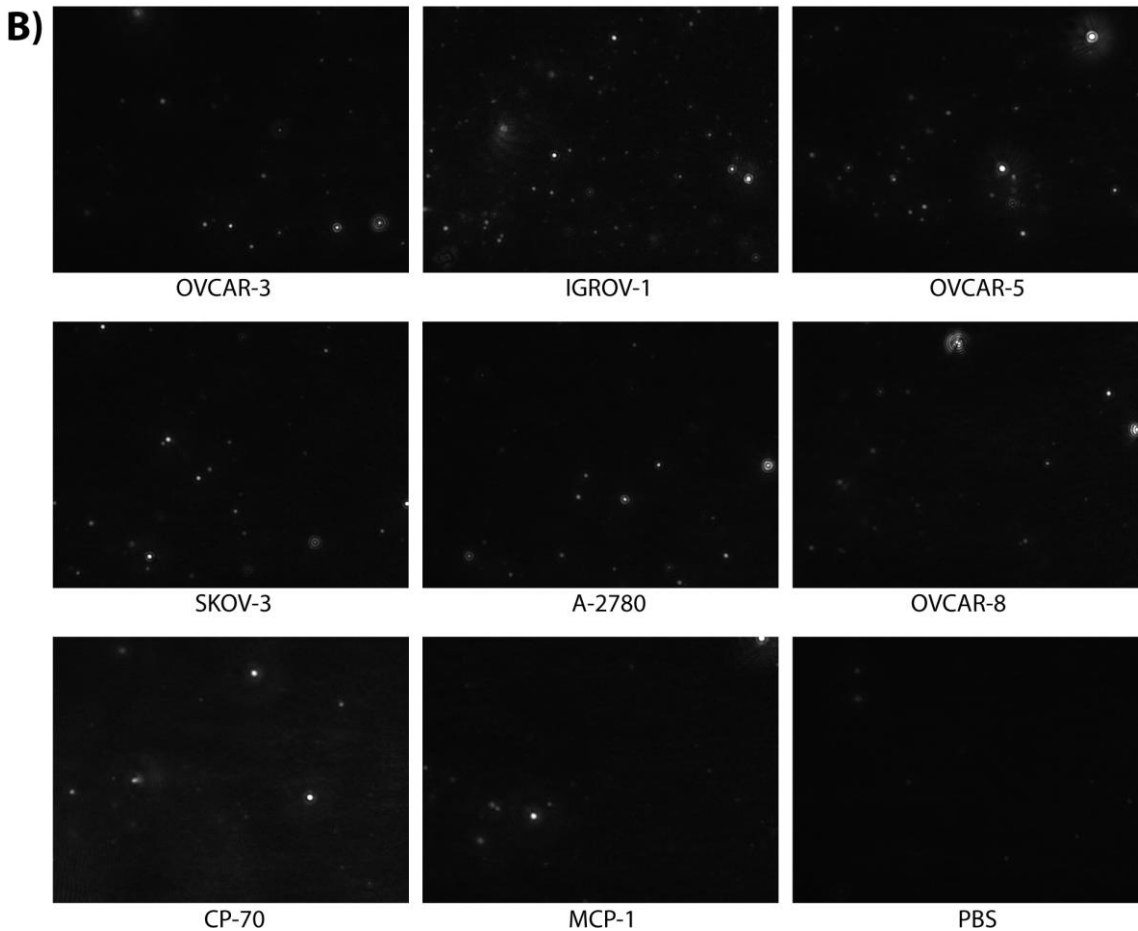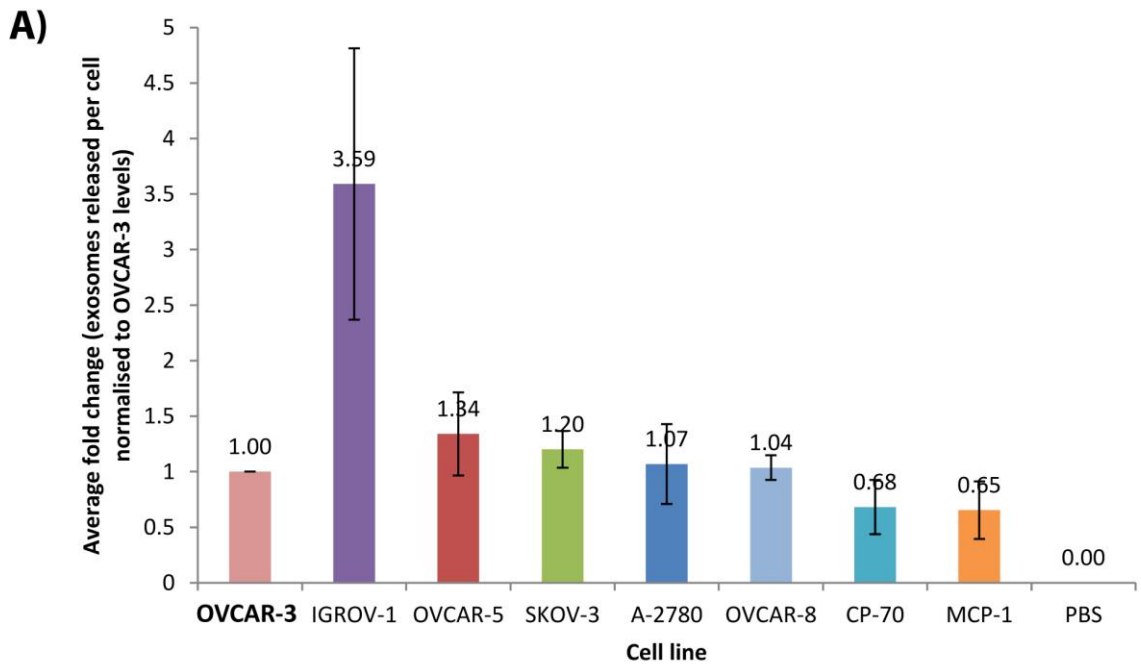
Figure 3.5: Average number of exosomes released per cell from eight different ovarian cancer cell lines, quantified by NTA. A) The average number of exosomes released per cell, quantified by NTA, from three biological replicates is demonstrated. Each biological replicate was collected on a different day over a seven day period. Values were normalised to OVCAR-3 levels of exosome secretion per cell; error bars represent the standard error of the mean of the average of three biological replicates. B) Screen shots of NTA videos recorded during quantification of exosome samples showing differences in particle concentration.

3.3. Discussion

In this chapter, exosomes extracted from both ovarian and breast cancer cell lines were characterised using four different methods available to our research group. These methods were WB, TEM, confocal microscopy, and NTA. There have been no reports of different ovarian cancer cell lines with distinct characteristics secreting exosomes of varying size or at a different concentration. Exosomes have been reported to be 30–160 nm in diameter (Ludwig and Giebel, 2012; Théry *et al.*, 2002; Théry, 2011), the EM and NTA data collected both show that exosomes from eight different ovarian cancer cell lines lie within this range (**Figure 3.2** and **Figure 3.4**). Cells from which exosomes were extracted were conditioned in EFM therefore, the exosomes characterised were mostly of human origin, although it should be noted that the FBS clearing procedure is not 100% reliable therefore it is likely that the exosome samples were not completely free of bovine exosomes (section **3.3.1.2**) (Webber and Clayton, 2013). Because of the ultracentrifugal exosome extraction procedure used in this project, it was possible that the vesicle population isolated contained microvesicles and possibly small apoptotic blebs that lie within the size range of exosomes. However, WB results showed that exosomes contained the specific exosome marker HSP70 and also the positive/loading control GAPDH. They were also free from organelle and apoptotic bleb contaminants (**Figure 3.1**). The confocal microscopic results suggest that the exosomes interacted with cells so were biologically viable following the extraction, fluorescent labelling, and short-term storage at -20°C (**Figure 3.3**).

NTA has been used to assess the exosome output of three ovarian cancer cell lines (Zhang *et al.*, 2015), but in this project a more comprehensive analysis of exosome secretion levels of ovarian cancer cells was performed. NTA was used to determine the exosome secretion rates of eight ovarian cancer cell lines, this has not previously been reported in literature and provides valuable information for ovarian cancer researchers to assist future experimental/study design (**Figure 3.5**). Exosome secretion from a single cell line and between different cell lines was inconsistent, this may have been because of the experimental conditions during each sample collection. However, NTA is known to have limitations, particularly when applied to exosome quantification; therefore it may not be the most appropriate method for exosome quantification. Despite detecting clean exosome preparations containing vesicles of the correct size and structure using four different exosome characterisation methods, there are limitations of the exosome isolation and classification techniques used (Raposo and Stoorvogel, 2013).

3.3.1. Current issues with exosome isolation, purification and nomenclature

Exosomes are classified based upon size, density, and protein composition. However these properties are insufficient for clear distinction between different classes of EV (Bobrie *et al.*, 2011). All exosome preparations invariably contain different proportions of other membranous vesicles that co-purify with exosomes including microvesicles and apoptotic blebs (Tauro *et al.*, 2012). Only once the ability to interfere with molecular mechanisms required for EV formation are developed, will the origins of EVs be determined. This will also enable elucidation of the respective functions of different types of EV (Raposo and Stoorvogel, 2013).

Confusion on the origin and nomenclature of EVs is evident throughout literature and is an issue that has still not been resolved (Raposo and Stoorvogel, 2013). Currently, the available purification methods, namely differential/sequential ultracentrifugation and density gradient centrifugation (Simpson and Mathivanan, 2012), isolate EVs by size and/or density and cannot distinguish between exosomes that are of endosomal origin, and microvesicles and apoptotic blebs that bud from the plasma membrane. This is a problem as microvesicles range in size from 50–1000 nm (Théry *et al.*, 2009), and exosomes are 30–160 nm in diameter (Ludwig and Giebel, 2012), so there is an overlap in size between the two types of EV (Booth *et al.*, 2006). Because exosome purification depends upon EV size, when 'exosomes' are isolated the population of vesicles represents a mixture of exosomes and other EVs. Hence, a major challenge that remains in the EV research field is to improve and standardise methods for exosome characterisation and analysis (Théry *et al.*, 2006).

3.3.1.1. Nomenclature

The term 'exosome' is currently used in three different ways: (1) to refer to secreted vesicles of MVB/endosomal origin; (2) in a broader sense to describe EVs that have a biological function; and (3) to define vesicles that sediment only after centrifugation at ~70,000–120,000 × *g* (Booth *et al.*, 2006; Gould and Raposo, 2013; Johnstone *et al.*, 1987; Raposo *et al.*, 1996; Théry *et al.*, 2006; Trams *et al.*, 1981). Taking into account the issues discussed concerning exosome extraction procedure and nomenclature, throughout this project the term 'exosome' refers to EVs that are extracted from cell culture media following differential/sequential centrifugation with a final ultracentrifugation step at 120,000 × *g* for 90 minutes at 4°C (Eldh *et al.*, 2012; Gould and Raposo, 2013).

3.3.1.2.   Exosome sample contamination

Measurement of exosome sample purity is important for experimentation involving functional exosomes. Contamination by, for example, high levels of protein aggregates could affect experimental results, the effects seen may have been caused by the protein rather than exosomes themselves giving false positive results (Webber and Clayton, 2013). Bovine exosomes are another common contaminant of exosome samples extracted from culture media. Bovine exosomes form part of the FBS that supplements the media to support normal cell growth. Additionally bovine serum may contaminate exosome samples by introducing bovine proteins and RNAs that could interfere with functional, and proteomic or sequencing exosome experiments (Eitan *et al.*, 2015), as mentioned in section **3.3**.

When quantifying exosomes using the BCA assay or NTA, bovine exosome contamination could lead to overestimation of exosome concentration (Eitan *et al.*, 2015). Fluorescently labelled exosomes may be used on the NTA to ensure that only exosomes of interest are considered for the analysis. This can only be achieved by extracting exosomes from cells that stably express a fluorescent protein/exosomal marker fusion protein, fluorescent labelling would not selectively target human exosomes. It is possible to remove bovine exosomes completely by growing cells in SFM prior to extraction; however, serum starvation could induce a cellular response to stress that could affect the experimental results. This is particularly unfavourable for experiments performed to examine the effect of stressed cell-derived exosomes upon the stress response in the recipient cell (Fader *et al.*, 2008). The best solution is to culture cells from which exosomes are to be extracted in media containing FBS cleared of exosomes (EFM) (by ultracentrifugation at 120,000 × *g* overnight). If exosome depleted FBS was used in media continually, cell growth may be affected, however, for short periods during exosomal experiments (typically a maximum of 48 hours), biological changes to cells cultured in the absence of bovine exosomes are minimal (Eitan *et al.*, 2015).

All exosome extraction procedures carried out during this project involved culture of cells with EFM for 24 hours prior to exosome extraction. EFM was made by clearing FBS of exosomes by ultracentrifugation at 120,000 × *g* overnight at 4°C. This does not guarantee, however, that all the bovine exosomes had been removed from the FBS before it was added to the media (final concentration of 10%).

3.3.2. Limitations of exosome characterisation techniques

The techniques used in this project to characterise exosomes are used frequently in the EV research field however, there are limitations. Since the EV research field is still relatively young, the gold standard method(s) for exosome characterisation have not yet been established.

3.3.2.1. Limitations of exosome quantification by WB

HSP70 is a good marker for exosomes because it is well-regarded that HSP70 is involved in exosome biogenesis (Théry, 2011). Ideally other proteins known as exosome markers such as Alix and TSG101 would also have been identified by WB in the exosome samples. Unfortunately, these proteins were not optimised even though considerable efforts were made.

The apoptotic body marker cytochrome C oxidase was used and its presence in whole cell protein lysates and absence in exosome samples suggests that apoptotic body concentration in the exosome samples was low. However, the exosome samples may have contained high levels of microvesicles.

Most exosome research publications identify at least one of the exosome tetraspanin markers CD9, CD63 and/or CD81. At the present time, these tetraspanin markers are the best for characterising exosomes because they are amongst the most common proteins identified in exosomes (Mathivanan *et al.*, 2012). Despite substantial efforts, it was not possible to optimise these exosome markers for WB in this project. Conversely, tetraspanin exosome markers are enriched in exosomes but are also found on the cell membrane so cannot be used as markers to distinguish exosomes from microvesicles. Knowledge within the EV research field of marker proteins to distinguish different types of EV is not yet sufficient for identification of exosomes (Raposo and Stoorvogel, 2013).

3.3.2.2. Limitations of exosome quantification by TEM

TEM is an indicator of the structure and size of exosomes extracted but may not represent the entire sample, especially in this project where the formvar coated grids were not prepared correctly by hydrophilisation to give a negative charge. This may have prevented a large fraction of the exosome sample from fixing to the grids and also gave high background signal making it difficult to distinguish exosome structure on some sections of the grids. This may also explain why a relatively low number of exosomes were identified.

3.3.2.3.   Limitations of exosome quantification by NTA

When quantifying exosomes it is important to note that exosomes are not only being released by cells but are also being taken up by recipient cells so the concentration represents the net number of exosomes that have been released but not internalised by neighbouring cells. Therefore, the calculated exosome concentrations may not represent the levels of exosome secretion by different cell types because some types of cells may take up more exosomes but secrete less, or vice versa. When measured by NTA, of the eight cell lines tested, IGROV-1 cells appeared to secrete the highest number of exosomes. IGROV-1 cells may secrete similar numbers of exosomes compared with other ovarian cancer cell lines but the rate of exosome uptake by IGROV-1 cells may be much lower, hence the higher concentration of exosomes detected in conditioned media. It is currently difficult to distinguish exosomes from other small particles in solution, including protein aggregates and other debris, when analysing exosome samples by NTA. The PBS control sample should account for this. However, without the ability to specifically tag exosomes for subsequent detection by NTA it is impossible to exclude non-exosomal particles. It is unclear whether the inconsistency in exosomes released per cell in the eight cell lines was because of true inconsistency in exosome release or because of limitations of the NTA method for quantifying exosomes.

3.3.2.4.   Limitations of exosome quantification by confocal microscopy

Confocal microscopy is subjective, time consuming and allows for only a small fraction of the total cell number to be analysed (Franzen *et al.*, 2014; Lässer *et al.*, 2011). In terms of exosome characterisation, the major limitation of lipid dyes is that they are not specific to exosomes. They were designed to label cell membranes so the amount of dye leeching is difficult to determine. The best way to resolve this problem would be to specifically tag exosomes by creating fluorescent fusion proteins with exosome markers e.g. CD63-GFP. This is achieved by creating a stable CD63-GFP expressing cell line that will consequently produce CD63-GFP expressing exosomes (Koumangoye *et al.*, 2011). This would enable visualisation of their activity by confocal microscopy. Because of the small diameter of exosomes (maximum of 160 nm [Ludwig and Giebel, 2012]) it may be difficult to visualise tagged proteins associated with exosomes. Furthermore, the number of proteins inside exosomes is unknown, CD63-GFP incorporation into exosomes must be great enough to give a signal that can be detected, i.e. it may not be possible to detect a single CD63-GFP protein on a single exosome.

A major limitation of the use of confocal microscopy for visualisation of exosome activity is that the wavelength of visible light is approximately 390–700 nm therefore resolution is limited. Single

exosomes that are typically 30–160 nm in diameter (Ludwig and Giebel, 2012), or clusters of exosomes that are less than 390 nm in diameter, would be indistinguishable from one another. This should not affect the general detection of exosome uptake inside recipient cells but may affect tracking and localisation analysis of individual exosomes.

3.3.3. Additional exosome isolation techniques

Differential/sequential ultracentrifugation was used throughout this project, however, additional exosome isolation procedures exist that may have been more suitable. Each technique has both benefits and limitations.

3.3.3.1. Sucrose density gradient centrifugation

In addition to ultracentrifugation, sucrose density gradient centrifugation has frequently been used to extract exosomes. This method exploits the buoyant density of exosomes for purification and can be used in either a continuous gradient (Raposo *et al.*, 1996) or in a linear stepped gradient (sucrose cushion) (Lamparski *et al.*, 2002). Sucrose density gradient centrifugation minimises protein contamination from large protein aggregates that co-sediment with exosomes during ultracentrifugation (Tauro *et al.*, 2012). However, unless sucrose is substituted for iodoxanol (OptiPrep™, SigmaAldrich), this technique is unable to separate exosomes from viruses or large EVs with comparable sedimentation velocities (Cantin *et al.*, 2008). The main limitations of this method are that sucrose gradients are difficult to make accurately, and following centrifugation it is difficult to remove separate fractions without mixing them.

3.3.3.2. Immunoadsorption/immunoaffinity capture

Immunoadsorption is an alternative exosome isolation technique (Wubbolts *et al.*, 2003) using magnetic beads coated with a specific protein antigen that selects for exosomes with an outward orientation (as achieved during inward budding of the endosomal membrane during exosome biogenesis). Initially this technique was reported to yield high quality exosome samples enriched for exosome markers Alix, TSG101, and HSP70 (Tauro *et al.*, 2012). However, since the technique utilises a specific membrane antigen, only exosomes with the antigen are isolated while the exosome population without the antigen are excluded (Simpson and Mathivanan, 2012). This could eliminate a substantial fraction of the exosome sample. The exosome sample would contain only vesicles that have the specific antigen and therefore the sample would not be representative

of the total exosome population. In order to use this immunoaffinity method to accurately separate different types of EVs, an antigen specific to each class of EV, that is always present, must be used. Many of the antigens present on the exosomal surface are common to other types of EV and the knowledge of the exosomal membrane within the EV research field is not adequate, hence, specifically isolating exosomes is not possible using this method (Simpson and Mathivanan, 2012).

3.3.3.3. Ultrafiltration

Ultrafiltration is a method used to concentrate exosomes from biological fluids, typically urine (Cheruvanky *et al.*, 2007). Exosomes in suspension (in culture media) are forced through a semi-permeable membrane that separates them from other components of the media including protein aggregates, which commonly contaminate exosome preparations (Nordin *et al.*, 2015). This method has been used in some exosome research studies and has become more popular with exosome researchers over the last few years (Cheruvanky *et al.*, 2007; Lamparski *et al.*, 2002; Lobb *et al.*, 2015). The method is less time consuming and does not require the use of an ultracentrifuge, however, would probably not be ideal for extracting exosomes from cell culture media because of the lower concentration of exosomes in culture media compared with biological fluids.

3.3.3.4. Size exclusion chromatography

Recently an investigation was performed to compare standard ultracentrifugation with ultrafiltration liquid chromatography (UF-LC) where the ultrafiltered exosomes were loaded onto a sephacryl column for subsequent size-exclusion fractionation. This method yielded exosome samples of higher concentration and purity than ultracentrifugation (Nordin *et al.*, 2015). Data were also collected that suggested that exosomes fuse, erupt, and aggregate during the ultracentrifugation procedure, these issues were evaded with UF-LC (Nordin *et al.*, 2015).

3.3.3.5. Commercial 'exosome' isolation kits

Because of the rapid and growing interest in exosomes as future biomarkers and their possible use in therapeutics, many commercially available kits have been designed for easy isolation of exosomes, which generally do not require ultracentrifugation. These kits usually extract all lipid material in the sample, including cell debris, and do not distinguish between different EV subtypes

(including apoptotic and membrane blebs of up to ~1000 nm in size) and membrane-free macromolecular aggregates (Raposo and Stoorvogel, 2013).

3.3.4. Additional exosome characterisation methods

In addition to the exosome characterisation methods used in this project, other methods exist. Ideally all characterisation methods would have been used but because of time and money constraints this was not possible.

3.3.4.1. Cryo-electron microscopy

Often exosomes have a cup-shaped morphology because the spherical structure collapses during the drying stage prior to the fixing process when preparing grids for TEM (Raposo *et al.*, 1996). Rapidly frozen, vitrified exosomes visualised using cryo-electron microscopy are round in shape (they have not collapsed) (Conde-Vancells *et al.*, 2008). This method may give a more representative depiction of exosome structure than standard TEM.

3.3.4.2. High resolution flow cytometry

Conventional flow cytometry cannot detect vesicles <300 nm in diameter (Raposo and Stoorvogel, 2013). Currently available exosome characterisation methods allow analysis of exosomes in bulk but are not suitable for accurate quantification. They often fail to analyse single exosomes within a population, and do not examine phenotypic heterogeneity within exosome samples (Nolte-'t Hoen *et al.*, 2012b). A high-throughput flow cytometric method for analysis of individual exosomes has recently been developed using PKH67-labelled exosomes (Nolte-'t Hoen *et al.*, 2012b; van der Vlist *et al.*, 2012). The method was further optimised for selection of exosomes specifically expressing major histocompatibility complex class 2 (MHC-II) and milk-fat globule-epidermal growth factor 8 (MFG-E8) (Nolte-'t Hoen *et al.*, 2012b). The main disadvantage of this method is that only exosomes expressing the specific proteins are selected, vesicles that are negative for the target proteins will not be analysed, therefore analysis may not be representative of the entire exosome sample. Additionally, specific antigens selected must only be present on the membranes of exosomes, our knowledge of EV protein components is limited at the present time, so it is difficult to select antigens that will specifically isolate the exosome population of an EV sample (Bobrie *et al.*, 2011).

3.4. Conclusion

Despite its limitations, sequential/differential ultracentrifugation is the most widely used method for exosome extraction (Zhang *et al.*, 2014) and was used to isolate exosomes throughout this project. On reflection, it may have been better to isolate exosomes using iodoxanol density gradient centrifugation or UF-LC to minimise protein aggregate and viral contamination (Cantin *et al.*, 2008; Nordin *et al.*, 2015; Tauro *et al.*, 2012). However, density gradient centrifugation does not prevent contamination of the exosome sample with other types of EV that have an equal density to exosomes. Strategies to separate EVs dependent upon their origin (endosomal or membranous) are yet to be robustly developed (Raposo and Stoorvogel, 2013; Théry *et al.*, 2006).

Future work should strive to characterise exosomes using as many of the characterisation techniques discussed in this chapter as possible, to ensure that the exosome sample has the desired characteristics and is free from impurities. Because of time and money constraints this is not always possible.

Regardless of the limitations discussed in this chapter, throughout this project all exosome samples were characterised using four different methods: WB, TEM (on non-hydrophilised formvar grids), NTA, and confocal microscopy. All four methods recognised EVs with typical exosomal features and there was no evidence to suggest that the exosome samples were contaminated.

Chapter 4

The effect of exosomes on cell motility

4.   The effect of exosomes on cell motility

4.1. Introduction

4.1.1.   Mechanisms of cell motility

To facilitate metastasis, cancer cells must escape the primary tumour and relocate to a secondary site (section **1.2**). In order for this to happen they must acquire an increased motile capacity (Brooks *et al.*, 2010; Birchmeier *et al.*, 2003; Friedl and Wolf, 2003). Invasive and migratory behaviours facilitate movement of cells from the primary tumour mass into the circulation or lymphatics for dissemination around the body (**Figure 1.2** and **Figure 1.3**) (Shayan *et al.*, 2006). To move within tissues and escape the primary tumour, neoplastic cells migrate in a similar way to cells during normal physiological processes, including: embryonic morphogenesis, wound-healing, and immune-cell trafficking (Friedl and Wolf, 2003). Cell migration occurs through a continuous cycle of four key steps, shown in **Figure 4.1**: (1) Firstly, the motile cell becomes polarised and elongates (Conklin and Keely, 2012), (2) as a result of projection of the leading edge, a long finger-like protrusion (known as a pseudopod) forms, (3) this attaches to the ECM through focal-adhesions and extends and contracts pulling the cell body forward, (4) a traction force is generated that causes gradual forward gliding of the cell body and its trailing edge across the ECM (Friedl and Wolf, 2003).
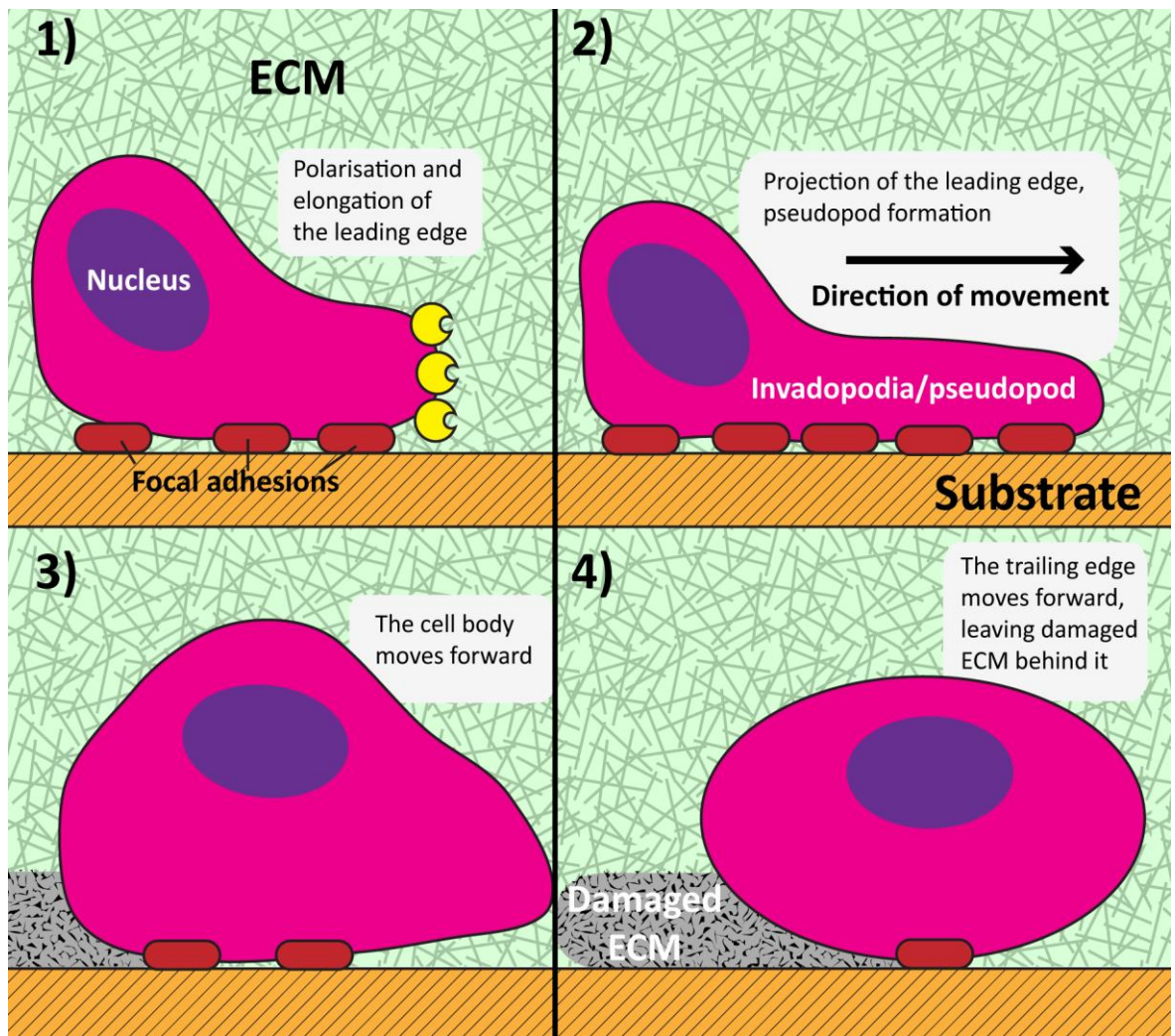
Figure 4.1: Mechanisms of cell motility. 1) The motile cell becomes polarised and elongates. Enzymes break down ECM making room for the cell to move forward. 2) As a result of projection of the leading edge, a long finger-like protrusion, known as a pseudopod, forms. 3) This attaches to the ECM through focal-adhesions and extends and contracts pulling the cell body forward. 4) A traction force is generated that causes gradual forward gliding of the cell body and its trailing edge across the ECM. A trail of damaged ECM is left behind the cell that has moved.

In order for cell migration to occur, the cell body shape is altered and the cell interacts with the adjacent ECM. The ECM provides both a support scaffold for the cell to move along and also acts as a barrier to cell migration. The migrating cell destroys the ECM through the activity of interstitial collagenases, gelatinases, and stromelysins at the leading edge, as the cell body moves towards the ECM framework (Conklin and Keely, 2012; Friedl and Wolf, 2003). Whilst the cell body increases in volume, the ECM is degraded, which provides the space required for the cell to move forward. The motile cell leaves behind a trail of tube-like defects in the ECM along the migration path (Friedl *et al.*, 1997), like a snail's trail. Additional protein types involved in neoplastic cell migration include integrins, cell-cell adhesion molecules, and proteins involved in intracellular communication (Conklin and Keely, 2012; Friedl and Wolf, 2003). Conversely, ECM

degradation is not essential to effective cell motility, some cancer cell types are able to physically deform their shapes to allow them to squeeze between cells of a complex tissue in the absence of protease activity (Brooks *et al.*, 2010; Friedl and Wolf, 2003; Sahai, 2005; Sahai, 2007).

Neoplastic cells migrate in several ways. Specifically, epithelial cancers migrate through single-cell migration collective/clustered cell migration or chain migration. Single-cell migration, as the name suggests, involves movement of single cancer cells. Collective/clustered migration involves movement of small clusters of cells or sheets of cells. This occurs in normal physiology during embryonic development, and development of glands and ducts in mammary tissue. Chain migration involves synchronised movement of a string of cells aligned between stromal fibres (Friedl and Wolf, 2003). Chain migration has been visualised in both breast (Roussos *et al.*, 2011), and ovarian (Sood *et al.*, 2001) cancers. In some cases, following extensive dedifferentiation, epithelial cancers migrate via mesenchymal migration where cells embrace a fibroblast-like spindle-shaped morphology (section **1.2**). Other types of cancer cell migrate in a less adhesive, amoeboid-like manner, which allows them to crawl faster through tissues (Brooks *et al.*, 2010; Friedl and Wolf, 2003).

4.1.2. The scratch assay

The scratch assay is a simple, cost-effective and well-established method used to measure basic cell migration factors such as speed, persistence, and polarity *in vitro*. A cell monolayer is grown to 100% confluency and a scratch is made using a pipette tip, scratch width is then observed at regular intervals (Todaro *et al.*, 1965) (**Figure 2.2**). Cells at the wound edge polarise and migrate inwards, eventually the scratch heals. Aside from being both straightforward and economical, the major advantage of the scratch assay is that it generates a strong directional migratory response in the cells allowing for easy analysis of cell migration rates (Cory, 2011).

4.1.2.1.   The use of the scratch assay in exosome research

The effect of exosomes on motility of human cells *in vitro* has been assessed using the scratch wound healing assay in many studies over the past six years (Salomon *et al.*, 2013a). Cytotrophoblast-derived exosomes statistically significantly increased motility of first trimester extravillous trophoblast cells (Salomon *et al.*, 2013a). Cancer studies have shown that exosomes influence the motile potential of recipient cells using the scratch assay. Motility of breast cancer cells and glioma cells was shown to increase in the presence of parent cell-derived exosomes in a HSP90α dependent manner (McCready *et al.*, 2010). Primary effusion lymphoma patient pleural

fluid-derived exosomes were shown to increase the motility of human telomerase reverse transcriptase (hTERT)-immortalised human umbilical vein endothelial cells, this process was shown to be mediated by phosphatidylserine on the exosomal surface (Chugh *et al.*, 2013). Exosomes derived from a colon adenocarcinoma cell line have been shown to increase proangiogenic motility of human dermal microvascular endothelial cells by 4.1 fold (Yoon *et al.*, 2014). Human embryonic kidney cell-derived exosomes positive for LMP1 were shown to increase movement of immortalised nasopharyngeal epithelial cells and an EBV-negative human nasopharyngeal carcinoma cell line (Aga *et al.*, 2014).

Exosome donor cells with increased drug resistance and metastatic potential have been explored as possible mediators of increased cell motility in cancer cells. Exosomes derived from human prostate cancer cells both resistant and sensitive to Docetaxel did not differentially affect cell motility (Corcoran *et al.*, 2012). Even though the drug resistance status of a cell does not affect the ability of the exosomes it secretes to induce cell movement in recipient cancer cells, there is evidence to suggest that the metastatic capacity of an exosome's parental cell can influence recipient cell motility (Harris *et al.*, 2015). Exosomes derived from aggressive triple-negative breast cancer cells were able to increase motility of three breast cancer cell lines more than exosomes derived from their less invasive sister cell line (section **4.1.2.2**) (O'Brien *et al.*, 2013).

4.1.2.2. The linear relationship between breast cancer exosome donor cell metastatic status and invasive capacity induced by exosomes

A relationship has been established between increasing breast cancer cell motility and increasing metastatic capacity of exosome donor cells (Harris *et al.*, 2015). Whereby, presence of highly metastatic breast cancer cell-derived exosomes increased motility the greatest, followed by intermediately metastatic cell-derived exosomes. Whereas, exosomes derived from cells with a low metastatic capacity had minimal effect on cell motility. This suggests an association between the metastatic potential of the exosome donor cells and the ability of exosomes to increase cell motility (Harris *et al.*, 2015).

4.1.3. Hypothesis

As exosomes derived from cells with higher metastatic capacity have been shown to increase motility of breast cancer cells to a greater degree than exosomes isolated from less metastatic breast cancer cells (Harris *et al.*, 2015), it was predicted that this mechanism may be active in other epithelial cancers, including ovarian cancer. For this reason, the effect of exosomes isolated

from a range of ovarian cancer cell lines with different metastatic abilities upon motility of ovarian cancer cells was investigated using the scratch wound healing assay. It was hypothesised that exosomes derived from highly motile ovarian cancer cell lines increase the motile capacity of inherently less motile ovarian cancer cell lines. In addition to this, it was hypothesised that cells that are more motile or that multiply faster may secrete exosomes of a distinctive size or at varied concentrations.

4.2. Results

4.2.1. Scratch assay method optimisation

The cell seeding concentration for the scratch assay was optimised for each different cell line (**Figure 4.2**). The optimum seeding concentrations are summarised in **Table 2.2**. Different tools to create the scratches were tested. P200 pipette tips were found to leave the least residual cells within the scratch region in comparison with the P20 and P2 pipette tips. The straight needle probe was insufficient for making a wide clean scratch (**Figure 4.3**).
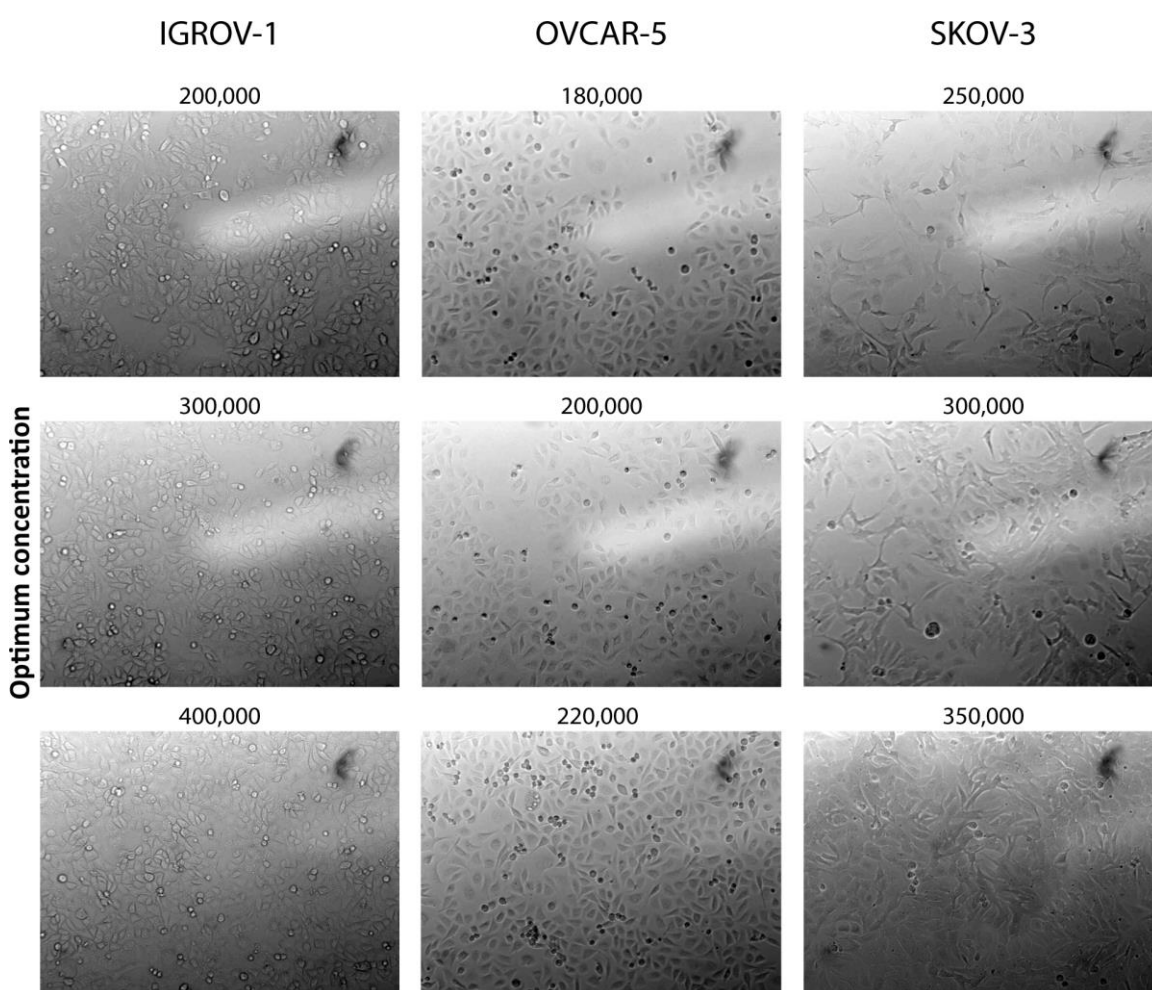
Figure 4.2: Optimising cell seeding concentration for scratch assay. Each cell line was seeded at different concentrations to find the optimum. The lowest concentration at which 100% confluency was achieved over 48 hours was used for subsequent scratch experimentation.

A) P2 pipette tip
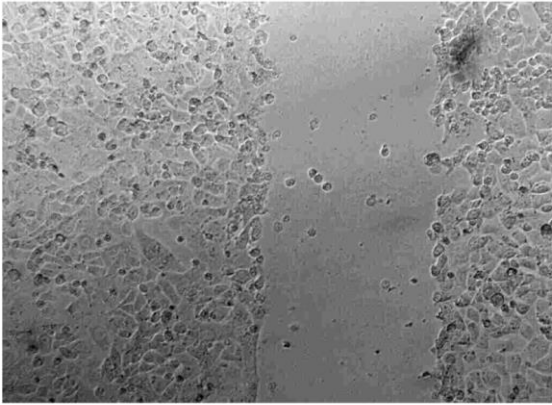
B) P20 pipette tip
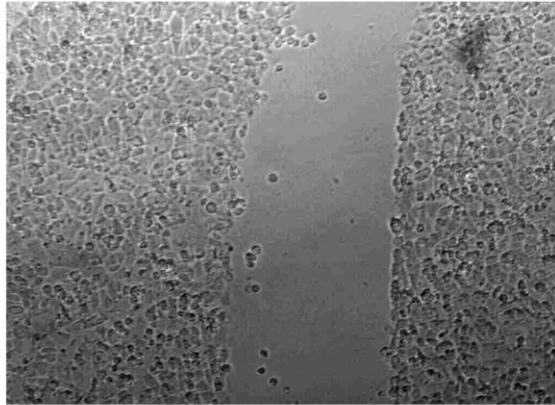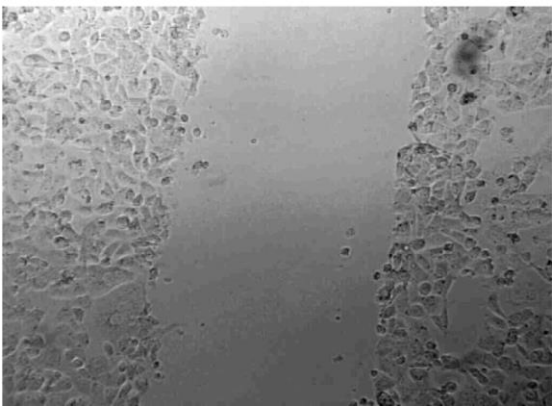
C) P200 pipette tip

D) Straight needle probe
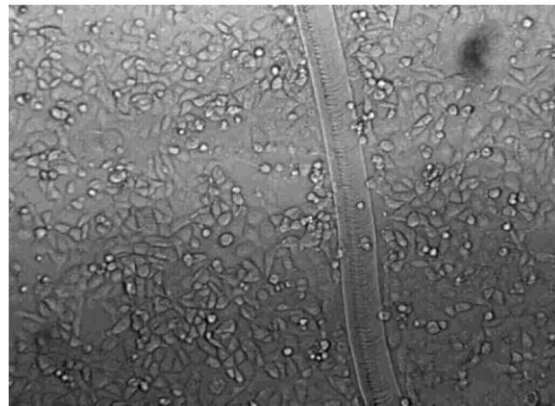
Figure 4.3: Testing scratch making tools on a cell monolayer. A) P2 pipette tip, B) P20 pipette tip, C) P200 pipette tip, and D) the straight needle probe were tested for their efficiency in creating a scratch on a monolayer of MCF-7 breast cancer cells.

4.2.2. Motility and proliferation rates of nine ovarian cancer cell lines

4.2.2.1.   Motility rates of nine ovarian cancer cell lines

The difference in motile capacity of these nine ovarian cancer cell lines has not previously been reported in literature. To assess the motility rates of different cancer cell lines, the scratch assay was used (**Figure 2.2** and **Figure 2.4**). Cells were seeded in 24-well plates and left to settle and reach 100% confluency over 48 hours. A scratch was made down the centre of the cell monolayer using a P200 pipette tip, and the cells were visualised every 12 hours to determine rate of scratch closure. SKOV-3 cells were found to have the greatest motile capacity, closely followed by OVCAR-8. IGROV-1 cells moved the slowest (**Figure 4.4A**). The two tailed T-test calculations indicate that cell motility (in terms of normalised scratch closure width at the 24 hour time point) of all nine cell lines were statistically significantly different from one another, except for A-2780 and MCP-1; A-2780 and OVCAR-4; CP-70 and OVCAR-3; CP-70 and OVCAR-4; IGROV-1 and MCP-1; MCP-1 and OVCAR-4 (**Table 4.1**). The average scratch closure rate is shown in **Figure 4.4B** for the

nine ovarian cancer cell lines of interest. Average scratch closure rates show a similar pattern to the scratch closure curves in **Figure 4.4A**, except CP-70 cells were shown to move slower overall than OVCAR-3 cells in terms of average scratch closure rate (1.95%/hour and 2.18%/hour, respectively). The scratch closure curves in **Figure 4.4A** show that at the 120 hour time point the scratch was wider (i.e. the cells moved slower) for OVCAR-3 cells compared with CP-70 cells. See Appendix B (section **8.2**) for raw motility data.

Table 4.1: Two tailed T-test for cell motility in terms of average scratch closure speed (% area reduction/hour) shown in Figure 4.4B.

Two tailed T-test	CP-70 (solid tumour)	IGROV-1 (solid tumour)	MCP-1 (solid tumour)	OVCAR-3 (malignant ascites)	OVCAR-4 (malignant ascites)	OVCAR-5 (malignant ascites)	OVCAR-8 (unknown origin)	SKOV-3 (malignant ascites)
A-2780 (solid tumour)	3.24×10^{-5}	5.75×10^{-4}	0.442	0.009	0.311	3.37×10^{-5}	7.94×10^{-6}	7.70×10^{-8}
CP-70 (solid tumour)		3.05×10^{-6}	0.010	0.289	0.051	2.47×10^{-4}	2.58×10^{-5}	2.63×10^{-7}
IGROV-1 (solid tumour)			0.117	2.11×10^{-4}	0.001	3.62×10^{-6}	2.03×10^{-6}	1.52×10^{-8}
MCP-1 (solid tumour)				0.007	0.191	6.10×10^{-6}	1.29×10^{-6}	1.62×10^{-9}
OVCAR-3 (malignant ascites)					0.044	6.69×10^{-4}	1.31×10^{-5}	8.48×10^{-9}
OVCAR-4 (malignant ascites)						3.13×10^{-5}	5.41×10^{-6}	1.48×10^{-8}
OVCAR-5 (malignant ascites)							0.004	9.77×10^{-7}
OVCAR-8 (unknown origin)								0.005

P = >0.05
P = <0.05

4.2.2.2.   Proliferation rates of nine ovarian cancer cell lines

The scratch assay is used to determine how fast cells move, however it is also important to appreciate that cell proliferation (i.e. increase in cell number) also contributes to closure of the scratch. To find the proliferation rates of the cell lines, cells were seeded at a known concentration at time = 0 and cell concentration was calculated every 24 hours over a period of 120 hours. The proliferation curves of nine ovarian cancer cell lines are shown in **Figure 4.4C**. Despite healing the scratch the fastest, SKOV-3 cells proliferate slower than most of the cell lines (**Figure 4.4A&C**). Of the nine cell lines tested, SKOV-3 cells were the third slowest in terms of proliferation with a doubling time of 36.24 hours (**Figure 4.4D**). A-2780 cells, and the A-2780 sister cell lines MCP-1 and CP-70, were shown to proliferate the fastest of the nine cell lines tested (**Figure 4.4C&D**), however aside from IGROV-1, these cell lines were the least motile (**Figure 4.4A&B**). The two tailed T-test values indicate that cell proliferation (in terms of doubling time calculated using 0–96 hour time points) between A-2780 and OVCAR-3; A-2780 and OVCAR-4;

A-2780 and SKOV-3; CP-70 and MCP-1; CP-70 and OVCAR-3; CP-70 and SKOV-3; MCP-1 and OVCAR-3; MCP-1 and OVCAR-4; MCP-1 and SKOV-3; OVCAR-3 and SKOV-3, were statistically significantly different from one another (**Table 4.2**). See Appendix B (section **8.2**) for raw proliferation data.

Table 4.2: Two tailed T-test for cell proliferation in terms of doubling time shown in Figure 4.4D.

Two tailed T-test	CP-70 (solid tumour)	IGROV-1 (solid tumour)	MCP-1 (solid tumour)	OVCAR-3 (malignant ascites)	OVCAR-4 (malignant ascites)	OVCAR-5 (malignant ascites)	OVCAR-8 (unknown origin)	SKOV-3 (malignant ascites)
A-2780 (solid tumour)	0.084	0.401	0.086	1.55×10^{-4}	0.048	0.276	0.315	4.70×10^{-4}
CP-70 (solid tumour)		0.433	0.030	3.45×10^{-4}	0.060	0.406	0.435	0.001
IGROV-1 (solid tumour)			0.376	0.647	0.737	0.521	0.533	0.573
MCP-1 (solid tumour)				0.002	0.042	0.205	0.242	0.003
OVCAR-3 (malignant ascites)					0.454	0.330	0.436	0.025
OVCAR-4 (malignant ascites)						0.194	0.266	0.214
OVCAR-5 (malignant ascites)							0.945	0.629
OVCAR-8 (unknown origin)								0.744

| P = >0.05 |
| P = <0.05 |

113

Figure 4.4: Motility and proliferation rates of nine ovarian cancer cell lines. A) Motility rate of nine ovarian cancer cell lines determined using the scratch assay. There were nine biological replicates for each cell line. Within each biological replicate there were three technical replicates i.e. three points on each scratch were measured. B) Average scratch closure speed per hour. Values from A) were used to calculate the average percentage scratch reduction per hour. C) Proliferation rate of nine ovarian cancer cell lines determined by cell counting, there were three biological replicates per cell line. Cells were seeded at 500,000 per flask in 15 T25 flasks at time = 0. Every 24 hours, cell concentration of three flasks of each cell line was determined using a haemocytometer. The average of three cell counts per flask was used to calculate total cell number at each time point for each cell line. D) Doubling time of nine ovarian cancer cell lines. Doubling time was calculated using cell concentrations from C) for time points between 0 and 96 hours. Error bars represent standard error of the mean.
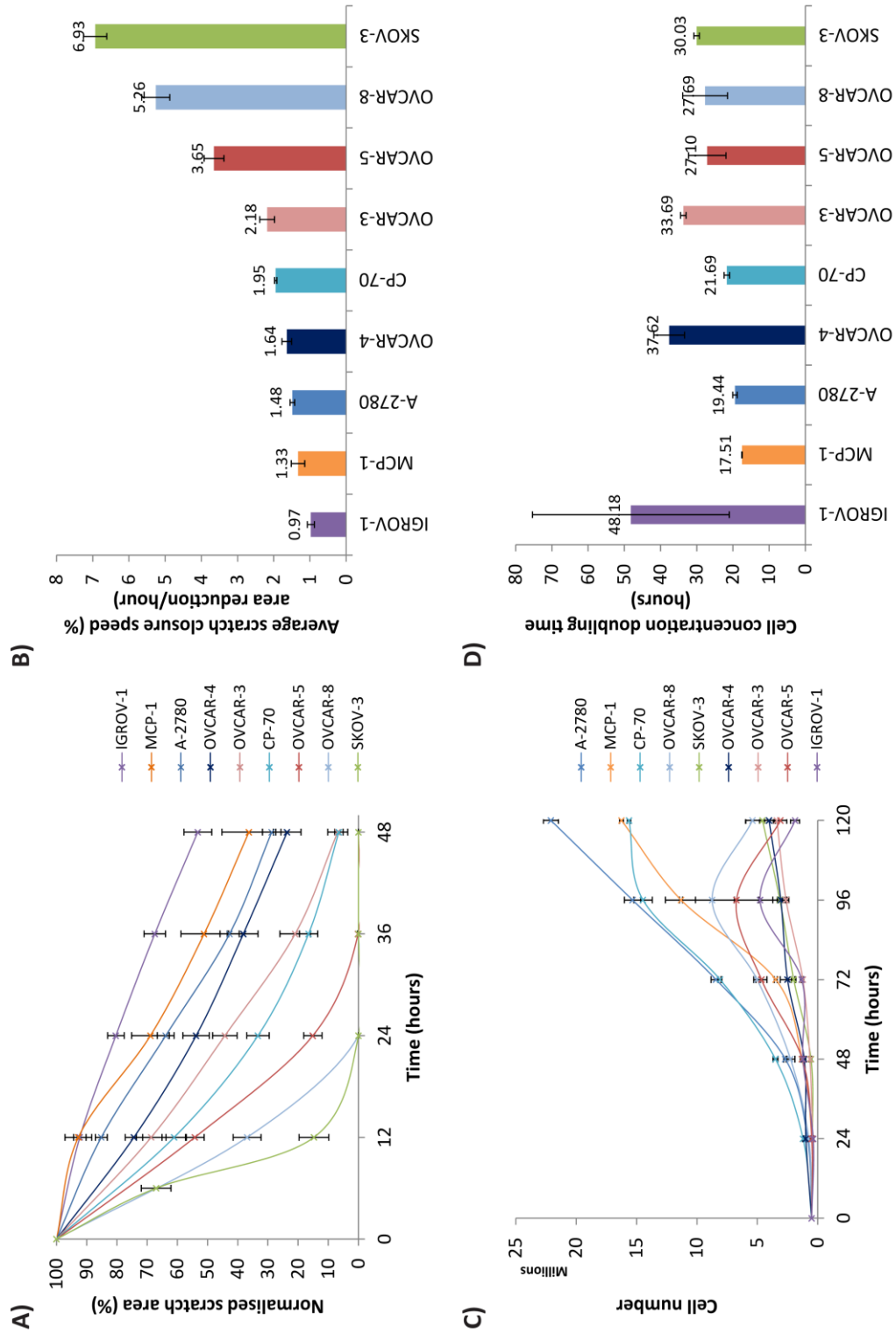
4.2.3. Scratch closure speed normalised to cell proliferation rates

Once scratch closure speed (**Figure 4.4B**) and cell proliferation rates, in terms of cell concentration doubling time (**Figure 4.4D**), had been determined for all nine cell lines, scratch closure speed was normalised to cell proliferation levels (**Figure 4.5**). Generally, scratch closure speed was not greatly affected by cell proliferation rate because SKOV-3 cells remained the most motile (0.23), followed by OVCAR-8 (0.19) and OVCAR-5 (0.13). IGROV-1 remained the least motile cell line (0.02) (**Figure 4.4B** and **Figure 4.5**). Cell proliferation was shown to have minimal effect upon MCP-1 cell motility with a normalised scratch closure speed of 0.11. Of the nine cell lines tested they were the fourth most motile (**Figure 4.5**) as opposed to the second slowest as indicated by average scratch closure speed (**Figure 4.4B**).

Scratch closure speed normalisation to proliferation rate suggested that OVCAR-3 (0.05) was the equal third slowest cell line in terms of cell motility (**Figure 4.5**) contrasting with fourth fastest when motility was assessed by average scratch closure speed only (**Figure 4.4B**). Similar results were found with the OVCAR-4 cell line when scratch closure speed was normalised to proliferation, a value of 0.04 represented the second slowest moving cell line of the nine lines tested whereas, when cell proliferation was not considered, OVCAR-4 cells were regarded as the fourth slowest cell line. These results suggest that for both OVCAR-3 and OVCAR-4 cell lines, cell proliferation contributed to closure of the scratch, more so than for the other cell lines tested.
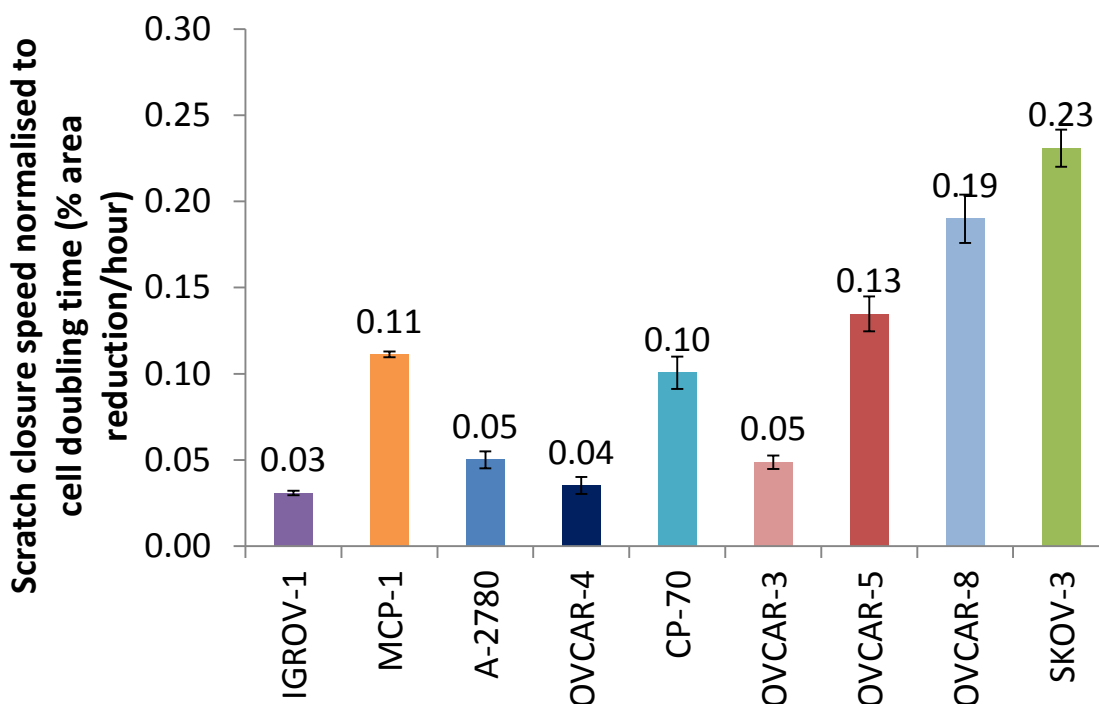
Figure 4.5: Scratch closure speed normalised to cell proliferation rates. Average scratch closure speed was divided by cell doubling time to give normalised values for scratch closure speed for each cell line. There were nine biological replicates for scratch closure speed for each cell line.

The correlation between cell proliferation and motility rate shows that there was lack of correlation between these two cellular phenotypes (**Figure 4.6**). The motility rate of each cell line was assessed in terms of both scratch width after 24 hours, and percentage scratch area reduction per hour. For doubling time plotted against scratch width after 24 hours for each cell line (**Figure 4.6A**), the regression line represents a Pearson's correlation coefficient of 0.200 (p = 0.606), demonstrating that there was a weak relationship between the two sets of data. The R^2 value of 0.040, and Spearman's rank correlation coefficient of 0.949 indicate that the variables have a weak linear but strongly monotonic relationship. For doubling time plotted against percentage scratch area reduction per hour for each cell line (**Figure 4.6B**), the Pearson's correlation coefficient was calculated as -0.081 (p = 0.836) indicating that there was a weak relationship between these cellular characteristics. The R^2 value of 0.007 suggests that cell motility, and exosome secretion rates have no linear relationship. Spearman's rank correlation coefficient was calculated as 0.898, further indicating a weak linear, but moderately monotonic relationship. This shows that irrespective of whether cell motility is analysed in terms of scratch width after 24 hours, or percentage scratch area reduction per hour, cell motility is not greatly influenced by cell proliferation.

The Grubbs' test indicated that there were no outliers in the data sets for both cell motility (in terms of both average scratch closure speed and scratch width at 24 hours) and proliferation (doubling time) rates. This results suggests that there was no association between cell motility and cell proliferation. The speed at which cells replicated did not affect their ability to close the scratch; hence, scratch closure occurred as a result of cell movement rather than faster proliferation.

A)

B)
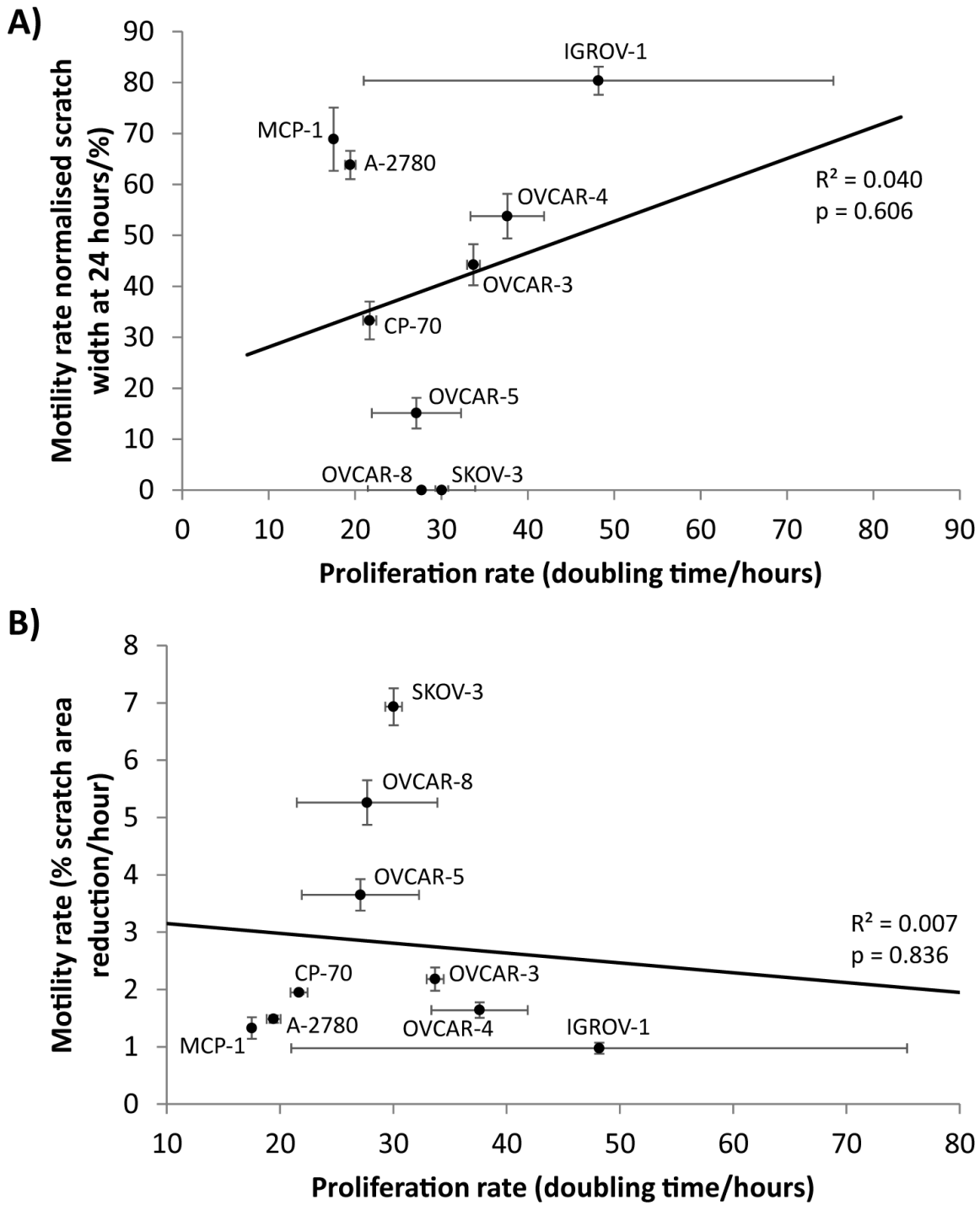
Figure 4.6: Correlation between motility and proliferation capabilities of nine ovarian cancer cell lines. Nine cancer cell lines were assessed for their motile capacity using the scratch assay and their proliferation rate by calculating cell number increase over 120 hours (five days). Average doubling time between 0–96 hours was used as a measure of cell proliferation. The relationship between cell proliferation and cell motility was determined in terms of A) scratch width at 24 hours and B) percentage scratch area reduction per hour. The correlation between the two cellular phenotypes for each cell line is shown. R^2 and p values were calculated using Pearson's correlation coefficient.

4.2.4. The relationship between cell motility and exosome secretion rates

It is possible that exosome secretion from cells that migrate more rapidly is elevated because of the increased need for cell-cell communication. An increase in circulating exosome concentration has been linked with poorly differentiated tumours and shorter overall survival (Silva *et al.*, 2012). Since a greater motile capacity is also a characteristic of more aggressive and well developed tumours (Guarino, 2007; Huber *et al.*, 2005), it was hypothesised that more motile cells secrete more exosomes. To investigate this, the relationship between exosome secretion and motility rate was determined by plotting exosome secretion and motility rates against one another. The correlation between exosome secretion and motility rate shows that there was no relationship between these two cellular phenotypes (**Figure 4.7**).

Where motility rate was assessed in terms of percentage scratch area reduction per hour, a Pearson's correlation coefficient of -0.303 (p = 0.465) suggests a weak negative correlation between the variables, this is represented by the regression line in **Figure 4.7A**. The R^2 value of 0.092 indicates that the data points had a weak linear relationship. The Spearman's rank correlation coefficient of 0.610 indicates an intermediary monotonic relationship between motility rate (in terms of percentage scratch area reduction per hour) and exosome secretion rates.

These results suggest a moderate relationship between cell motility and exosome secretion. The Grubbs' test was applied to identify outliers. The Grubbs' test confirmed that in terms of average number of exosomes released per cell, IGROV-1 was an outlier. When the IGROV-1 anomalous data point was removed, the direction of the relationship between exosome secretion and cell motility (in terms of both average scratch closure speed and scratch width at 24 hours) changed from positive to negative, or vice versa. For this reason, the IGROV-1 data point was not included in the analysis.

When the IGROV-1 data point was removed (**Figure 4.7B**), the R^2 value was 0.238, the Pearson's correlation coefficient was 0.488 (p = 0.536), and the Spearman's rank correlation coefficient was 0.337, suggesting a weak, positively correlated, mildly monotonic relationship between cell motility and exosome secretion.

Many publications use scratch width at 24 hours to assess cell motility (Kaur *et al.*, 2012; Liu *et al.*, 2013; Yang *et al.*, 2010), so the data was also analysed in terms of normalised percentage scratch width at 24 hours. The relationship between cell motility in terms of scratch width at 24 hours and exosome secretion is presented in **Figure 4.7C**. The Pearson's correlation coefficient was calculated as 0.457 (p = 0.255) suggesting a moderate positive correlation. The R^2 value of 0.208 indicates that the data points have a weak linear relationship, and Spearman's rank correlation

coefficient was 0.670 suggesting an intermediary monotonic relationship between cell motility (in terms of scratch width at 24 hours) and exosome secretion. When the IGROV-1 anomaly was removed (**Figure 4.7D**), the Pearson's correlation coefficient was re-calculated to -0.617 (p = 0.140) suggesting a moderate negative correlation between the variables. The R^2 value of 0.380 suggests a weak linear relationship between cell motility and exosome secretion. Spearman's rank correlation coefficient was 0.041 indicating absence of a monotonic relationship between scratch width at 24 hours and exosome secretion rates.

Figure 4.7: Correlation between motility and exosome secretion rates of nine ovarian cancer cell lines. Nine ovarian cancer cell lines were assessed for their motile capacity using the scratch assay and their exosome secretion rate, which was calculated by NTA. Exosome levels in cell culture media conditioned for 24 hours were measured. The relationship between cell proliferation and exosome secretion was determined in terms of A) percentage scratch area reduction per hour, B) percentage scratch area reduction per hour excluding the IGROV-1 anomaly, C) scratch width at 24 hours, and D) scratch width at 24 hours excluding the IGROV-1 anomaly. The correlation between the two cellular phenotypes for each cell line is shown. R^2 and p values were calculated using Pearson's correlation coefficient.
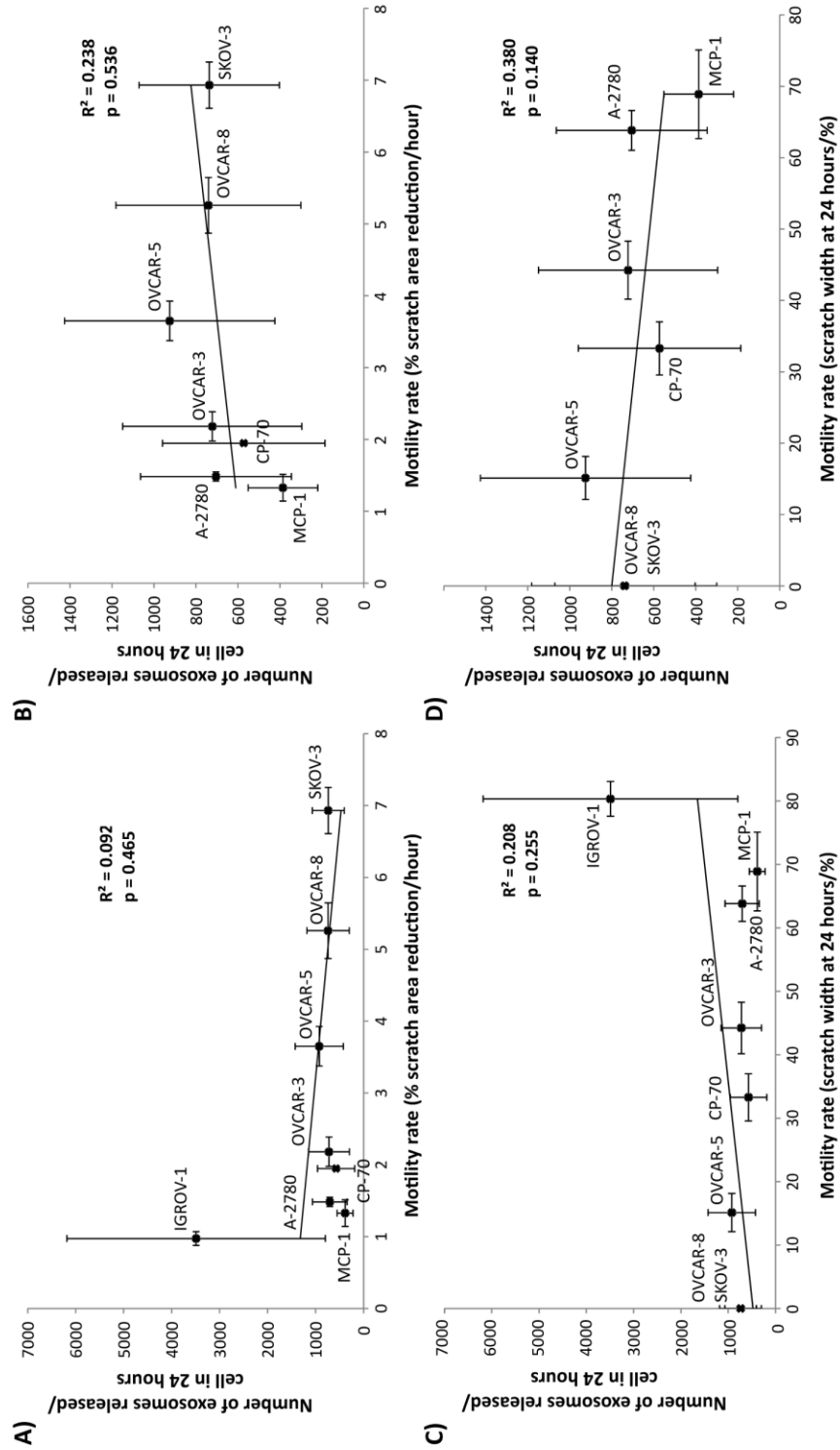
4.2.5.   The effect of exosomes derived from highly motile cells on less motile cells

It was predicted that exosomes may have the ability to transfer signals to recipient cells to increase their metastatic behaviour, in particular, cell motility. Having established the most motile cell lines from the least motile, exosome swapping experiments were performed where ovarian cancer cells were cultured in EFM. Twenty-four hours prior to, and immediately after the scratch was created, exosomes derived from more/less motile cells were administered, and their effect on cell motility was explored. To determine the effect of exosomes on motility of OVCAR-5 cells, exosomes were extracted from OVCAR-5 and SKOV-3 cells and applied to OVCAR-5 cells (**Figure 2.3**). OVCAR-5 cells were selected as their motile capacity was in the middle of the range of the ovarian cancer cell lines tested (**Figure 4.4A&B**), so their motility could be increased or decreased by exosome treatment. It was predicted that their motile capacity may be enhanced by SKOV-3-derived exosomes because SKOV-3 cells had the greatest motile capacity.

Exosomes were collected from media that had conditioned approximately 6 million cells over a 24 hour time period and applied to cells in the scratch assay. OVCAR-5 and SKOV-3-derived exosomes enhanced motility of OVCAR-5 cells resulting in faster closure of the scratch, but the effect induced did not reach significance. Despite the differences in the motility rate curve (**Figure 4.8A**) and increase in average scratch closure speed (**Figure 4.8B**), the T-test of normalised scratch width at 24 hours and average scratch closure speed, showed that neither OVCAR-5 nor SKOV-3 exosomes statistically significantly increased cell motility (**Table 4.2**). The experiment was repeated three more times to generate a total of 12 biological replicates (**Figure 4.9**), but significance was not reached (**Table 4.4**). It was hypothesised that SKOV-3 exosomes would increase motility more than exosomes derived from other cell lines because SKOV-3 cells are the most motile. However, the results suggest that SKOV-3 cell-derived exosomes do not increase the motility of OVCAR-5 cells. Also, OVCAR-5 cell-derived exosomes, used as a control, did not increase OVCAR-5 cell motility, indicating that increased exosome concentration also does not increase cell motility.

Table 4.3: Two tailed T-test results for exosome 'swapping' treatments on OVCAR-5 cells shown in Figure 4.8.

Average scratch closure speed (% area reduction/hour)				Scratch width at 12 hours		
	Control (no exosomes)	Control (OVCAR-5) exosomes			Control (no exosomes)	Control (OVCAR-5) exosomes
Control (OVCAR-5) exosomes	0.270			Control (OVCAR-5) exosomes	0.255	
SKOV-3 exosomes	0.198	0.394		SKOV-3 exosomes	0.181	0.394
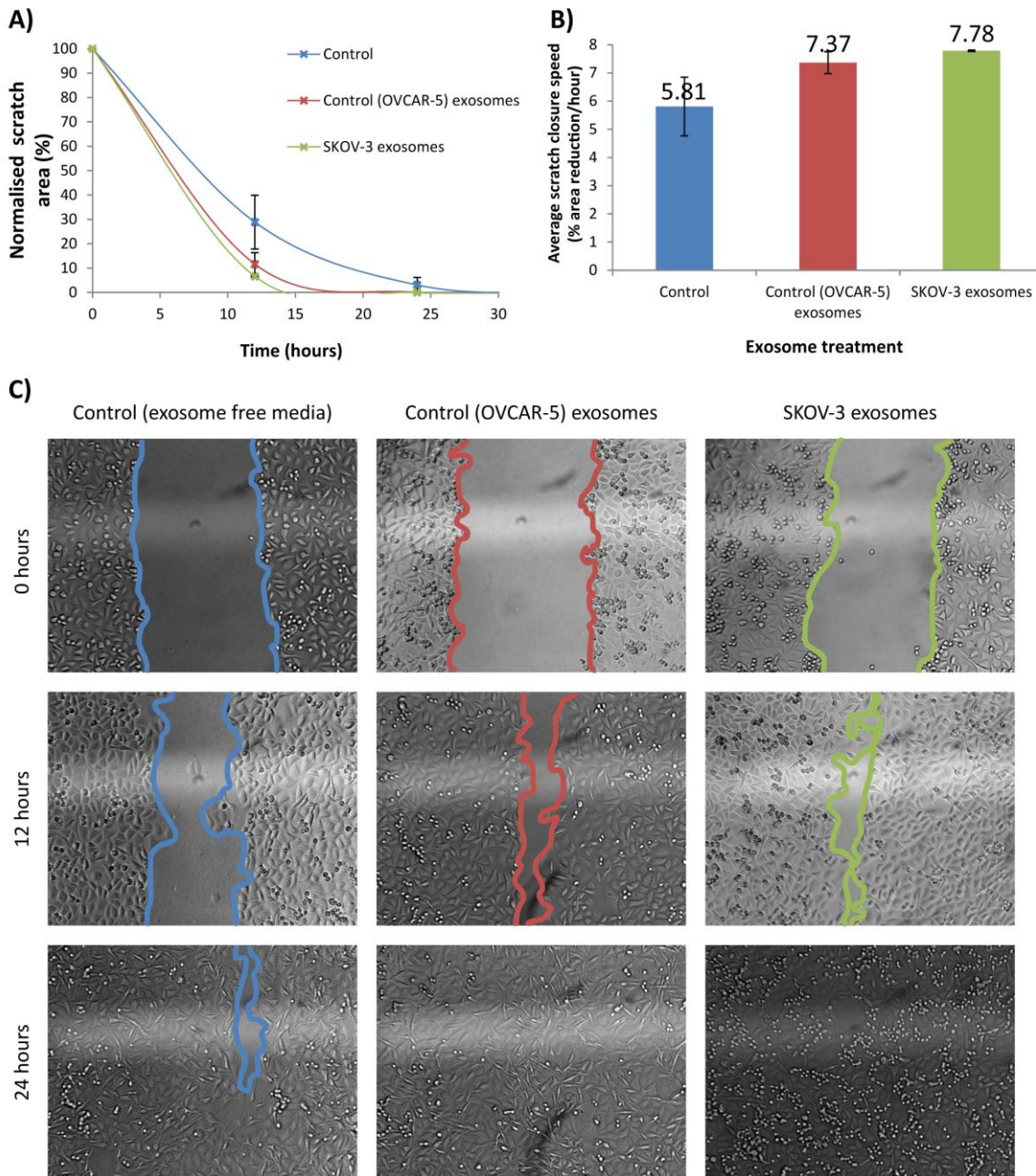
Figure 4.8: The effect of OVCAR-5 and SKOV-3-derived exosomes on motility of OVCAR-5 cells. A) The curve represents scratch closure rate of OVCAR-5 cells that received no exosomes, or OVCAR-5 or SKOV-3 cell-derived exosomes. B) Average scratch closure speed in terms of percentage scratch area decrease per hour. Each sample group contained three biological replicates, within each replicate there were three technical replicates. Error bars represent standard error of the mean of three biological replicates. C) Representative images of the cells at different time points showing the effect that exosomes had on cell movement. Each exosome treatment contained exosomes secreted by approximately 2 million cells over 24 hour period, there were approximately 220,000 cells in each receiver well.

Table 4.4: Two tailed T-test results for 12 replicates of exosome 'swapping' treatments on OVCAR-5 cells shown in Figure 4.9.

Average scratch closure speed (% area reduction/hour)				Scratch width at 12 hours		
	Control (no exosomes)	Control (OVCAR-5) exosomes			Control (no exosomes)	Control (OVCAR-5) exosomes
Control (OVCAR-5) exosomes	0.999			Control (OVCAR-5) exosomes	0.480	
SKOV-3 exosomes	0.241	0.204		SKOV-3 exosomes	0.820	0.725
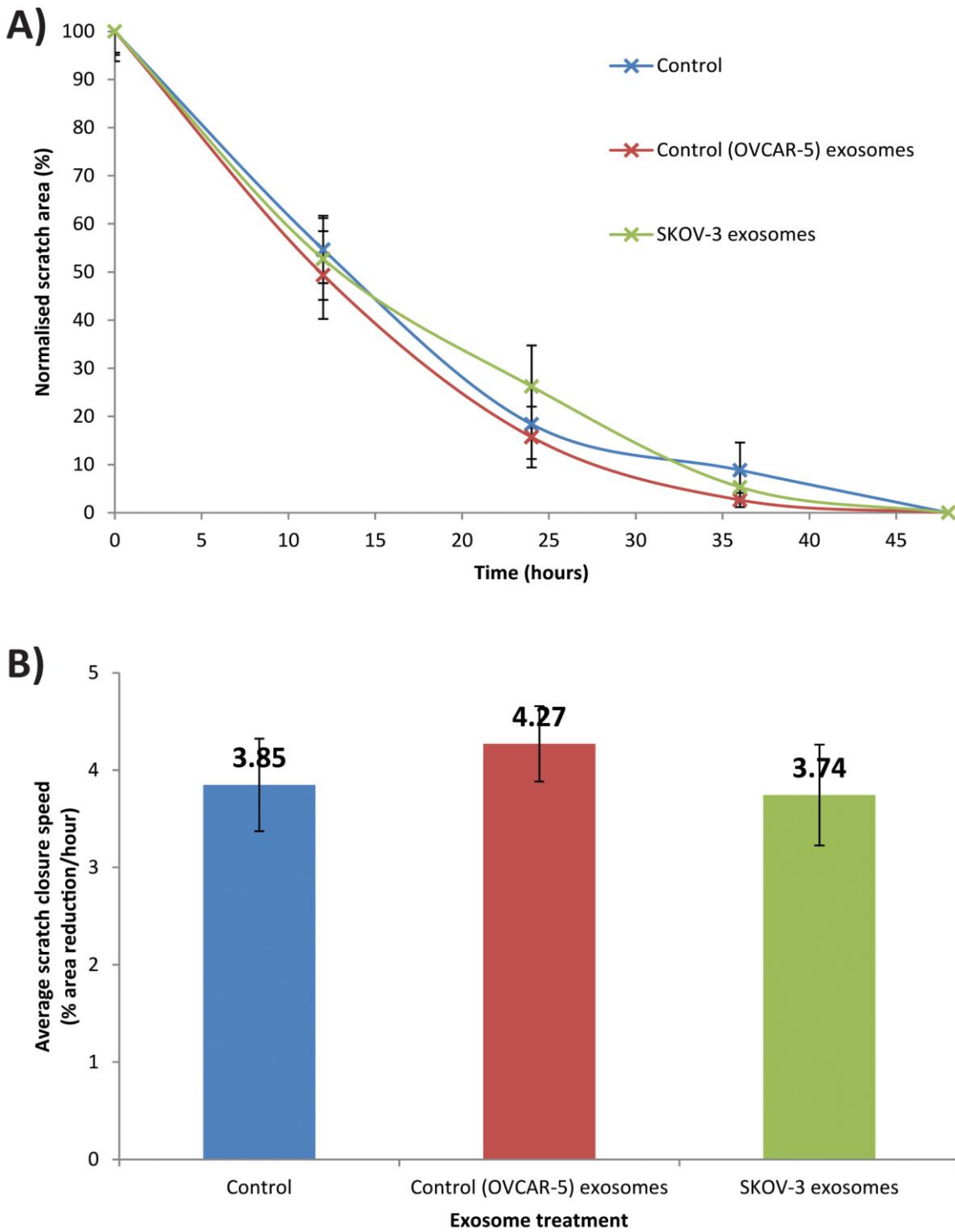
Figure 4.9: The effect of OVCAR-5 and SKOV-3-derived exosomes on motility of OVCAR-5 cells with 12 biological replicates. A) The curve represents scratch closure rate of OVCAR-5 cells that received no exosomes, or OVCAR-5 or SKOV-3 cell-derived exosomes. B) Average scratch closure speed in terms of percentage scratch area decrease per hour. Each sample group contained 12 biological replicates, within each replicate there were three technical replicates. Error bars represent standard error of the mean of 12 biological replicates.

4.2.6. The effect of exosomes derived from less motile cells on highly motile cells

To investigate the effect of exosomes on motility of SKOV-3 cells, exosomes were extracted from OVCAR-5 and SKOV-3 cells and applied to SKOV-3 cells (as shown in **Figure 2.3**, except SKOV-3 cells were the recipient cells instead of OVCAR-5 cells). It was hypothesised that OVCAR-5 exosomes may have the ability to reduce the motility of SKOV-3 cells because the parent cells had a lower motile capacity.

As above in **Figure 4.8**, exosomes were collected from media that had conditioned approximately 6 million cells over a 24 hour time period. Both OVCAR-5 and SKOV-3-derived exosomes increased motility of SKOV-3 cells resulting in faster closure of the scratch (**Figure 4.10**). The T-test of normalised average scratch closure speed indicates that both SKOV-3 and OVCAR-5 exosomes statistically significantly increased SKOV-3 cell motility, with p values of 0.001 and 0.012, respectively (**Table 4.5**). As shown in OVCAR-5 cells, both SKOV-3 and OVCAR-5 exosomes induced a similar effect upon SKOV-3 cell motility. This suggests that the signal responsible for increased motility was transferred by exosomes, but was not necessarily provided by exosomes derived from cells that have a more motile phenotype. Increased motility may be caused more generally by cancer-derived exosomes, independent of the motility status of the cells from which they were derived.

Table 4.5: Two tailed T-test results for exosome 'swapping' treatments on SKOV-3 cells shown in Figure 4.10.

Average scratch closure speed (% area reduction/hour)		
	Control (no exosomes)	**OVCAR-5 exosomes**
OVCAR-5 exosomes	0.012	
Control (SKOV-3) exosomes	0.001	0.394
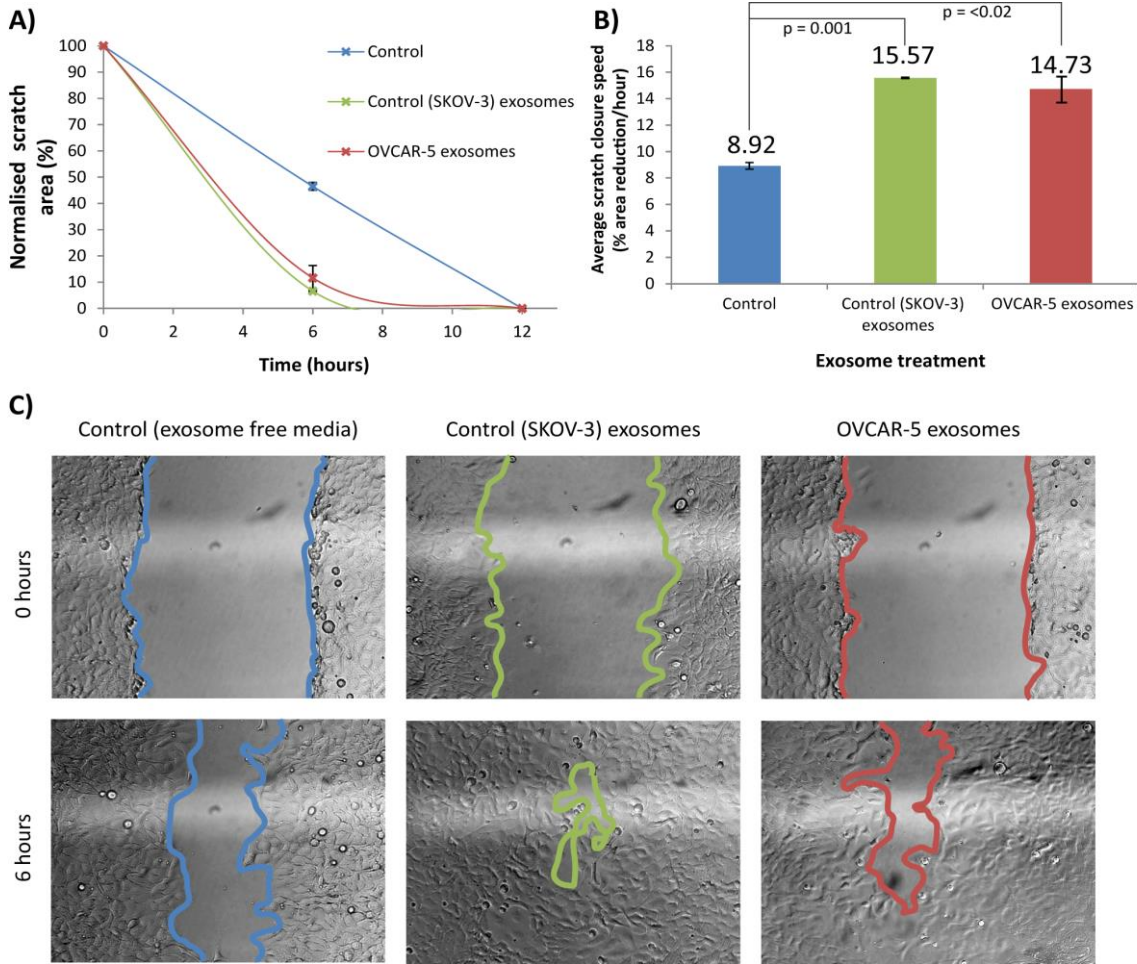
Figure 4.10: The effect of SKOV-3 and OVCAR-5-derived exosomes on motility of SKOV-3 cells. A) The curve represents scratch closure rate of SKOV-3 cells that received no exosomes, or SKOV-3 or OVCAR-5 cell-derived exosomes. B) Average scratch closure speed in terms of percentage scratch area decrease per hour. Each sample group contained three biological replicates, within each replicate there were three technical replicates. Error bars represent standard error of the mean of three biological replicates. P values were calculated using the two tailed T-test. C) Representative images of the cells at different time points showing the effect that exosomes had on cell movement. Each exosome treatment contained exosomes secreted by approximately 2 million cells over 24 hour period, there were approximately 350,000 cells in each receiver well.

4.3. Discussion

4.3.1. Establishment of ovarian cancer cell line motile capacity

Prior to this project, adherent epithelial ovarian cancer cell lines had been used in many experiments to study cancer *in vitro* (Comamala *et al.*, 2011; Flate and Stalvey, 2014; Zhao *et al.*, 2012). However, a comprehensive comparison of cell motility within a panel of ovarian cancer cell lines had not been carried out. Nine ovarian cancer cell lines (**Table 2.1**) were ranked in order of motile capacity using the scratch assay, with SKOV-3 cells found to be the most motile, and IGROV-1 cells the least motile (**Figure 4.4**). Establishment of the cellular motility status of these cell lines will assist ovarian cancer researchers in the future by influencing cell line choice in experimental design.

4.3.2. The association between cellular motile capacity, proliferation, and exosome secretion rates

The effect of cell proliferation on the ability of cells to heal the wound in the scratch assay was established (**Figure 4.5**). The speed at which cells grow and replicate was shown not to influence motility rates (**Figure 4.6**). In addition, there was no association between cellular motility and exosome secretion rates (**Figure 4.7**). These findings are important for the ovarian cancer research field. Investigation into the relationship between cell motility, proliferation, and exosome secretion rates will save researchers time, money and resources in the future; and will assist with selection of cell lines suitable for the experimental design. It was important to determine the effect of proliferation on cell motility to validate the use of the scratch assay for analysis of motile capacity of cell lines.

4.3.3. The effect of exosomes from motile cell lines on recipient cell motility rates

Exosomes derived from both OVCAR-5 and SKOV-3 cells were shown to increase the motility (assessed using the scratch assay) of SKOV-3 cells (**Figure 4.10**). A trend was established whereby exosomes derived from both OVCAR-5 and SKOV-3 cells were shown to increase the motility of OVCAR-5 cells (**Figure 4.8**) (although not to a statistically significant degree). However when the experiment was repeated in OVCAR-5 cells, to generate 12 biological replicates, the same results were not attained. When all 12 biological replicates were considered, OVCAR-5 and SKOV-3 exosomes did not consistently increase the motility of OVCAR-5 cells (**Figure 4.9**), despite the initial increase with three biological replicates shown in **Figure 4.8**. It was concluded that OVCAR-5 and SKOV-3 exosomes do not consistently induce increased OVCAR-5 cell motility.

In addition, several exosome swapping experiments with different exosome donor cell lines and different recipient cell lines were performed, but statistically significant differences in cell motility between control and exosome-treated cells were not found (results not shown). This suggests that more motile cell line-derived exosomes did not increase the motile capacity of less motile recipient cells, and vice versa.

Further experimentation with more scratch replicates would confirm whether exosomes from more motile cells can affect motility of recipient cells. Additionally, the trans-well migration assay (**Figure 2.6**) may provide an alternative method for analysis of cell migration and may generate more accurate results.

4.3.4. The effect of cell origin and chemotherapeutic resistance status on cell motility

4.3.4.1. Cell origin

The origin of each of the ovarian cancer cell lines is shown in **Table 2.1**. In terms of motility (average scratch closure speed), all nine cell lines were statistically significantly different from one another (calculated using the two tailed T-test) (**Table 4.1**), except for CP-70 (solid tumour) and OVCAR-3 (ascites); IGROV-1 (solid) and MCP-1 (ascites); A-2780 (solid) and OVCAR-4 (ascites); MCP-1 (solid) and OVCAR-4 (ascites). This indicates that the origin of the cell line does not affect its motile capacity. However, SKOV-3 and OVCAR-5, two of the most motile cell lines were derived from ascites whereas IGROV-1, the least motile cell line, was derived from the solid tumour mass. It was predicted that cells with a greater motile capacity would originate from the ascites as opposed to the solid tumour mass because these cells have acquired the ability to detach from the primary tumour; this phenotype is associated with cells of a metastatic nature (Brooks *et al.*, 2010).

4.3.4.2. Resistance to chemotherapeutics

A-2780 cell line was derived from a solid untreated ovarian tumour (Godwin *et al.*, 1992), MCP-1 were generated by culturing A-2780 cells in the presence of cisplatin and therefore have a moderate resistance to cisplatin (Anthoney *et al.*, 1996), CP-70 were also generated by culturing A-2780 cells in the presence of cisplatin but have a higher resistance to cisplatin than MCP-1, 10-fold greater than their A-2780 parental cell line (Louie *et al.*, 1985). CP-70 were statistically significantly more motile than both A-2780 and MCP-1 cell lines suggesting that with increased resistance to chemotherapeutics, cells acquire a more aggressive and migratory phenotype, this result is consistent with previous studies (Seo *et al.*, 2015; Yue *et al.*, 2012) (**Table 2.1**). This could

be further tested with different cell lines with varying resistance to different chemotherapeutic agents.

4.3.5. Experimental limitations

4.3.5.1. Constraints of using SKOV-3 cells for assessing the effect of exosomes on cell motility

Of the nine cell lines assessed, SKOV-3 cells have the greatest motility (**Figure 4.4B** and **Figure 4.5**). Because of their highly motile phenotype, it may be difficult to identify the effects caused by different types of exosomes. This could have been resolved, perhaps, by taking measurements of scratch area at more regular intervals, for example, every two hours. However, the four hour time interval was initially chosen for SKOV-3 cells as a compromise between collection of more frequent data points and the impact that regularly removing the cells from the incubator would have on the experimental results. To alleviate the issue of SKOV-3 cells healing the wound too quickly (before the effect of exosomes could be determined) OVCAR-5 cells, that have a reduced motile capacity compared with SKOV-3 cells, were used for most experimentation to investigate the effect of exosome swapping on cell motility.

4.3.5.2. Limitations of the scratch assay

There are a number of limitations of the scratch assay in comparison to other available methods to measure cell motility e.g. the trans-well migration/chemotaxis assay. The main disadvantage is that direct physiological relevance is poor (Cory, 2011). The Boyden chamber trans-well migration and invasion (Matrigel) assays are more representative of the processes undertaken by metastasizing tumour cells *in vivo* (Marshall, 2011).

Additionally, the assay is relatively long, 48 hours are required for growth of the cell monolayer and then a further 48 hours for scratch closure, for most cell lines (Liang *et al.*, 2007). Another disadvantage is that it is impossible to create the same size scratch twice, therefore all scratches were of varying widths (Liang *et al.*, 2007). Despite accounting for this during calculation of scratch width (by normalising data so that the time = 0 value equalled 100%), this prevented attainment of consistent results and created variation between scratches, even though multiple points along the same scratch were measured. For these reasons it was difficult to obtain the required number of replicates to reduce the amount of error to an acceptable level.

Furthermore, scratching the cell monolayer causes damage to the cells at the edge of the wound, and cells in the monolayer can become over-crowded. Both of these factors can prevent normal

cell migratory activity (Sammak *et al.*, 1997). In spite of these limitations, the *in vitro* scratch assay is the preferred method for analysis of cell migration as it is easy to establish, inexpensive, does not require any specialist materials and, most importantly, provides a good measure of cell motility (Liang *et al.*, 2007).

4.3.5.3. Excessive concentration of exosomes

The physiological concentration of exosomes in peripheral blood of healthy donors is currently predicted to be 5–50 µg/mL (Hunter *et al.*, 2008; Lee *et al.*, 2014; Müller, 2012). Efforts were made to determine exosome protein concentration prior to administration onto cells so that the amount of exosomes administered fell within this range. However, this involved multiple freeze-thaw cycles, which it is best to avoid so that the biological viability of the exosomes is not lost (Théry *et al.*, 2006). A decision was made not to quantify the exosomes prior to administration, and instead fresh exosomes were used immediately following extraction, with the anticipation that in future experimentation, the exosomes would be quantified following collection of preliminary data that supported the theory that exosomes from more motile cells had an effect upon recipient cell motility. Unfortunately lacking confidence in the data collected meant that this experiment was not optimised further.

Since the exosome dose administered to the cells in the scratch assay exceeded the predicted physiological concentration, one third of the exosomes extracted from a T175 flask (exosomes secreted from approximately 3 million cells in 24 hours) was administered to a single well of a 24-well plate (seeded at 220,000 OVCAR-5 cells or 350,000 SKOV-3 cells). Since SKOV-3 cells were the most motile cell line tested, an increase in SKOV-3 cell motility may have suggested that the effect of exosomes upon motility was concentration dependent, rather than specific to the cell line that the exosomes were derived from.

4.3.5.4. Scratch width at 24 hours is not an accurate measure of cell motility

Scratch width at 24 hours is a commonly used method for assessing cellular motile capacity (Funari *et al.*, 2013; Wang *et al.*, 2013). The statistical analysis performed to describe the relationship between exosome secretion rates, and cell motility in terms of scratch width at 24 hours, involved two points (for SKOV-3 and OVCAR-8) where the scratch width at 24 hours was 0 because the cells were very motile and healed the wound within this time period. It may have been more effective to use the 12 hour time point for this analysis; although, the majority of the

cell lines tested, the differences in cell motility were not distinguishable between the different cell lines using the 12 hour time point.

4.3.6. Experimental improvements

4.3.6.1.   Time-lapse visualisation

Had the technology been available in our department, it would have been ideal to make time-lapse video recordings of the cells moving throughout the scratch assay. An environmental control chamber that would maintain the cells at 37°C and 5% CO_2 was required to collect this data. This would have allowed the identification of cells that moved the fastest, that moved first (following scratch creation), and those that moved the slowest or did not move among the population that were associated with each scratch. This would also have made it easier to identify whether scratch closure was because of cell proliferation rather than cell movement. Alternatively, more regular observations of scratch width could have been made to better estimate cell motility, 12 hours between data collection points (6 hours for SKOV-3 cells) may not have been sufficient to accurately determine cell motility.

4.3.6.2.   Immunocytochemistry

To investigate the phenotypes of motile cells further, immunocytochemical analysis of EMT markers may have revealed a relationship between more motile cell lines and less motile cell lines. E-cadherin is a tumour suppressor gene that also acts as a marker of EMT and is regularly used not only in academic research, but also in the clinic to determine patient prognosis (section **1.2.2.1**) (Takai *et al.*, 2014). Additionally vimentin, a marker of mesenchymal cells, is used to recognise mesenchymal-like cells and can identify cells that have undergone or are in the later stages of EMT (section **1.2.2.1**). Increased vimentin expression has been associated with increased motility and invasiveness of prostate cancer cells. Furthermore, in the same study E-cadherin and vimentin expression had an inversely linear relationship (Zhao *et al.*, 2008).

It would be interesting to investigate whether more motile cells associated with the scratch express greater levels of vimentin compared with E-cadherin. Additionally, cells may alter their phenotype in response to creation of the scratch, e.g. cells along the scratch edge may start to express more vimentin. Perhaps, in the cell lines that have a more stationary phenotype E-cadherin expression is greater than vimentin. These questions could be answered using this immunocytochemical staining method.

4.4. Conclusion

Because of the inconsistency in statistically significant results when treating OVCAR-5 and SKOV-3 cells with OVCAR-5 and SKOV-3 exosomes, and the inability to detect changes in cell motility as a result of other exosome swapping experiments, the hypothesis that exosomes derived from highly motile ovarian cancer cell lines increase the motile capacity of inherently less motile ovarian cancer cell lines was not supported. Exosomes, irrespective of their cell of origin, had no clear effect on cell migration. It appears that unlike in breast cancer (Harris *et al.*, 2015), more motile ovarian cancer cell line-derived exosomes do not affect motility of less motile ovarian cancer cell lines. An explanation for this may be that ovarian cancer metastasis has a similar, yet distinct, mode of action to breast cancer metastasis. Ovarian cancer metastasis occurs when metastatic cells evade the ovarian tumour into the peripheral environment and travel to secondary organs in the peritoneal fluid (**Figure 1.3**, section **1.2.3**). Whereas metastatic breast cancer cells must develop the ability to hijack the circulation in order to access to secondary sites (**Figure 1.2**, section **1.2.1**). Although these metastatic mechanisms differ, they both rely greatly upon cancerous cells increasing their motile capacity compared with healthy cells. It is likely that exosomes derived from more motile cells affect less motile cells through a different mechanism, possibly their invasive capacity is affected. The trans-well migration/chemotaxis assay assesses the invasive capacity of cells, and is possibly more physiologically relevant than the scratch assay in terms of testing cell motility and invasive potential (Cory, 2011; Liang *et al.*, 2007), therefore this assay may be more suitable for determining the effect of exosomes upon cell migration.

4.4.1. Future direction

Exosomes derived from cells that have undergone stress have been shown to affect recipient cells in various ways. In collaboration with Professor Munira Kadhim, our group were the first to show that exosomes are involved in mediating radiation-induced bystander effect, whereby non-irradiated cells that received exosomes derived from irradiated cells exhibited DNA damage characteristics corresponding to those of irradiated cells (Al-Mayah *et al.*, 2012). Other studies have shown that exosomes derived from cells stressed by radiation, hypoxia and oxidative stress contribute to neighbouring cell resilience to stress (Arscott *et al.*, 2013; Eldh *et al.*, 2010; Salomon *et al.*, 2013b). Until now, there have been no published studies that investigate the effect of heat shock cell-derived or chemotherapy treated cell-derived exosomes upon recipient cell invasive capacity. Therefore the hypothesis that cells stressed by heat shocking or chemical stress (chemotherapeutics) have the ability to increase cell migration in recipient cells was investigated in **Chapter 5**.

Chapter 5

The effect of stressed cell-derived exosomes upon the invasive capacity of cancer cell lines *in vitro*

5. The effect of stressed cell-derived exosomes upon the invasive capacity of cancer cell lines *in vitro*

5.1. Introduction

5.1.1. Cellular stress response

Tissue homeostasis ensures that equilibrium is maintained between cell proliferation and death rates (Lockshin and Zakeri, 2007). Stress stimuli imbalance this physiological mechanism causing potential harm to the organism because excessive loss or gain of tissue is fatal. Cellular stress response is the term used to describe a number of different mechanisms that occur inside the cell as a result of environmental stress. The most common stressors include extremes of temperature and exposure to toxins. Cells respond to stress in various different ways. One approach is to activate mechanisms to promote cell survival; alternatively, programmed cell death pathways are triggered to eliminate damaged cells (Fulda *et al.*, 2010). There is an immediate stress response that has the purpose of maximising imminent cell survival, minimising damage to overall cell integrity, and helping the cell recover from the insult. If the toxic stimulus is unresolved and exceeds the stress resilience threshold then cell death processes are activated (Perkins and Gilmore, 2006; Weston and Davis, 2007). There is also is long-term cellular stress response that increases cellular resilience to subsequent exposure to environmental stresses (Fulda *et al.*, 2010).

5.1.2. Stress proteins

Cellular stress is tackled by a family of proteins called 'stress proteins'. Stress proteins often are not restricted to function during periods of stress, many are also essential to the function of cells in a normal environment (Calabrese *et al.*, 2010). Since a cell's survival depends on its ability to mount an appropriate response to environmental or intracellular stress, stress proteins are well conserved across phyla. Similarities in the expression pattern of stress proteins is maintained from singular prokaryotic cells through to cells of complex eukaryotic organisms (Fulda *et al.*, 2010).

5.1.3. The heat shock response

The heat shock response is a protective response activated by extreme temperature but also by other types of stress. It was originally described as a response to mild increases in temperature of only 3–5°C above normal (Craig, 1985; Lindquist and Craig, 1988). Heat stress causes protein damage that causes accumulation of unfolded protein aggregates. In response to this the cell

increases chaperone protein, namely HSP, activity inside the cell, which improves the protein folding capacity of the cell. Misfolded proteins are refolded, alleviating protein aggregation; hence, cell survival is promoted. This process confers transient protection, otherwise known as thermotolerance, whereby cells become more resistant to subsequent stress stimuli (Fulda *et al.*, 2010; Pallepati and Averill-Bates, 2011).

5.1.4. Heat shock proteins

HSPs (also exosome marker proteins, section **1.4.3.2**) are a group of evolutionary conserved proteins that are either constitutively expressed e.g. HSP90 or are inducible e.g. HSP70. HSP90 not only has chaperone duties but also prevents premature folding of nascent polypeptides (Lindquist and Craig, 1988). HSP70 is expressed at low basal levels and expression increases in response to stressors (Samali and Orrenius, 1998). HSP70 has been shown to protect the cell from induction of controlled cell death by directly inhibiting cell death pathways and indirectly by pro-survival protein refolding activity (Hartl and Hayer-Hartl, 2002). HSP70 also inhibits downstream c-Jun N-terminal kinases (JNK)-pro-apoptotic activity (Gabai *et al.*, 2000; Mosser *et al.*, 1997; Park and Liu, 2001).

5.1.5. DNA damage response

Stress conditions caused by chemotherapeutic agents induce DNA damage as an initial response. DNA double-strand breaks (DSBs) are considered a key lesion in activation of the DNA damage response. Depending upon the type of lesion, DNA damage initiates one of several repair pathways. Following a DSB, two major mechanisms responsible for DNA repair are non-homologous end joining (which involves the DNA-PK repair protein), and homologous recombination. These processes restore the continuity of the DNA double strand (Jackson, 2002; Valerie and Povirk, 2003). Mismatch repair subsequently corrects any mistakes made during DNA repair (Stojic *et al.*, 2004). Cisplatin is a crosslinking agent that forms platinum-DNA adducts and subsequently produces DSBs; as a result, cell division is disrupted and induction of apoptosis ensues (Roos and Kaina, 2006; Takahara *et al.*, 1995). Cisplatin is a standard chemotherapy drug in the treatment of ovarian cancer patients (Helm and States, 2009).

5.1.6.   The role of exosomes in transferring stress-tolerance to neighbouring cells

Our research group has shown that CP-70 cisplatin-resistant cells can transfer resistance to A-2780 cisplatin-sensitive cells via exosomes (Pink *et al.*, 2015). These results initiated the theory that protection against other types of cell stress may also be communicated between cells through exosomes. Other research groups have published data that supports this concept, as described below.

5.1.6.1.   Radiation stress

Our group (in collaboration with Professor Munira Kadhim) have shown that exosomes extracted from irradiated MCF-7 cells can transfer resilience to radiation stress to naïve MCF-7 cells, via exosomes, in a RNA dependent manner (Al-Mayah *et al.*, 2012). DNA damage increased in cells that had not been irradiated but had received exosomes from irradiated cells (Al-Mayah *et al.*, 2012). A similar study in glioblastoma cells and normal astrocytes also showed that exosomes released by cells that had been exposed to radiation stress were able to increase cell migration in recipient cells (Arscott *et al.*, 2013).

5.1.6.2.   Hypoxia

It has been shown that under hypoxic conditions epidermoid (Park *et al.*, 2010), breast (Wang *et al.*, 2014), and prostate (Ramteke *et al.*, 2015) cancer cells produce exosomes that have the ability to stimulate invasion and metastasis in recipient cells. More than 50% of the proteins secreted by epidermoid cancer cells under hypoxia were found to be associated with the exosome population. Additionally, many of these proteins were identified to have functions in the control of metastasis, hence, it was predicted that exosomes derived from cells under hypoxic conditions may support increased metastatic activity in recipient cells (Park *et al.*, 2010). Hypoxia increased the concentration of exosomal C4.4A; a protein known for its involvement in wound healing, tissue remodelling and cell motility (Ngora *et al.*, 2012). Prostate cancer exosomal proteome analysis identified a higher protein concentration in hypoxic exosomes (160 proteins) compared with control exosomes (62 proteins). Hypoxic exosome proteins were mostly associated with the remodelling of epithelial adherens junction pathway. This protein signature encompasses proteins that have the ability to increase cellular invasiveness and modulate the microenvironment; thus, supporting prostate cancer progression (Ramteke *et al.*, 2015).

5.1.6.3.   Oxidative stress

Pre-treating cells with exosomes derived from cells that had undergone oxidative stress provided protection against subsequent oxidative stress in the recipients, measured as an attenuated loss of cell viability (Eldh *et al.*, 2010). Furthermore, microarray analysis identified that exosomal mRNA content differs between exosomes derived from cells grown under conditions of oxidative stress compared with normal conditions (Eldh *et al.*, 2010).

5.1.7. Inhibition of stress exosome induced responses

5.1.7.1.   Exosome uptake inhibition

Several agents have been used by other research groups to inhibit exosome uptake (Mulcahy *et al.*, 2014) including Heparin (Christianson *et al.*, 2013; Franzen *et al.*, 2014) and proteinase K (Escrevente *et al.*, 2011). These agents were chosen for optimisation in our lab to investigate the effects of inhibition of stress exosome uptake.

5.1.7.2.   Inhibition of the DNA-PK protein

NU7441, an inhibitor of DNA-PK, was used in this project to inhibit the non-homologous end joining and homology-directed repair pathways of DNA repair that are mediated by DNA-PK (Smith and Jackson, 1999).

5.1.8. Evidence for increased exosome secretion following stress

There is substantial evidence to suggest that the concentration of exosomes secreted by cancer cells increases with disease progression (Muralidharan-Chari *et al.*, 2010), but the molecular mechanisms regulating the biogenesis of exosomes have not been described. The concentration of exosomes secreted by stressed cells has been shown to increase in response to heat stress (Clayton *et al.*, 2005), exposure to anti-cancer drugs (Lv *et al.*, 2012), irradiation (Al-Mayah *et al.*, 2015; Jella *et al.*, 2014), and hypoxia (King *et al.*, 2012; Ngora *et al.*, 2012; Salomon *et al.*, 2013a; Wang *et al.*, 2014); suggesting that exosomes have a functional role in intercellular communication following stress. Stress-induced exosome release has been shown to occur within 20 minutes (Koumangoye *et al.*, 2011). Further molecular studies are required to determine whether there are qualitative differences in cargo carried by exosomes generated in stressed cells compared with control cells (Wang *et al.*, 2014).

5.1.9. Cellular invasive capacity

One of the rate-limiting steps of the metastatic cascade is basement membrane penetration (Brooks *et al.*, 2010; Volk *et al.*, 1984). Invasion results from a combination of abnormal cell motility, reduced cellular cohesion, and production of proteolytic enzymes (Chambers *et al.*, 2002; Fidler, 2003); metastasis follows, where formation of secondary tumours at distant sites occurs.

5.1.9.1. Proteolytic enzymes

Protease activity is tightly regulated under normal conditions and is typically required for processes including ovulation (Hulboy *et al.*, 1997) and mammary gland involution (Wiesen and Werb, 2000). These control mechanisms are lost during metastasis enabling ECM degradation and subsequent cell invasion (section **4.1.1**). Binding of the tumour cell to the basement membrane triggers signal transduction pathways that result in the release of several hydrolytic enzymes that are responsible for ECM breakdown (Brooks *et al.*, 2010). These enzymes are either released by the tumour cells themselves, or by neighbouring cells (Price *et al.*, 1997). Examples of proteolytic enzymes associated with metastasis include: urokinase-type plasminogen activator protein (Danø *et al.*, 2005; Duffy *et al.*, 1999; Duffy, 2004), cathepsins (Price *et al.*, 1997), and several MMPs (Blood and Zetter, 1990; Brown, 1999; Deryugina and Quigley, 2006; Egeblad and Werb, 2002).

5.1.10. Matrigel trans-well assay

To establish the invasive capacity of nine ovarian cancer cell lines the Matrigel trans-well invasion assay was used. Matrigel is a solubilised basement membrane formulation encompassing mostly laminin, collagen IV, and heparan sulphate proteoglycan extracted from the Engelbreth-Holm-Swarm mouse sarcoma (Kleinman *et al.*, 1982). Matrigel is coated onto the trans-well membranes with 8.0 μm pores and acts as a barrier to invading cells. Metastatic cells are able to attach and invade the Matrigel, and subsequently pass through the 8.0 μm pores (Marshall, 2011). The trans-well Matrigel invasion assay assesses the invasive capacity of cells and is more physiologically relevant than the scratch assay in terms of testing cell motility and metastatic potential (Cory, 2011; Kenny *et al.*, 2009; Liang *et al.*, 2007). This assay has been used extensively in cancer research to investigate the complex mechanisms that contribute to cell invasiveness and metastasis.

5.1.11. Hypothesis

Exosomes derived from metastatic cells have been shown to influence the invasive capacity of recipient cells. Additionally, previous studies have shown that exosomes can transfer protection to stress from cells that have experienced stress to naïve cells. Since the adaptive response of cells to stress correlates with cell fate, it is likely that cells undergoing stress communicate with their neighbours to help prepare them for adverse environmental stimuli and, hence, promote survival of the organism. It was hypothesised that exosomes mediate transfer of signals that increase invasiveness in recipient cells and provide a vehicle for transfer of stress precautionary messages to neighbouring cells.

5.2. Results

5.2.1. Invasive capacity of cancer cell lines

In addition to the scratch motility assay, the trans-well migration and trans-well invasion assays were performed to further investigate some aspects of the invasive potential of the nine ovarian cancer cell lines of interest. The MCF-7 breast cancer cell line was also assessed using the trans-well migration and invasion assays. The trans-well migration assay, like the scratch assay, also assesses cell motility but in terms of the cell's ability to pass through a membrane with 8.0 µm pores as opposed to the ability of the cells to close a scratch. This migration assay also assesses cellular chemotaxis, in terms of the movement of cell towards an environment with a higher concentration of serum. The trans-well invasion assay investigates the same principle, however, the cells must also have the ability to adhere to, then sufficiently degrade and invade an artificial ECM barrier, in addition to passing through the semi-permeable membrane.

Cells were seeded in trans-wells that had membranes with 8.0 µm pores. Uncoated membranes were used for the trans-well migration assay, whilst ECM invasion-testing membranes were used for the trans-well invasion assay, these were supplied pre-coated in Matrigel (BD Biosciences). Cells were left to migrate/invade over a 24 hour period. The cells that successfully passed through the membrane were stained and counted. Migration/invasion was calculated by counting the number of cells on the base of the membrane following the migration/invasion period. A diagram of the Matrigel trans-well assay is shown in **Figure 2.6**. The invasive capacity of ten cancer cell lines was established using the Matrigel invasion assay. Cell invasion through uncoated membranes was indicative of the proportion of cells that had the ability to compress and pass through membranes. Cells that can pass through Matrigel coated membranes have the additional capacity to sufficiently degrade and invade ECM. CP-70, MCP-1, OVCAR-4, OVCAR-5, OVCAR-8, and SKOV-3 cells were all statistically significantly more capable of invading uncoated membranes than Matrigel coated membranes. This was calculated using the one tailed T-test that generated p values of 3.39×10^{-5}, 5.39×10^{-6}, and 5.73×10^{-6}, respectively (**Figure 5.1**). This indicates that these cell lines have the capacity to pass through porous membranes but have reduced ability to degrade and invade ECM. OVCAR-5 and SKOV-3 cells were both more invasive than the other cell lines through both uncoated and Matrigel membranes. When seeded at 100,000 cells/trans-well insert, on average 21,272 SKOV-3 cells invaded Matrigel membranes. For OVCAR-5 cells an average of 8525 cells had the capacity to invade Matrigel membranes (**Figure 5.1A**). This suggests that of the ten cell lines, OVCAR-5 and SKOV-3 cells are the most invasive through both porous membranes and Matrigel membranes. SKOV-3 cells are the most efficient at degrading ECM

allowing for subsequent membrane invasion. See Appendix B (**8.2**) for raw migration and invasion data.

Aside from OVCAR-5 and SKOV-3 cells, the other cell lines had reduced invasive capacity. This is shown in **Figure 5.1B**, where data for OVCAR-5 and SKOV-3 was removed to show the differences between the eight less invasive cell lines more clearly.

CP-70, MCP-1, OVCAR-4, and OVCAR-8 cells have intermediate capacity to invade membranes, of the ten cell lines tested, and this was statistically significantly prevented by artificial ECM (Matrigel). CP-70 cells were approximately 35 times more efficient at crossing uncoated membranes than Matrigel coated membranes, with 2828 cells on average capable of penetrating uncoated membranes and 81 cells capable of penetrating Matrigel membranes. An average of 2731 MCP-1 cells were capable of migrating across the uncoated membrane and 112 through the Matrigel membrane. On average, 6176 OVCAR-8 cells penetrated the uncoated membrane compared with 307 that invaded the Matrigel membrane. IGROV-1 cells were approximately three times more effective at migrating through uncoated membranes, with 2725 invasive cells compared with an average of 895 cells capable of invading Matrigel membranes. OVCAR-4 cells were the third most invasive cells, after OVCAR-5 and SKOV-3 cells, with 10,616 cells on average capable of crossing the uncoated membrane and 67 capable of penetrating the Matrigel membrane.

A-2780, MCF-7, and OVCAR-3 cell lines were the least invasive, and the presence of the ECM layer did not have a great effect on invasion (**Figure 5.1**). For MCF-7 cells, the number of invasive cells was greater in the presence of the Matrigel layer, with an average of 303 cells invading the uncoated membrane and 527 cells penetrating the Matrigel membrane. For A-2780 cells, there was little difference in the number of cells capable of invading the uncoated and Matrigel membranes with an average of 528 and 450, respectively. OVCAR-3 cells were the least invasive with an average of 99 and 50 invasive cells for uncoated and Matrigel membranes, respectively.

Representative images of the trans-well membranes further support these results. It is clear to see that SKOV-3 cells were the most migratory (**Figure 5.1C**) and invasive (**Figure 5.1D**), followed by OVCAR-5 cells, then OVCAR-4 cells. OVCAR-3 cells were the least invasive.

After investigating some aspects of the invasive potential of the cells using the scratch, trans-well migration and trans-well invasion assay, it was confirmed that SKOV-3 cells were both the most motile and invasive, and IGROV-1 cells were both the least motile and invasive (**Figure 4.4A&B** and **Figure 5.1**).
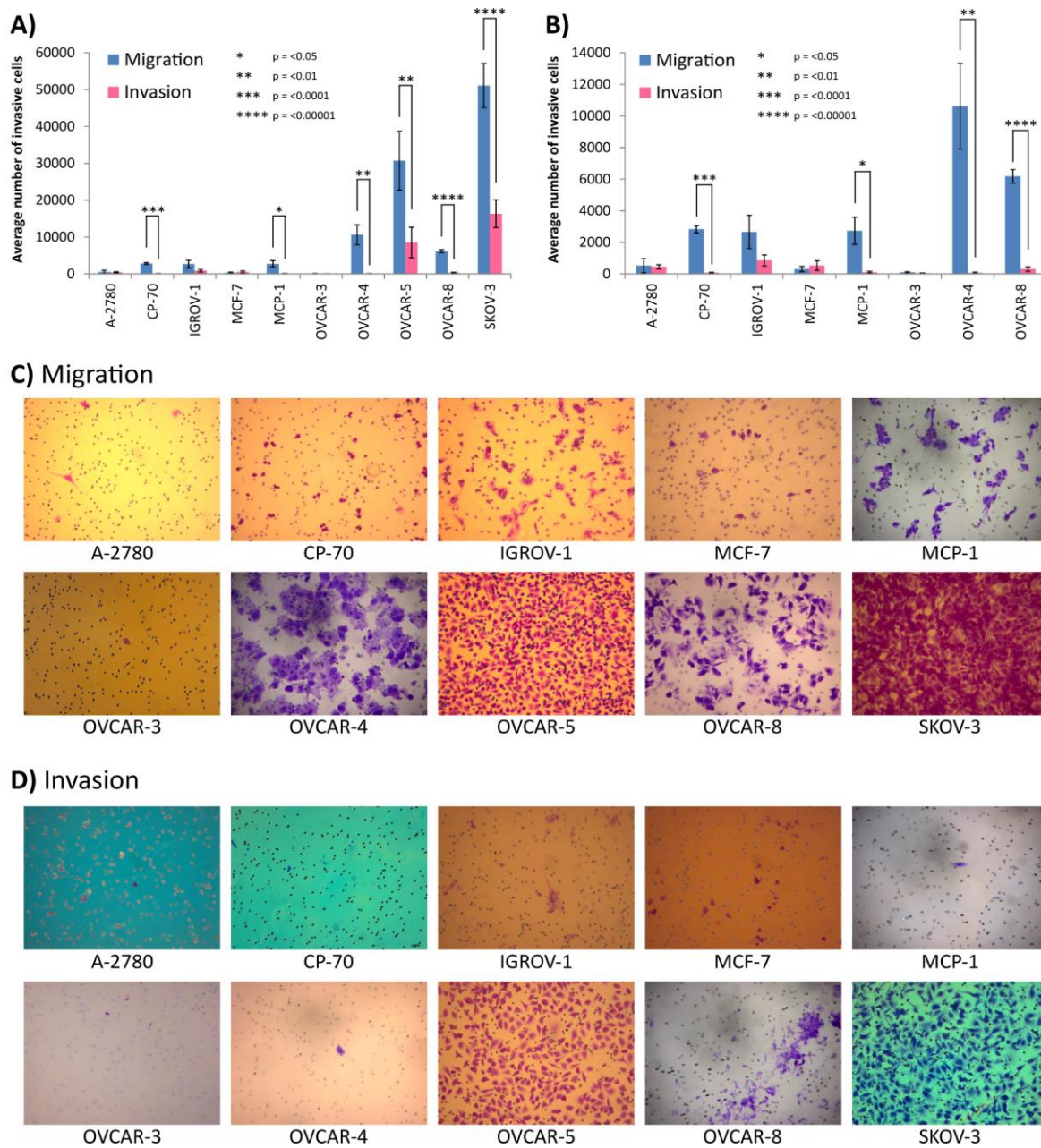
Figure 5.1: Invasive capacity of ten cancer cell lines. Cells were starved of FBS for 24 hours prior to being seeded at 100,000 cells/trans-well. Trans-wells had membranes with 8.0 µm pores coated in Matrigel or uncoated membranes. 10.0% FBS was used as chemoattractant; cell invasion over 24 hour period was calculated. A) The average number of cells with migratory and invasive capacities of each cell line through uncoated and Matrigel coated membranes. B) Zoomed in version of graph shown in A) without OVCAR-5 and SKOV-3 cell lines. C) Representative images of the Matrigel and uncoated membranes following the invasion period and crystal violet staining. Each sample group contained six biological replicates, within each replicate there were five technical replicates. Error bars represent standard error of the mean of the biological replicates. P values were calculated using the one tailed T-test.

5.2.2. Correlation between cell invasiveness, migratory phenotype, and motile capacity

The correlation between cell invasiveness and migration rate shows that there was a strong relationship between these two cellular phenotypes (**Figure 5.2A**). The regression line represents a Pearson's correlation coefficient of 0.987 (p = <0.001) demonstrating the nature of the

relationship between the two sets of data. The R^2 value of 0.987 and Spearman's rank correlation coefficient of 0.394 indicate that the invasion and migration rates have a strong linear but weakly monotonic relationship. The Grubbs' test was applied to identify outliers between cell invasiveness and migration rate. The Grubbs' test confirmed that in terms of cell invasiveness, OVCAR-5 and SKOV-3 cells were outliers; in terms of migration rate, OVCAR-4, OVCAR-5, and SKOV-3 cells were outliers. When the OVCAR-4, OVCAR-5, and SKOV-3 anomalous data points were removed, the relationship between cell invasiveness and migration rate changed from positive to neutral (no clear relationship) (**Figure 5.2B**). The R^2 value was <0.001, the Pearson's correlation coefficient was -0.013 (p = 0.978), and the Spearman's rank correlation coefficient was -0.036, suggesting no correlation between cell invasiveness and migration rate once the outliers had been removed.

For cell invasiveness versus motility (**Figure 5.2C**), the Pearson's correlation coefficient was calculated as 0.786 (p = 0.012) indicating that there was a moderately positively correlated relationship between these cellular characteristics. The R^2 value of 0.618 suggests that cell motility and invasiveness have a weak linear relationship. Spearman's rank correlation coefficient was calculated as 0.233, further indicating a weakly monotonic relationship. The Grubbs' test identified no outliers in the motility dataset, but OVCAR-5 and SKOV-3 cell data points were outliers in the cell invasiveness dataset. When the OVCAR-5 and SKOV-3 anomalous data points were removed, the relationship between cell invasiveness and motile capacity changed from moderately positive to weakly positive. The R^2 value was 0.094, the Pearson's correlation coefficient was 0.306 (p = 0.504), and the Spearman's rank correlation coefficient was 0.214, suggesting weak positive correlation between cell invasiveness and motile capacity, once the outliers had been removed.

For cell migratory phenotype versus motile capacity (**Figure 5.2E**), the regression line represents a Pearson's correlation coefficient of 0.805 (p = 0.009) signifying a positively correlated relationship between these cellular characteristics. The R^2 value of 0.649 indicates that cell motility and migratory rates have a weak linear relationship. Spearman's rank correlation coefficient was calculated as 0.600, indicating a moderately monotonic relationship. Since increased cell motility is required for increased cell migration, an association between these two cellular characteristics was anticipated. When the OVCAR-4, OVCAR-5, and SKOV-3 anomalous data points were removed, the positive correlation between cell migration rate and motile capacity became slightly weaker. The R^2 value was 0.611, the Pearson's correlation coefficient was 0.782 (p = 0.066), and the Spearman's rank correlation coefficient was 0.257, suggesting weak positive correlation between cell migration rate and motile capacity once the outliers had been removed.

Cell invasiveness, migratory abilities and motility are acquired by cells as they become more metastatic, therefore, as predicted, there was an association between all three of these cellular characteristics.
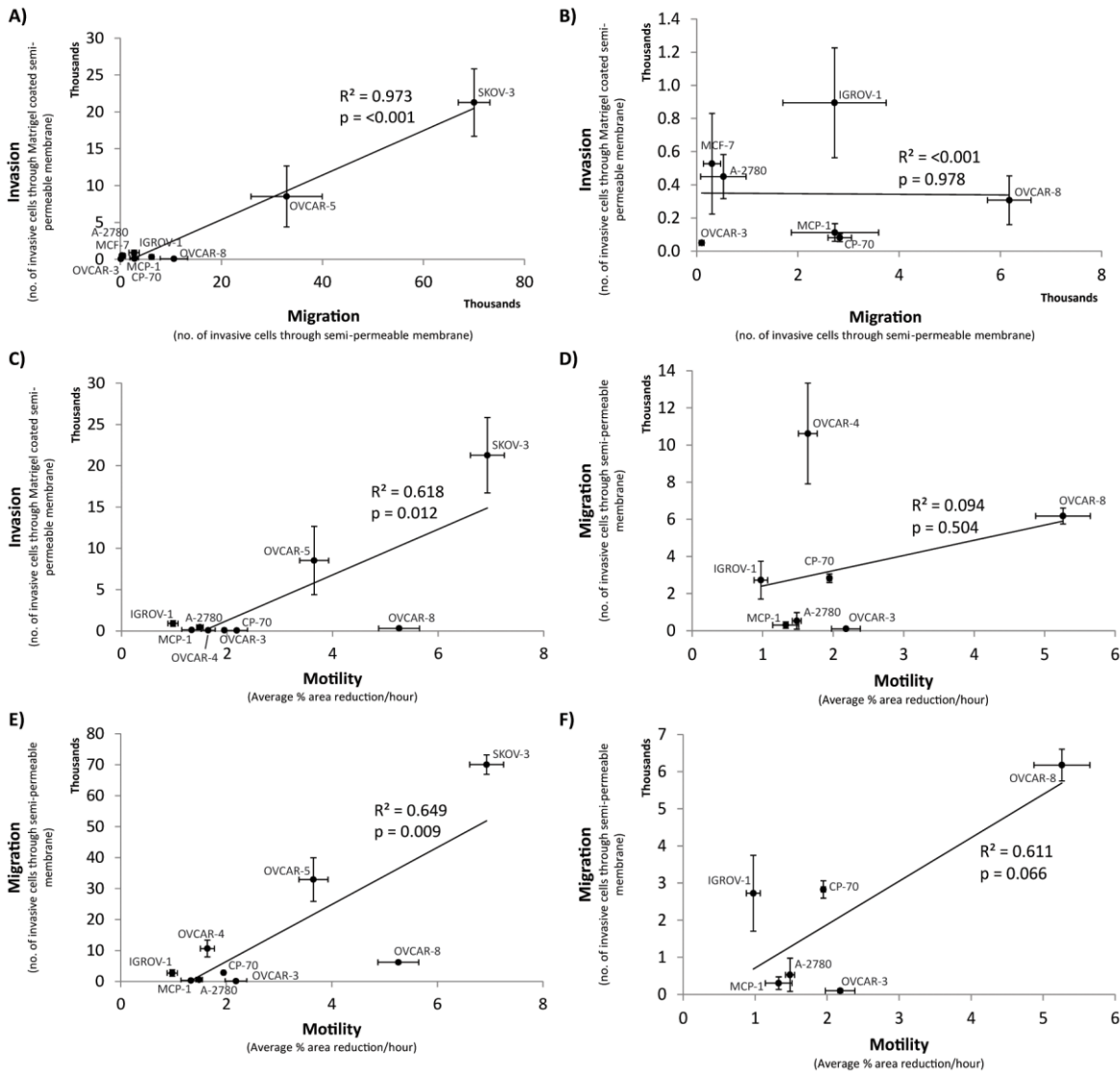
Figure 5.2: Correlation between invasion with migration and motility rates of nine ovarian and one breast cancer cell lines. Nine ovarian and one breast cancer cell lines were assessed for their invasive capacity using the Matrigel trans-well invasion assay, migratory capacity was determined using the trans-well migration/chemotaxis assay and motile capacity using the scratch assay. A) The relationship between cell invasiveness and migratory phenotype in terms of the ability of cells to cross semi-permeable membranes. B) Correlation between cell invasiveness and migratory phenotype excluding the OVCAR-4, OVCAR-5, and SKOV-3 anomalies. C) The relationship between cell invasiveness and motile capacity in terms of the speed at which cells could close a scratch. D) Correlation between cell invasiveness and motile capacity excluding the OVCAR-5 and SKOV-3 anomalies. E) The relationship between cellular migratory phenotype and motile capacity in terms of the speed at which cells could close a scratch. F) Correlation between cellular migratory phenotype and motile capacity excluding the OVCAR-4, OVCAR-5, and SKOV-3 anomalies. The correlation between the different cellular characteristics for each cell line is shown. R^2 and p values were calculated using the Pearson's correlation coefficient.

5.2.3. Heat stress method validation by western blotting

Hyperthermia is a treatment for cancer, used alongside other anti-cancer therapies because heat shocking malignant cells has been shown to increase their sensitivity to radiation and some chemotherapy drugs. Heat is applied to a small area, in the form of microwaves, radiowaves, or ultrasound. The location of the tumour influences the heat-shocking method used (van der Zee, 2002; Wust *et al.*, 2002). People with cancer who have received heat treatment have been shown to have increased five year survival rates (Colombo *et al.*, 2011). However, high heat also traumatises and damages cells, often leading to cell death. This is ideal when the tumour cells are affected; however there may also be off-target effects in neighbouring cancer cells and surrounding tissues (Wust *et al.*, 2002). To determine the effect of exosomes derived from heat shocked cells on recipient cancer cells, a number of trans-well invasion experiments were performed.

To verify that the heat shocking procedure was sufficiently stressing cells and inducing a cellular response to increased temperature, heat shocked cell protein lysates were probed for HSP70 (and GAPDH as a positive/loading control). Three protein samples of heat shocked and control cells were loaded into a gel and electrophoresis was performed (**Figure 5.3A**). The protein was transferred from the gel (**Figure 5.3B**) onto a membrane (**Figure 5.3C**) and the membrane was probed for HSP70 first (**Figure 5.3D**), followed by detection of GAPDH as a positive/loading control (**Figure 5.3E**) to show that the protein samples were viable. The HSP70 band had partially washed away during probing for GAPDH. The blot shows that HSP70 is more concentrated in the heat shocked cells. GAPDH was comparable across the six cell samples, indicating that HSP70 was upregulated in the heat shocked cells as part of the stress response.

The relative intensities of WB bands (**Figure 5.3**) were quantified using Image Lab software version 5.2.1. Control cell band intensity was used as the reference band for each antibody. This confirmed that heat shocking MCF-7 cells at 45°C for 1 hour was sufficient to induce the heat shock response, since the p value was 0.001 for the difference in intensity of the HSP70 bands in control cells compared with heat shocked cells (**Table 5.1**). The positive/loading control GAPDH bands were not statistically significantly different in intensity suggesting that the increased band intensity observed in HSP70 bands for the heat shocked cells is because of an increase in protein expression rather than an error in sample loading.

Table 5.1: The relative intensities of HSP70 and GAPDH bands on Figure 5.3 western blots of heat shocked MCF-7 cells compared with control MCF-7 cells.

Sample	Relative intensity					
	HSP70 (Figure 5.3D)	Average (STEM)	Student's two tailed T-test	GAPDH (Figure 5.3E)	Average (STEM)	Student's two tailed T-test
Control 1	1.00			1.00		
Control 2	0.77			1.56		
Control 3	0.53	**0.767** (0.136)		0.92	**1.160** (0.201)	
Heat shock 1	2.16			0.81		
Heat shock 2	2.50			0.84		
Heat shock 3	2.62	**2.427** (0.138)	**0.001**	1.58	**1.077** (0.252)	**0.809**
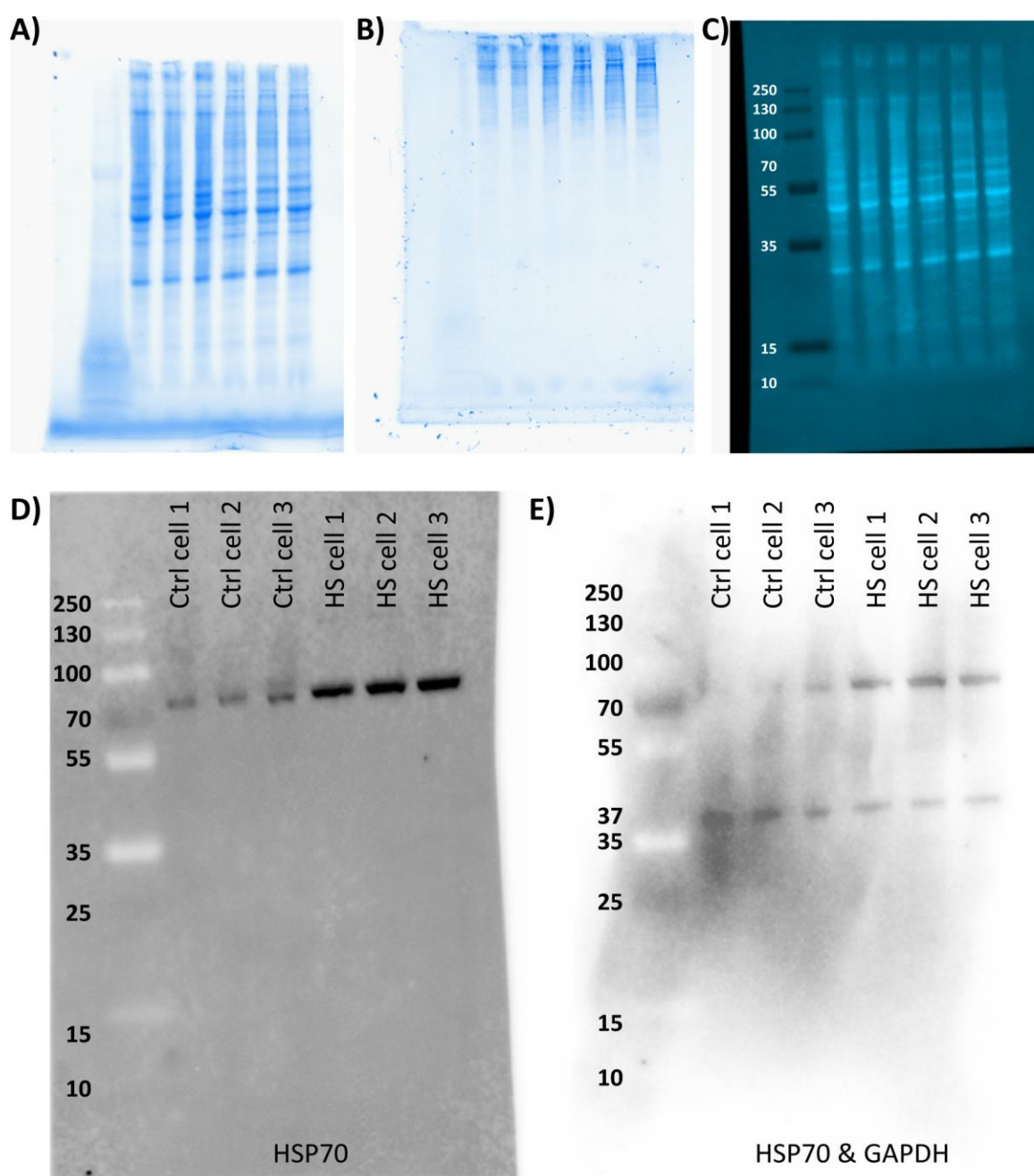
Figure 5.3: Validation of heat shocking stress procedure by western blotting. A) Gel electrophoresis of three heat shocked and three control cell protein samples, 2.829 second exposure of stain-free gel. B) Polyacrylamide gel after transfer of protein onto PVDF membrane, 2.829 second exposure of stain-free gel. C) Stain-free PVDF membrane after protein transfer. D) Blot after probing with anti-HSP70 antibody. E) Blot after probing with anti-GAPDH antibody (blot was initially probed for HSP70).

5.2.4.   The effect of heat shocked cell-derived exosomes on invasive behaviour of cancer cells

The effect of heat shocked cell-derived exosomes (heat shock exosomes) on invasive capacity of four cancer cell lines: MCF-7, IGROV-1, OVCAR-5, and SKOV-3, was investigated. To determine whether heat stress exosomes can increase invasive capacity of cells, parental cells were incubated at 45°C for 1 hour then returned to 37°C atmosphere for 23 hours; exosomes were collected from the tissue culture media and incubated with serum-starved cells for 24 hours. The stress exosome collection procedure was repeated 24 hours later and a second batch of heat shock exosomes were added to the cells immediately after they had been seeded in the Matrigel trans-well assay. The effect of heat stress exosomes on invasive capacity compared with cells treated with control cell-derived exosomes (control exosomes) was established. A one tailed T-test value of 0.015 confirmed that invasive capacity of MCF-7 cells increased in the presence of heat shock exosomes compared with cells that received control exosomes (**Figure 5.4**). Invasive capacity of three other cell lines (IGROV-1, OVCAR-5, and SKOV-3) showed the same trend but the increase in invasiveness was not significant. These results suggest that following heat-induced stress response the exosomes released by MCF-7 cells have the ability to induce greater invasive potential in neighbouring cells.
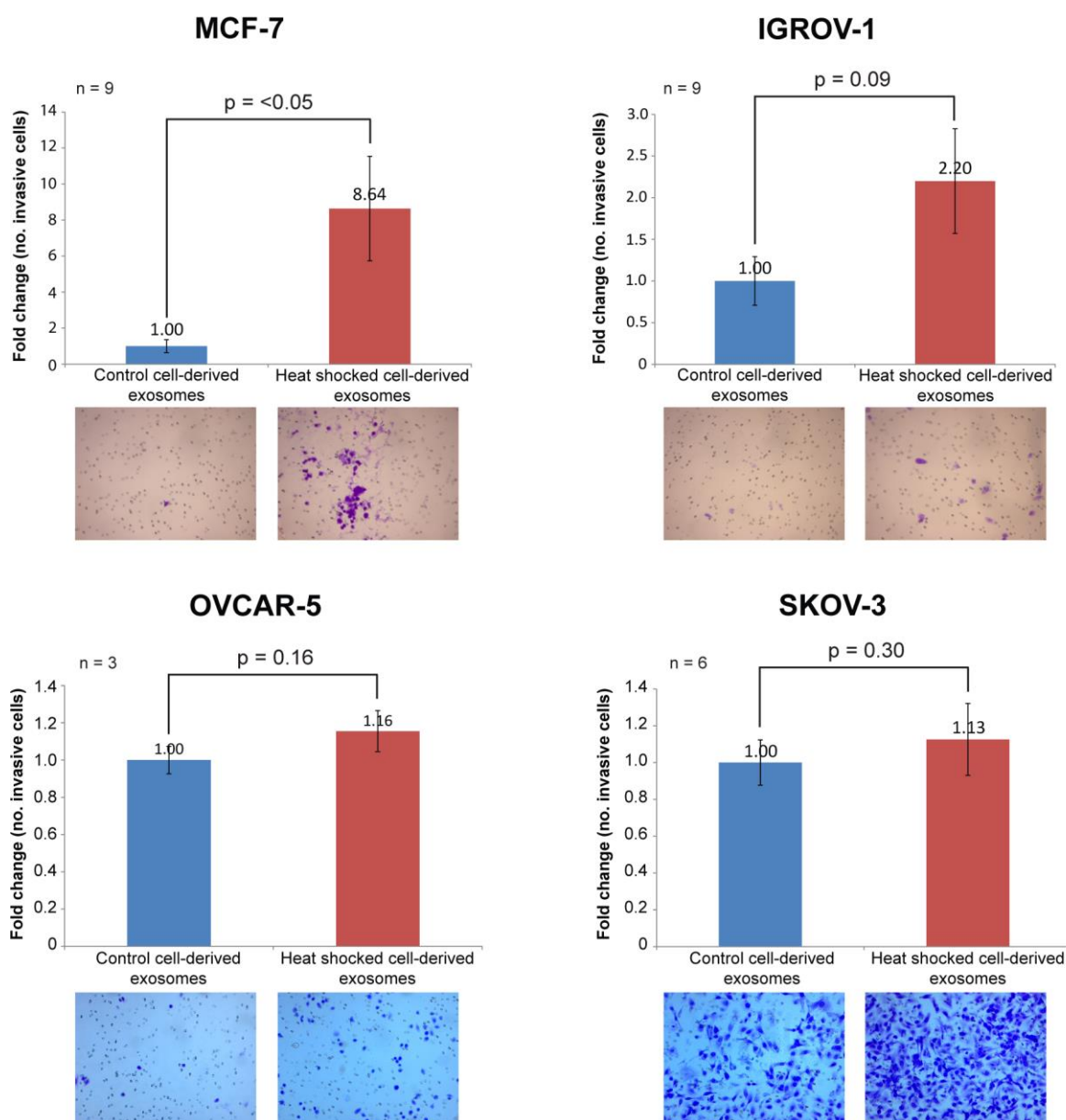
Figure 5.4: The effect of heat shocked cell-derived exosomes upon the invasive capacity of four cancer cell lines. The Matrigel trans-well invasion assay was used to determine the effect of heat shocked cell-derived exosomes on invasive potential of four cancer cell lines. Exosomes were extracted from approximately 6 million cells that had been heat shocked 24 hours prior to exosome extraction and 6 million control cells that had been maintained at 37°C, for each cell line. Extracted exosomes were administered to approximately 1 million cells. 24 hours later the exosome extraction procedure was repeated to harvest more heat shocked and control cell-derived exosomes. 100,000 cells were distributed into each insert of the trans-well assay. Following extraction exosomes were immediately transferred into Matrigel trans-wells (the dose was equivalent to exosomes extracted from 6 million cells). Cells invaded Matrigel membranes over 24 hours. Matrigel membranes were cleared of non-invasive cells and invasive cells were stained with crystal violet. The number of invasive cells on each membrane was counted, where it was impossible to count the total number of cells five representative areas were counted. The counts were used to accurately calculate the total number of invasive cells. The graphs represent fold change in terms of the total number of cells that invaded the Matrigel membrane following treatment with either control or heat shocked cell-derived exosomes. Each sample group contained either three, six or nine biological replicates depending upon the cell type. Error bars represent standard error of the mean of the biological replicates. P values were calculated using the one tailed T-test. The images represent the Matrigel membranes following the cell invasion period after the cells received either control or heat shock exosomes.

5.2.5. Characterisation and further investigation into the effect of heat shocked cell-derived exosomes on invasive behaviour of MCF-7 cells

Heat shocked MCF-7 cell-derived exosomes were characterised by WB (**Figure 5.5A**). HSP70, a marker of exosomes, and GAPDH were both identified in the exosome samples. Cytochrome C oxidase and calnexin were not detected by WB in the exosome samples indicating that the samples contained exosomes and were not contaminated by intracellular organelles or other types of EV during the extraction process. All four proteins were identified in the MCF-7 cell samples indicating that the WB procedure was effective. HSP70 was upregulated in cells that had experienced heat shock and in the exosomes derived from these cells.

The relative intensities of WB bands (**Figure 5.5A**) for protein samples extracted from directly heat shocked and control MCF-7 cells, and their secreted exosomes, were quantified using Image Lab software version 5.2.1. Control cell band intensity was used as the reference band for each antibody. The results show that HSP70 was enriched in heat shock exosomes with a band intensity of 0.13 compared with 0.08 for control exosomes (**Table 5.2**). HSP70 was also enriched in heat shocked cells (1.30) compared with control cells (1.00). The positive/loading control GAPDH bands were more intense in control cells (1.00) compared with heat shocked cells (0.88), and in heat shock exosomes (0.34) compared with control exosomes (0.05). Calnexin was detected in control and heat shocked cells (1.00 and 0.67, respectively), as expected, but was also present in heat shocked exosomes (0.18) (although the band is not visible on the blot [**Figure 5.5A**]). This was unexpected because calnexin is an endoplasmic reticulum marker. Cytocrome C oxidase, a marker of apoptotic bodies and mitochondria, was present in both heat shocked and control cells (1.00 and 1.11, respectively) and absent in both exosome samples, as anticipated (**Table 5.2**). This indicates that the exosome samples contained low levels of apoptotic bodies.

Table 5.2: The relative intensities of HSP70, GAPDH, calnexin, and cytochrome C oxidase bands on Figure 5.5A western blots of directly heat shocked MCF-7 cells and exosomes derived from heat shocked MCF-7 cells compared with control MCF-7 cells and exosomes.

Sample	Relative intensity			
	HSP70	**GAPDH**	**Calnexin**	**Cytochrome C oxidase**
Control cells	1.00	1.00	1.00	1.00
Control exosomes	0.08	0.05	0.00	0.01
Directly heat shocked cells	1.30	0.88	0.67	1.11
Heat shocked cell-derived exosomes	0.13	0.34	0.18	0.00

Since exosomes were not quantified prior to being added to cells, it was speculated that the increase in cell invasiveness in the presence of heat shock exosomes may have been because of increased exosome concentration, i.e. cells release more exosomes into the environment in response to heat stress, and it was the number, rather than a specific component of heat shock exosomes, that caused an increase in cellular invasive behaviour. NTA was performed on three samples of control exosomes and three samples of heat shock exosomes derived from MCF-7 cells. The six T175 flasks were seeded at equal concentration of MCF-7 cells and once 70% confluency was reached three of the flasks were heat shocked for 1 hour at 45°C; the remaining three flasks were maintained at 37°C. Exosomes were extracted the following day and exosome concentration was determined by NTA. There was no significant difference between the concentration of exosomes released by control MCF-7 cells (32.33×10^8 particles/mL) compared with heat shocked MCF-7 cells (39.72×10^8 particles/mL) (**Figure 5.5B**). This indicates that exosomes transfer a stress-induced signal to recipient cells that in turn causes increased cell invasiveness.

TEM identified vesicles within the size range of exosomes (30–160 nm) for both control and heat-shock exosomes (**Figure 5.5C&D**). Previous reports have identified smaller sized exosomes secreted by stressed cells (de Jong *et al.*, 2012). In our group, for example, cells irradiated with 2.0 Gy secrete exosomes that are statistically significantly smaller in diameter than those released by non-irradiated cells (Jacobs *et al.*, unpublished). Consistent with this, heat shocked MCF-7 cells also released exosomes that were statistically significantly smaller in diameter than those secreted by control cells (p = 0.047).

To further investigate the effect of exosome concentration upon MCF-7 cell invasiveness, the Matrigel invasion experiment was repeated with control exosomes (1X) (exosomes extracted from approximately 6 million cells, cultured for 24 hours in EFM), doubled concentration of control exosomes (2X) (exosomes extracted from approximately 12 million cells, cultured for 24 hours in EFM), and heat shock exosome treatments. This time an additional control was added: control cells that received no exosomes (**Figure 5.5E**). Treatment with control exosomes did not affect MCF-7 cell invasiveness regardless of exosome concentration. Despite an increase in fold change from 1.00 for cells with no exosome treatment to 1.88 for cells treated with 1X control exosomes and a fold change value of 4.13 for cells treated with 2X control exosomes, none of the differences in MCF-7 cell invasiveness were statistically significantly different. Heat shock exosomes increased MCF-7 cell invasiveness by 46 fold. Despite the increase in fold change, the effect of heat shock exosomes on MCF-7 cell invasiveness was not statistically significantly different from other exosome treatments. This was because of one of the heat shocked exosome treated biological replicates having a similar number of invasive cells to the three control types

(no exosomes, 1X control exosomes and 2X control exosomes). Representative images of the Matrigel membranes are shown in **Figure 5.5F**. Low numbers of invasive cells are shown on the three control types (no exosomes, 1X control exosomes and 2X control exosomes) but areas of the heat shock exosome treated cell membranes have a higher concentration of invasive cells. This indicates that groups of invasive cells invade the Matrigel membrane together.
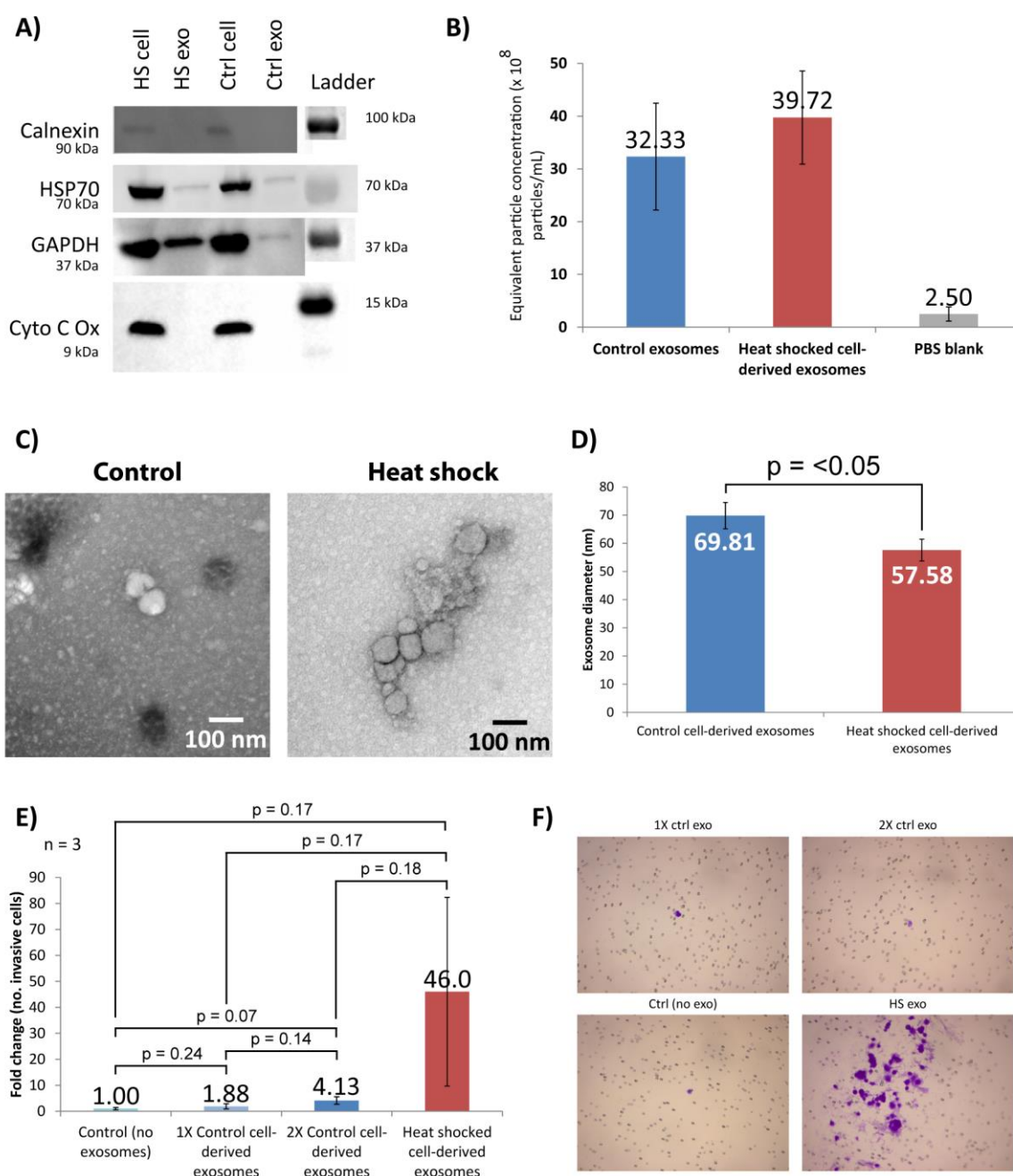
Figure 5.5: Characterisation of heat shock and control exosomes derived from MCF-7 cells and their effect on invasive behaviour on naïve MCF-7 cells. A) Control and heat shocked cell and exosome protein lysates were characterised by western blotting, samples were probed for GAPDH, calnexin, HSP70, and cytochrome C oxidase. B) Quantification of exosomes secreted by control and heat shocked MCF-7 cells by nanoparticle tracking analysis. C) Images of electron microscopy grids of control and heat shock exosomes visualised by transmission electron microscopy. D) Average diameter of exosomes secreted by heat shocked and control MCF-7 cells measured on electron microscopy grids (C). There were two biological replicates containing diameter measurements of 50 exosomes. The p value was calculated using the two tailed T-test. E) Matrigel assay performed to investigate the effect of exosome concentration and heat shock exosomes upon invasive capacity of MCF-7 cells. 1X control exosomes was equivalent to exosomes extracted from approximately 6 million cells, cultured in exosome-free media for 24 hours. 2X control exosomes was equivalent to exosomes extracted from 12 million cells. F) Representative images of Matrigel membranes showing invasive MCF-7 cells following treatment with different concentrations and types of exosomes (in the Matrigel invasion experiment, E).

5.2.6. The effect of heat stress cell conditioned media on motility of MCF-7 cells

In addition to enhanced cell invasiveness, increased cell motility is another important factor in cancer metastasis. Because of the significant increase in invasiveness caused by heat shock exosomes (**Figure 5.4** and **Figure 5.5E)**, their effect on cell motility was also investigated using the scratch assay. Exosomes were not isolated from the heat shock cell conditioned media, as in previous experiments that investigated the effects of exosomes on cell motility; whole media transfer was performed instead of directly adding exosomes to naïve cells. Control MCF-7 cells that did not receive heat shocked cell conditioned media had a similar motility rate curve to those that received heat shocked cell conditioned media (**Figure 5.6A**). Directly heat shocking cells slowed their motility rate (**Figure 5.6**); this was expected as the cells had become damaged and were recovering from the heat stress. The average percentage scratch closure per hour (**Figure 5.6B**) was not statistically significantly different between the three different treatment types: control, heat shocked cell conditioned media transfer and direct heat shocking; rates were 2.03%/hour, 2.41%/hour and 1.55%/hour, respectively. To determine whether the different treatments affect cell motility immediately after their administration or whether the response occurs a few hours after the stress alert has been received, the average scratch closure rate per hour was calculated for the time periods between each data collection point (**Figure 5.6C**). Again, there was no statistically significant difference between the motility rates of the three different treatment types (control, heat shocked cell conditioned media and direct heat shocking) suggesting that heat shocked cell conditioned media, and hence, heat shocked cell-derived exosomes, did increase MCF-7 cell motility in terms of average scratch closure speed but not to a significant level.
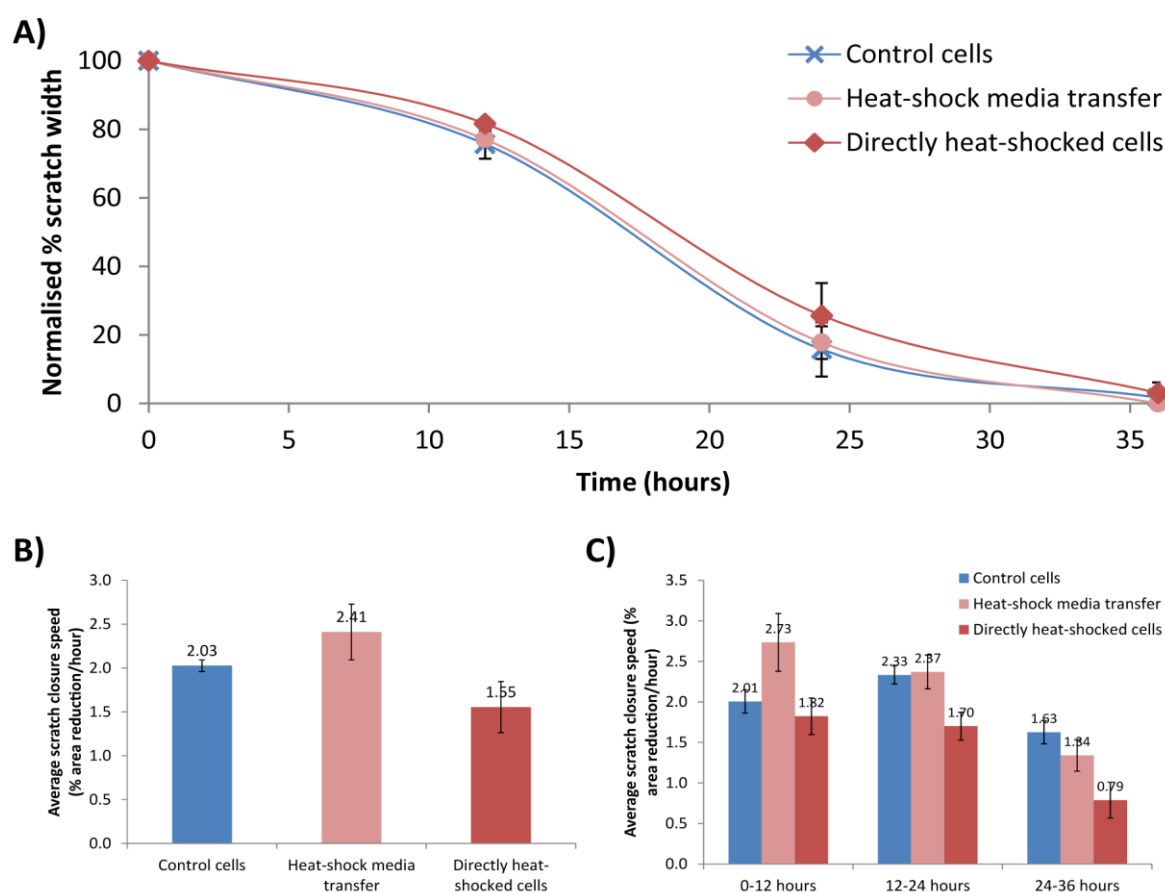
Figure 5.6: Scratch assay performed to investigate the effect of heat shock media transfer and direct heat shocking upon motility of MCF-7 cells. A) The curve represents scratch closure rate of MCF-7 cells that were treated with heat shocked cell conditioned media or were directly heat shocked compared with control cells that received no treatment. B) Average scratch closure speed in terms of percentage scratch area decrease per hour over the entire assay. C) Average scratch closure speed was analysed for the time periods between each data collection point. Each sample group contained six biological replicates, within each replicate there were three technical replicates. Error bars represent standard error of the mean of six biological replicates.

5.2.7. The role of kinases in heat shock exosome mediated increase in MCF-7 cell invasiveness

With the aim of improving our understanding of the mechanism responsible for increased cell invasiveness induced by heat shock exosomes, the proteome profiler human phospho-MAPK array was used. The assay simultaneously determined the relative phosphorylation levels of 26 kinases (including nine mitogen-activated protein kinases [MAPKs]) of MCF-7 cells treated with either control exosomes or heat shock exosomes. Each cell lysate was combined with a cocktail of biotinylated detection antibodies and incubated overnight on a nitrocellulose membrane (spotted with capture and control antibodies in duplicate). Antibody signal was detected using streptavidin-HRP and chemiluminescent reagents (**Figure 5.7A**). The signal intensity at each capture spot represented bound phosphorylated protein and was used to calculate relative phosphorylation levels of each kinase. Significant differences in protein kinase phosphorylation between samples were calculated using the two tailed T-test. Five kinases were statistically

significantly downregulated in the cell treated with heat shock exosomes compared with control exosome treatment. The downregulated kinases were: Akt2 (p = 0.033), CREB (p = 0.046), HSP27 (p = 0.0037), p38γ (p = 0.031), and p53 (p = 0.0081) (**Figure 5.7B**). This result indicates that down-regulation of the protein kinases Akt2, CREB, HSP27, p38γ, and p53 may have a role in the mechanism responsible for heat shock exosome-induced increased MCF-7 cell invasiveness.
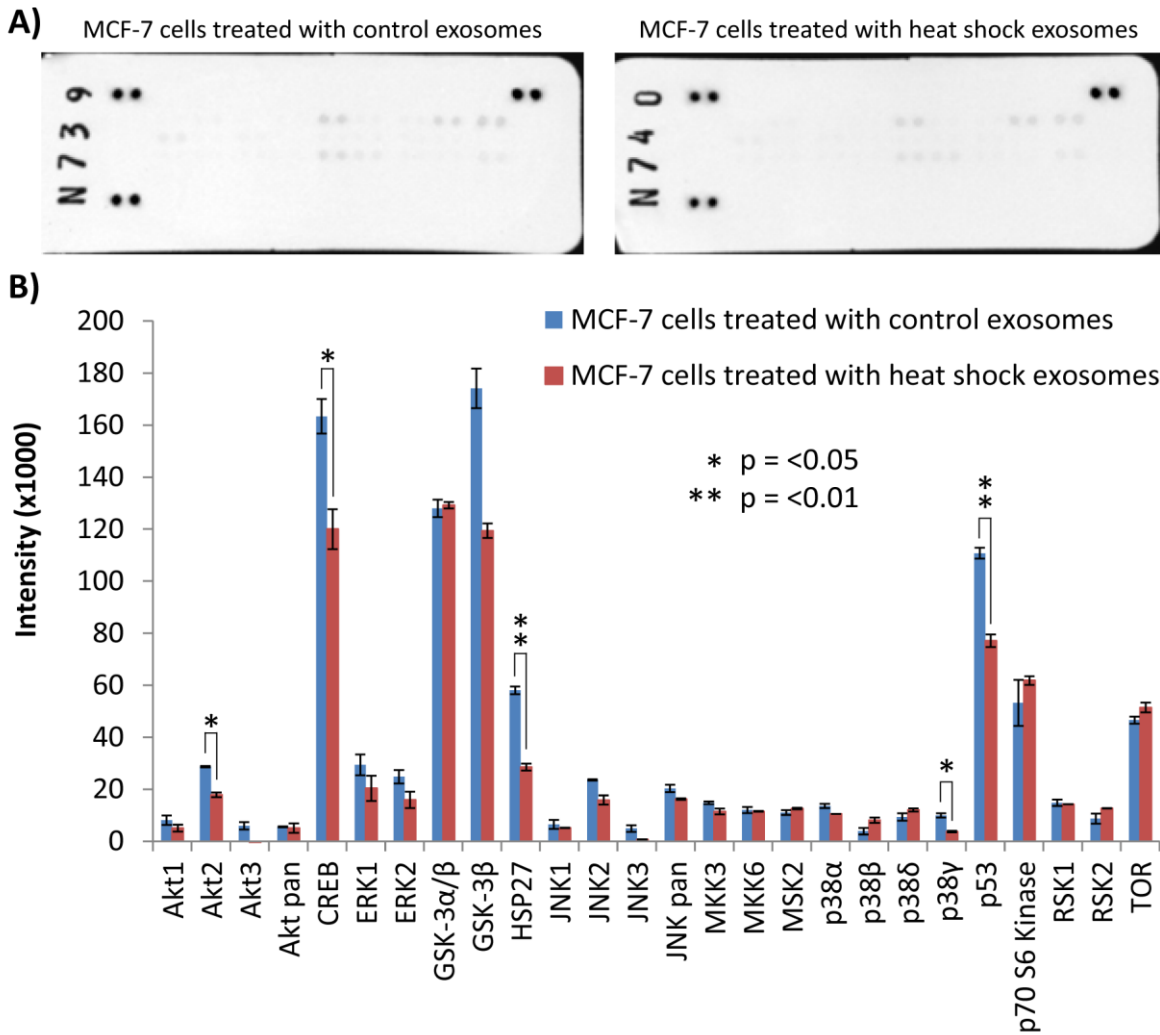
Figure 5.7: Relative phosphorylation levels of 26 kinases in MCF-7 cells following treatment with either control or heat shock exosomes determined using the proteome profiler human phospho-MAPK array. A) Blots showing intensity for each kinase on duplicate spots for each exosome treatment. B) Intensity levels of each kinase in MCF-7 cells treated with either control or heat shock exosomes. P values were calculated using the two tailed T-test.

5.2.8. Gene expression microarray indicates pathways possibly involved in exosome mediated increased cell invasiveness

To explain the increased invasiveness of heat shock exosome recipient MCF-7 cells analysis of the relative gene expression profiles of control MCF-7 cells, directly heat shocked MCF-7 cells, control exosome recipient MCF-7 cells, and heat shock exosome recipient MCF-7 cells was performed. In order to identify genes that were up- or down-regulated, following each treatment type, total RNA was extracted, amplified, and labelled using the Agilent Low Input Quick Amp labelling two colour kit, hybridised to an Agilent G3 8plex × 60k gene human transcriptome microarray, processed and scanned, converted to probe intensity, and Loess- and quartile-normalised. Fold change and p values were calculated using ArrayStar software (DNASTAR®, Madison, USA). Gene expression correlation between experiments were generated by plotting hybridisation signal values for each analysed gene. All four gene expression correlations showed strong positive correlation indicating that differential gene expression between experiments was minimal (**Figure 5.8**), as expected with such a large number of genes, and show reliable dye normalisation. The green lines represent hybridisation signal fold change threshold of 2.0. The number of genes that had differential expression of more than two-fold between the experiments are shown above and below these thresholds.
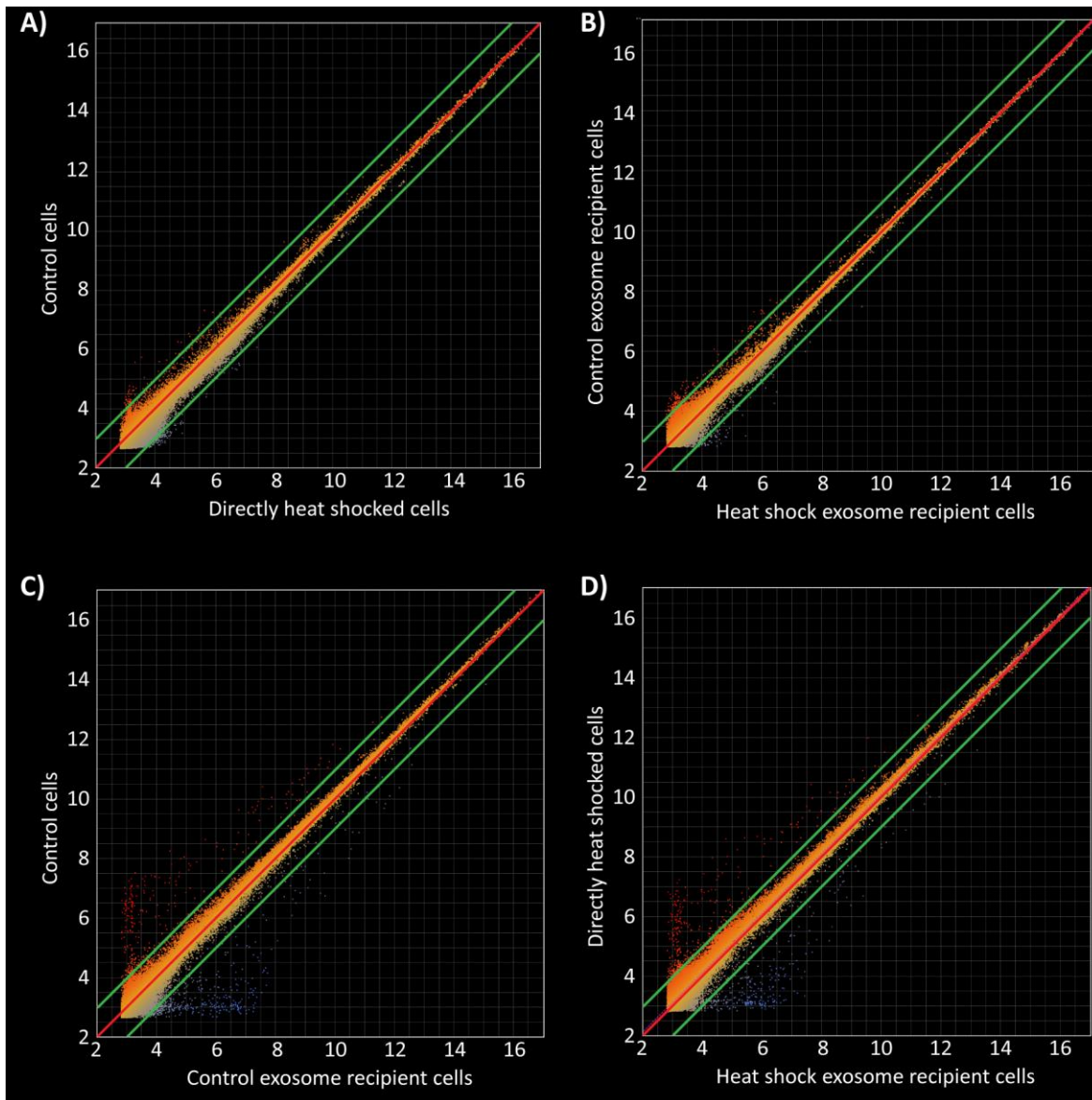
Figure 5.8: Scatter plots of gene expression correlation in MCF-7 cells. A) Control cells versus directly heat shocked cells. B) Control exosome recipient cells versus heat shock exosome recipient cells. C) Control cells versus control exosome recipient cells. D) Directly heat shocked cells versus heat shock exosome recipient cells. The red 45° line marks the line of best-fit for all probe signals. The green lines represent 2-fold change thresholds for hybridisation signal.

5.2.9. Gene expression most greatly affected by heat shock exosomes and directly heat shocking MCF-7 cells

Typically, only genes with 2.0 or greater fold change in gene expression and a significant p value of ≤0.05 are regarded as exhibiting differential expression. However, for directly heat shocked MCF-7 cells versus heat shock exosome recipient MCF-7 cells, only five genes held both of these attributes, and no genes for the other three treatment comparisons (control MCF-7 cells versus directly heat shocked MCF-7 cells, control exosome recipient MCF-7 cells versus heat shock exosome recipient MCF-7 cells, and control MCF-7 cells versus control exosome recipient MCF-7

cells). Because of the low number of differentially expressed genes with fold change greater than 2.0, genes were ranked in descending order of fold change to determine the 20 greatest up-regulated genes and the 20 greatest down-regulated genes for each gene expression sample set comparisons (**Table 5.3**).

Table 5.3: The 20 greatest up- and down-regulated genes for each gene expression comparison in MCF-7 cells. A) Control cells versus directly heat shocked cells. B) Control exosome recipient cells versus heat shock exosome recipient cells. C) Control cells versus control exosome recipient cells. D) Directly heat shocked cells versus heat shock exosome recipient cells. Highlighted genes were most greatly up-/down-regulated in more than one sample comparison. The colours represent the same genes that are most up-/down-regulated in more than one experiment comparison.

A)   **Control MCF-7 cells versus directly heat shocked MCF-7 cells**

Up-regulated in directly heat shocked cells			Down-regulated in directly heat shocked cells		
Gene name	Fold change	P value	Gene name	Fold change	P value
HTRA3	3.341921	0.384	XLOC_009974	0.405076	0.799
ITGAL	2.796371	0.284	DSC1	0.403809	0.308
LOC100130849	2.709529	0.744	CXCL2	0.399461	0.509
TRIM55	2.679796	0.119	XLOC_007302	0.393999	0.448
XLOC_l2_009510	2.665921	0.412	XLOC_010238	0.386404	0.712
CD70	2.661669	0.153	XLOC_l2_000138	0.38567	0.381
FLJ32255	2.635503	0.167	PCSK1	0.383093	0.414
PTGES	2.624374	0.167	XLOC_008708	0.379768	0.384
AGBL2	2.616214	0.306	LOC100507156	0.373974	0.728
XLOC_011633	2.610768	0.115	XLOC_010163	0.373097	0.384
LOC100506421	2.59553	0.167	TP53AIP1	0.371366	0.511
GOLGA6L6	2.582582	0.130	XLOC_005263	0.366258	0.628
XLOC_005531	2.581694	0.152	LIMS3L	0.362595	0.299
ESYT3	2.581647	0.139	SLCO1A2	0.358111	0.306
ZNF3	2.578119	0.598	SLITRK2	0.356211	0.105
RRAGD	2.553797	0.621	PPP1R1A	0.350085	0.664
PSG8	2.542537	0.237	KISS1R	0.323405	0.290
NPPB	2.53951	0.290	GAB3	0.316999	0.091
LOC100132356	2.525886	0.217	ABCC4	0.217219	0.719
PSAT1	2.51985	0.132	UGT3A1	0.210625	0.360

B)   **Control exosome recipient MCF-7 cells versus heat shock exosome recipient MCF-7 cells**

Up-regulated in heat shock exosome recipient cells			Down-regulated in heat shock exosome recipient cells		
Gene name	Fold change	P value	Gene name	Fold change	P value
NSUN7	4.352195	0.216	XLOC_007277	0.392912	0.275
MAK16	3.554827	0.178	TRAPPC6B	0.391662	0.659
GZF1	3.550008	0.131	OR52L1	0.389641	0.118
LOC286149	3.199528	0.447	XLOC_l2_012388	0.389072	0.137
LOC100128922	3.155415	0.511	XLOC_l2_008313	0.385202	0.145
XLOC_000909	3.144326	0.324	LIMS3L	0.384464	0.110

XLOC_l2_011924	3.04401	0.224	*ARL10*	0.378097	0.769
ENG	2.970951	0.367	*PTGS2*	0.371292	0.380
XLOC_013795	2.855058	0.281	*XLOC_012079*	0.370785	0.786
XLOC_004426	2.760932	0.203	*DUSP26*	0.363442	0.077
XLOC_007420	2.749519	0.395	*XLOC_l2_001138*	0.361445	0.102
MARCO	2.713181	0.527	*TNF*	0.35333	0.068
BAALC	2.70135	0.786	*PEG3*	0.35049	0.132
PGCP1	2.551168	0.562	*XLOC_l2_014423*	0.348687	0.155
XLOC_l2_000696	2.526436	0.545	*XLOC_l2_005692*	0.3438	0.244
DEFB107A	2.511197	0.734	*LAMA1*	0.338534	0.143
XLOC_l2_015288	2.504192	0.353	*DAGLA*	0.333836	0.362
XLOC_l2_010897	2.495157	0.191	*LBH*	0.33187	0.362
NDP	2.466298	0.176	*XLOC_009893*	0.326386	0.750
CTTNBP2NL	2.43161	0.346	*ANP32A*	0.314603	0.133

C)   **Control MCF-7 cells versus control exosome recipient MCF-7 cells**

Up-regulated in control exosome recipient cells			*Down-regulated in control exosome recipient cells*		
Gene name	**Fold change**	**P value**	**Gene name**	**Fold change**	**P value**
XLOC_l2_003911	21.0027	0.323	*XLOC_l2_014024*	0.08197	0.321
TM4SF19	19.73313	0.291	*XLOC_002049*	0.081768	0.342
LINC00290	18.72338	0.284	*XLOC_l2_008321*	0.081471	0.357
PRDM9	18.14694	0.323	*LOC100293612*	0.081142	0.357
LOC400756	17.98568	0.226	*DDTL*	0.080851	0.336
LBH	17.86589	0.314	*XLOC_001795*	0.079146	0.365
XLOC_l2_001011	17.32759	0.284	*SERPINE1*	0.077292	0.379
XLOC_001776	16.31838	0.281	*FAM190A*	0.0753	0.320
LOC643723	16.25609	0.282	*XLOC_002174*	0.074166	0.394
XLOC_l2_015037	16.18181	0.353	*XLOC_005194*	0.073272	0.326
ARL10	16.1636	0.301	*AKD1*	0.072093	0.296
GUCY2F	15.23669	0.287	*GAB3*	0.071955	0.320
XLOC_012079	15.22509	0.340	*CHST10*	0.070909	0.390
XLOC_l2_002761	15.18733	0.287	*XLOC_002049*	0.068169	0.295
XLOC_004851	14.43412	0.319	*GUCY2D*	0.067104	0.348
LOC100133123	14.27681	0.280	*XLOC_005081*	0.065717	0.356
PPIH	14.04792	0.280	*XLOC_000133*	0.058433	0.325
SNORD115-37	14.00694	0.286	*XLOC_002134*	0.055497	0.321
OR51S1	13.93371	0.324	*XLOC_009974*	0.055082	0.355
CLEC4GP1	13.86039	0.280	*SULT1C3*	0.052455	0.355

D)   **Directly heat shocked MCF-7 cells versus heat shock exosome recipient MCF-7 cells**

Up-regulated in heat shock exosome recipient cells			*Down-regulated in heat shock exosome recipient cells*		
Gene name	**Fold change**	**P value**	**Gene name**	**Fold change**	**P value**
MARCO	16.93904	0.334	*XLOC_l2_007656*	0.106307	0.347
XLOC_008358	13.28133	0.350	*FAM190A*	0.102325	0.378
FBN3	11.88516	0.351	*XLOC_002134*	0.097451	0.340

LOC100129894	11.57543	0.312	FASLG	0.097355	0.415
XLOC_004851	11.41059	0.320	XLOC_005081	0.097065	0.336
XLOC_l2_008124	11.11305	0.417	XLOC_l2_014024	0.096003	0.154
XLOC_004851	10.33849	0.316	ZNF3	0.094102	0.336
KIAA0556	10.3313	0.314	HIST2H4A	0.09292	0.308
XLOC_000550	10.32035	0.360	TACR3	0.090907	0.376
NEFL	9.869531	0.311	SULT1C3	0.084926	0.372
GSTP1	9.59684	0.316	CHST10	0.079697	0.264
XLOC_009912	9.547468	0.398	LOC100130849	0.078929	0.267
XLOC_l2_015037	9.535888	0.417	XLOC_l2_008321	0.078702	0.300
XLOC_l2_003911	9.447515	0.456	SERPINE1	0.077911	0.412
BHMT2	9.340737	0.317	LOC100293612	0.073924	0.286
TM4SF19	9.327131	0.421	RCAN3	0.070968	0.264
XLOC_l2_000696	9.220111	0.287	FP588	0.070215	0.232
XLOC_010714	8.822661	0.395	MIB2	0.063713	0.268
XLOC_000505	8.783594	0.315	APLNR	0.063397	0.316
CACNA1B	8.603439	0.372	AKD1	0.061339	0.333

5.2.10. Cellular biological and molecular functional pathways implicated in heat shock exosome recipient MCF-7 cells and by directly heat shocking MCF-7 cells

In order to accurately predict the pathways that are activated by heat shock exosomes or by directly heat shocking MCF-7 cells, approximately 100 genes are required. Typically genes that have at least a 2-fold change in their expression, and a p value of ≤0.05 are selected for accurate prediction of the pathways activated in the different experiments. However, when these thresholds were applied to the genes, there were not enough genes to perform an accurate analysis. Therefore, all genes with p values of ≤0.05 were selected (irrespective of their fold change); there were 15 differentially expressed genes for directly heat shocked cells versus control cells, 120 for control exosome recipient cells versus heat shock exosome recipient cells, 326 genes for control cells versus control exosome recipient cells, and 481 for directly heat shocked cells versus heat shock exosome recipient cells. These gene lists were input into DAVID Bioinformatics Resources 6.7 and KEGG Pathways were selected for each gene expression sample set comparison.

Enriched molecular functions in each list of differentially expressed genes were identified by this tool. The gene ontology (GO) terms are shown with their corresponding p values. For control MCF-7 cells versus directly heat shocked MCF-7 cells, two genes that participate in calcium-dependent phospholipid binding were identified to have differential gene expression with a statistically significant p value of 1.6×10^{-2} (**Table 5.4**). Additionally, three genes (**Table 5.5**) in

the SNARE interactions in vesicular transport pathway (**Figure 5.9**) were identified to have differential gene expression with a statistically significant p value of 5.4×10^{-4}.

Eight GO terms were recognised for containing differentially expressed genes between control exosome recipient MCF-7 cells versus heat shock exosome recipient MCF-7 cells (**Table 5.6**). The p53 signalling pathway (**Figure 5.10**) was also identified to have differential gene expression between these two experiments, with a statistically significant p value of 5.7×10^{-2}, expression of three genes were affected (**Table 5.7**).

Ten GO terms (**Table 5.8**) and ten KEGG pathways (**Table 5.9**) were identified to be affected in control exosome recipient MCF-7 cells compared with control MCF-7 cells. Seven of the identified KEGG pathways were related to cancer and the endocytosis pathway was also influenced by control exosomes.

Fourty-one GO terms (**Table 5.10**) and ten KEGG pathways (**Table 5.11**) were also identified to be affected in directly heat shocked MCF-7 cells versus heat shock exosome recipient MCF-7 cells. GO terms identified included 'heat shock protein binding' ($p = 6.0 \times 10^{-2}$) and 'damaged DNA binding' ($p = 7.8 \times 10^{-2}$). Four of the KEGG pathways were related to cancer and the lysosome and phagocytosis pathways were also influenced by heat shock exosomes compared with direct heat shocking.

Table 5.4: GO terms and the number of differentially expressed genes associated with each term for control MCF-7 cells versus directly heat shocked MCF-7 cells.

GO Term (molecular function)	Gene count	P value
calcium-dependent phospholipid binding	2	1.6×10^{-2}

Table 5.5: KEGG pathways associated with differentially expressed genes in control MCF-7 cells versus directly heat shocked MCF-7 cells.

KEGG Pathway	Differentially expressed genes	P value
SNARE interactions in vesicular transport	1) *Blocked early in transport 1 homolog (S. cerevisiae)-like (Bet-1)* 2) *Synaptosomal-associated protein, 23kDa (SNAP23)* 3) *Vesicle-associated membrane protein 4 (VAMP4)*	5.4×10^{-4}
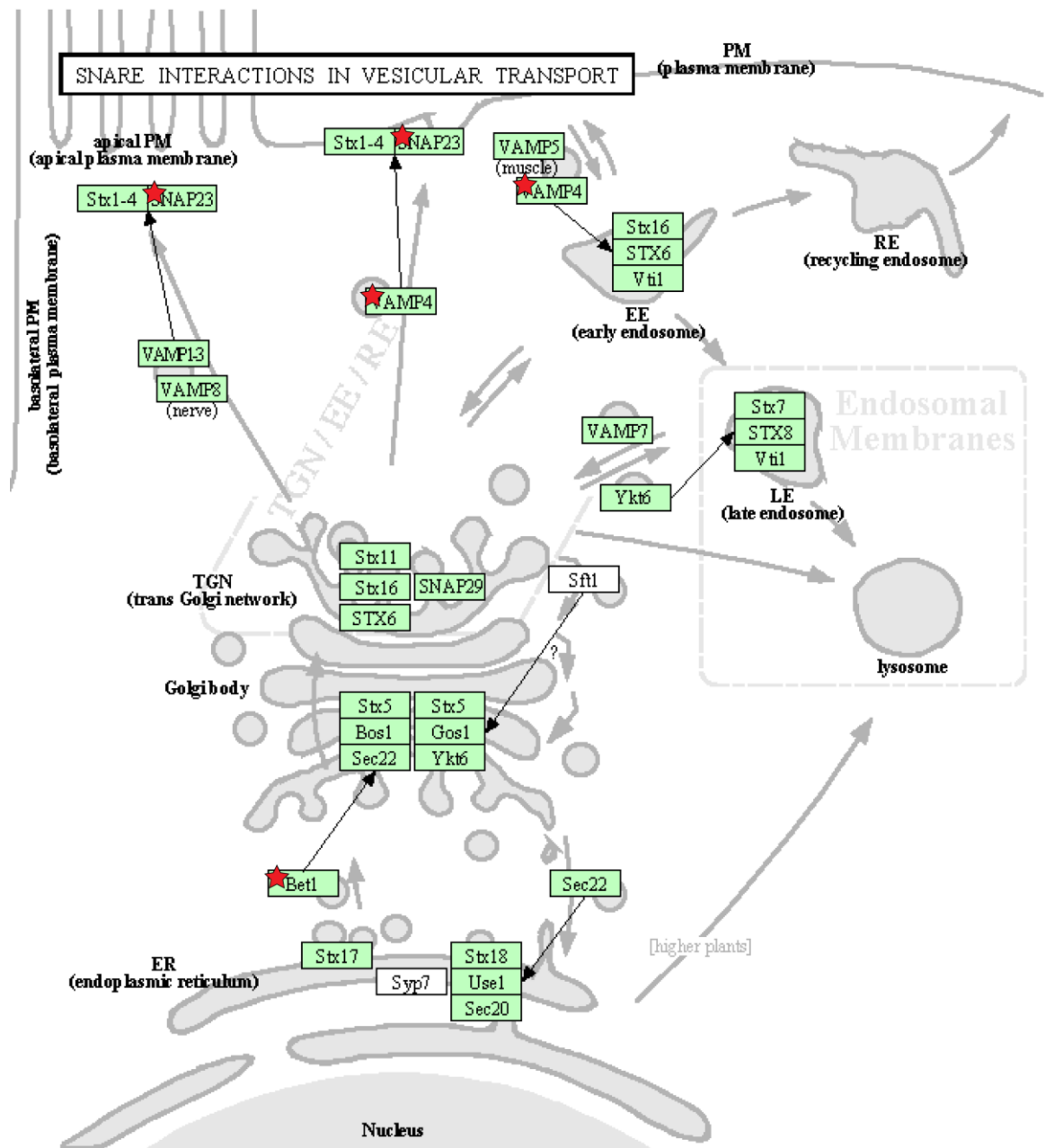
Figure 5.9: The SNARE interactions in vesicular transport KEGG pathway generated by DAVID Bioinformatics Resources 6.7 (Huang *et al.*, 2009a; Huang *et al.*, 2009b). The pathway shows the interaction of various genes in cellular vesicular transport. The red stars represent the differentially expressed genes in control MCF-7 cells versus directly heat shocked MCF-7 cells.

Table 5.6: GO terms and the number of differentially expressed genes associated with each term for control exosome recipient MCF-7 cells versus heat shock exosome recipient MCF-7 cells.

	GO Term (molecular function)	Gene count	P value
1	phosphatase activity	6	8.6×10^{-3}
2	laminin-1 binding	2	1.5×10^{-2}
3	oxidoreductase activity, acting on the CH-NH group of donors, oxygen as acceptor	2	1.5×10^{-2}
4	protein phosphatase regulator activity	3	3.0×10^{-2}
5	phosphatase regulator activity	3	3.3×10^{-2}
6	laminin binding	2	5.5×10^{-2}
7	cAMP-dependent protein kinase regulator activity	2	7.8×10^{-2}
8	protein domain specific binding	5	8.8×10^{-2}

Table 5.7: KEGG pathways associated with differentially expressed genes in control exosome recipient MCF-7 cells versus heat shock exosome recipient MCF-7 cells.

KEGG Pathway	Differentially expressed genes	P value
p53 signalling pathway	1) *Fas (TNF receptor superfamily, member 6)* 2) *insulin-like growth factor binding protein 3 (IGF-BP3)* 3) *phosphatase and tensin homolog (PTEN); phosphatase and tensin homolog pseudogene 1 (PTENP1)*	5.7×10^{-2}
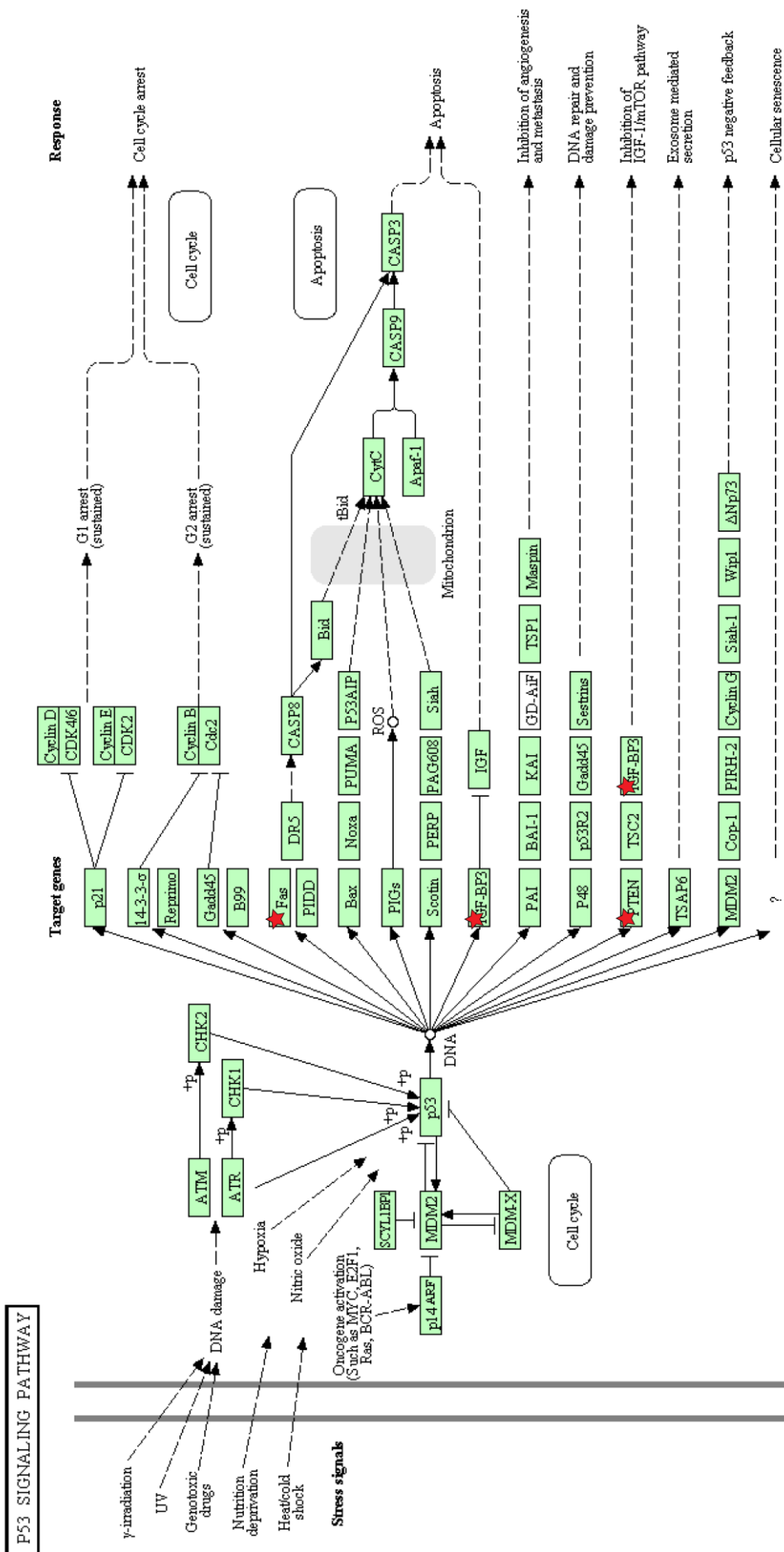
Figure 5.10: p53 signalling KEGG pathway generated by DAVID Bioinformatics Resources 6.7 (Huang *et al.*, 2009a; Huang *et al.*, 2009b). The pathway shows the interaction of various genes in the p53 signalling pathway and downstream effects on various pathways including cell cycle and apoptosis. The red stars represent the differentially expressed genes in control MCF-7 cells versus directly heat shocked MCF-7 cells.

Table 5.8: GO terms and the number of differentially expressed genes associated with each term for control MCF-7 cells versus control exosome recipient MCF-7 cells.

	GO Term (molecular function)	Gene count	P value
1	protein phosphatase regulator activity	5	6.2×10^{-3}
2	phosphatase regulator activity	5	7.5×10^{-3}
3	cadherin binding	3	2.3×10^{-2}
4	cytoskeletal protein binding	14	2.3×10^{-2}
5	enzyme binding	14	3.0×10^{-2}
6	protein transporter activity	5	3.3×10^{-2}
7	promoter binding	4	4.4×10^{-2}
8	beta-N-acetylhexosaminidase activity	2	5.4×10^{-2}
9	cell adhesion molecule binding	3	6.5×10^{-2}
10	microtubule binding	4	7.8×10^{-2}

Table 5.9: KEGG pathways and the number of differentially expressed genes in each pathway for control MCF-7 cells versus control exosome recipient MCF-7 cells.

	KEGG Pathway	Number of genes up-/down-regulated	P value
1	Endometrial cancer	5	1.1×10^{-2}
2	Leukocyte transendothelial migration	6	4.9×10^{-2}
3	Pathways in cancer	11	4.9×10^{-2}
4	Small cell lung cancer	5	5.3×10^{-2}
5	Progesterone-mediated oocyte maturation	5	5.7×10^{-2}
6	Non-small cell lung cancer	4	6.3×10^{-2}
7	Prostate cancer	5	6.3×10^{-2}
8	Vibrio cholerae infection	4	6.8×10^{-2}
9	Thyroid cancer	3	8.6×10^{-2}
10	Endocytosis	7	9.0×10^{-2}

Table 5.10: GO terms and the number of differentially expressed genes associated with each term for directly heat shocked MCF-7 cells versus heat shock exosome recipient MCF-7 cells.

	GO Term (molecular function)	Gene count	P value
1	cation-transporting ATPase activity	7	7.0×10^{-5}
2	proton-transporting ATPase activity, rotational mechanism	6	7.6×10^{-5}
3	hydrogen ion transporting ATP synthase activity, rotational mechanism	5	2.3×10^{-4}
4	ATPase activity, coupled to transmembrane movement of ions	8	6.7×10^{-4}
5	P-P-bond-hydrolysis-driven transmembrane transporter activity	9	3.1×10^{-3}
6	primary active transmembrane transporter activity	9	3.1×10^{-3}
7	oxidoreductase activity, acting on the CH-NH group of donors, NAD or NADP as acceptor	4	5.1×10^{-3}
8	ATPase activity, coupled to transmembrane movement of substances	8	6.1×10^{-3}
9	ATPase activity, coupled to movement of substances	8	6.5×10^{-3}
10	hydrolase activity, acting on acid anhydrides, catalyzing transmembrane movement of substances	8	6.8×10^{-3}
11	unfolded protein binding	8	8.2×10^{-3}
12	inorganic cation transmembrane transporter activity	9	1.1×10^{-2}
13	monovalent inorganic cation transmembrane transporter activity	7	1.8×10^{-2}
14	NF-kappaB binding	4	2.0×10^{-2}
15	oxidoreductase activity, acting on the CH-NH group of donors	4	2.0×10^{-2}
16	hydrolase activity, acting on carbon-nitrogen (but not peptide) bonds, in linear amides	5	2.8×10^{-2}
17	identical protein binding	21	3.1×10^{-2}
18	hydrogen ion transmembrane transporter activity	6	3.4×10^{-2}
19	aldo-keto reductase activity	3	3.5×10^{-2}
20	protein homodimerization activity	13	3.6×10^{-2}
21	peptidyl-prolyl cis-trans isomerase activity	4	3.7×10^{-2}
22	cis-trans isomerase activity	4	4.2×10^{-2}
23	cytoskeletal protein binding	17	4.5×10^{-2}
24	protein serine/threonine kinase activity	15	5.0×10^{-2}
25	RNA binding	22	5.1×10^{-2}
26	transcription factor binding	17	5.1×10^{-2}
27	FAD binding	5	5.6×10^{-2}
28	nucleotide binding	56	5.6×10^{-2}

29	TPR domain binding	2	5.9×10^{-2}
30	heat shock protein binding	5	6.0×10^{-2}
31	SMAD binding	4	6.4×10^{-2}
32	structure-specific DNA binding	7	7.0×10^{-2}
33	nucleoside-triphosphatase regulator activity	14	7.1×10^{-2}
34	protein dimerization activity	17	7.6×10^{-2}
35	damaged DNA binding	4	7.8×10^{-2}
36	iron-sulfur cluster binding	4	7.8×10^{-2}
37	metal cluster binding	4	7.8×10^{-2}
38	guanyl-nucleotide exchange factor activity	7	8.4×10^{-2}
39	4 iron, 4 sulfur cluster binding	3	8.8×10^{-2}
40	ATPase activity, coupled	10	9.5×10^{-2}
41	pyrroline-5-carboxylate reductase activity	2	9.6×10^{-2}

Table 5.11: KEGG pathways and the number of differentially expressed genes in each pathway for directly heat shocked MCF-7 cells versus heat shock exosome recipient MCF-7 cells.

	KEGG Pathway	Number of genes up-/down-regulated	P value
1	Vibrio cholerae infection	7	1.9×10^{-3}
2	Epithelial cell signaling in Helicobacter pylori infection	7	5.1×10^{-3}
3	Lysosome	9	6.1×10^{-3}
4	Acute myeloid leukemia	6	1.1×10^{-2}
5	Steroid biosynthesis	3	6.0×10^{-2}
6	Fc gamma R-mediated phagocytosis	6	7.3×10^{-2}
7	Bladder cancer	4	7.6×10^{-2}
8	Pathways in cancer	13	8.5×10^{-2}
9	Pancreatic cancer	5	8.9×10^{-2}
10	Natural killer cell mediated cytotoxicity	7	9.3×10^{-2}

5.2.11. The effect of cisplatin treated cell-derived exosomes on invasive behaviour of ovarian cancer cells

After establishing that heat shock exosomes increase the invasive capacity of MCF-7 cells, the effect of exosomes derived from cells stressed in a different way, by treatment with a chemotherapeutic drug, was investigated. The hypothesis was that invasive capacity of cancer cells increased in response to exosomes derived from cells that had been stressed by several different types of stressor and was not limited to heat stress exosomes. To test this hypothesis, cisplatin treated cell-derived exosomes (cisplatin exosomes) were extracted and their effect on the invasive capacity of two ovarian cancer cell lines, A-2780 and IGROV-1, was explored. To generate cisplatin exosomes, parental cells were incubated in 40 µM cisplatin for 2 hours. This concentration of cisplatin (40 µM) was optimised in our research group in A-2780 cells by Dr Priya Samuel. Dr Samuel determined the ideal concentration and duration of stress induction by calculating the IC_{50} (the concentration at which cisplatin reduced cellular metabolic activity by half) using the MTT assay. Chemotherapy-containing media was removed, the cells were washed in PBS, and fresh EFM was added to the cells. The cells were incubated for a further 2 hours, then the media was replaced with EFM once more. This step removes cisplatin pumped out of the cells following the treatment period. 20 hours later exosomes were collected from the tissue culture media and incubated with serum-starved cells for 24 hours. The stress exosome collection procedure was repeated 24 hours later, and a second batch of heat shock exosomes were added to the cells immediately after they had been seeded in the Matrigel trans-well assay. The effect of cisplatin exosomes on invasive capacity compared with control cells was established. A one tailed T-test value of 0.0082 confirmed that the invasive capacity of A-2780 cells increased in the presence of cisplatin exosomes compared with cells that received no exosomes (**Figure 5.11**). Cisplatin exosomes also increased invasive activity compared with control exosome treatment (p = 0.0067). There was not a significant difference between invasiveness of control cells treated with no exosomes, and cells treated with control exosomes (p = 0.218).

The invasive capacity of IGROV-1 cells also increased in response to cisplatin exosomes compared with control cells that received no exosomes (p = 0.042), and in comparison to control exosome treatment (p = 0.039). There was no significant difference between invasiveness of control cells treated with no exosomes, and cells treated with control exosomes (p = 0.436).

These results suggest that following cisplatin-induced stress response the exosomes released by both A-2780 and IGROV-1 cells have the ability to induce greater invasive potential in neighbouring recipient cells. Increased invasive capacity was induced by exosomes derived from cells that were stressed by both heat shocking (**Figure 5.4**) and cisplatin treatment (**Figure 5.11**).
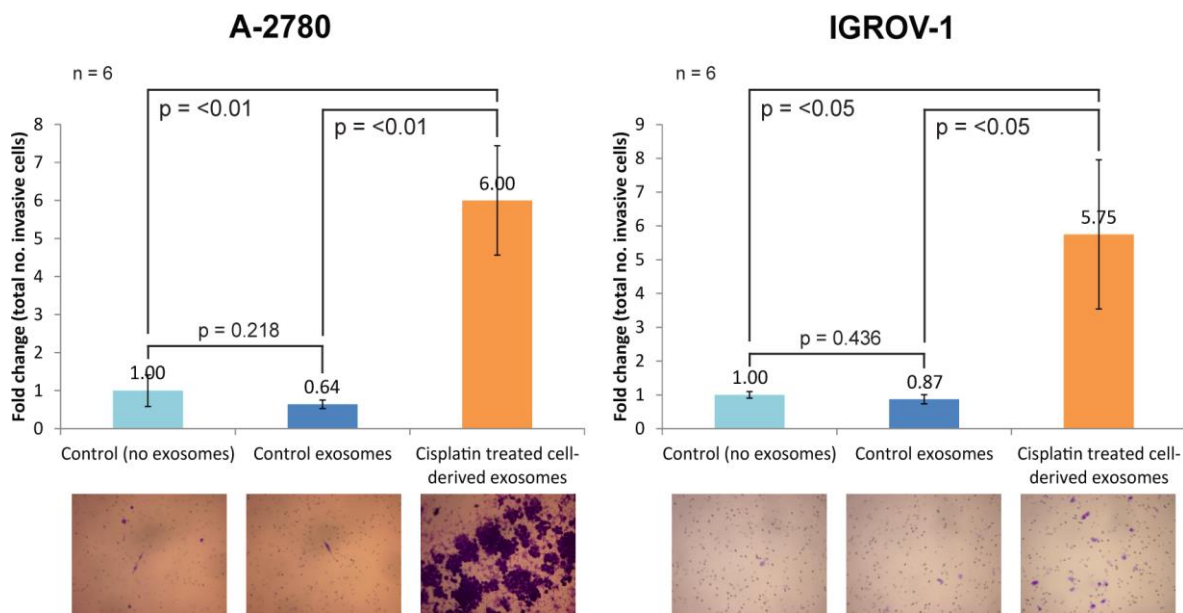
Figure 5.11: The effect of cisplatin treated cell-derived exosomes upon the invasive capacity of ovarian cancer cell lines. The Matrigel trans-well invasion assay was used to determine the effect of cisplatin treated cell-derived exosomes on invasive potential of two ovarian cancer cell lines. Exosomes were extracted from approximately 6 million cells that had been cisplatin treated 24 hours prior to exosome extraction and 6 million control cells, for each cell line. Extracted exosomes were administered to approximately 1 million cells. 24 hours later the exosome extraction procedure was repeated to harvest more cisplatin treated and control cell-derived exosomes. 100,000 cells were distributed into each insert of the trans-well assay. Following extraction exosomes were immediately transferred into Matrigel trans-wells (the dose was equivalent to exosomes extracted from 6 million cells). Cells invaded Matrigel membranes over 24 hours. Matrigel membranes were cleared of non-invasive cells and invasive cells were stained with crystal violet. The number of invasive cells on each membrane was counted. The graphs represent fold change in terms of the total number of cells that invaded the Matrigel membrane following treatment with either control or cisplatin treated cell-derived exosomes. Each sample group contained six biological replicates. Error bars represent standard error of the mean of the biological replicates. P values were calculated using the one tailed T-test. The images represent the Matrigel membranes following the cell invasion period after the cells received either control or heat shock exosomes.

5.2.12. Characterisation and further investigation into the effect of cisplatin treated cell--derived exosomes on invasive behaviour of A-2780 cells

Cisplatin treated A-2780 cell-derived exosomes were characterised by WB (**Figure 5.12A**). As for the heat shock exosomes, HSP70 (an exosome marker) and GAPDH (a cytoplasmic marker) were both identified in the cisplatin and control exosome samples. Cytochrome C oxidase and calnexin were not detected by WB in the exosome samples indicating that the samples were not contaminated by intracellular organelles or other types of EV during the extraction process. All four proteins were identified in the A-2780 control and cisplatin treated cell samples signifying that the WB procedure was successful.

The relative intensities of WB bands (**Figure 5.12A**) for protein samples extracted from directly cisplatin treated and control A-2780 cells, and their secreted exosomes, were quantified using Image Lab software version 5.2.1. Control cell band intensity was used as the reference band for each antibody. The results show that HSP70 expressed at approximately equal levels in both cisplatin (0.08) and control exosomes (0.09) (**Table 5.12**). HSP70 was detected in both cisplatin treated and control cells (0.74 and 1.00, respectively). The positive/loading control GAPDH bands were more intense in control cells (1.00) compared with cisplatin treated cells (0.71), and in cisplatin exosomes (0.42) compared with control exosomes (0.17). Calnexin was detected in control and cisplatin treated cells (1.00 and 0.36, respectively), as expected, and at very low levels in control and cisplatin exosome samples (0.01 and 0.04, respectively). Cytocrome C oxidase was present in both cisplatin treated and control cells (0.43 and 1.00, respectively), and absent in both exosome samples (0.00 and 0.02), as predicted (**Table 5.12**).

Table 5.12: The relative intensities of HSP70, GAPDH, calnexin, and cytochrome C oxidase bands on Figure 5.12A western blots of directly cisplatin treated A-2780 cells and exosomes derived from cisplatin treated A-2780 cells compared with control A-2780 cells and exosomes.

Sample	Relative intensity			
	HSP70	**GAPDH**	**Calnexin**	**Cytochrome C oxidase**
Control cells	1.00	1.00	1.00	1.00
Control exosomes	0.09	0.17	0.01	0.00
Directly cisplatin treated cells	0.74	0.71	0.36	0.43
Cisplatin treated cell-derived exosomes	0.08	0.42	0.04	0.02

To determine the effect of cisplatin treatment on exosome secretion levels, NTA was performed on three samples of control exosomes and three samples of cisplatin exosomes derived from A-2780 cells. Six T175 flasks were seeded at equal concentration of A-2780 cells, and once 70% confluency was reached, three of the flasks were cisplatin treated for 2 hours at a concentration of 40 µM. The remaining three flasks were maintained at 37°C and used as control exosome donating cells. Exosomes were extracted the following day, and exosome concentration was determined by NTA. There was no significant difference between the concentration of exosomes released by control A-2780 cells (13.00×10^8 particles/mL) compared with cisplatin treated A-2780 cells (17.22×10^8 particles/mL) (**Figure 5.12B**). This indicates that stress-induced by cisplatin does not affect the number of exosomes released by A-2780 cells.

TEM identified vesicles within the size range of exosomes (30–160 nm) for both control and cisplatin exosomes (**Figure 5.12C&D**). In addition to irradiation and heat shocking (**Figure 5.5C&D**), cisplatin exosomes were also shown to be statistically significantly smaller in diameter than control A-2780 cell-derived exosomes (p = 2.112×10^{-8}).

To check that the increase in cell invasion was caused specifically by cisplatin exosomes rather than increased exosome number induced by the cisplatin treatment, the Matrigel invasion assay was repeated with A-2780 cells treated with 1X control exosomes (exosomes extracted from approximately 10 million cells, cultured for 24 hours in EFM), 2X control exosomes (exosomes extracted from approximately 20 million cells, cultured for 24 hours in EFM), or 1X cisplatin exosomes (**Figure 5.12E**). This experiment generated different results to those obtained previously. Compared with 1X control exosome treatment, both 2X control and 1X cisplatin exosome treatments caused statistically significantly fewer invasive A-2780 cells (p = 0.001 and p = 0.0003, respectively). This suggests that doubling the concentration of exosomes administered does not increase invasive behaviour of A-2780 cells. However on this occasion, cisplatin exosomes were not capable of increasing A-2780 cell invasive capacity.

Representative images of the Matrigel membranes are shown in **Figure 5.12F**. The highest number of invasive cells were found on the Matrigel membranes that contained cells treated with 1X control exosomes. Lower numbers of invasive cells are shown on membranes treated with either 2X control exosomes or 1X cisplatin exosomes.
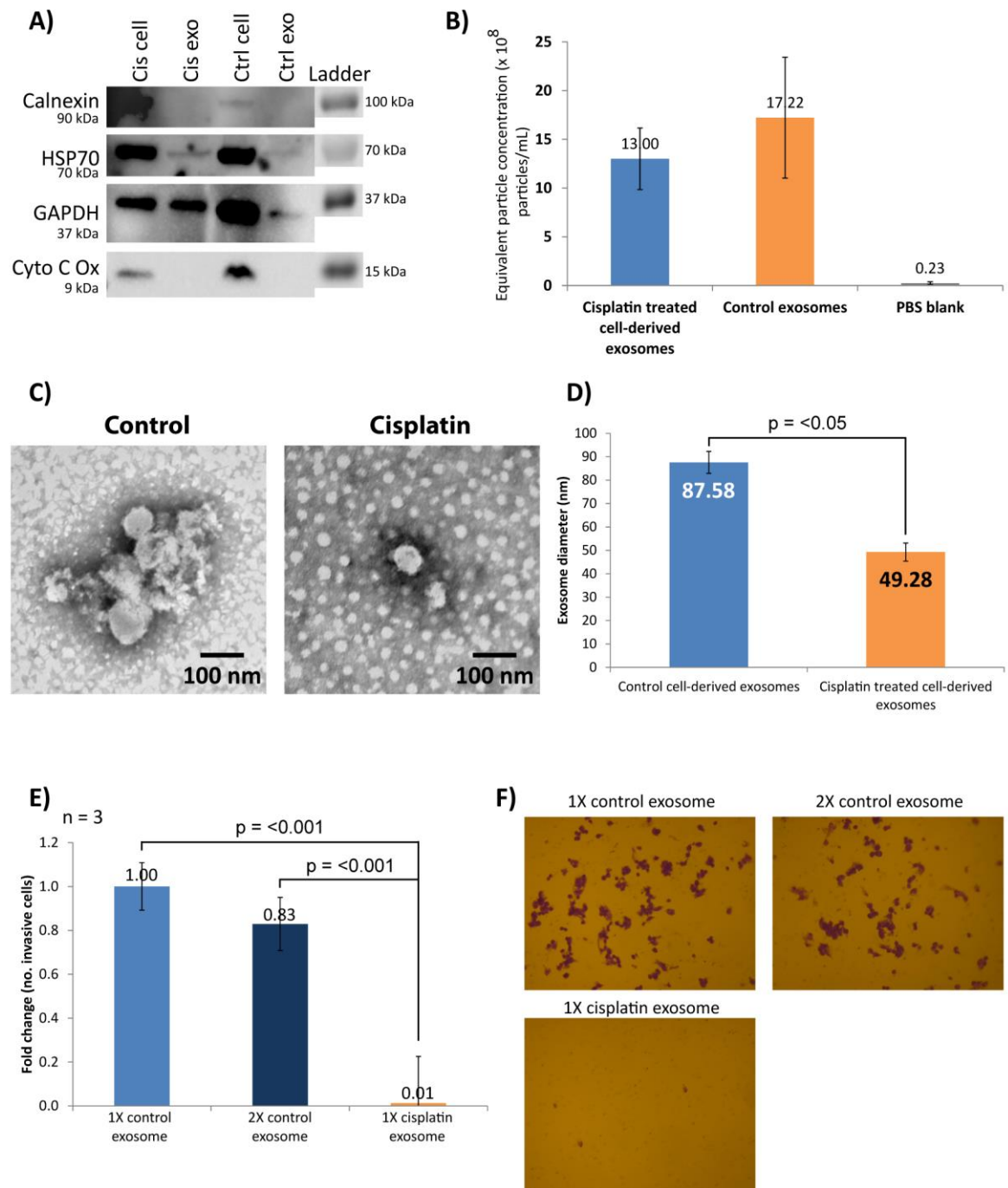
Figure 5.12: Characterisation of cisplatin and control exosomes derived from A-2780 cells and their effect on invasive behaviour on naïve A-2780 cells. A) Control and cisplatin treated cell and exosome protein lysates were characterised by western blotting, samples were probed for GAPDH, calnexin, HSP70, and cytochrome C oxidase. B) Quantification of exosomes secreted by control and cisplatin treated A-2780 cells by nanoparticle tracking analysis. C) Images of electron microscopy grids of control and cisplatin exosomes visualised by transmission electron microscopy. D) Average diameter of exosomes secreted by cisplatin treated and control A-2780 cells measured on electron microscopy grids (C). There were two biological replicates containing diameter measurements of 50 exosomes. E) Matrigel assay performed to investigate the effect of exosome concentration and cisplatin exosomes upon invasive capacity of A-2780 cells. 1X control exosomes was equivalent to exosomes extracted from approximately 10 million cells, cultured in exosomes-free media for 24 hours. 2X control exosomes was equivalent to exosomes extracted from 20 million cells. F) Representative images of Matrigel membranes showing invasive A-2780 cells following treatment with different concentrations and types of exosomes (in the Matrigel invasion experiment, E). P values were calculated using the two tailed T-test.

5.2.13. Optimisation of exosome uptake inhibition with heparin and proteinase K

To further confirm that cisplatin exosomes increase invasiveness of recipient cells, experiments were planned to show reversal of this effect by inhibiting exosome uptake. Heparin and proteinase K were chosen for optimisation in our lab. Heparin pre-treatment of cells and exosomes at 10.0 mg/mL heparin for 30 minutes at 37°C prior to exosome administration onto cells, and proteinase K pre-treatment of exosomes prior to their administration onto cells at 1.0 mg/mL proteinase K for 30 minutes at 37°C were both successful methods for inhibition of exosome uptake. The average volume of PKH26-exosomes identified inside cells following exosome uptake inhibition was statistically significantly reduced from 11.00 μm^3 to 0.09 μm^3 for heparin treatment and from 143.26 μm^3 to 0.50 μm^3 for proteinase K treatment (**Figure 5.13**). Heparin binds many ECM proteins (Sarrazin *et al.*, 2011) so is not a suitable exosome uptake inhibitor for invasion experiments involving Matrigel. Therefore, proteinase K was selected for subsequent Matrigel invasion experiments involving exosome uptake inhibition of cisplatin exosomes.

Figure 5.13: Exosome uptake inhibition with heparin and proteinase K. A) Confocal images of exosome uptake by A-2780 after control (no heparin) and heparin treatment of cells and exosomes. B) Bar graph representing exosome uptake in terms of average PKH26-exosome volume per cell for control and heparin treated cells and exosomes. C) Confocal images of exosome uptake by A-2780 after control (no proteinase K) and proteinase K treatment of exosomes. D) Bar graph representing exosome uptake in terms of average PKH26-exosome volume per cell for control and proteinase K treated exosomes. There were three biological replicates for each treatment type; within each biological replicate, the exosome volume inside 40 cells was measured. Confocal images were taken at x630 magnification. Red signal represents PKH26-stained exosomes inside cells; blue signal represents DAPI-stained cell nuclei. Error bars represent standard error of the mean. P values were calculated using the two tailed T-test.
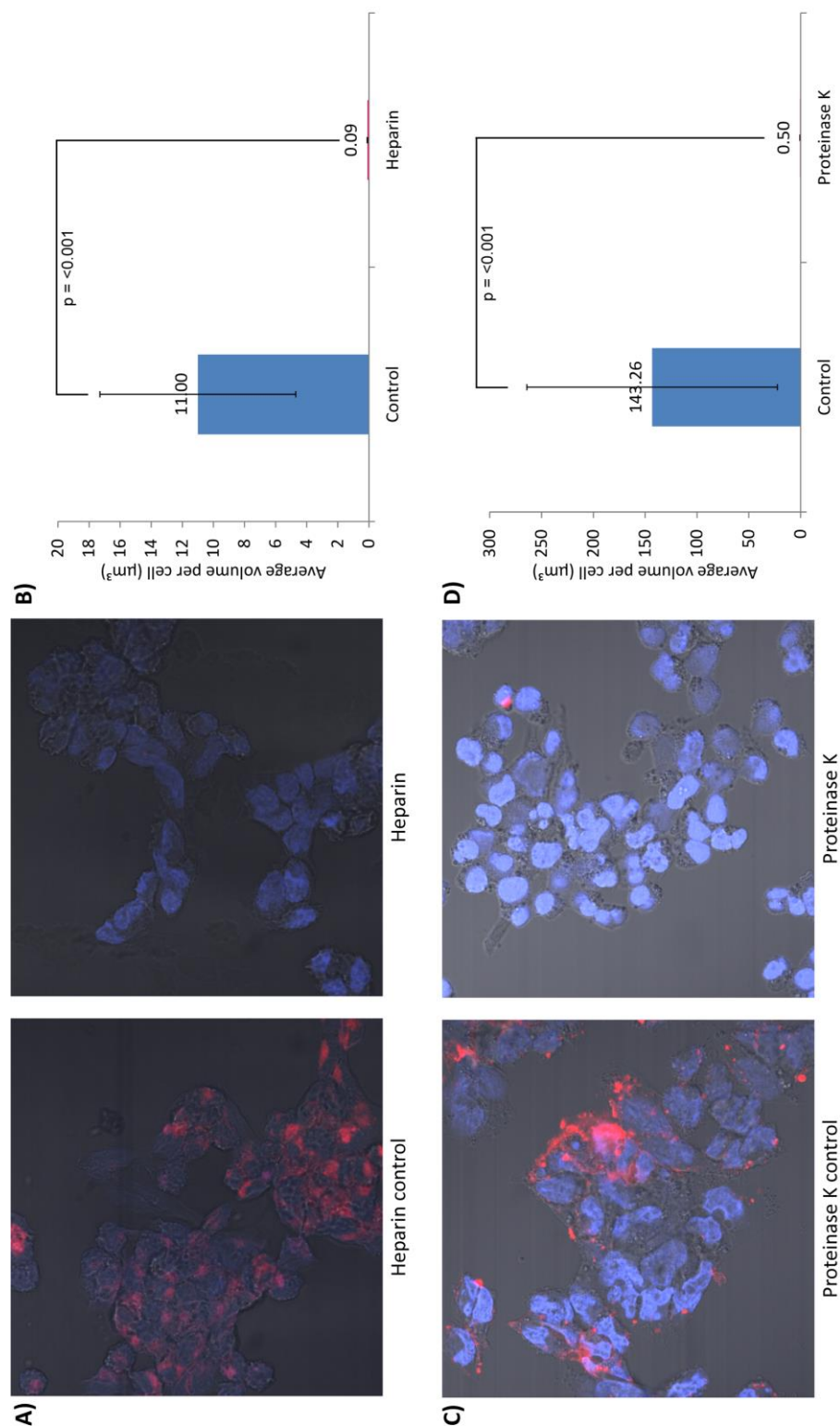
5.2.14. The effect of exosome uptake and DNA repair inhibitors on the ability of cisplatin exosomes to increase invasiveness of A-2780 cells

In an attempt to describe, at least in part, the mechanism responsible for cisplatin exosome-mediated increase in cellular invasive capacity, proteinase K (previously shown to inhibit exosome uptake [**Figure 5.13**]) and the DNA-PK inhibitor NU7441 were used. Proteinase K was added to cisplatin exosomes for 30 minutes, then inhibited by boiling for 10 minutes, prior to their administration onto cells. In addition to cisplatin exosomes, 10.0 µM NU7441 was administered to cells over a 24 hour treatment period. Proteinase K and NU7441 treatments occurred both 24 hours before and immediately after cells were seeded in the Matrigel trans-well inserts. Compared with control A-2780 exosome treatments, cisplatin exosomes did not increase cellular invasiveness (**Figure 5.14**), unlike in previous experiments (**Figure 5.11**). Inhibiting cisplatin exosome uptake with proteinase K was predicted to reduce cellular invasiveness, however, invasiveness did not decrease compared with cells treated with control exosomes or cisplatin exosomes (**Figure 5.14**). NU7441 treatment in addition to cisplatin exosomes statistically significantly reduced cellular invasiveness in comparison with cells treated with control exosomes, cisplatin exosomes, and control exosomes (**Figure 5.14**).

A)

n = 3

B)
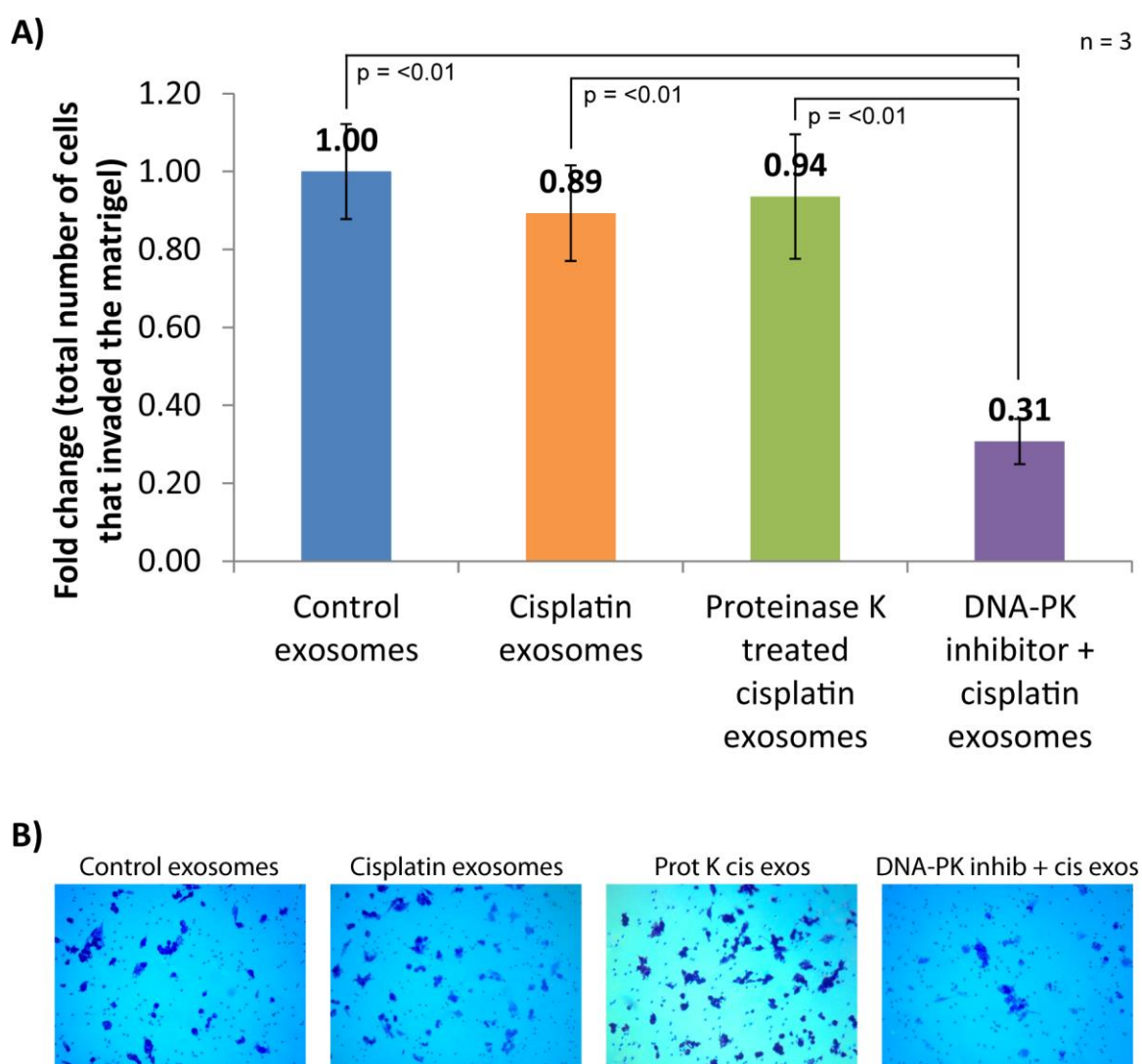
Figure 5.14: The effect of inhibiting exosome uptake and DNA-PK activity upon the ability of cisplatin exosomes to influence invasive capacity of A-2780 ovarian cancer cells. A) Matrigel assay performed to investigate the effect of A-2780 cell invasiveness following cisplatin exosome uptake inhibition with proteinase K and DNA-PK inhibition with NU7441 in cisplatin exosome recipient cells. B) Representative images of Matrigel membranes showing invasive A-2780 cells following treatment with different compounds and types of exosomes (in the Matrigel invasion experiment, A). There were three biological replicates for each treatment type, all of the cells were counted on each Matrigel membrane. P values were calculated using the two tailed T-test.

5.2.15. The role of kinases in cisplatin exosome mediated increase in A-2780 cell invasiveness

With the aim of improving our understanding of the mechanism responsible for increased cell invasiveness induced by cisplatin exosomes, the proteome profiler human phospho-MAPK array was used. The relative phosphorylation levels of 26 kinases was determined for A-2780 cells treated with either control exosomes or cisplatin exosomes. The signal intensity at each capture spot represented bound phosphorylated protein and was used to calculate relative phosphorylation levels of each kinase (**Figure 5.15A**). Phosphorylation of each kinase was measured in duplicate (two spots for each kinase). Significant differences in protein kinase phosphorylation between samples were calculated using the two tailed T-test. Seven kinases had statistically significantly different relative levels of phosphorylation between the cells treated with cisplatin exosomes and the control exosome treatment. The downregulated kinases were: CREB ($p = 0.019$), extracellular signal-regulated kinases (ERK) 2 ($p = 0.050$), and TOR ($p = 0.0021$); upregulated kinases were: JNK2 ($p = 0.00087$), JNKpan ($p = 0.044$), p38α ($p = 0.038$), and p53 ($p = 0.015$) (**Figure 5.15B**). These results indicate that CREB, ERK2, TOR, JNK2, JNKpan, p38α, and p53 may have a role in the mechanism responsible for cisplatin exosome-induced increased A-2780 cell invasiveness.

Statistically significant down-regulation of CREB phosphorylation levels was consistent between heat shock exosome treated MCF-7 cells and cisplatin exosome treated A-2780 cells (compared with control exosome treated cell equivalents). p53 expression was different in both types of stress exosome treated cells but was statistically significantly increased in cisplatin exosome treated A-2780 cells and statistically significantly decreased in heat shock exosome treated MCF-7 cells.
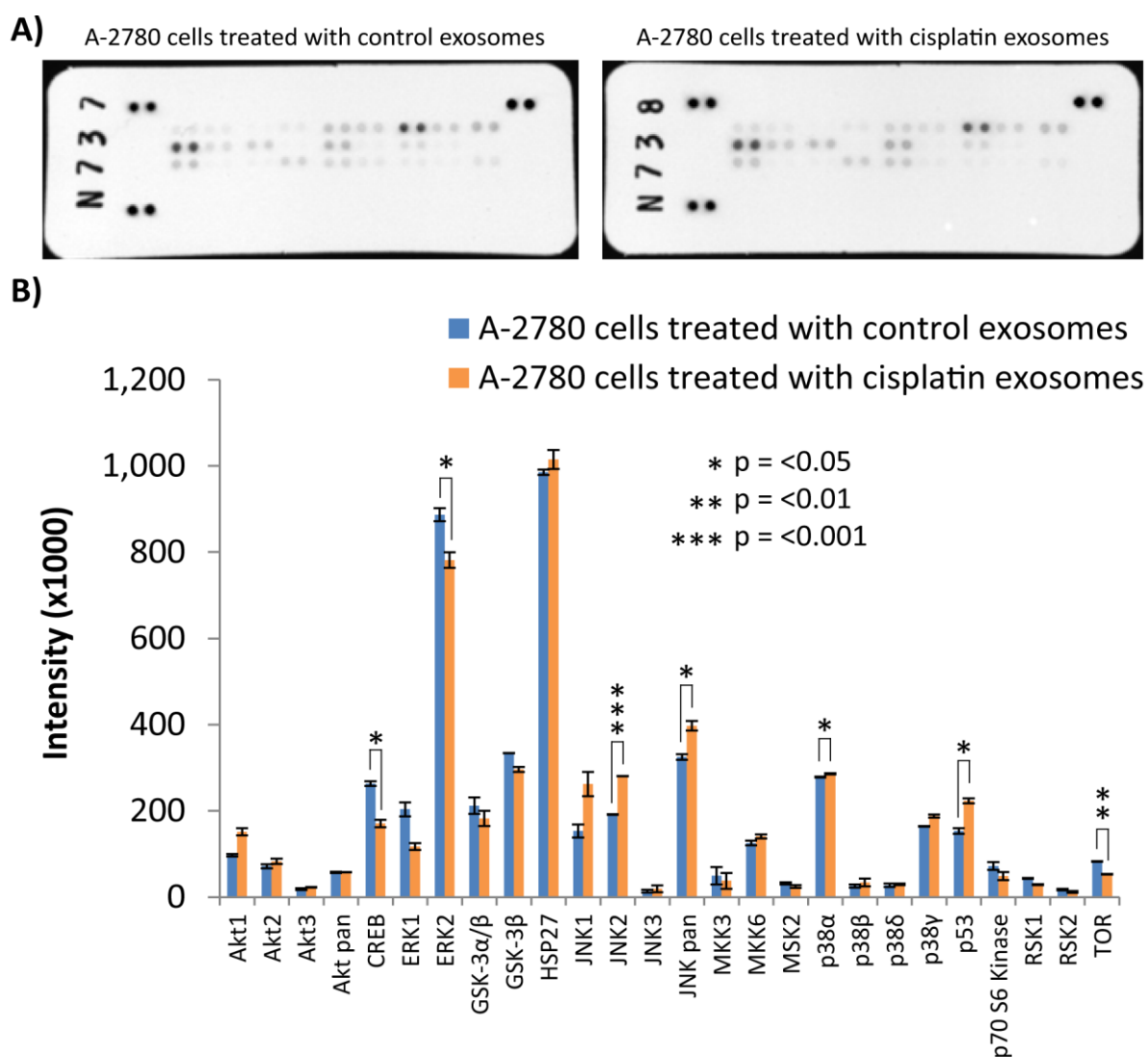
Figure 5.15: Relative phosphorylation levels of 26 kinases in A-2780 cells following treatment with either control or cisplatin exosomes determined using the proteome profiler human phospho-MAPK array. A) Blots showing intensity for each kinase on duplicate spots for each exosome treatment. B) Intensity levels of each kinase in A-2780 cells treated with either control or cisplatin exosomes. Differences in kinase phosphorylation were calculated using the two tailed T-test.

5.3. Discussion

There is evidence to suggest that exosomes can transfer protection to stress from cells that have experienced stress to naïve cells (Al-Mayah *et al.*, 2012; Arscott *et al.*, 2013; Eldh *et al.*, 2010; Ngora *et al.*, 2012; Park *et al.*, 2010; Ramteke *et al.*, 2015; Wang *et al.*, 2014). Cells undergoing stress may send signals to their neighbours to help them respond to adverse environmental conditions, and as a result improve their chance of survival. Increased recipient cell motility and invasive capacity as a consequence of receipt of such a signal would enable cells to escape the potential threat. It was predicted that stress alerts are transferred between cells via exosomes. In support of this idea, results in this chapter demonstrate that exosomes derived from both heat shocked (**Figure 5.4**) and cisplatin treated cells (**Figure 5.11**) increase the invasiveness of some lines of recipient cancer cells.

5.3.1.   Stressed cell derived exosomes increase recipient cell invasiveness

Exosomes were extracted from heat shocked cells and applied to cells in the Matrigel invasion assay. This experiment showed that heat shock exosomes statistically significantly increased the invasiveness of MCF-7 cells (**Figure 5.4**). A-2780 and IGROV-1 cells were treated with cisplatin, then exosomes were extracted from these stressed cells, and applied to cells in the Matrigel invasion assay. This experiment showed that cisplatin exosomes statistically significantly increased the invasiveness of A-2780 cells (**Figure 5.11**).

5.3.2.   Establishment of cancer cell line invasive capacity

With the purpose of distinguishing more invasive ovarian cancer cell lines from less invasive cell lines, the Matrigel invasion assay was used. Prior to commencement of this project a comparison between the invasive capacities of a range of ovarian cancer cell lines had not been made, despite the Matrigel invasion assay being used as an *in vitro* model for analysis of cellular invasive competence. This project established that SKOV-3 cells were the most invasive, of the nine ovarian cancer cell lines tested, and A-2780 and OVCAR-3 cell lines were the least invasive (**Figure 5.1**). The ECM layer did not affect the invasive capacity of A-2780, IGROV-1 nor OVCAR-3 cells. However, CP-70, MCP-1, OVCAR-4, OVCAR-5, OVCAR-8, and SKOV-3 cell invasive capacities were statistically significantly reduced by the ECM barrier. This suggests that these cell lines migrate easily across semi-permeable membranes but their ECM-degradation ability restricts the number of cells that can invade the membrane. The invasive competence of the breast cancer cell line MCF-7 was also established; their invasive capacity through semi-permeable membranes and

membranes coated in Matrigel was similar to that of A-2780 and OVCAR-3 ovarian cancer cell lines (**Figure 5.1**). Analysis of gene expression differences between the cell lines may explain differences in their invasive capacities. The establishment of cellular invasive competencies will provide a useful tool for ovarian cancer researchers in the future for more sophisticated experimental design.

5.3.3. Optimisation of the heat shocking procedure

Heat shocking cells for 1 hour was shown to increase cellular protein expression of HSP70 (**Figure 5.3**) and therefore strongly suggested that cells were sufficiently heat shocked, inducing a cellular stress response. The GO terms 'heat shock protein binding' and 'damaged DNA binding' were identified by differential gene expression data for heat shock exosome recipient cell versus directly heat shocked cells (**Table 5.10**). This may be a consequence of the exposure of the cells to the extreme temperature of 45°C. Up-regulation of components of these pathways further suggest that the heat shocking procedure was sufficiently stressing cells.

5.3.4. Stress exosome characterisation

Heat shock exosomes derived from MCF-7 cells, and cisplatin exosomes derived from A-2780 cells were characterised by WB, TEM, and NTA. WB results showed that heat shock exosomes contained HSP70 at an elevated level compared with control exosomes (**Figure 5.5A**). An increase in exosomal HSP70 concentration has also been shown by Clayton and colleagues in 2005, where exosomes were collected after heat shocking B-cells for 3 hours at 42°C (Clayton *et al.*, 2005). These results indicate that the method used in this project, of heat shocking cells at 45°C for 1 hour, also increases expression of HSP70 in heat stressed cells resulting in a higher concentration of HSP70 in the exosomes secreted by these cells. Cisplatin exosomes contained the exosome marker HSP70 and the positive/loading control protein GAPDH (present in both cells and exosomes) (**Figure 5.12A**). Heat shock and cisplatin exosome samples were also free of organelle and apoptotic body contamination. TEM identified exosomes within the expected size range, 30–160 nm (Ludwig and Giebel, 2012), but stress (both heat shock and cisplatin) exosomes were statistically significantly smaller in diameter (**Figure 5.5C&D** and **Figure 5.12C&D**). These results are consistent with previous findings in our research group, where Dr Laura Jacobs showed that exosomes secreted by irradiated MCF-7 cells were also significantly smaller than those secreted by control cells (Jacobs *et al.*, unpublished data).

5.3.5. The effect of exosome concentration on cellular invasiveness

Previous studies (section **5.1.8**) have shown that stress causes an increase in exosome secretion concentration (Al-Mayah *et al.*, 2015; Clayton *et al.*, 2005; Jella *et al.*, 2014; King *et al.*, 2012; Lv *et al.*, 2012; Ngora *et al.*, 2012; Salomon *et al.*, 2013a; Wang *et al.*, 2014). Therefore, one explanation for the observed increase in cell invasiveness in response to stress (both heat shock and cisplatin) exosome treatment was a higher exosomal dose instead of specific components of stress exosomes. To investigate this, exosome secretion following stress was compared with secretion under control conditions. Exosomes were extracted and quantified using NTA (**Figure 5.5B** and **Figure 5.12B**) – stress did not cause an increase in exosome secretion. To further confirm this, cell invasiveness was measured using the Matrigel invasion assay to compare treatment with control exosomes extracted from 6 million cells with treatment with control exosomes extracted from 12 million cells. The difference in cellular invasiveness was not statistically significantly different (**Figure 5.5E** and **Figure 5.12E**). This indicates that a specific exosome component of heat shock and cisplatin exosomes, rather than exosome concentration, is responsible for the increased invasive capacity observed in cancer cell lines. For the heat shock exosome treatment, cellular invasiveness was increased, although did not quite reach significance (because of high intra-assay variability) (**Figure 5.5E**). However, cisplatin exosomes did not increase cellular invasiveness in this experiment (**Figure 5.12E**); this may have been caused by accumulation of mutations as a result of successive passaging of the A-2780 cell line (causing alterations to cellular characteristics), insufficient cisplatin exposure of parental cells caused by discrepancy in cisplatin administration, or expired cisplatin.

Microarray data suggests that relative expression levels of three genes: *Bet-1*, *SNAP23*, and *VAMP4* (**Figure 5.8A** and **Table 5.5**), were statistically significantly different in MCF-7 cells that were directly heat shocked compared with control cells. These genes are all involved in SNARE interactions in vesicular transport (**Figure 5.9**). These results are consistent with previous studies that provide evidence for increased secretion of exosomes following cellular stress (section **5.1.8**) (Al-Mayah *et al.*, 2015; Clayton *et al.*, 2005; Jella *et al.*, 2014; King *et al.*, 2012; Lv *et al.*, 2012; Ngora *et al.*, 2012; Salomon *et al.*, 2013a; Wang *et al.*, 2014).

5.3.6. Invasive cell distribution on Matrigel membranes

The invasive cells were observed on the Matrigel coated membranes, small clusters of MCF-7 cells were shown on the membranes, suggesting that MCF-7 cells invade more effectively in groups rather than single cells (**Figure 5.5F**) (section **4.1.1**). However, A-2780 cell spread across Matrigel

membranes was more uniform (**Figure 5.12F**) suggesting that they are more capable of invading as single cells.

5.3.7. The effect of heat shock exosomes on cell motility

To determine whether heat shock exosomes had the same effect on cell motility as they do on cell invasiveness, the scratch assay was used. Twenty-four hours after heat shocking, the media was aspirated, filtered, and administered to naïve cells. Then 24 hours later, the scratch assay was performed, and a second dose of heat shocked cell media was added to the cells. For comparison, and to confirm cellular damage, cell motility was also analysed in directly heat shocked cells using the scratch assay. As expected, directly heat shocked cells were less motile than control and heat shock media transfer recipient cells. This is likely to result from the damage caused during the heat shocking procedure. Heat shock media transfer did not affect the motility of recipient cells compared with control cells, suggesting that, unlike cellular invasiveness, heat shock exosomes (that were suspended in the conditioned media) did not affect cell motility (**Figure 5.6**). Had an effect been observed, this experiment would have been repeated but heat shock exosomes would have been extracted from the media and administered directly onto MCF-7 cells to determine whether that the increase in cell motility was caused by heat shock exosomes or another component of the heat shock media.

5.3.8. Exosome uptake inhibition experiment

In order to show that cellular invasiveness induced by stress exosomes is reversed when exosome uptake is inhibited, an experiment was optimised to inhibit exosome uptake using heparin (**Figure 5.11A&B**). Heparin has been used as an inhibitor of exosome uptake in previous studies (Christianson *et al.*, 2013; Mulcahy *et al.*, 2014; Svensson *et al.*, 2013). However, exosome uptake inhibition needed to be used in synchrony with the Matrigel invasion assay, since heparin binds with HSPG components of the Matrigel it was not suitable for this experiment. Therefore, proteinase K was optimised as an alternative exosome uptake inhibitor (**Figure 5.12C&D**). Protein interactions are key for exosomal uptake, and proteinase K has been shown to abrogate internalisation of EVs (Escrevente *et al.*, 2011). Both heparin and proteinase K statistically significantly reduced the level of PKH26-exosome signal detected inside A-2780 cells.

5.3.9. The role of cisplatin exosomes in the increased invasiveness of A-2780 cells

Following the discovery of increased A-2780 invasiveness in response to cisplatin exosomes, exosome uptake inhibition by pre-treatment of cisplatin-exosomes with proteinase K was expected to reduce cellular invasion compared with cells treated only with cisplatin exosomes as exosome uptake had been inhibited. Had this result been obtained, it would have further indicated that cisplatin exosomes are responsible for increased cellular invasion. However, on this occasion, cisplatin exosomes did not increase invasiveness of recipient cells significantly more than control exosomes, and a reduction in invasiveness was not induced by proteinase K treatment (**Figure 5.14**). Reasons for this include: (1) exosome uptake may not be required to increase cell invasiveness; (2) exosome-cell protein-protein interactions are necessary for transfer of the signal from stress exosomes to cells to induce a more invasive phenotype; (3) the interaction on the cell surface between the cell and exosomal membranes may be sufficient for signal transduction (Rana and Zöller, 2011; Record *et al.*, 2014); (4) the A-2780 cell line had been passaged too many times so the characteristics of the cell line had evolved, and their response to cisplatin exosomes changed.

5.3.10. Elucidating the mechanism responsible for stress exosome-mediated increases in cellular invasiveness

5.3.10.1. The role of DNA-PK

DNA-PK is a nuclear serine/threonine protein kinase, an essential participant in the DNA repair pathway. It has an important role in the DNA damage response and maintenance of genomic stability. DNA-PK is activated upon association with DNA (Smith and Jackson, 1999), and recognises and then re-joins DSBs in DNA through non-homologous end joining (Smith and Jackson, 1999; Yoo and Dynan, 1999). DNA-PK expression has been shown to be significantly elevated in patients with advanced disease and has been correlated with decreased therapeutic response to DNA-damaging agents in several malignancies (Beskow *et al.*, 2009; Bouchaert *et al.*, 2012). This suggests that DNA-PK-mediated DNA repair is a mechanism involved in tumour cell survival and cancer development. High DNA-PK levels have also been associated with poor prognosis in the absence of DNA-damaging therapies (Evert *et al.*, 2013; Willmore *et al.*, 2008), suggesting a DNA damage response-independent role for DNA-PK in human cancers. DNA-PK has been identified as a mediator of cancer-promoting pathways distinct from DNA repair, including hypoxia, metabolism, inflammatory response, and transcriptional regulation (Goodwin and Knudsen, 2014). Goodwin and colleagues (2015) have shown that DNA-PK has a pivotal role in transcriptional regulation of cell migration, invasion, and metastasis of prostate cancer (Goodwin

et al., 2015). In the same study, suppression of DNA-PK inhibited prostate cancer metastasis (Goodwin *et al.*, 2015). It is possible that DNA-PK is active in other solid tumours. The stress exosome-associated increase in cancer cell invasiveness may be activated via a DNA-PK dependent pathway. To test this, DNA-PK was inhibited with NU7441 in cisplatin exosome recipient cells. Invasion was statistically significantly reduced in these cells in comparison with cells treated with cisplatin exosomes (**Figure 5.14**). However, since cells treated with cisplatin exosomes and proteinase K (to inhibit exosome uptake) and control exosomes were not statistically significantly less invasive than those treated with cisplatin exosomes, it is possible that the decreased cellular invasion observed was because of the NU7441 concentration being too high or the treatment period too long i.e. cell integrity caused reduced cell invasiveness. Because of time constraints, NU7441 concentration and treatment period were not optimised prior to performing the Matrigel invasion experiment, and the experiment was not repeated with altered conditions. Therefore, further experimentation is required to determine the role of DNA-PK in stress exosome-mediated increased cellular invasiveness.

5.3.10.2. Potential pathways involved in stress exosome-mediated increased cellular invasiveness

Carcinogenesis is a consequence of the disrupted balance between cell proliferation and apoptosis (programmed cell death). Therefore, proteins that regulate cell proliferation, differentiation, development, and apoptosis sustain oncogenic changes more frequently than molecules involved in other signalling pathways (Fresno Vara *et al.*, 2004). During cancer progression, the phosphorylation status of three major families of MAPKs: ERK1/2, JNK1–3, and different p38 isoforms (α/β/δ/γ), influence the aggressiveness of the tumour (Sebolt-Leopold and Herrera, 2004). Expression levels of signal transduction regulatory proteins, including: Akt, GSK-3, p70 S6 Kinase, TOR, p53, and CREB, which mediate cell development and proliferation, also indicate the pathways that are active inside the cell (Robinson and Cobb, 1997).

5.3.10.2.1. Effects upon the MAPK and PI-3K pathways in response to heat shock exosomes in MCF-7 recipient cells

Microarray data suggested that relative expression levels of three genes: *Fas*, *IGF-BP3*, and *PTEN* and/or *PTENP1* (**Figure 5.8B** and **Table 5.7**), were statistically significantly different in MCF-7 cells that received heat shock exosomes compared with control exosomes. These genes are all involved in the p53 signalling pathway (**Figure 5.10**). In addition to this, the proteome profiler

human phospho-MAPK array identified Akt2, CREB, HSP27, p38γ, and p53 as statistically significantly less phosphorylated in MCF-7 cells treated with heat shock exosomes compared with cells that received control exosomes (**Figure 5.7**). Akt2 overexpression is associated with a more malignant and aggressive phenotype in ovarian and pancreatic tumours (Cheng *et al.*, 1992; Cheng *et al.*, 1996). This protein kinase is capable of phosphorylating a number of known proteins. HSP27 is involved in stress resistance (Garrido *et al.*, 1997; Huot *et al.*, 1996; Wang *et al.*, 2002), its expression is induced by environmental stress, and the protein translocates from the cytoplasm to the nucleus upon stress induction (Bryantsev *et al.*, 2007). p53 is an essential tumour suppressor protein that responds to a diverse range of cellular stressors to regulate expression of cell cycle arrest, apoptosis, senescence, DNA repair, and metabolism (Levine *et al.*, 1991; Liu *et al.*, 2014b). p53 is mutated or deleted in 60–70% of cancers (Hollstein *et al.*, 1991; Levine *et al.*, 1991; Liu *et al.*, 2014b). p38 regulates cellular activity including proliferation, differentiation, transcription regulation, and development (Koul *et al.*, 2013). This kinase is triggered under conditions of environmental stress and its stimulation requires its phosphorylation by MAP kinase kinases or autophosphorylation (Raingeaud *et al.*, 1995; Zarubin and Han, 2005). p38 modulates stress-induced transcription and cell cycle regulation, with substrates of this kinase including many transcription regulators; one such protein is the tumour suppressor p53 (Koul *et al.*, 2013). Down-regulated p53 phosphorylation in heat shock exosome recipient MCF-7 cells may explain the reduction in p38γ phosphorylation levels.

Akt2, CREB, p38γ, and p53 have roles in cancer and its progression to invasive disease and HSP27, p38γ, and p53 participate in the stress response. Phosphorylation of all of these proteins was statistically significantly reduced in MCF-7 cells that received heat shock exosomes compared with control exosomes, therefore, the results obtained were unanticipated. Since heat shock exosomes increased invasive capacity of MCF-7 cells in previous experiments (**Figure 5.4** and **Figure 5.7E**), it was expected that phosphorylation of proteins involved in both cell invasiveness and stress response would increase.

5.3.10.2.2. *Effects on the MAPK and PI-3K pathways in response to cisplatin exosomes in A-2780 recipient cells*

The proteome profiler human phospho-MAPK array identified ERK2 and TOR as statistically significantly less phosphorylated, and JNK2, JNKpan, p38α, p53 had statistically significantly greater phosphorylation in A-2780 cells treated with cisplatin exosomes compared with cells that received control exosomes (**Figure 5.15**). ERK2 acts as an integration point for multiple biochemical signals, which affect proliferation, differentiation, transcription regulation, and

development. ERK2 mutations can drive the development of cancer (Samatar and Poulikakos, 2014; Dhillon *et al.*, 2007). TOR is a kinase that regulates the cellular stress response. It participates in cell cycle arrest following DNA damage (Shen *et al.*, 2007). JNK2 and JNKpan are closely related kinases that target specific transcription factors, which mediate immediate-early gene expression in response to cellular stimuli (Hirsch and Stork, 1997). Both of these kinases participate in UV radiation induced apoptosis that has been shown to be associated with the cytochrome C-mediated cell death pathway (Staples *et al.*, 2010; Wu *et al.*, 2002). JNK2 inhibits ubiquitination of p53 that stabilises p53 in non-stressed cells (Fuchs *et al.*, 1998).

Disruption of CREB, ERK2, JNK2, JNKpan, p38α, and p53 expression have detrimental effects on cells and contribute to the development of aggressive cancers. TOR, p38α, and p53 participate in the stress response. Despite this, phosphorylation of CREB, ERK2, and TOR was statistically significantly reduced in A-2780 cells that received cisplatin exosomes compared with control exosomes. This result was unexpected because of the results obtained previously showing that cisplatin exosomes had the ability to increase invasiveness of A-2780 cells compared with control exosomes (**Figure 5.11** and **Figure 5.12**), and also because of the roles that these proteins have in both cancer development and the stress response pathways. JNK2, JNKpan, p38α, and p53, however, were upregulated. This may explain, at least in part, the mechanism responsible for increased invasive activity of cells following treatment with cisplatin exosomes. All four of these up-regulated proteins are involved in the MAPK signalling pathway and the phosphoinositide 3-kinase (PI-3K) cascade. The MAPK signalling pathway and the PI-3K cascade are essential pathways for the regulation of the cell cycle. They modulate proliferation, quiescence, apoptosis, migration, and cancer. Deregulation of these pathways contributes considerably to cancer progression (Dhillon *et al.*, 2007; Fresno Vara *et al.*, 2004).

Increased cellular invasiveness in response to stress exosomes is not solely induced by activation of the MAPK and PI-3K pathways. Other pathways may also influence the increased invasion following stress exosome administration, but phosphorylation levels of proteins involved in only the MAPK signalling pathway were analysed.

5.3.11. Experimental limitations and future directions

5.3.11.1.   The reliability of cell cultures

After initially becoming more invasive following treatment with stress exosomes (**Figure 5.4** and **Figure 5.11**), stress exosomes failed to increase invasive competency of MCF-7 and A-2780 cells in subsequent experiments (**Figure 5.5E**, **Figure 5.12E** and **Figure 5.14**). The same batch of cell lines

(both MCF-7 and A-2780) were maintained for the duration of stress exosome experimentation, from initial establishment of an increase in cellular invasiveness induced by stress exosomes, throughout exosome uptake inhibition experiment optimisation, scratch assay experimentation to determine the effect of stress exosomes on cell motility, and also for investigations into the possible mechanism responsible for stress exosome-induced increased invasiveness. Using the cells for this length of time (approximately 40 passages), may have contributed to the inconsistency in the results because of selective pressures and genetic drift that cell lines can exhibit, and reduced or altered functions when kept in culture for too long (Hughes *et al.*, 2007). Cell lines with high passage numbers have often acquired a substantial number of mutations meaning that they no longer represent reliable models of their original source material (Yu *et al.*, 1997). Long-term sub-culturing forces selective pressure within the cell population, for example, rapidly dividing cells will eventually outcompete slower proliferating cells. Two of the main issues are that it is impossible to determine the age of a cancer cell in culture, and there is no marker that depicts a cell's age or how many times it has divided (Hughes *et al.*, 2007).

Then again, 40 passages is not generally regarded as a high passage number. Cells of this age would not typically have acquired enough mutations to induce substantial changes to their normal functions. The same batch of cells were used throughout because it was suspected that changing the batch of cells may have increased variation in experimental results. Retrospectively, more consistent results may have been achieved using cells with the same passage number (i.e. the cells were of similar age), and the cells should have been characterised not only visually but also by short tandem repeat polymorphism profiling (Nims *et al.*, 2010).

5.3.11.2. More evidence required to support increased metastatic capacity in stress exosome recipient cells

The effect of stress exosomes on cell invasiveness was tested using two experimental procedures, the Matrigel assay that examines cell invasiveness and also the scratch assay that determines cell motility (stressed cell conditioned culture media was introduced to recipient cells instead of isolated stress exosomes). Invasiveness increased in response to stress exosomes (**Figure 5.4** and **Figure 5.11**), however stressed cell conditioned culture media did not affect the motility of recipient cells. In order to further validate the results additional analysis of stress exosome recipient cells should be performed. Three-dimensional culture systems arguably better mimic the tumour microenvironment and tumour cell activity (Breslin and O'Driscoll, 2013), therefore this technique could be used to further determine how stress exosomes affect metastatic activity of cancer cells. Additionally, it is important to understand the mechanism responsible for any

changes in cellular characteristics. Attempts were made to show differences in phosphorylation levels of various MAPKs to help understand the pathways involved in increased invasiveness caused by stress exosomes (**Figure 5.7** and **Figure 5.15**), but future work should aim to specifically identify the proteins involved, enabling confident proposal of a suitable mechanism. Experimentation should not be restricted to the MAPK signalling pathway. Microarray data identified the genes *Fas*, *IGF-BP3*, and *PTEN* and/or *PTENP1*, which are all active in the p53 signalling pathway, differentially expressed between cells that received heat shock exosomes compared with control exosomes (**Figure 5.8B**). This concept should be investigated further through gene knockdown experimentation and quantitative polymerase chain reaction (qPCR).

5.4. Conclusion

The results in this chapter have provided evidence to show that exosomes extracted from two different cancer cell lines of different organs that were stressed using two different types of stressor, increase invasive capacity of some recipient cells. This is novel work to the cancer and exosome research fields. The results presented have great potential for further research. Future experiments should focus on investigating the effect of different types of environmental stressors (not restricted to heat shock and drug treatment) on exosome composition, and the effects of different types of stress exosomes upon cellular invasiveness. It is of primary importance to define the cellular mechanism responsible for the characteristic changes that occur in response to stress exosomes.

Chapter 6

Discussion

6.   Discussion

6.1. Novel contributions and impact of this project

This project was the first to provide evidence to suggest that exosomes secreted from stressed cells can increase the invasive capacity of cells that internalise and process them. Invasion of recipient cells was assessed using the Matrigel trans-well invasion assay and showed that heat shocked cell-derived exosomes had the ability to statistically significantly increase invasiveness of MCF-7 breast cancer cell line (**Figure 5.4**), and cisplatin treated cell-derived exosomes were able to increase invasiveness of A-2780 and IGROV-1 ovarian cancer cell lines (**Figure 5.11**). These results are interesting because tumour cells that resist, but become stressed during administration of cancer therapy, could be expelling exosomes that increase the invasiveness of neighbouring cancer cells. The effect of stress exosomes upon healthy cells was not investigated in this project but should be considered for future research.

6.1.1.   The potential impact of heparin on ovarian cancer metastasis

Heparin is a molecule typically used as an anti-coagulant (Hirsh *et al.*, 1998), although, its use as an exosome uptake inhibitor has recently been discovered (Christianson *et al.*, 2013; Franzen *et al.*, 2014; Svensson *et al.*, 2013). It was used in this project to confirm exosome uptake inhibition but could not be used in conjunction with the Matrigel trans-well invasion assay because it interacts with components of the Matrigel. Therefore, the effect of inhibition of cisplatin exosome uptake using heparin in recipient ovarian cancer cells could not be analysed. However, the use of heparin alongside chemotherapy for the treatment of ovarian cancer has shown improved patient survival (Mousa *et al.*, 2006, Stevenson *et al.*, 2007).

Low molecular weight heparin is routinely used for anti-thrombotic treatment of cancer patients (Lee *et al.*, 2003). Retrospective analysis of clinical data implied that heparin treatment, reduced metastasis, alongside other prognostic advantages, and hence, provided a survival benefit for patients with cancer (Hettiarachchi *et al.*, 1999); this was later confirmed by numerous prospective clinical trials (Akl *et al.*, 2008; Akl *et al.*, 2014; Noble, 2014). Decreased metastasis following chemotherapeutic treatment alongside heparin has been associated with increased efficacy of chemotherapeutics, whereby heparin reduces interstitial pressure that improves the accessibility of tumour tissue to anti-cancer drugs (Bendas and Borsig, 2012; Gil-Bernabé *et al.*, 2013). It is also possible that the exosome uptake inhibition activity of heparin may also contribute to the reductions in metastasis observed in patients following chemotherapy and heparin combination treatment. Should the increased invasiveness of cells in response to receipt

of exosomes secreted by cisplatin treated cells be confirmed, the value of heparin administration, alongside chemotherapeutics, would be recognised and could potentially be used as a standard frontline treatment option for patients with ovarian cancer.

6.2. Exosome extraction optimisation

Although there has been substantial progress in exosome research, the best method for isolating biologically intact exosomes is yet to be agreed upon within the exosome research field. Differential ultracentrifugation is the standard protocol for exosome isolation and is the most frequently used extraction technique within the field (Théry *et al.*, 2006). Problems associated with ultracentrifugation for exosome isolation have been identified, including low yields and operator-dependent inconsistencies in efficiency (Momen-Heravi *et al.*, 2013). Alternative strategies including sucrose density gradient centrifugation (Cantin *et al.*, 2008), immuno-affinity capture (Tauro *et al.*, 2012), and polymer based precipitation (Alvarez *et al.*, 2012) have limitations also, e.g. vesicle disruption, and co-purification of non-vesicular protein aggregates (Momen-Heravi *et al.*, 2013). Development of an exosome isolation method that consistently yields high recovery of functional exosomes is essential for progression of exosome research. In this project exosomes were extracted using classic differential ultracentrifugation; this may not be the most ideal method since this method does not eliminate impurities e.g. protein aggregates and other material that also pellet at $120,000 \times g$. Future work should strive to make use of more sophisticated exosome extraction techniques, where possible, to improve the quality of the exosome samples yielded.

6.3. Characterisation of exosomes

Secretion of a variety of types of EVs from cells has become appreciated over the past 20 years. Despite the release of apoptotic bodies during apoptosis being well-established (Hristov *et al.*, 2004), the concept that healthy cells also shed vesicles from their plasma membrane (now referred to as microvesicles) has only recently become widely acknowledged (Cocucci *et al.*, 2009; György *et al.*, 2011; Raposo and Stoorvogel, 2013). The definition of an 'exosome' has become more strict over the past few years, they are now widely regarded as vesicles 30–160 nm in diameter that are secreted from cells and specifically are of endosomal origin (Gould and Raposo, 2013).

Exosome characterisation remains a major challenge for the exosome research field (Théry *et al.*, 2006). Partly restricted by their small size, optimisation of exosome characterisation methods is

ongoing. There are no standard methods in place that have been agreed upon by the field's experts (Raposo and Stoorvogel, 2013; Taylor, 2015). Instead, exosome characterisation is carried out using as many techniques as feasibly possible with small sample quantities of exosomes (~50 µL). This often leaves minimal volume of the exosome sample remaining for functional experimentation. In this project exosomes were characterised by WB, TEM, NTA, and their biological viability was assessed by fluorescent staining coupled with confocal microscopy.

With the methods currently available, different types of EVs can be differentiated by size and density but it is impossible to distinguish their intracellular origins. Because of their small size, there is limited quantities of protein, mRNA, and miRNA material available to analyse for membrane or organelle markers. Additionally, there is cross-over between membrane and organelle markers, no single designated markers for each type of EV that can uniquely distinguish them have been identified (Kalra *et al.*, 2013; Tauro *et al.*, 2012). Until this issue has been overcome, exosomes are best characterised based on multiple techniques (Yáñez-Mó *et al.*, 2015).

Because of the current insufficient means for distinguishing different types of EVs, it is quite inaccurate to describe vesicles of 30–160 nm in diameter as exosomes because it is possible that vesicles within this size range did not originate in the endosome. Microvesicles and apoptotic bodies could also lie within this range. Nevertheless, throughout this thesis the term 'exosome' has been used to refer to material (vesicles) of less than 200 nm in size that were extracted by filtering of culture media through 0.22 µm filters and subsequent ultracentrifugation at $120,000 \times g$. The intracellular origin of the vesicles used throughout this project was not determined.

6.3.1. Distinct characteristics of stressed cell-derived exosomes

Stressed cell derived exosomes in this project were identified to be statistically significantly smaller than exosomes secreted by control (non-stressed) cells. Stressors included heat shocking (**Figure 5.5D**) and cisplatin treatment (**Figure 5.12D**). Previous data collected by Dr Laura Jacobs, a member of our research group, supports this. She discovered that when MCF-7 cells were irradiated under a 2.0 Gy dose, secreted exosomes were statistically significantly smaller (Jacobs *et al.*, unpublished data). It would be of interest to investigate whether smaller exosomes are secreted by cells in response to a variety of stressors, or whether this effect is limited to stress induced by heat shocking, cisplatin treatment, and irradiation.

In addition, HSP70 (known for its activity during the stress response – particularly in the cell's reaction to extreme heat [section **5.1.3**]) was more enriched in heat shock exosomes compared with control exosomes (**Figure 5.5A**). Cisplatin exosomes were not enriched for HSP70, this may suggest that cisplatin treatment does not activate the heat shock response pathway to the same degree as extreme heat, and as a result the components loaded into stress exosomes are dependent upon the stress type.

6.4. Motility, invasion, proliferation, and exosome secretion rates of different cancer cell lines

Motility, invasion, proliferation, and exosome secretion rates of different cancer cell lines were established during this project (**Figure 4.4** and **Figure 5.1**). These properties of the cell lines have not previously been determined and recorded. This information provides a useful tool for cancer researchers, they could use this information to enhance their experimental design. Cell lines with desirable characteristics, whether it be that they secrete high levels of exosomes, or they have a very motile phenotype, could be selected for their suitability to the desired experimental design.

The data collected in this project could be expanded to create a database that could be used by researchers worldwide. The number of cell lines and number of cellular characteristics analysed could be increased, the data would not need to be limited to cancer cell lines, and information about a range of different cell lines of different origins could be recorded. The database could be designed in a similar way to ExoCarta where researchers deposit their own experimental results to populate the database (Keerthikumar *et al.*, 2016; Mathivanan and Simpson, 2009; Mathivanan *et al.*, 2012; Simpson *et al.*, 2012). One of the major limitations of the scratch assay is unreliability and inconsistency in the results, generation of a public database would improve the reliability of the results because of accumulation of an increased number of biological replicates. As for the ExoCarta database, researchers would need to provide their methods to ensure that the experimental results can be compared and summarised.

6.5. The mechanism responsible for stress exosome-induced increased invasiveness of recipient cells

The mechanism responsible for increased invasiveness following receipt of stress exosomes needs to be further investigated. Experiments performed in this project suggest the involvement of members of the MAPK family of protein kinases (**Figure 5.7** and **Figure 5.15**), and the p53 signalling pathway (**Figure 5.10**). The increased invasiveness mechanism is not restricted to these

proteins and gene expression components. There are an extensive number of proteins that were not investigated for their potential role. qPCR experimentation should be performed to further confirm the down-/up-regulation of genes contributing to the effect. The increased invasiveness of recipient cells could also be a result of exosome mediated transfer of mRNA and miRNA to recipient cells.

6.5.1. The role of miRNA in exosome-mediated metastasis

Various studies have shown that exosomal transfer of miRNAs increases metastasis, e.g. miR-21 in oesophageal squamous cell carcinoma (Tanaka *et al.*, 2013), let-7 miRNAs in gastric cancer (Ohshima *et al.*, 2010), miR-10b in breast cancer (Singh *et al.*, 2014), miR-223 transferred by tumour-associated macrophages-derived exosomes in breast cancer (Yang *et al.*, 2011), miR-126 in chronic myelogenous leukaemia (Taverna *et al.*, 2014), and miR-192 in lung cancer (Valencia *et al.*, 2014). The RNA content of stress exosomes should be extracted, sequenced, and compared with that of control exosomes. The RNA signatures identified may correspond with cellular protein and gene expression changes detected in response to stress exosomes, and could provide evidence to further support the mechanism conjectured.

6.5.2. Future developments

This research could be extended by investigating the effect of exosomes extracted from cells treated with other types of stressor to determine whether increased cell invasiveness is limited to heat shock and cisplatin exosomes, or is a general effect of stress exosomes irrespective of the type of stress their parental cells endured. Research has been performed in our group using exosomes extracted from irradiated cells (donor cells received 2.0 Gy radiation) but the effect of these exosomes upon invasiveness of naïve cells was not investigated. This experiment could be performed along with testing exosomes extracted from cells that have endured other types of stress including hypoxia, oxidative stress, and other types of drugs or toxins (other than cisplatin).

6.6. Conclusion

Novel research findings of this thesis were: (1) the discovery of increased invasiveness of cells following receipt of exosomes that were extracted from cells that had endured either heat shock or cisplatin treatment; (2) the identification of secretion of significantly smaller exosomes from stressed cells; and (3) establishment of the motility rates, proliferation rates, exosome secretion levels, and invasive capacities of ten cancer cell lines. Additional experimentation performed as part of this project included: (1) exosome characterisation using WB, TEM, NTA, and confocal microscopy; (2) assessment of the effect of exosomes upon cell motility using the scratch assay; and (3) exosome uptake analysis and inhibition. Attempts were made to elucidate the mechanism responsible for increased cancer cell invasiveness in response to receiving stress exosomes, with CREB and p53 proteins, and the p53 signalling pathway identified as possible contributors.

References

7. <u>References</u>

Abedin, M. and King, N. (2010) 'Diverse evolutionary paths to cell adhesion', *Trends Cell Biol,* 20(12), pp. 734–42.

Adams, J. C. and Watt, F. M. (1993) 'Regulation of development and differentiation by the extracellular matrix', *Development,* 117(4), pp. 1183–98.

Aga, M., Bentz, G. L., Raffa, S., Torrisi, M. R., Kondo, S., Wakisaka, N., Yoshizaki, T., Pagano, J. S. and Shackelford, J. (2014) 'Exosomal HIF1α supports invasive potential of nasopharyngeal carcinoma-associated LMP1-positive exosomes', *Oncogene,* 33(37), pp. 4613–22.

Akl, E. A., Barba, M., Rohilla, S., Terrenato, I., Sperati, F., Muti, P. and Schünemann, H. J. (2008) 'Low-molecular-weight heparins are superior to vitamin K antagonists for the long term treatment of venous thromboembolism in patients with cancer: a cochrane systematic review', *J Exp Clin Cancer Res,* 27, pp. 21.

Akl, E. A., Kahale, L., Neumann, I., Barba, M., Sperati, F., Terrenato, I., Muti, P. and Schünemann, H. (2014) 'Anticoagulation for the initial treatment of venous thromboembolism in patients with cancer', *Cochrane Database Syst Rev,* 6, pp. CD006649.

Al-Mayah, A. H., Irons, S. L., Pink, R. C., Carter, D. R. and Kadhim, M. A. (2012) 'Possible role of exosomes containing RNA in mediating nontargeted effect of ionizing radiation', *Radiat Res,* 177(5), pp. 539–45.

Al-Mayah, A., Bright, S., Chapman, K., Irons, S., Luo, P., Carter, D., Goodwin, E. and Kadhim, M. (2015) 'The non-targeted effects of radiation are perpetuated by exosomes', *Mutat Res,* 772, pp. 38–45.

Al-Nedawi, K., Meehan, B., Micallef, J., Lhotak, V., May, L., Guha, A. and Rak, J. (2008) 'Intercellular transfer of the oncogenic receptor EGFRvIII by microvesicles derived from tumour cells', *Nat Cell Biol,* 10(5), pp. 619–24.

Alvarez, M. L., Khosroheidari, M., Kanchi Ravi, R. and DiStefano, J. K. (2012) 'Comparison of protein, microRNA, and mRNA yields using different methods of urinary exosome isolation for the discovery of kidney disease biomarkers', *Kidney Int,* 82(9), pp. 1024–32.

Alvarez-Erviti, L., Seow, Y., Yin, H., Betts, C., Lakhal, S. and Wood, M. J. (2011) 'Delivery of siRNA to the mouse brain by systemic injection of targeted exosomes', *Nat Biotechnol,* 29(4), pp. 341–5.

Anderson, H. C., Mulhall, D. and Garimella, R. (2010) 'Role of extracellular membrane vesicles in the pathogenesis of various diseases, including cancer, renal diseases, atherosclerosis, and arthritis', *Lab Invest,* 90(11), pp. 1549–57.

Andre, F., Schartz, N. E., Movassagh, M., Flament, C., Pautier, P., Morice, P., Pomel, C., Lhomme, C., Escudier, B., Le Chevalier, T., Tursz, T., Amigorena, S., Raposo, G., Angevin, E. and Zitvogel, L. (2002) 'Malignant effusions and immunogenic tumour-derived exosomes', *Lancet,* 360(9329), pp. 295–305.

Andreasen, P. A., Egelund, R. and Petersen, H. H. (2000) 'The plasminogen activation system in tumor growth, invasion, and metastasis', *Cell Mol Life Sci,* 57(1), pp. 25–40.

Anthoney, D. A., McIlwrath, A. J., Gallagher, W. M., Edlin, A. R. and Brown, R. (1996) 'Microsatellite instability, apoptosis, and loss of p53 function in drug-resistant tumor cells', *Cancer Res,* 56(6), pp. 1374–81.

Antonyak, M. A., Li, B., Boroughs, L. K., Johnson, J. L., Druso, J. E., Bryant, K. L., Holowka, D. A. and Cerione, R. A. (2011) 'Cancer cell-derived microvesicles induce transformation by transferring tissue transglutaminase and fibronectin to recipient cells', *Proc Natl Acad Sci U S A,* 108(12), pp. 4852–7.

Appleton, K., Mackay, H. J., Judson, I., Plumb, J. A., McCormick, C., Strathdee, G., Lee, C., Barrett, S., Reade, S., Jadayel, D., Tang, A., Bellenger, K., Mackay, L., Setanoians, A., Schätzlein, A., Twelves, C., Kaye, S. B. and Brown, R. (2007) 'Phase I and pharmacodynamic trial of the DNA methyltransferase inhibitor decitabine and carboplatin in solid tumors', *J Clin Oncol,* 25(29), pp. 4603–9.

Arscott, W. T., Tandle, A. T., Zhao, S., Shabason, J. E., Gordon, I. K., Schlaff, C. D., Zhang, G., Tofilon, P. J. and Camphausen, K. A. (2013) 'Ionizing radiation and glioblastoma exosomes: implications in tumor biology and cell migration', *Transl Oncol,* 6(6), pp. 638–48.

Atay, S., Banskota, S., Crow, J., Sethi, G., Rink, L. and Godwin, A. K. (2014) 'Oncogenic KIT-containing exosomes increase gastrointestinal stromal tumor cell invasion', *Proc Natl Acad Sci U S A,* 111(2), pp. 711–6.

Babst, M. (2005) 'A protein's final ESCRT', *Traffic,* 6(1), pp. 2–9.

Bache, K. G., Brech, A., Mehlum, A. and Stenmark, H. (2003) 'Hrs regulates multivesicular body formation via ESCRT recruitment to endosomes', *J Cell Biol,* 162(3), pp. 435–42.

Badylak, S. F., Freytes, D. O. and Gilbert, T. W. (2015) 'Reprint of: Extracellular matrix as a biological scaffold material: Structure and function', *Acta Biomater,* 23 Suppl, pp. S17–26.

Baj-Krzyworzeka, M., Szatanek, R., Weglarczyk, K., Baran, J., Urbanowicz, B., Brański, P., Ratajczak, M. Z. and Zembala, M. (2006) 'Tumour-derived microvesicles carry several surface determinants and mRNA of tumour cells and transfer some of these determinants to monocytes', *Cancer Immunol Immunother,* 55(7), pp. 808–18.

Balkwill, F. R., Capasso, M. and Hagemann, T. (2012) 'The tumor microenvironment at a glance', *J Cell Sci,* 125(Pt 23), pp. 5591–6.

Banyard, J. and Bielenberg, D. R. (2015) 'The role of EMT and MET in cancer dissemination', *Connect Tissue Res*, 56(5), pp. 403–13.

Barreto, A., Rodríguez, L. S., Rojas, O. L., Wolf, M., Greenberg, H. B., Franco, M. A. and Angel, J. (2010) 'Membrane vesicles released by intestinal epithelial cells infected with rotavirus inhibit T-cell function', *Viral Immunol,* 23(6), pp. 595–608.

Bartel, D. P. (2004) 'MicroRNAs: genomics, biogenesis, mechanism, and function', *Cell,* 116(2), pp. 281–97.

Bartel, D. P. (2009) 'MicroRNAs: target recognition and regulatory functions', *Cell,* 136(2), pp. 215–33.

Bedoui, S., Prato, S., Mintern, J., Gebhardt, T., Zhan, Y., Lew, A. M., Heath, W. R., Villadangos, J. A. and Segura, E. (2009) 'Characterization of an immediate splenic precursor of CD8+ dendritic cells capable of inducing antiviral T cell responses', *J Immunol,* 182(7), pp. 4200–7.

Bénard, J., Da Silva, J., De Blois, M. C., Boyer, P., Duvillard, P., Chiric, E. and Riou, G. (1985) 'Characterization of a human ovarian adenocarcinoma line, IGROV1, in tissue culture and in nude mice', *Cancer Res,* 45(10), pp. 4970–9.

Bendas, G. and Borsig, L. (2012) 'Cancer cell adhesion and metastasis: selectins, integrins, and the inhibitory potential of heparins', *Int J Cell Biol,* 2012, pp. 676731.

Beskow, C., Skikuniene, J., Holgersson, A., Nilsson, B., Lewensohn, R., Kanter, L. and Viktorsson, K. (2009) 'Radioresistant cervical cancer shows upregulation of the NHEJ proteins DNA-PKcs, Ku70 and Ku86', *Br J Cancer,* 101(5), pp. 816–21.

Bidard, F. C., Pierga, J. Y., Vincent-Salomon, A. and Poupon, M. F. (2008) 'A "class action" against the microenvironment: do cancer cells cooperate in metastasis?', *Cancer Metastasis Rev,* 27(1), pp. 5–10.

Bijnsdorp, I. V., Geldof, A. A., Lavaei, M., Piersma, S. R., van Moorselaar, R. J. and Jimenez, C. R. (2013) 'Exosomal ITGA3 interferes with non-cancerous prostate cell functions and is increased in urine exosomes of metastatic prostate cancer patients', *J Extracell Vesicles,* 2, pp. 22097.

Birchmeier, C., Birchmeier, W., Gherardi, E. and Vande Woude, G. F. (2003) 'Met, metastasis, motility and more', *Nat Rev Mol Cell Biol,* 4(12), pp. 915–25.

Blood, C. H. and Zetter, B. R. (1990) 'Tumor interactions with the vasculature: angiogenesis and tumor metastasis', *Biochim Biophys Acta,* 1032(1), pp. 89–118.

Bobrie, A., Colombo, M., Raposo, G. and Théry, C. (2011) 'Exosome secretion: molecular mechanisms and roles in immune responses', *Traffic,* 12(12), pp. 1659–68.

Bobrie, A., Krumeich, S., Reyal, F., Recchi, C., Moita, L. F., Seabra, M. C., Ostrowski, M. and Théry, C. (2012) 'Rab27a supports exosome-dependent and -independent mechanisms that modify the tumor microenvironment and can promote tumor progression', *Cancer Res,* 72(19), pp. 4920–30.

Bockhorn, M., Jain, R. K. and Munn, L. L. (2007) 'Active versus passive mechanisms in metastasis: do cancer cells crawl into vessels, or are they pushed?', *Lancet Oncol,* 8(5), pp. 444–8.

Bonnans, C., Chou, J. and Werb, Z. (2014) 'Remodelling the extracellular matrix in development and disease', *Nat Rev Mol Cell Biol,* 15(12), pp. 786–801.

Booth, A. M., Fang, Y., Fallon, J. K., Yang, J. M., Hildreth, J. E. and Gould, S. J. (2006) 'Exosomes and HIV Gag bud from endosome-like domains of the T cell plasma membrane', *J Cell Biol,* 172(6), pp. 923–35.

Bose, N. and Masellis, A. M. (2005) 'Secretory products of breast cancer cells upregulate hyaluronan production in a human osteoblast cell line', *Clin Exp Metastasis,* 22(8), pp. 629–42.

Bouchaert, P., Guerif, S., Debiais, C., Irani, J. and Fromont, G. (2012) 'DNA-PKcs expression predicts response to radiotherapy in prostate cancer', *Int J Radiat Oncol Biol Phys,* 84(5), pp. 1179–85.

Breslin, S. and O'Driscoll, L. (2013) 'Three-dimensional cell culture: the missing link in drug discovery', *Drug Discov Today,* 18(5–6), pp. 240–9.

Brooks, S. A., Lomax-Browne, H. J., Carter, T. M., Kinch, C. E. and Hall, D. M. (2010) 'Molecular interactions in cancer cell metastasis', *Acta Histochem,* 112(1), pp. 3–25.

Brown, P. D. (1999) 'Clinical studies with matrix metalloproteinase inhibitors', *APMIS,* 107(1), pp. 174–80.

Brownlee, C. (2002) 'Role of the extracellular matrix in cell-cell signalling: paracrine paradigms', *Curr Opin Plant Biol,* 5(5), pp. 396–401.

Bryantsev, A. L., Kurchashova, S. Y., Golyshev, S. A., Polyakov, V. Y., Wunderink, H. F., Kanon, B., Budagova, K. R., Kabakov, A. E. and Kampinga, H. H. (2007) 'Regulation of stress-induced intracellular sorting and chaperone function of Hsp27 (HspB1) in mammalian cells', *Biochem J,* 407(3), pp. 407–17.

Butler, T. P. and Gullino, P. M. (1975) 'Quantitation of cell shedding into efferent blood of mammary adenocarcinoma', *Cancer Res,* 35(3), pp. 512–6.

Calabrese, V., Cornelius, C., Dinkova-Kostova, A. T., Calabrese, E. J. and Mattson, M. P. (2010) 'Cellular stress responses, the hormesis paradigm, and vitagenes: novel targets for therapeutic intervention in neurodegenerative disorders', *Antioxid Redox Signal,* 13(11), pp. 1763–811.

Camacho, L., Guerrero, P. and Marchetti, D. (2013) 'MicroRNA and protein profiling of brain metastasis competent cell-derived exosomes', *PLoS One,* 8(9), pp. e73790.

Cancer Research UK (2014a) *Breast cancer Key Stats*. Cancer Research UK. Available at: http://publications.cancerresearchuk.org/downloads/Product/CS_KF_BREAST.pdf (Accessed: 24th January 2016).

Cancer Research UK (2014b) *Ovarian cancer Key Stats*. Cancer Research UK. Available at: http://publications.cancerresearchuk.org/downloads/Product/CS_KF_OVARY.pdf (Accessed: 24th January 2016).

Cantin, R., Diou, J., Bélanger, D., Tremblay, A. M. and Gilbert, C. (2008) 'Discrimination between exosomes and HIV-1: purification of both vesicles from cell-free supernatants', *J Immunol Methods,* 338(1–2), pp. 21–30.

Chaffer, C. L., Thompson, E. W. and Williams, E. D. (2007) 'Mesenchymal to epithelial transition in development and disease', *Cells Tissues Organs,* 185(1–3), pp. 7–19.

Chairoungdua, A., Smith, D. L., Pochard, P., Hull, M. and Caplan, M. J. (2010) 'Exosome release of β-catenin: a novel mechanism that antagonizes Wnt signaling', *J Cell Biol,* 190(6), pp. 1079–91.

Chambers, A. F., Groom, A. C. and MacDonald, I. C. (2002) 'Dissemination and growth of cancer cells in metastatic sites', *Nat Rev Cancer,* 2(8), pp. 563–72.

Chaput, N. and Théry, C. (2011) 'Exosomes: immune properties and potential clinical implementations', *Semin Immunopathol,* 33(5), pp. 419–40.

Charpentier, M. and Martin, S. (2013) 'Interplay of Stem Cell Characteristics, EMT, and Microtentacles in Circulating Breast Tumor Cells', *Cancers (Basel),* 5(4), pp. 1545–65.

Chen, X., Liang, H., Zhang, J., Zen, K. and Zhang, C. Y. (2012) 'Secreted microRNAs: a new form of intercellular communication', *Trends Cell Biol,* 22(3), pp. 125–32.

Chen, G., Zhang, Y. and Wu, X. (2014) '786-0 Renal cancer cell line-derived exosomes promote 786-0 cell migration and invasion *in vitro*', *Oncol Lett,* 7(5), pp. 1576–1580.

Cheng, J. Q., Godwin, A. K., Bellacosa, A., Taguchi, T., Franke, T. F., Hamilton, T. C., Tsichlis, P. N. and Testa, J. R. (1992) 'AKT2, a putative oncogene encoding a member of a subfamily of protein-serine/threonine kinases, is amplified in human ovarian carcinomas', *Proc Natl Acad Sci U S A,* 89(19), pp. 9267–71.

Cheng, J. Q., Ruggeri, B., Klein, W. M., Sonoda, G., Altomare, D. A., Watson, D. K. and Testa, J. R. (1996) 'Amplification of AKT2 in human pancreatic cells and inhibition of AKT2 expression and tumorigenicity by antisense RNA', *Proc Natl Acad Sci U S A,* 93(8), pp. 3636–41.

Cheruvanky, A., Zhou, H., Pisitkun, T., Kopp, J. B., Knepper, M. A., Yuen, P. S. and Star, R. A. (2007) 'Rapid isolation of urinary exosomal biomarkers using a nanomembrane ultrafiltration concentrator', *Am J Physiol Renal Physiol,* 292(5), pp. F1657–61.

Choquet, D., Felsenfeld, D. P. and Sheetz, M. P. (1997) 'Extracellular matrix rigidity causes strengthening of integrin-cytoskeleton linkages', *Cell,* 88(1), pp. 39–48.

Christianson, H. C., Svensson, K. J., van Kuppevelt, T. H., Li, J. P. and Belting, M. (2013) 'Cancer cell exosomes depend on cell-surface heparan sulfate proteoglycans for their internalization and functional activity', *Proc Natl Acad Sci U S A,* 110(43), pp. 17380–5.

Chugh, P. E., Sin, S. H., Ozgur, S., Henry, D. H., Menezes, P., Griffith, J., Eron, J. J., Damania, B. and Dittmer, D. P. (2013) 'Systemically circulating viral and tumor-derived microRNAs in KSHV-associated malignancies', *PLoS Pathog,* 9(7), pp. e1003484.

Clayton, A., Turkes, A., Navabi, H., Mason, M. D. and Tabi, Z. (2005) 'Induction of heat shock proteins in B-cell exosomes', *J Cell Sci,* 118(Pt 16), pp. 3631–8.

Cocucci, E., Racchetti, G. and Meldolesi, J. (2009) 'Shedding microvesicles: artefacts no more', *Trends Cell Biol,* 19(2), pp. 43–51.

Colombo, R., Salonia, A., Leib, Z., Pavone-Macaluso, M. and Engelstein, D. (2011) 'Long-term outcomes of a randomized controlled trial comparing thermochemotherapy with mitomycin-C alone as adjuvant treatment for non-muscle-invasive bladder cancer (NMIBC)', *BJU Int,* 107(6), pp. 912–8.

Comamala, M., Pinard, M., Thériault, C., Matte, I., Albert, A., Boivin, M., Beaudin, J., Piché, A. and Rancourt, C. (2011) 'Downregulation of cell surface CA125/MUC16 induces epithelial-to-mesenchymal transition and restores EGFR signalling in NIH:OVCAR3 ovarian carcinoma cells', *Br J Cancer,* 104(6), pp. 989–99.

Conde-Vancells, J., Rodriguez-Suarez, E., Embade, N., Gil, D., Matthiesen, R., Valle, M., Elortza, F., Lu, S. C., Mato, J. M. and Falcon-Perez, J. M. (2008) 'Characterization and comprehensive proteome profiling of exosomes secreted by hepatocytes', *J Proteome Res,* 7(12), pp. 5157–66.

Conklin, M. W. and Keely, P. J. (2012) 'Why the stroma matters in breast cancer: insights into breast cancer patient outcomes through the examination of stromal biomarkers', *Cell Adh Migr,* 6(3), pp. 249–60.

Corcoran, C., Rani, S., O'Brien, K., O'Neill, A., Prencipe, M., Sheikh, R., Webb, G., McDermott, R., Watson, W., Crown, J. and O'Driscoll, L. (2012) 'Docetaxel-resistance in prostate cancer: evaluating associated phenotypic changes and potential for resistance transfer via exosomes', *PLoS One,* 7(12), pp. e50999.

Cory, G. (2011) 'Scratch-wound assay', *Methods Mol Biol,* 769, pp. 25–30.

Craig, E. A. (1985) 'The heat shock response', *CRC Crit Rev Biochem,* 18(3), pp. 239–80.

Danø, K., Behrendt, N., Høyer-Hansen, G., Johnsen, M., Lund, L. R., Ploug, M. and Rømer, J. (2005) 'Plasminogen activation and cancer', *Thromb Haemost,* 93(4), pp. 676–81.

de Jong, O. G., Verhaar, M. C., Chen, Y., Vader, P., Gremmels, H., Posthuma, G., Schiffelers, R. M., Gucek, M. and van Balkom, B. W. (2012) 'Cellular stress conditions are reflected in the

protein and RNA content of endothelial cell-derived exosomes', *J Extracell Vesicles,* 1, pp. 18396.

Deng, Z., Cheng, Z., Xiang, X., Yan, J., Zhuang, X., Liu, C., Jiang, H., Ju, S., Zhang, L., Grizzle, W., Mobley, J., Roman, J., Miller, D. and Zhang, H. G. (2012) 'Tumor cell cross talk with tumor-associated leukocytes leads to induction of tumor exosomal fibronectin and promotes tumor progression', *Am J Pathol,* 180(1), pp. 390–8.

Denzer, K., Kleijmeer, M. J., Heijnen, H. F., Stoorvogel, W. and Geuze, H. J. (2000) 'Exosome: from internal vesicle of the multivesicular body to intercellular signaling device', *J Cell Sci,* 113 Pt 19, pp. 3365–74.

Deregibus, M. C., Cantaluppi, V., Calogero, R., Lo Iacono, M., Tetta, C., Biancone, L., Bruno, S., Bussolati, B. and Camussi, G. (2007) 'Endothelial progenitor cell derived microvesicles activate an angiogenic program in endothelial cells by a horizontal transfer of mRNA', *Blood,* 110(7), pp. 2440–8.

Deryugina, E. I. and Quigley, J. P. (2006) 'Matrix metalloproteinases and tumor metastasis', *Cancer Metastasis Rev,* 25(1), pp. 9–34.

Dhillon, A. S., Hagan, S., Rath, O. and Kolch, W. (2007) 'MAP kinase signalling pathways in cancer', *Oncogene,* 26(22), pp. 3279–90.

Di Lullo, G. A., Sweeney, S. M., Korkko, J., Ala-Kokko, L. and San Antonio, J. D. (2002) 'Mapping the ligand-binding sites and disease-associated mutations on the most abundant protein in the human, type I collagen', *J Biol Chem,* 277(6), pp. 4223–31.

Dragovic, R. A., Gardiner, C., Brooks, A. S., Tannetta, D. S., Ferguson, D. J., Hole, P., Carr, B., Redman, C. W., Harris, A. L., Dobson, P. J., Harrison, P. and Sargent, I. L. (2011) 'Sizing and phenotyping of cellular vesicles using Nanoparticle Tracking Analysis', *Nanomedicine,* 7(6), pp. 780–8.

Duffy, M. J., Maguire, T. M., McDermott, E. W. and O'Higgins, N. (1999) 'Urokinase plasminogen activator: a prognostic marker in multiple types of cancer', *J Surg Oncol,* 71(2), pp. 130–5.

Duffy, M. J. (2004) 'The urokinase plasminogen activator system: role in malignancy', *Curr Pharm Des,* 10(1), pp. 39–49.

Dutta, S., Warshall, C., Bandyopadhyay, C., Dutta, D. and Chandran, B. (2014) 'Interactions between exosomes from breast cancer cells and primary mammary epithelial cells leads to generation of reactive oxygen species which induce DNA damage response, stabilization of p53 and autophagy in epithelial cells', *PLoS One,* 9(5), pp. e97580.

Eccles, S. A. and Welch, D. R. (2007) 'Metastasis: recent discoveries and novel treatment strategies', *Lancet,* 369(9574), pp. 1742–57.

Egeblad, M. and Werb, Z. (2002) 'New functions for the matrix metalloproteinases in cancer progression', *Nat Rev Cancer,* 2(3), pp. 161–74.

Eitan, E., Zhang, S., Witwer, K. W. and Mattson, M. P. (2015) 'Extracellular vesicle-depleted fetal bovine and human sera have reduced capacity to support cell growth', *J Extracell Vesicles,* 4, pp. 26373.

Eldh, M., Ekström, K., Valadi, H., Sjöstrand, M., Olsson, B., Jernås, M. and Lötvall, J. (2010) 'Exosomes communicate protective messages during oxidative stress; possible role of exosomal shuttle RNA', *PLoS One,* 5(12), pp. e15353.

Eldh, M., Lötvall, J., Malmhäll, C. and Ekström, K. (2012) 'Importance of RNA isolation methods for analysis of exosomal RNA: evaluation of different methods', *Mol Immunol,* 50(4), pp. 278–86.

Engler, A. J., Sen, S., Sweeney, H. L. and Discher, D. E. (2006) 'Matrix elasticity directs stem cell lineage specification', *Cell,* 126(4), pp. 677–89.

Epple, L. M., Griffiths, S. G., Dechkovskaia, A. M., Dusto, N. L., White, J., Ouellette, R. J., Anchordoquy, T. J., Bemis, L. T. and Graner, M. W. (2012) 'Medulloblastoma exosome proteomics yield functional roles for extracellular vesicles', *PLoS One,* 7(7), pp. e42064.

Escola, J. M., Kleijmeer, M. J., Stoorvogel, W., Griffith, J. M., Yoshie, O. and Geuze, H. J. (1998) 'Selective enrichment of tetraspan proteins on the internal vesicles of multivesicular endosomes and on exosomes secreted by human B-lymphocytes', *J Biol Chem,* 273(32), pp. 20121–7.

Escrevente, C., Keller, S., Altevogt, P. and Costa, J. (2011) 'Interaction and uptake of exosomes by ovarian cancer cells', *BMC Cancer,* 11, pp. 108.

Esquivel-Velázquez, M., Ostoa-Saloma, P., Palacios-Arreola, M. I., Nava-Castro, K. E., Castro, J. I. and Morales-Montor, J. (2015) 'The role of cytokines in breast cancer development and progression', *J Interferon Cytokine Res,* 35(1), pp. 1–16.

Eustace, B. K., Sakurai, T., Stewart, J. K., Yimlamai, D., Unger, C., Zehetmeier, C., Lain, B., Torella, C., Henning, S. W., Beste, G., Scroggins, B. T., Neckers, L., Ilag, L. L. and Jay, D. G. (2004) 'Functional proteomic screens reveal an essential extracellular role for hsp90 alpha in cancer cell invasiveness', *Nat Cell Biol,* 6(6), pp. 507–14.

Evert, M., Frau, M., Tomasi, M. L., Latte, G., Simile, M. M., Seddaiu, M. A., Zimmermann, A., Ladu, S., Staniscia, T., Brozzetti, S., Solinas, G., Dombrowski, F., Feo, F., Pascale, R. M. and Calvisi, D. F. (2013) 'Deregulation of DNA-dependent protein kinase catalytic subunit contributes to human hepatocarcinogenesis development and has a putative prognostic value', *Br J Cancer,* 109(10), pp. 2654–64.

Fader, C. M., Sánchez, D., Furlán, M. and Colombo, M. I. (2008) 'Induction of autophagy promotes fusion of multivesicular bodies with autophagic vacuoles in k562 cells', *Traffic,* 9(2), pp. 230–50.

Fader, C. M. and Colombo, M. I. (2009) 'Autophagy and multivesicular bodies: two closely related partners', *Cell Death Differ,* 16(1), pp. 70–8.

Fan, W., Tian, X. D., Huang, E. and Zhang, J. J. (2013) 'Exosomes from CIITA-Transfected CT26 Cells Enhance Anti- tumor Effects', *Asian Pac J Cancer Prev,* 14(2), pp. 987–91.

Fernández-Medarde, A. and Santos, E. (2011) 'Ras in cancer and developmental diseases', *Genes Cancer,* 2(3), pp. 344–58.

Février, B. and Raposo, G. (2004) 'Exosomes: endosomal-derived vesicles shipping extracellular messages', *Curr Opin Cell Biol,* 16(4), pp. 415–21.

Fidler, I. J. and Kripke, M. L. (1977) 'Metastasis results from preexisting variant cells within a malignant tumor', *Science,* 197(4306), pp. 893–5.

Fidler, I. J. (2003) 'The pathogenesis of cancer metastasis: the 'seed and soil' hypothesis revisited', *Nat Rev Cancer,* 3(6), pp. 453–8.

Finucane, D. M., Bossy-Wetzel, E., Waterhouse, N. J., Cotter, T. G. and Green, D. R. (1999) 'Bax-induced caspase activation and apoptosis via cytochrome c release from mitochondria is inhibitable by Bcl-xL', *J Biol Chem,* 274(4), pp. 2225–33.

Flate, E. and Stalvey, J. R. (2014) 'Motility of select ovarian cancer cell lines: effect of extra-cellular matrix proteins and the involvement of PAK2', *Int J Oncol,* 45(4), pp. 1401–11.

Fogh, J., Wright, W. C. and Loveless, J. D. (1977) 'Absence of HeLa cell contamination in 169 cell lines derived from human tumors', *J Natl Cancer Inst,* 58(2), pp. 209–14.

Foulds, L. (1954) 'The experimental study of tumor progression: a review', *Cancer Res,* 14(5), pp. 327–39.

Franzen, C. A., Simms, P. E., Van Huis, A. F., Foreman, K. E., Kuo, P. C. and Gupta, G. N. (2014) 'Characterization of uptake and internalization of exosomes by bladder cancer cells', *Biomed Res Int,* 2014, pp. 619829.

Franzen, C. A., Blackwell, R. H., Todorovic, V., Greco, K. A., Foreman, K. E., Flanigan, R. C., Kuo, P. C. and Gupta, G. N. (2015) 'Urothelial cells undergo epithelial-to-mesenchymal transition after exposure to muscle invasive bladder cancer exosomes', *Oncogenesis,* 4, pp. e163.

Fresno Vara, J. A., Casado, E., de Castro, J., Cejas, P., Belda-Iniesta, C. and González-Barón, M. (2004) 'PI3K/Akt signalling pathway and cancer', *Cancer Treat Rev,* 30(2), pp. 193–204.

Fridman, J. S. and Lowe, S. W. (2003) 'Control of apoptosis by p53', *Oncogene,* 22(56), pp. 9030–40.

Friedl, P., Maaser, K., Klein, C. E., Niggemann, B., Krohne, G. and Zänker, K. S. (1997) 'Migration of highly aggressive MV3 melanoma cells in 3-dimensional collagen lattices results in local matrix reorganization and shedding of alpha2 and beta1 integrins and CD44', *Cancer Res,* 57(10), pp. 2061–70.

Friedl, P. and Wolf, K. (2003) 'Tumour-cell invasion and migration: diversity and escape mechanisms', *Nat Rev Cancer,* 3(5), pp. 362–74.

Fuchs, S. Y., Adler, V., Buschmann, T., Yin, Z., Wu, X., Jones, S. N. and Ronai, Z. (1998) 'JNK targets p53 ubiquitination and degradation in nonstressed cells', *Genes Dev,* 12(17), pp. 2658–63.

Fulda, S., Gorman, A. M., Hori, O. and Samali, A. (2010) 'Cellular stress responses: cell survival and cell death', *Int J Cell Biol,* 2010, pp. 214074.

Funari, V. A., Winkler, M., Brown, J., Dimitrijevich, S. D., Ljubimov, A. V. and Saghizadeh, M. (2013) 'Differentially expressed wound healing-related microRNAs in the human diabetic cornea', *PLoS One,* 8(12), pp. e84425.

Futter, C. E., Pearse, A., Hewlett, L. J. and Hopkins, C. R. (1996) 'Multivesicular endosomes containing internalized EGF-EGF receptor complexes mature and then fuse directly with lysosomes', *J Cell Biol,* 132(6), pp. 1011–23.

Gabai, V. L., Yaglom, J. A., Volloch, V., Meriin, A. B., Force, T., Koutroumanis, M., Massie, B., Mosser, D. D. and Sherman, M. Y. (2000) 'Hsp72-mediated suppression of c-Jun N-terminal kinase is implicated in development of tolerance to caspase-independent cell death', *Mol Cell Biol,* 20(18), pp. 6826–36.

Gan, X. and Gould, S. J. (2011) 'Identification of an inhibitory budding signal that blocks the release of HIV particles and exosome/microvesicle proteins', *Mol Biol Cell,* 22(6), pp. 817–30.

Gardiner, C., Ferreira, Y. J., Dragovic, R. A., Redman, C. W. and Sargent, I. L. (2013) 'Extracellular vesicle sizing and enumeration by nanoparticle tracking analysis', *J Extracell Vesicles,* 2, pp. 19671.

Garnier, D., Magnus, N., Meehan, B., Kislinger, T. and Rak, J. (2013) 'Qualitative changes in the proteome of extracellular vesicles accompanying cancer cell transition to mesenchymal state', *Exp Cell Res,* 319(17), pp. 2747–57.

Garrido, C., Ottavi, P., Fromentin, A., Hammann, A., Arrigo, A. P., Chauffert, B. and Mehlen, P. (1997) 'HSP27 as a mediator of confluence-dependent resistance to cell death induced by anticancer drugs', *Cancer Res,* 57(13), pp. 2661–7.

Gastpar, R., Gehrmann, M., Bausero, M. A., Asea, A., Gross, C., Schroeder, J. A. and Multhoff, G. (2005) 'Heat shock protein 70 surface-positive tumor exosomes stimulate migratory and cytolytic activity of natural killer cells', *Cancer Res,* 65(12), pp. 5238–47.

Gil-Bernabé, A. M., Lucotti, S. and Muschel, R. J. (2013) 'Coagulation and metastasis: what does the experimental literature tell us?', *Br J Haematol,* 162(4), pp. 433-41.

Godwin, A. K., Meister, A., O'Dwyer, P. J., Huang, C. S., Hamilton, T. C. and Anderson, M. E. (1992) 'High resistance to cisplatin in human ovarian cancer cell lines is associated with marked increase of glutathione synthesis', *Proc Natl Acad Sci U S A,* 89(7), pp. 3070–4.

Goodwin, J. F. and Knudsen, K. E. (2014) 'Beyond DNA repair: DNA-PK function in cancer', *Cancer Discov,* 4(10), pp. 1126–39.

Goodwin, J. F., Kothari, V., Drake, J. M., Zhao, S., Dylgjeri, E., Dean, J. L., Schiewer, M. J., McNair, C., Jones, J. K., Aytes, A., Magee, M. S., Snook, A. E., Zhu, Z., Den, R. B., Birbe, R. C., Gomella, L. G., Graham, N. A., Vashisht, A. A., Wohlschlegel, J. A., Graeber, T. G., Karnes, R. J., Takhar, M., Davicioni, E., Tomlins, S. A., Abate-Shen, C., Sharifi, N., Witte, O. N., Feng, F. Y. and Knudsen, K. E. (2015) 'DNA-PKcs-Mediated Transcriptional Regulation Drives Prostate Cancer Progression and Metastasis', *Cancer Cell,* 28(1), pp. 97–113.

Gould, S. J. and Raposo, G. (2013) 'As we wait: coping with an imperfect nomenclature for extracellular vesicles', *J Extracell Vesicles,* 2, pp. 20389.

Grange, C., Tapparo, M., Collino, F., Vitillo, L., Damasco, C., Deregibus, M. C., Tetta, C., Bussolati, B. and Camussi, G. (2011) 'Microvesicles released from human renal cancer stem cells stimulate angiogenesis and formation of lung premetastatic niche', *Cancer Res,* 71(15), pp. 5346–56.

Guarino, M. (2007) 'Epithelial-mesenchymal transition and tumour invasion', *Int J Biochem Cell Biol,* 39(12), pp. 2153–60.

Guo, S., Lok, J., Liu, Y., Hayakawa, K., Leung, W., Xing, C., Ji, X. and Lo, E. H. (2014) 'Assays to examine endothelial cell migration, tube formation, and gene expression profiles', *Methods Mol Biol,* 1135, pp. 393–402.

György, B., Szabó, T. G., Pásztói, M., Pál, Z., Misják, P., Aradi, B., László, V., Pállinger, E., Pap, E., Kittel, A., Nagy, G., Falus, A. and Buzás, E. I. (2011) 'Membrane vesicles, current state-of-the-art: emerging role of extracellular vesicles', *Cell Mol Life Sci,* 68(16), pp. 2667–88.

Hamilton, T. C., Young, R. C., McKoy, W. M., Grotzinger, K. R., Green, J. A., Chu, E. W., Whang-Peng, J., Rogan, A. M., Green, W. R. and Ozols, R. F. (1983) 'Characterization of a human ovarian carcinoma cell line (NIH:OVCAR-3) with androgen and estrogen receptors', *Cancer Res,* 43(11), pp. 5379–89.

Hanahan, D. and Coussens, L. M. (2012) 'Accessories to the crime: functions of cells recruited to the tumor microenvironment', *Cancer Cell,* 21(3), pp. 309–22.

Hanahan, D. and Weinberg, R. A. (2000) 'The hallmarks of cancer', *Cell,* 100(1), pp. 57–70.

Hanahan, D. and Weinberg, R. A. (2011) 'Hallmarks of cancer: the next generation', *Cell,* 144(5), pp. 646–74.

Hao, S., Ye, Z., Li, F., Meng, Q., Qureshi, M., Yang, J. and Xiang, J. (2006) 'Epigenetic transfer of metastatic activity by uptake of highly metastatic B16 melanoma cell-released exosomes', *Exp Oncol,* 28(2), pp. 126–31.

Harris, D. A., Patel, S. H., Gucek, M., Hendrix, A., Westbroek, W. and Taraska, J. W. (2015) 'Exosomes released from breast cancer carcinomas stimulate cell movement', *PLoS One,* 10(3), pp. e0117495.

Hartl, F. U. and Hayer-Hartl, M. (2002) 'Molecular chaperones in the cytosol: from nascent chain to folded protein', *Science,* 295(5561), pp. 1852–8.

Heath, R. M., Jayne, D. G., O'Leary, R., Morrison, E. E. and Guillou, P. J. (2004) 'Tumour-induced apoptosis in human mesothelial cells: a mechanism of peritoneal invasion by Fas Ligand/Fas interaction', *Br J Cancer,* 90(7), pp. 1437–42.

Heijnen, H. F., Schiel, A. E., Fijnheer, R., Geuze, H. J. and Sixma, J. J. (1999) 'Activated platelets release two types of membrane vesicles: microvesicles by surface shedding and exosomes derived from exocytosis of multivesicular bodies and alpha-granules', *Blood,* 94(11), pp. 3791–9.

Helm, C. W. and States, J. C. (2009) 'Enhancing the efficacy of cisplatin in ovarian cancer treatment - could arsenic have a role', *J Ovarian Res,* 2, pp. 2.

Hemler, M. E. (2003) 'Tetraspanin proteins mediate cellular penetration, invasion, and fusion events and define a novel type of membrane microdomain', *Annu Rev Cell Dev Biol,* 19, pp. 397–422.

Hemler, M. E. (2005) 'Tetraspanin functions and associated microdomains', *Nat Rev Mol Cell Biol,* 6(10), pp. 801–11.

Hendrix, A. and Hume, A. N. (2011) 'Exosome signaling in mammary gland development and cancer', *Int J Dev Biol,* 55(7–9), pp. 879–87.

Henne, W. M., Buchkovich, N. J. and Emr, S. D. (2011) 'The ESCRT pathway', *Dev Cell,* 21(1), pp. 77–91.

Hettiarachchi, R. J., Smorenburg, S. M., Ginsberg, J., Levine, M., Prins, M. H. and Büller, H. R. (1999) 'Do heparins do more than just treat thrombosis? The influence of heparins on cancer spread', *Thromb Haemost,* 82(2), pp. 947–52.

Higginbotham, J. N., Demory Beckler, M., Gephart, J. D., Franklin, J. L., Bogatcheva, G., Kremers, G. J., Piston, D. W., Ayers, G. D., McConnell, R. E., Tyska, M. J. and Coffey, R. J. (2011) 'Amphiregulin exosomes increase cancer cell invasion', *Curr Biol,* 21(9), pp. 779–86.

Hirsch, D. D. and Stork, P. J. (1997) 'Mitogen-activated protein kinase phosphatases inactivate stress-activated protein kinase pathways *in vivo*', *J Biol Chem,* 272(7), pp. 4568–75.

Hirsh, J., Warkentin, T. E., Raschke, R., Granger, C., Ohman, E. M. and Dalen, J. E. (1998) 'Heparin and low-molecular-weight heparin: mechanisms of action, pharmacokinetics, dosing considerations, monitoring, efficacy, and safety', *Chest,* 114(5 Suppl), pp. 489S–510S.

Hoffman, R. M. (2013) 'Stromal-cell and cancer-cell exosomes leading the metastatic exodus for the promised niche', *Breast Cancer Res,* 15(3), pp. 310.

Hollstein, M., Sidransky, D., Vogelstein, B. and Harris, C. C. (1991) 'p53 mutations in human cancers', *Science,* 253(5015), pp. 49–53.

Hong, B. S., Cho, J. H., Kim, H., Choi, E. J., Rho, S., Kim, J., Kim, J. H., Choi, D. S., Kim, Y. K., Hwang, D. and Gho, Y. S. (2009) 'Colorectal cancer cell-derived microvesicles are enriched in cell cycle-related mRNAs that promote proliferation of endothelial cells', *BMC Genomics,* 10, pp. 556.

Hood, J. L., San, R. S. and Wickline, S. A. (2011) 'Exosomes released by melanoma cells prepare sentinel lymph nodes for tumor metastasis', *Cancer Res,* 71(11), pp. 3792–801.

Hoshino, D., Kirkbride, K. C., Costello, K., Clark, E. S., Sinha, S., Grega-Larson, N., Tyska, M. J. and Weaver, A. M. (2013) 'Exosome secretion is enhanced by invadopodia and drives invasive behavior', *Cell Rep,* 5(5), pp. 1159–68.

Hoshino, A., Costa-Silva, B., Shen, T. L., Rodrigues, G., Hashimoto, A., Tesic Mark, M., Molina, H., Kohsaka, S., Di Giannatale, A., Ceder, S., Singh, S., Williams, C., Soplop, N., Uryu, K., Pharmer, L., King, T., Bojmar, L., Davies, A. E., Ararso, Y., Zhang, T., Zhang, H., Hernandez, J., Weiss, J. M., Dumont-Cole, V. D., Kramer, K., Wexler, L. H., Narendran, A., Schwartz, G. K., Healey, J. H., Sandstrom, P., Jørgen Labori, K., Kure, E. H., Grandgenett, P. M., Hollingsworth, M. A., de Sousa, M., Kaur, S., Jain, M., Mallya, K., Batra, S. K., Jarnagin, W. R., Brady, M. S., Fodstad, O., Muller, V., Pantel, K., Minn, A. J., Bissell, M. J., Garcia, B. A., Kang, Y., Rajasekhar, V. K., Ghajar, C. M., Matei, I., Peinado, H., Bromberg, J. and Lyden, D. (2015) 'Tumour exosome integrins determine organotropic metastasis', *Nature,* 527(7578), pp. 329–35.

Hosseini-Beheshti, E., Pham, S., Adomat, H., Li, N. and Tomlinson Guns, E. S. (2012) 'Exosomes as biomarker enriched microvesicles: characterization of exosomal proteins derived from a panel of prostate cell lines with distinct AR phenotypes', *Mol Cell Proteomics,* 11(10), pp. 863–85.

Hristov, M., Erl, W., Linder, S. and Weber, P. C. (2004) 'Apoptotic bodies from endothelial cells enhance the number and initiate the differentiation of human endothelial progenitor cells *in vitro*', *Blood,* 104(9), pp. 2761–6.

Huang, d. W., Sherman, B. T. and Lempicki, R. A. (2009a) 'Bioinformatics enrichment tools: paths toward the comprehensive functional analysis of large gene lists', *Nucleic Acids Res,* 37(1), pp. 1–13.

Huang, d. W., Sherman, B. T. and Lempicki, R. A. (2009b) 'Systematic and integrative analysis of large gene lists using DAVID bioinformatics resources', *Nat Protoc,* 4(1), pp. 44–57.

Huber, V., Fais, S., Iero, M., Lugini, L., Canese, P., Squarcina, P., Zaccheddu, A., Colone, M., Arancia, G., Gentile, M., Seregni, E., Valenti, R., Ballabio, G., Belli, F., Leo, E., Parmiani, G. and Rivoltini, L. (2005) 'Human colorectal cancer cells induce T-cell death through release of proapoptotic microvesicles: role in immune escape', *Gastroenterology,* 128(7), pp. 1796–804.

Hughes, P., Marshall, D., Reid, Y., Parkes, H. and Gelber, C. (2007) 'The costs of using unauthenticated, over-passaged cell lines: how much more data do we need?', *Biotechniques,* 43(5), pp. 575, 577–8, 581–2 passim.

Hulboy, D. L., Rudolph, L. A. and Matrisian, L. M. (1997) 'Matrix metalloproteinases as mediators of reproductive function', *Mol Hum Reprod,* 3(1), pp. 27–45.

Hunter, M. P., Ismail, N., Zhang, X., Aguda, B. D., Lee, E. J., Yu, L., Xiao, T., Schafer, J., Lee, M. L., Schmittgen, T. D., Nana-Sinkam, S. P., Jarjoura, D. and Marsh, C. B. (2008) 'Detection of microRNA expression in human peripheral blood microvesicles', *PLoS One,* 3(11), pp. e3694.

Huot, J., Houle, F., Spitz, D. R. and Landry, J. (1996) 'HSP27 phosphorylation-mediated resistance against actin fragmentation and cell death induced by oxidative stress', *Cancer Res,* 56(2), pp. 273–9.

Hurley, J. H. and Stenmark, H. (2011) 'Molecular mechanisms of ubiquitin-dependent membrane traffic', *Annu Rev Biophys,* 40, pp. 119–42.

Iozzo, R. V. (1998) 'Matrix proteoglycans: from molecular design to cellular function', *Annu Rev Biochem,* 67, pp. 609–52.

Jackson, S. P. (2002) 'Sensing and repairing DNA double-strand breaks', *Carcinogenesis,* 23(5), pp. 687–96.

Jang, J. Y., Lee, J. K., Jeon, Y. K. and Kim, C. W. (2013) 'Exosome derived from epigallocatechin gallate treated breast cancer cells suppresses tumor growth by inhibiting tumor-associated macrophage infiltration and M2 polarization', *BMC Cancer,* 13, pp. 421.

Jella, K. K., Rani, S., O'Driscoll, L., McClean, B., Byrne, H. J. and Lyng, F. M. (2014) 'Exosomes are involved in mediating radiation induced bystander signaling in human keratinocyte cells', *Radiat Res,* 181(2), pp. 138–45.

Jeppesen, D. K., Nawrocki, A., Jensen, S. G., Thorsen, K., Whitehead, B., Howard, K. A., Dyrskjøt, L., Ørntoft, T. F., Larsen, M. R. and Ostenfeld, M. S. (2014) 'Quantitative proteomics of fractionated membrane and lumen exosome proteins from isogenic metastatic and nonmetastatic bladder cancer cells reveal differential expression of EMT factors', *Proteomics,* 14(6), pp. 699–712.

Ji, H., Greening, D. W., Barnes, T. W., Lim, J. W., Tauro, B. J., Rai, A., Xu, R., Adda, C., Mathivanan, S., Zhao, W., Xue, Y., Xu, T., Zhu, H. J. and Simpson, R. J. (2013) 'Proteome profiling of exosomes derived from human primary and metastatic colorectal cancer cells reveal differential expression of key metastatic factors and signal transduction components', *Proteomics,* 13(10–11), pp. 1672–86.

Johnstone, R. M., Adam, M., Hammond, J. R., Orr, L. and Turbide, C. (1987) 'Vesicle formation during reticulocyte maturation. Association of plasma membrane activities with released vesicles (exosomes)', *J Biol Chem,* 262(19), pp. 9412–20.

Johnstone, R. M., Mathew, A., Mason, A. B. and Teng, K. (1991) 'Exosome formation during maturation of mammalian and avian reticulocytes: evidence that exosome release is a major route for externalization of obsolete membrane proteins', *J Cell Physiol,* 147(1), pp. 27–36.

Kahlert, C., Melo, S. A., Protopopov, A., Tang, J., Seth, S., Koch, M., Zhang, J., Weitz, J., Chin, L., Futreal, A. and Kalluri, R. (2014) 'Identification of double-stranded genomic DNA spanning all chromosomes with mutated KRAS and p53 DNA in the serum exosomes of patients with pancreatic cancer', *J Biol Chem,* 289(7), pp. 3869–75.

Kalluri, R. and Weinberg, R. A. (2009) 'The basics of epithelial-mesenchymal transition', *J Clin Invest,* 119(6), pp. 1420–8.

Kalra, H., Adda, C. G., Liem, M., Ang, C. S., Mechler, A., Simpson, R. J., Hulett, M. D. and Mathivanan, S. (2013) 'Comparative proteomics evaluation of plasma exosome isolation

techniques and assessment of the stability of exosomes in normal human blood plasma', *Proteomics,* 13(22), pp. 3354–64.

Kamińska, K., Szczylik, C., Bielecka, Z. F., Bartnik, E., Porta, C., Lian, F. and Czarnecka, A. M. (2015) 'The role of the cell-cell interactions in cancer progression', *J Cell Mol Med,* 19(2), pp. 283–96.

Kaplan, R. N., Riba, R. D., Zacharoulis, S., Bramley, A. H., Vincent, L., Costa, C., MacDonald, D. D., Jin, D. K., Shido, K., Kerns, S. A., Zhu, Z., Hicklin, D., Wu, Y., Port, J. L., Altorki, N., Port, E. R., Ruggero, D., Shmelkov, S. V., Jensen, K. K., Rafii, S. and Lyden, D. (2005) 'VEGFR1-positive haematopoietic bone marrow progenitors initiate the pre-metastatic niche', *Nature,* 438(7069), pp. 820–7.

Kaplan, R. N., Psaila, B. and Lyden, D. (2006) 'Bone marrow cells in the 'pre-metastatic niche': within bone and beyond', *Cancer Metastasis Rev,* 25(4), pp. 521–9.

Kaur, H., Phillips-Mason, P. J., Burden-Gulley, S. M., Kerstetter-Fogle, A. E., Basilion, J. P., Sloan, A. E. and Brady-Kalnay, S. M. (2012) 'Cadherin-11, a marker of the mesenchymal phenotype, regulates glioblastoma cell migration and survival *in vivo*', *Mol Cancer Res,* 10(3), pp. 293–304.

Keerthikumar, S., Chisanga, D., Ariyaratne, D., Al Saffar, H., Anand, S., Zhao, K., Samuel, M., Pathan, M., Jois, M., Chilamkurti, N., Gangoda, L. and Mathivanan, S. (2016) 'ExoCarta: A Web-Based Compendium of Exosomal Cargo', *J Mol Biol*, 428(4), pp. 688–92.

Keller, S., König, A. K., Marmé, F., Runz, S., Wolterink, S., Koensgen, D., Mustea, A., Sehouli, J. and Altevogt, P. (2009) 'Systemic presence and tumor-growth promoting effect of ovarian carcinoma released exosomes', *Cancer Lett,* 278(1), pp. 73–81.

Kenny, H. A., Krausz, T., Yamada, S. D. and Lengyel, E. (2007) 'Use of a novel 3D culture model to elucidate the role of mesothelial cells, fibroblasts and extra-cellular matrices on adhesion and invasion of ovarian cancer cells to the omentum', *Int J Cancer,* 121(7), pp. 1463–72.

Kenny, H. A., Dogan, S., Zillhardt, M., K Mitra, A., Yamada, S. D., Krausz, T. and Lengyel, E. (2009) 'Organotypic models of metastasis: A three-dimensional culture mimicking the human peritoneum and omentum for the study of the early steps of ovarian cancer metastasis', *Cancer Treat Res,* 149, pp. 335–51.

Kenny, H. A., Leonhardt, P., Ladanyi, A., Yamada, S. D., Montag, A., Im, H. K., Jagadeeswaran, S., Shaw, D. E., Mazar, A. P. and Lengyel, E. (2011) 'Targeting the urokinase plasminogen activator receptor inhibits ovarian cancer metastasis', *Clin Cancer Res,* 17(3), pp. 459–71.

Kharaziha, P., Ceder, S., Li, Q. and Panaretakis, T. (2012) 'Tumor cell-derived exosomes: a message in a bottle', *Biochim Biophys Acta,* 1826(1), pp. 103–11.

Kim, S. H., Turnbull, J. and Guimond, S. (2011) 'Extracellular matrix and cell signalling: the dynamic cooperation of integrin, proteoglycan and growth factor receptor', *J Endocrinol,* 209(2), pp. 139–51.

King, H. W., Michael, M. Z. and Gleadle, J. M. (2012) 'Hypoxic enhancement of exosome release by breast cancer cells', *BMC Cancer,* 12, pp. 421.

Kleinman, H. K., McGarvey, M. L., Liotta, L. A., Robey, P. G., Tryggvason, K. and Martin, G. R. (1982) 'Isolation and characterization of type IV procollagen, laminin, and heparan sulfate proteoglycan from the EHS sarcoma', *Biochemistry,* 21(24), pp. 6188–93.

Koga, K., Matsumoto, K., Akiyoshi, T., Kubo, M., Yamanaka, N., Tasaki, A., Nakashima, H., Nakamura, M., Kuroki, S., Tanaka, M. and Katano, M. (2005) 'Purification, characterization and biological significance of tumor-derived exosomes', *Anticancer Res,* 25(6A), pp. 3703–7.

Kogure, T., Lin, W. L., Yan, I. K., Braconi, C. and Patel, T. (2011) 'Intercellular nanovesicle-mediated microRNA transfer: a mechanism of environmental modulation of hepatocellular cancer cell growth', *Hepatology,* 54(4), pp. 1237–48.

Koul, H. K., Pal, M. and Koul, S. (2013) 'Role of p38 MAP Kinase Signal Transduction in Solid Tumors', *Genes Cancer,* 4(9–10), pp. 342–59.

Koumangoye, R. B., Sakwe, A. M., Goodwin, J. S., Patel, T. and Ochieng, J. (2011) 'Detachment of breast tumor cells induces rapid secretion of exosomes which subsequently mediate cellular adhesion and spreading', *PLoS One,* 6(9), pp. e24234.

Kowal, J., Tkach, M. and Théry, C. (2014) 'Biogenesis and secretion of exosomes', *Curr Opin Cell Biol,* 29, pp. 116–25.

Lakhal, S. and Wood, M. J. (2011) 'Exosome nanotechnology: an emerging paradigm shift in drug delivery: exploitation of exosome nanovesicles for systemic *in vivo* delivery of RNAi heralds new horizons for drug delivery across biological barriers', *Bioessays,* 33(10), pp. 737–41.

Lakkaraju, A. and Rodriguez-Boulan, E. (2008) 'Itinerant exosomes: emerging roles in cell and tissue polarity', *Trends Cell Biol,* 18(5), pp. 199–209.

Lamparski, H. G., Metha-Damani, A., Yao, J. Y., Patel, S., Hsu, D. H., Ruegg, C. and Le Pecq, J. B. (2002) 'Production and characterization of clinical grade exosomes derived from dendritic cells', *J Immunol Methods,* 270(2), pp. 211–26.

Lancaster, J. M., Dressman, H. K., Clarke, J. P., Sayer, R. A., Martino, M. A., Cragun, J. M., Henriott, A. H., Gray, J., Sutphen, R., Elahi, A., Whitaker, R. S., West, M., Marks, J. R., Nevins, J. R. and Berchuck, A. (2006) 'Identification of genes associated with ovarian cancer metastasis using microarray expression analysis', *Int J Gynecol Cancer,* 16(5), pp. 1733–45.

Lässer, C., Alikhani, V. S., Ekström, K., Eldh, M., Paredes, P. T., Bossios, A., Sjöstrand, M., Gabrielsson, S., Lötvall, J. and Valadi, H. (2011) 'Human saliva, plasma and breast milk exosomes contain RNA: uptake by macrophages', *J Transl Med,* 9, pp. 9.

Laulagnier, K., Motta, C., Hamdi, S., Roy, S., Fauvelle, F., Pageaux, J. F., Kobayashi, T., Salles, J. P., Perret, B., Bonnerot, C. and Record, M. (2004) 'Mast cell- and dendritic cell-derived exosomes display a specific lipid composition and an unusual membrane organization', *Biochem J,* 380(Pt 1), pp. 161–71.

Lee, A. Y., Levine, M. N., Baker, R. I., Bowden, C., Kakkar, A. K., Prins, M., Rickles, F. R., Julian, J. A., Haley, S., Kovacs, M. J., Gent, M. and Randomized Comparison of Low-Molecular-Weight Heparin versus Oral Anticoagulant Therapy for the Prevention of Recurrent Venous Thromboembolism in Patients with Cancer (CLOT) Investigators. (2003) 'Low-molecular-weight heparin versus a coumarin for the prevention of recurrent venous thromboembolism in patients with cancer', *N Engl J Med,* 349(2), pp. 146–53.

Lee, H. D., Kim, Y. H. and Kim, D. S. (2014) 'Exosomes derived from human macrophages suppress endothelial cell migration by controlling integrin trafficking', *Eur J Immunol,* 44(4), pp. 1156–69.

Lengyel, E. (2010) 'Ovarian cancer development and metastasis', *Am J Pathol,* 177(3), pp. 1053–64.

Levine, A. J., Momand, J. and Finlay, C. A. (1991) 'The p53 tumour suppressor gene', *Nature,* 351(6326), pp. 453–6.

Liang, C. C., Park, A. Y. and Guan, J. L. (2007) '*In vitro* scratch assay: a convenient and inexpensive method for analysis of cell migration *in vitro*', *Nat Protoc,* 2(2), pp. 329–33.

Liao, W. T., Ye, Y. P., Deng, Y. J., Bian, X. W. and Ding, Y. Q. (2014) 'Metastatic cancer stem cells: from the concept to therapeutics', *Am J Stem Cells,* 3(2), pp. 46–62.

Lin, R., Wang, S. and Zhao, R. C. (2013) 'Exosomes from human adipose-derived mesenchymal stem cells promote migration through Wnt signaling pathway in a breast cancer cell model', *Mol Cell Biochem,* 383(1–2), pp. 13–20.

Lindquist, S. and Craig, E. A. (1988) 'The heat-shock proteins', *Annu Rev Genet,* 22, pp. 631–77.

Liotta, L. A., Saidel, M. G. and Kleinerman, J. (1976) 'The significance of hematogenous tumor cell clumps in the metastatic process', *Cancer Res,* 36(3), pp. 889–94.

Liu, C., Yu, S., Zinn, K., Wang, J., Zhang, L., Jia, Y., Kappes, J. C., Barnes, S., Kimberly, R. P., Grizzle, W. E. and Zhang, H. G. (2006) 'Murine mammary carcinoma exosomes promote tumor growth by suppression of NK cell function', *J Immunol,* 176(3), pp. 1375–85.

Liu, S., Patel, S. H., Ginestier, C., Ibarra, I., Martin-Trevino, R., Bai, S., McDermott, S. P., Shang, L., Ke, J., Ou, S. J., Heath, A., Zhang, K. J., Korkaya, H., Clouthier, S. G., Charafe-Jauffret, E., Birnbaum, D., Hannon, G. J. and Wicha, M. S. (2012) 'MicroRNA93 regulates proliferation and differentiation of normal and malignant breast stem cells', *PLoS Genet,* 8(6), pp. e1002751.

Liu, X. L., Xiao, K., Xue, B., Yang, D., Lei, Z., Shan, Y. and Zhang, H. T. (2013) 'Dual role of TGFBR3 in bladder cancer', *Oncol Rep,* 30(3), pp. 1301–8.

Liu, C., Qu, L., Lian, S., Tian, Z., Zhao, C., Meng, L. and Shou, C. (2014a) 'Unconventional secretion of synuclein-γ promotes tumor cell invasion', *FEBS J,* 281(22), pp. 5159–71.

Liu, J., Zhang, C. and Feng, Z. (2014b) 'Tumor suppressor p53 and its gain-of-function mutants in cancer', *Acta Biochim Biophys Sin (Shanghai),* 46(3), pp. 170–9.

Llorente, A., de Marco, M. C. and Alonso, M. A. (2004) 'Caveolin-1 and MAL are located on prostasomes secreted by the prostate cancer PC-3 cell line', *J Cell Sci,* 117(Pt 22), pp. 5343–51.

Lo, C. M., Wang, H. B., Dembo, M. and Wang, Y. L. (2000) 'Cell movement is guided by the rigidity of the substrate', *Biophys J,* 79(1), pp. 144–52.

Lobb, R. J., Becker, M., Wen, S. W., Wong, C. S., Wiegmans, A. P., Leimgruber, A. and Möller, A. (2015) 'Optimized exosome isolation protocol for cell culture supernatant and human plasma', *J Extracell Vesicles,* 4, pp. 27031.

Lockshin, R. A. and Zakeri, Z. (2007) 'Cell death in health and disease', *J Cell Mol Med,* 11(6), pp. 1214–24.

Logozzi, M., De Milito, A., Lugini, L., Borghi, M., Calabrò, L., Spada, M., Perdicchio, M., Marino, M. L., Federici, C., Iessi, E., Brambilla, D., Venturi, G., Lozupone, F., Santinami, M., Huber, V., Maio, M., Rivoltini, L. and Fais, S. (2009) 'High levels of exosomes expressing CD63 and caveolin-1 in plasma of melanoma patients', *PLoS One,* 4(4), pp. e5219.

Louie, K. G., Behrens, B. C., Kinsella, T. J., Hamilton, T. C., Grotzinger, K. R., McKoy, W. M., Winker, M. A. and Ozols, R. F. (1985) 'Radiation survival parameters of antineoplastic drug-sensitive and -resistant human ovarian cancer cell lines and their modification by buthionine sulfoximine', *Cancer Res,* 45(5), pp. 2110–5.

Lu, Q., Hope, L. W., Brasch, M., Reinhard, C. and Cohen, S. N. (2003) 'TSG101 interaction with HRS mediates endosomal trafficking and receptor down-regulation', *Proc Natl Acad Sci U S A,* 100(13), pp. 7626–31.

Ludwig, A. K. and Giebel, B. (2012) 'Exosomes: small vesicles participating in intercellular communication', *Int J Biochem Cell Biol,* 44(1), pp. 11–5.

Luga, V., Zhang, L., Viloria-Petit, A. M., Ogunjimi, A. A., Inanlou, M. R., Chiu, E., Buchanan, M., Hosein, A. N., Basik, M. and Wrana, J. L. (2012) 'Exosomes mediate stromal mobilization of autocrine Wnt-PCP signaling in breast cancer cell migration', *Cell,* 151(7), pp. 1542–56.

Lv, L. H., Wan, Y. L., Lin, Y., Zhang, W., Yang, M., Li, G. L., Lin, H. M., Shang, C. Z., Chen, Y. J. and Min, J. (2012) 'Anticancer drugs cause release of exosomes with heat shock proteins from human hepatocellular carcinoma cells that elicit effective natural killer cell antitumor responses *in vitro*', *J Biol Chem,* 287(19), pp. 15874–85.

Maecker, H. T., Todd, S. C. and Levy, S. (1997) 'The tetraspanin superfamily: molecular facilitators', *FASEB J,* 11(6), pp. 428–42.

Maquart, F. X. and Monboisse, J. C. (2014) 'Extracellular matrix and wound healing', *Pathol Biol,* 62(2), pp. 91–5.

Marcucci, F., Bellone, M., Caserta, C. A. and Corti, A. (2013) 'Pushing tumor cells towards a malignant phenotype: Stimuli from the microenvironment, intercellular communications and alternative roads', *Int J Cancer,* 135(6), pp. 1265–76.

Marcus, M. E. and Leonard, J. N. (2013) 'FedExosomes: Engineering Therapeutic Biological Nanoparticles that Truly Deliver', *Pharmaceuticals,* 6(5), pp. 659–680.

Marshall, J. (2011) 'Transwell(®) invasion assays', *Methods Mol Biol,* 769, pp. 97–110.

Mathew, A., Bell, A. and Johnstone, R. M. (1995) 'Hsp-70 is closely associated with the transferrin receptor in exosomes from maturing reticulocytes', *Biochem J,* 308 (Pt 3), pp. 823–30.

Mathivanan, S. and Simpson, R. J. (2009) 'ExoCarta: A compendium of exosomal proteins and RNA', *Proteomics,* 9(21), pp. 4997–5000.

Mathivanan, S., Ji, H. and Simpson, R. J. (2010) 'Exosomes: extracellular organelles important in intercellular communication', *J Proteomics,* 73(10), pp. 1907–20.

Mathivanan, S., Fahner, C. J., Reid, G. E. and Simpson, R. J. (2012) 'ExoCarta 2012: database of exosomal proteins, RNA and lipids', *Nucleic Acids Res,* 40(Database issue), pp. D1241–4.

McCready, J., Sims, J. D., Chan, D. and Jay, D. G. (2010) 'Secretion of extracellular hsp90alpha via exosomes increases cancer cell motility: a role for plasminogen activation', *BMC Cancer,* 10, pp. 294.

McDonald, D. M. and Baluk, P. (2002) 'Significance of blood vessel leakiness in cancer', *Cancer Res,* 62(18), pp. 5381–5.

Meckes, D. G., Shair, K. H., Marquitz, A. R., Kung, C. P., Edwards, R. H. and Raab-Traub, N. (2010) 'Human tumor virus utilizes exosomes for intercellular communication', *Proc Natl Acad Sci U S A,* 107(47), pp. 20370–5.

Meckes, D. G. and Raab-Traub, N. (2011) 'Microvesicles and viral infection', *J Virol,* 85(24), pp. 12844–54.

Menck, K., Klemm, F., Gross, J. C., Pukrop, T., Wenzel, D. and Binder, C. (2013) 'Induction and transport of Wnt 5a during macrophage-induced malignant invasion is mediated by two types of extracellular vesicles', *Oncotarget,* 4(11), pp. 2057–66.

Merkerova, M., Belickova, M. and Bruchova, H. (2008) 'Differential expression of microRNAs in hematopoietic cell lineages', *Eur J Haematol,* 81(4), pp. 304–10.

Michel, G., Tonon, T., Scornet, D., Cock, J. M. and Kloareg, B. (2010) 'The cell wall polysaccharide metabolism of the brown alga Ectocarpus siliculosus. Insights into the evolution of extracellular matrix polysaccharides in Eukaryotes', *New Phytol,* 188(1), pp. 82–97.

Minciacchi, V. R., Freeman, M. R. and Di Vizio, D. (2015) 'Extracellular vesicles in cancer: exosomes, microvesicles and the emerging role of large oncosomes', *Semin Cell Dev Biol,* 40, pp. 41–51.

Mitchell, P. J., Welton, J., Staffurth, J., Court, J., Mason, M. D., Tabi, Z. and Clayton, A. (2009) 'Can urinary exosomes act as treatment response markers in prostate cancer?', *J Transl Med,* 7, pp. 4.

Miyanishi, M., Tada, K., Koike, M., Uchiyama, Y., Kitamura, T. and Nagata, S. (2007) 'Identification of Tim4 as a phosphatidylserine receptor', *Nature,* 450(7168), pp. 435–9.

Momen-Heravi, F., Balaj, L., Alian, S., Mantel, P. Y., Halleck, A. E., Trachtenberg, A. J., Soria, C. E., Oquin, S., Bonebreak, C. M., Saracoglu, E., Skog, J. and Kuo, W. P. (2013) 'Current methods for the isolation of extracellular vesicles', *Biol Chem,* 394(10), pp. 1253–62.

Montecalvo, A., Larregina, A. T., Shufesky, W. J., Stolz, D. B., Sullivan, M. L., Karlsson, J. M., Baty, C. J., Gibson, G. A., Erdos, G., Wang, Z., Milosevic, J., Tkacheva, O. A., Divito, S. J., Jordan, R., Lyons-Weiler, J., Watkins, S. C. and Morelli, A. E. (2012) 'Mechanism of transfer of functional microRNAs between mouse dendritic cells via exosomes', *Blood,* 119(3), pp. 756–66.

Morelli, A. E., Larregina, A. T., Shufesky, W. J., Sullivan, M. L., Stolz, D. B., Papworth, G. D., Zahorchak, A. F., Logar, A. J., Wang, Z., Watkins, S. C., Falo, L. D. and Thomson, A. W. (2004) 'Endocytosis, intracellular sorting, and processing of exosomes by dendritic cells', *Blood,* 104(10), pp. 3257–66.

Morikawa, S., Baluk, P., Kaidoh, T., Haskell, A., Jain, R. K. and McDonald, D. M. (2002) 'Abnormalities in pericytes on blood vessels and endothelial sprouts in tumors', *Am J Pathol,* 160(3), pp. 985–1000.

Mosser, D. D., Caron, A. W., Bourget, L., Denis-Larose, C. and Massie, B. (1997) 'Role of the human heat shock protein hsp70 in protection against stress-induced apoptosis', *Mol Cell Biol,* 17(9), pp. 5317–27.

Mousa, S. A., Linhardt, R., Francis, J. L. and Amirkhosravi, A. (2006) 'Anti-metastatic effect of a non-anticoagulant low-molecular-weight heparin versus the standard low-molecular-weight heparin, enoxaparin', *Thromb Haemost,* 96(6), pp. 816–21.

Mu, W., Rana, S. and Zöller, M. (2013) 'Host matrix modulation by tumor exosomes promotes motility and invasiveness', *Neoplasia,* 15(8), pp. 875–87.

Mulcahy, L. A., Pink, R. C. and Carter, D. R. (2014) 'Routes and mechanisms of extracellular vesicle uptake', *J Extracell Vesicles,* 3, pp. 24641.

Muralidharan-Chari, V., Clancy, J. W., Sedgwick, A. and D'Souza-Schorey, C. (2010) 'Microvesicles: mediators of extracellular communication during cancer progression', *J Cell Sci,* 123(Pt 10), pp. 1603–11.

Müller, G. (2012) 'Microvesicles/exosomes as potential novel biomarkers of metabolic diseases', *Diabetes Metab Syndr Obes,* 5, pp. 247–82.

Nakamura, N., Rabouille, C., Watson, R., Nilsson, T., Hui, N., Slusarewicz, P., Kreis, T. E. and Warren, G. (1995) 'Characterization of a cis-Golgi matrix protein, GM130', *J Cell Biol,* 131(6 Pt 2), pp. 1715–26.

National Institute for Health and Care Excellence (2010) Ovarian cancer: the recognition and initial management of ovarian cancer NICE guideline. National Institute for Health and Care Excellence. Available at: http://www.nice.org.uk/guidance/cg122/documents/ovarian-cancer-nice-guideline-for-consultation2 (Accessed: 27th January 2016).

Ngora, H., Galli, U. M., Miyazaki, K. and Zöller, M. (2012) 'Membrane-bound and exosomal metastasis-associated C4.4A promotes migration by associating with the α(6)β(4) integrin and MT1-MMP', *Neoplasia,* 14(2), pp. 95–107.

Nims, R. W., Sykes, G., Cottrill, K., Ikonomi, P. and Elmore, E. (2010) 'Short tandem repeat profiling: part of an overall strategy for reducing the frequency of cell misidentification', *In Vitro Cell Dev Biol Anim,* 46(10), pp. 811–9.

Noble, S. (2014) 'Heparins and cancer survival: where do we stand?', *Thromb Res,* 133 Suppl 2, pp. S133–8.

Nolte-'t Hoen, E. N., Buermans, H. P., Waasdorp, M., Stoorvogel, W., Wauben, M. H. and 't Hoen, P. A. (2012a) 'Deep sequencing of RNA from immune cell-derived vesicles uncovers the selective incorporation of small non-coding RNA biotypes with potential regulatory functions', *Nucleic Acids Res,* 40(18), pp. 9272–85.

Nolte-'t Hoen, E. N., van der Vlist, E. J., Aalberts, M., Mertens, H. C., Bosch, B. J., Bartelink, W., Mastrobattista, E., van Gaal, E. V., Stoorvogel, W., Arkesteijn, G. J. and Wauben, M. H. (2012b) 'Quantitative and qualitative flow cytometric analysis of nanosized cell-derived membrane vesicles', *Nanomedicine,* 8(5), pp. 712–20.

Nordin, J. Z., Lee, Y., Vader, P., Mäger, I., Johansson, H. J., Heusermann, W., Wiklander, O. P., Hällbrink, M., Seow, Y., Bultema, J. J., Gilthorpe, J., Davies, T., Fairchild, P. J., Gabrielsson, S., Meisner-Kober, N. C., Lehtiö, J., Smith, C. I., Wood, M. J. and El Andaloussi, S. (2015) 'Ultrafiltration with size-exclusion liquid chromatography for high yield isolation of extracellular vesicles preserving intact biophysical and functional properties', *Nanomedicine,* 11(4), pp. 879–83.

Nowell, P. C. (1976) 'The clonal evolution of tumor cell populations', *Science,* 194(4260), pp. 23–8.

O'Brien, K., Rani, S., Corcoran, C., Wallace, R., Hughes, L., Friel, A. M., McDonnell, S., Crown, J., Radomski, M. W. and O'Driscoll, L. (2013) 'Exosomes from triple-negative breast cancer cells can transfer phenotypic traits representing their cells of origin to secondary cells', *Eur J Cancer,* 49(8), pp. 1845–59.

O'Loughlin, A. J., Woffindale, C. A. and Wood, M. J. (2012) 'Exosomes and the emerging field of exosome-based gene therapy', *Curr Gene Ther,* 12(4), pp. 262–74.

Ohno, S., Takanashi, M., Sudo, K., Ueda, S., Ishikawa, A., Matsuyama, N., Fujita, K., Mizutani, T., Ohgi, T., Ochiya, T., Gotoh, N. and Kuroda, M. (2013) 'Systemically injected exosomes

targeted to EGFR deliver antitumor microRNA to breast cancer cells', *Mol Ther,* 21(1), pp. 185–91.

Ohshima, K., Inoue, K., Fujiwara, A., Hatakeyama, K., Kanto, K., Watanabe, Y., Muramatsu, K., Fukuda, Y., Ogura, S., Yamaguchi, K. and Mochizuki, T. (2010) 'Let-7 microRNA family is selectively secreted into the extracellular environment via exosomes in a metastatic gastric cancer cell line', *PLoS One,* 5(10), pp. e13247.

Paget, S. (1989) 'The distribution of secondary growths in cancer of the breast. 1889', *Cancer Metastasis Rev,* 8(2), pp. 98–101.

Pallepati, P. and Averill-Bates, D. A. (2011) 'Activation of ER stress and apoptosis by hydrogen peroxide in HeLa cells: protective role of mild heat preconditioning at 40°C', *Biochim Biophys Acta,* 1813(12), pp. 1987–99.

Palma, J., Yaddanapudi, S. C., Pigati, L., Havens, M. A., Jeong, S., Weiner, G. A., Weimer, K. M., Stern, B., Hastings, M. L. and Duelli, D. M. (2012) 'MicroRNAs are exported from malignant cells in customized particles', *Nucleic Acids Res,* 40(18), pp. 9125–38.

Paltridge, J. L., Belle, L. and Khew-Goodall, Y. (2013) 'The secretome in cancer progression', *Biochim Biophys Acta,* 1834(11), pp. 2233–41.

Pan, B. T., Teng, K., Wu, C., Adam, M. and Johnstone, R. M. (1985) 'Electron microscopic evidence for externalization of the transferrin receptor in vesicular form in sheep reticulocytes', *J Cell Biol,* 101(3), pp. 942–8.

Pan, Q., Ramakrishnaiah, V., Henry, S., Fouraschen, S., de Ruiter, P. E., Kwekkeboom, J., Tilanus, H. W., Janssen, H. L. and van der Laan, L. J. (2012) 'Hepatic cell-to-cell transmission of small silencing RNA can extend the therapeutic reach of RNA interference (RNAi)', *Gut,* 61(9), pp. 1330–9.

Park, J. and Liu, A. Y. (2001) 'JNK phosphorylates the HSF1 transcriptional activation domain: role of JNK in the regulation of the heat shock response', *J Cell Biochem,* 82(2), pp. 326–38.

Park, J. E., Tan, H. S., Datta, A., Lai, R. C., Zhang, H., Meng, W., Lim, S. K. and Sze, S. K. (2010) 'Hypoxic tumor cell modulates its microenvironment to enhance angiogenic and metastatic potential by secretion of proteins and exosomes', *Mol Cell Proteomics,* 9(6), pp. 1085–99.

Parolini, I., Federici, C., Raggi, C., Lugini, L., Palleschi, S., De Milito, A., Coscia, C., Iessi, E., Logozzi, M., Molinari, A., Colone, M., Tatti, M., Sargiacomo, M. and Fais, S. (2009) 'Microenvironmental pH is a key factor for exosome traffic in tumor cells', *J Biol Chem,* 284(49), pp. 34211–22.

Peach, R. J., Hollenbaugh, D., Stamenkovic, I. and Aruffo, A. (1993) 'Identification of hyaluronic acid binding sites in the extracellular domain of CD44', *J Cell Biol,* 122(1), pp. 257–64.

Peinado, H., Alečković, M., Lavotshkin, S., Matei, I., Costa-Silva, B., Moreno-Bueno, G., Hergueta-Redondo, M., Williams, C., García-Santos, G., Ghajar, C., Nitadori-Hoshino, A., Hoffman, C., Badal, K., Garcia, B. A., Callahan, M. K., Yuan, J., Martins, V. R., Skog, J., Kaplan, R. N., Brady, M. S., Wolchok, J. D., Chapman, P. B., Kang, Y., Bromberg, J. and Lyden, D. (2012) 'Melanoma exosomes educate bone marrow progenitor cells toward a pro-metastatic phenotype through MET', *Nat Med,* 18(6), pp. 883–91.

Perkins, N. D. and Gilmore, T. D. (2006) 'Good cop, bad cop: the different faces of NF-kappaB', *Cell Death Differ,* 13(5), pp. 759–72.

Pink, R. C., Samuel, P., Massa, D., Caley, D. P., Brooks, S. A. and Carter, D. R. (2015) 'The passenger strand, miR-21-3p, plays a role in mediating cisplatin resistance in ovarian cancer cells', *Gynecol Oncol,* 137(1), pp. 143–51.

Pistone Creydt, V., Fletcher, S. J., Giudice, J., Bruzzone, A., Chasseing, N. A., Gonzalez, E. G., Sacca, P. A. and Calvo, J. C. (2013) 'Human adipose tissue from normal and tumoral breast regulates the behavior of mammary epithelial cells', *Clin Transl Oncol,* 15(2), pp. 124–31.

Polyak, K. and Weinberg, R. A. (2009) 'Transitions between epithelial and mesenchymal states: acquisition of malignant and stem cell traits', *Nat Rev Cancer,* 9(4), pp. 265–73.

Pornillos, O., Higginson, D. S., Stray, K. M., Fisher, R. D., Garrus, J. E., Payne, M., He, G. P., Wang, H. E., Morham, S. G. and Sundquist, W. I. (2003) 'HIV Gag mimics the Tsg101-recruiting activity of the human Hrs protein', *J Cell Biol,* 162(3), pp. 425–34.

Price, J. T., Bonovich, M. T. and Kohn, E. C. (1997) 'The biochemistry of cancer dissemination', *Crit Rev Biochem Mol Biol,* 32(3), pp. 175–253.

Provenzano, P. P., Inman, D. R., Eliceiri, K. W. and Keely, P. J. (2009) 'Matrix density-induced mechanoregulation of breast cell phenotype, signaling and gene expression through a FAK-ERK linkage', *Oncogene,* 28(49), pp. 4326–43.

Qu, J. L., Qu, X. J., Zhao, M. F., Teng, Y. E., Zhang, Y., Hou, K. Z., Jiang, Y. H., Yang, X. H. and Liu, Y. P. (2009) 'Gastric cancer exosomes promote tumour cell proliferation through PI3K/Akt and MAPK/ERK activation', *Dig Liver Dis,* 41(12), pp. 875–80.

Rabinowits, G., Gerçel-Taylor, C., Day, J. M., Taylor, D. D. and Kloecker, G. H. (2009) 'Exosomal microRNA: a diagnostic marker for lung cancer', *Clin Lung Cancer,* 10(1), pp. 42–6.

Raingeaud, J., Gupta, S., Rogers, J. S., Dickens, M., Han, J., Ulevitch, R. J. and Davis, R. J. (1995) 'Pro-inflammatory cytokines and environmental stress cause p38 mitogen-activated protein kinase activation by dual phosphorylation on tyrosine and threonine', *J Biol Chem,* 270(13), pp. 7420–6.

Ramakrishna, R. and Rostomily, R. (2013) 'Seed, soil, and beyond: The basic biology of brain metastasis', *Surg Neurol Int,* 4(Suppl 4), pp. S256–64.

Ramteke, A., Ting, H., Agarwal, C., Mateen, S., Somasagara, R., Hussain, A., Graner, M., Frederick, B., Agarwal, R. and Deep, G. (2015) 'Exosomes secreted under hypoxia enhance invasiveness and stemness of prostate cancer cells by targeting adherens junction molecules', *Mol Carcinog,* 54(7), pp. 554–65.

Rana, S. and Zöller, M. (2011) 'Exosome target cell selection and the importance of exosomal tetraspanins: a hypothesis', *Biochem Soc Trans,* 39(2), pp. 559–62.

Rana, S., Malinowska, K. and Zöller, M. (2013) 'Exosomal tumor microRNA modulates premetastatic organ cells', *Neoplasia,* 15(3), pp. 281–95.

Raposo, G., Nijman, H. W., Stoorvogel, W., Liejendekker, R., Harding, C. V., Melief, C. J. and Geuze, H. J. (1996) 'B lymphocytes secrete antigen-presenting vesicles', *J Exp Med,* 183(3), pp. 1161–72.

Raposo, G. and Stoorvogel, W. (2013) 'Extracellular vesicles: exosomes, microvesicles, and friends', *J Cell Biol,* 200(4), pp. 373–83.

Rappa, G., Mercapide, J., Anzanello, F., Pope, R. M. and Lorico, A. (2013) 'Biochemical and biological characterization of exosomes containing prominin-1/CD133', *Mol Cancer,* 12, pp. 62.

Ratajczak, J., Miekus, K., Kucia, M., Zhang, J., Reca, R., Dvorak, P. and Ratajczak, M. Z. (2006) 'Embryonic stem cell-derived microvesicles reprogram hematopoietic progenitors: evidence for horizontal transfer of mRNA and protein delivery', *Leukemia,* 20(5), pp. 847–56.

Razi, M. and Futter, C. E. (2006) 'Distinct roles for Tsg101 and Hrs in multivesicular body formation and inward vesiculation', *Mol Biol Cell,* 17(8), pp. 3469–83.

Record, M., Carayon, K., Poirot, M. and Silvente-Poirot, S. (2014) 'Exosomes as new vesicular lipid transporters involved in cell-cell communication and various pathophysiologies', *Biochim Biophys Acta,* 1841(1), pp. 108–20.

Renzulli, J. F., Del Tatto, M., Dooner, G., Aliotta, J., Goldstein, L., Dooner, M., Colvin, G., Chatterjee, D. and Quesenberry, P. (2010) 'Microvesicle induction of prostate specific gene expression in normal human bone marrow cells', *J Urol,* 184(5), pp. 2165–71.

Robinson, M. J. and Cobb, M. H. (1997) 'Mitogen-activated protein kinase pathways', *Curr Opin Cell Biol,* 9(2), pp. 180–6.

Roccaro, A. M., Sacco, A., Maiso, P., Azab, A. K., Tai, Y. T., Reagan, M., Azab, F., Flores, L. M., Campigotto, F., Weller, E., Anderson, K. C., Scadden, D. T. and Ghobrial, I. M. (2013) 'BM mesenchymal stromal cell-derived exosomes facilitate multiple myeloma progression', *J Clin Invest,* 123(4), pp. 1542–55.

Rolfo, C., Castiglia, M., Hong, D., Alessandro, R., Mertens, I., Baggerman, G., Zwaenepoel, K., Gil-Bazo, I., Passiglia, F., Carreca, A. P., Taverna, S., Vento, R., Peeters, M., Russo, A. and Pauwels, P. (2014) 'Liquid biopsies in lung cancer: the new ambrosia of researchers', *Biochim Biophys Acta,* 1846(2), pp. 539–46.

Roos, W. P. and Kaina, B. (2006) 'DNA damage-induced cell death by apoptosis', *Trends Mol Med,* 12(9), pp. 440–50.

Roussos, E. T., Condeelis, J. S. and Patsialou, A. (2011) 'Chemotaxis in cancer', *Nat Rev Cancer,* 11(8), pp. 573–87.

Rubinstein, E. (2011) 'The complexity of tetraspanins', *Biochem Soc Trans,* 39(2), pp. 501–5.

Sahai, E. (2005) 'Mechanisms of cancer cell invasion', *Curr Opin Genet Dev,* 15(1), pp. 87–96.

Sahai, E. (2007) 'Illuminating the metastatic process', *Nat Rev Cancer,* 7(10), pp. 737–49.

Sahoo, S., Klychko, E., Thorne, T., Misener, S., Schultz, K. M., Millay, M., Ito, A., Liu, T., Kamide, C., Agrawal, H., Perlman, H., Qin, G., Kishore, R. and Losordo, D. W. (2011) 'Exosomes from human CD34(+) stem cells mediate their proangiogenic paracrine activity', *Circ Res,* 109(7), pp. 724–8.

Sahu, R., Kaushik, S., Clement, C. C., Cannizzo, E. S., Scharf, B., Follenzi, A., Potolicchio, I., Nieves, E., Cuervo, A. M. and Santambrogio, L. (2011) 'Microautophagy of cytosolic proteins by late endosomes', *Dev Cell,* 20(1), pp. 131–9.

Salomon, C., Kobayashi, M., Ashman, K., Sobrevia, L., Mitchell, M. D. and Rice, G. E. (2013a) 'Hypoxia-induced changes in the bioactivity of cytotrophoblast-derived exosomes', *PLoS One,* 8(11), pp. e79636.

Salomon, C., Ryan, J., Sobrevia, L., Kobayashi, M., Ashman, K., Mitchell, M. and Rice, G. E. (2013b) 'Exosomal signaling during hypoxia mediates microvascular endothelial cell migration and vasculogenesis', *PLoS One,* 8(7), pp. e68451.

Salvador, N., Aguado, C., Horst, M. and Knecht, E. (2000) 'Import of a cytosolic protein into lysosomes by chaperone-mediated autophagy depends on its folding state', *J Biol Chem,* 275(35), pp. 27447–56.

Samali, A. and Orrenius, S. (1998) 'Heat shock proteins: regulators of stress response and apoptosis', *Cell Stress Chaperones,* 3(4), pp. 228–36.

Samatar, A. A. and Poulikakos, P. I. (2014) 'Targeting RAS-ERK signalling in cancer: promises and challenges', *Nat Rev Drug Discov,* 13(12), pp. 928–42.

Sammak, P. J., Hinman, L. E., Tran, P. O., Sjaastad, M. D. and Machen, T. E. (1997) 'How do injured cells communicate with the surviving cell monolayer?', *J Cell Sci,* 110 (Pt 4), pp. 465–75.

Sarrazin, S., Lamanna, W. C. and Esko, J. D. (2011) 'Heparan sulfate proteoglycans', *Cold Spring Harb Perspect Biol,* 3(7), pp. a004952.

Schwartz, D. R., Kardia, S. L., Shedden, K. A., Kuick, R., Michailidis, G., Taylor, J. M., Misek, D. E., Wu, R., Zhai, Y., Darrah, D. M., Reed, H., Ellenson, L. H., Giordano, T. J., Fearon, E. R., Hanash, S. M. and Cho, K. R. (2002) 'Gene expression in ovarian cancer reflects both morphology and biological behavior, distinguishing clear cell from other poor-prognosis ovarian carcinomas', *Cancer Res,* 62(16), pp. 4722–9.

Scully, O. J., Bay, B. H., Yip, G. and Yu, Y. (2012) 'Breast cancer metastasis', *Cancer Genomics Proteomics,* 9(5), pp. 311–20.

Sebolt-Leopold, J. S. and Herrera, R. (2004) 'Targeting the mitogen-activated protein kinase cascade to treat cancer', *Nat Rev Cancer,* 4(12), pp. 937–47.

Seidler, N. W. (2013) 'Compartmentation of GAPDH', *Adv Exp Med Biol,* 985, pp. 61–101.

Seo, Y. H., Jo, Y. N., Oh, Y. J. and Park, S. (2015) 'Nano-mechanical reinforcement in drug-resistant ovarian cancer cells', *Biol Pharm Bull,* 38(3), pp. 389–95.

Seow, Y. and Wood, M. J. (2009) 'Biological gene delivery vehicles: beyond viral vectors', *Mol Ther,* 17(5), pp. 767–77.

Shayan, R., Achen, M. G. and Stacker, S. A. (2006) 'Lymphatic vessels in cancer metastasis: bridging the gaps', *Carcinogenesis,* 27(9), pp. 1729–38.

Sheldon, H., Heikamp, E., Turley, H., Dragovic, R., Thomas, P., Oon, C. E., Leek, R., Edelmann, M., Kessler, B., Sainson, R. C., Sargent, I., Li, J. L. and Harris, A. L. (2010) 'New mechanism for Notch signaling to endothelium at a distance by Delta-like 4 incorporation into exosomes', *Blood,* 116(13), pp. 2385–94.

Shen, C., Lancaster, C. S., Shi, B., Guo, H., Thimmaiah, P. and Bjornsti, M. A. (2007) 'TOR signaling is a determinant of cell survival in response to DNA damage', *Mol Cell Biol,* 27(20), pp. 7007–17.

Siekevitz, P. and Watson, M. L. (1956) 'Cytochemical studies of mitochondria. II. Enzymes associated with a mitochondrial membrane fraction', *J Biophys Biochem Cytol,* 2(6), pp. 653–69.

Silva, J., Garcia, V., Rodriguez, M., Compte, M., Cisneros, E., Veguillas, P., Garcia, J. M., Dominguez, G., Campos-Martin, Y., Cuevas, J., Peña, C., Herrera, M., Diaz, R., Mohammed, N. and Bonilla, F. (2012) 'Analysis of exosome release and its prognostic value in human colorectal cancer', *Genes Chromosomes Cancer,* 51(4), pp. 409–18.

Simpson, R. J., Kalra, H. and Mathivanan, S. (2012) 'ExoCarta as a resource for exosomal research', *J Extracell Vesicles,* 1, pp. 18374.

Simpson, R. J. and Mathivanan, S. (2012) 'Extracellular Microvesicles: The Need for Internationally Recognised Nomenclature and Stringent Purification Criteria', *J Proteomics Bioinform*, 5, pp. 2.

Singh, R., Pochampally, R., Watabe, K., Lu, Z. and Mo, Y. Y. (2014) 'Exosome-mediated transfer of miR-10b promotes cell invasion in breast cancer', *Mol Cancer,* 13, pp. 256.

Skog, J., Würdinger, T., van Rijn, S., Meijer, D. H., Gainche, L., Sena-Esteves, M., Curry, W. T., Carter, B. S., Krichevsky, A. M. and Breakefield, X. O. (2008) 'Glioblastoma microvesicles transport RNA and proteins that promote tumour growth and provide diagnostic biomarkers', *Nat Cell Biol,* 10(12), pp. 1470–6.

Skokos, D., Le Panse, S., Villa, I., Rousselle, J. C., Peronet, R., David, B., Namane, A. and Mécheri, S. (2001) 'Mast cell-dependent B and T lymphocyte activation is mediated by the secretion of immunologically active exosomes', *J Immunol,* 166(2), pp. 868–76.

Smith, G. C. and Jackson, S. P. (1999) 'The DNA-dependent protein kinase', *Genes Dev,* 13(8), pp. 916–34.

Sokolova, V., Ludwig, A. K., Hornung, S., Rotan, O., Horn, P. A., Epple, M. and Giebel, B. (2011) 'Characterisation of exosomes derived from human cells by nanoparticle tracking analysis and scanning electron microscopy', *Colloids Surf B Biointerfaces,* 87(1), pp. 146–50.

Soo, C. Y., Song, Y., Zheng, Y., Campbell, E. C., Riches, A. C., Gunn-Moore, F. and Powis, S. J. (2012) 'Nanoparticle tracking analysis monitors microvesicle and exosome secretion from immune cells', *Immunology,* 136(2), pp. 192–7.

Sood, A. K., Seftor, E. A., Fletcher, M. S., Gardner, L. M., Heidger, P. M., Buller, R. E., Seftor, R. E. and Hendrix, M. J. (2001) 'Molecular determinants of ovarian cancer plasticity', *Am J Pathol,* 158(4), pp. 1279–88.

Sorkin, A. and von Zastrow, M. (2009) 'Endocytosis and signalling: intertwining molecular networks', *Nat Rev Mol Cell Biol,* 10(9), pp. 609–22.

Soule, H. D., Vazquez, J., Long, A., Albert, S. and Brennan, M. (1973) 'A human cell line from a pleural effusion derived from a breast carcinoma', *J Natl Cancer Inst,* 51(5), pp. 1409–16.

St Croix, B., Rago, C., Velculescu, V., Traverso, G., Romans, K. E., Montgomery, E., Lal, A., Riggins, G. J., Lengauer, C., Vogelstein, B. and Kinzler, K. W. (2000) 'Genes expressed in human tumor endothelium', *Science,* 289(5482), pp. 1197–202.

Staples, C. J., Owens, D. M., Maier, J. V., Cato, A. C. and Keyse, S. M. (2010) 'Cross-talk between the p38alpha and JNK MAPK pathways mediated by MAP kinase phosphatase-1 determines cellular sensitivity to UV radiation', *J Biol Chem,* 285(34), pp. 25928–40.

Staubach, S., Razawi, H. and Hanisch, F. G. (2009) 'Proteomics of MUC1-containing lipid rafts from plasma membranes and exosomes of human breast carcinoma cells MCF-7', *Proteomics,* 9(10), pp. 2820–35.

Steeg, P. S. (2006) 'Tumor metastasis: mechanistic insights and clinical challenges', *Nat Med,* 12(8), pp. 895–904.

Stevenson, J. L., Varki, A. and Borsig, L. (2007) 'Heparin attenuates metastasis mainly due to inhibition of P- and L-selectin, but non-anticoagulant heparins can have additional effects', *Thromb Res,* 120 Suppl 2, pp. S107–11.

Stoeck, A., Keller, S., Riedle, S., Sanderson, M. P., Runz, S., Le Naour, F., Gutwein, P., Ludwig, A., Rubinstein, E. and Altevogt, P. (2006) 'A role for exosomes in the constitutive and stimulus-induced ectodomain cleavage of L1 and CD44', *Biochem J,* 393(Pt 3), pp. 609–18.

Stojic, L., Brun, R. and Jiricny, J. (2004) 'Mismatch repair and DNA damage signalling', *DNA Repair (Amst),* 3(8–9), pp. 1091–101.

Stoorvogel, W., Kleijmeer, M. J., Geuze, H. J. and Raposo, G. (2002) 'The biogenesis and functions of exosomes', *Traffic,* 3(5), pp. 321–30.

Stoorvogel, W. (2012) 'Functional transfer of microRNA by exosomes', *Blood,* 119(3), pp. 646–8.

Svensson, K. J., Christianson, H. C., Wittrup, A., Bourseau-Guilmain, E., Lindqvist, E., Svensson, L. M., Morgelin, M. and Belting, M. (2013) 'Exosome uptake depends on ERK1/2-heat shock protein 27 signalling and lipid raft-mediated endocytosis negatively regulated by caveolin-1', *J Biol Chem,* 288(24), pp. 17713–24.

Tadokoro, H., Umezu, T., Ohyashiki, K., Hirano, T. and Ohyashiki, J. H. (2013) 'Exosomes derived from hypoxic leukemia cells enhance tube formation in endothelial cells', *J Biol Chem,* 288(48), pp. 34343–51.

Takahara, P. M., Rosenzweig, A. C., Frederick, C. A. and Lippard, S. J. (1995) 'Crystal structure of double-stranded DNA containing the major adduct of the anticancer drug cisplatin', *Nature,* 377(6550), pp. 649–52.

Takai, M., Terai, Y., Kawaguchi, H., Ashihara, K., Fujiwara, S., Tanaka, T., Tsunetoh, S., Tanaka, Y., Sasaki, H., Kanemura, M., Tanabe, A. and Ohmichi, M. (2014) 'The EMT (epithelial-mesenchymal-transition)-related protein expression indicates the metastatic status and prognosis in patients with ovarian cancer', *J Ovarian Res,* 7, pp. 76.

Tanaka, Y., Kamohara, H., Kinoshita, K., Kurashige, J., Ishimoto, T., Iwatsuki, M., Watanabe, M. and Baba, H. (2013) 'Clinical impact of serum exosomal microRNA-21 as a clinical biomarker in human esophageal squamous cell carcinoma', *Cancer,* 119(6), pp. 1159–67.

Tarin, D., Price, J. E., Kettlewell, M. G., Souter, R. G., Vass, A. C. and Crossley, B. (1984) 'Mechanisms of human tumor metastasis studied in patients with peritoneovenous shunts', *Cancer Res,* 44(8), pp. 3584–92.

Tauro, B. J., Greening, D. W., Mathias, R. A., Ji, H., Mathivanan, S., Scott, A. M. and Simpson, R. J. (2012) 'Comparison of ultracentrifugation, density gradient separation, and immunoaffinity capture methods for isolating human colon cancer cell line LIM1863-derived exosomes', *Methods,* 56(2), pp. 293–304.

Tavaria, M., Gabriele, T., Anderson, R. L., Mirault, M. E., Baker, E., Sutherland, G. and Kola, I. (1995) 'Localization of the gene encoding the human heat shock cognate protein, HSP73, to chromosome 11', *Genomics,* 29(1), pp. 266–8.

Taverna, S., Amodeo, V., Saieva, L., Russo, A., Giallombardo, M., De Leo, G. and Alessandro, R. (2014) 'Exosomal shuttling of miR-126 in endothelial cells modulates adhesive and migratory abilities of chronic myelogenous leukemia cells', *Mol Cancer,* 13, pp. 169.

Tavoosidana, G., Ronquist, G., Darmanis, S., Yan, J., Carlsson, L., Wu, D., Conze, T., Ek, P., Semjonow, A., Eltze, E., Larsson, A., Landegren, U. D. and Kamali-Moghaddam, M. (2011) 'Multiple recognition assay reveals prostasomes as promising plasma biomarkers for prostate cancer', *Proc Natl Acad Sci U S A,* 108(21), pp. 8809–14.

Taylor, D. D. and Gercel-Taylor, C. (2008) 'MicroRNA signatures of tumor-derived exosomes as diagnostic biomarkers of ovarian cancer', *Gynecol Oncol,* 110(1), pp. 13–21.

Taylor, D. D. (2015) 'Isolation and molecular characterization of extracellular vesicles', *Methods,* 87, pp. 1–2.

Théry, C., Regnault, A., Garin, J., Wolfers, J., Zitvogel, L., Ricciardi-Castagnoli, P., Raposo, G. and Amigorena, S. (1999) 'Molecular characterization of dendritic cell-derived exosomes. Selective accumulation of the heat shock protein hsc73', *J Cell Biol,* 147(3), pp. 599–610.

Théry, C., Zitvogel, L. and Amigorena, S. (2002) 'Exosomes: composition, biogenesis and function', *Nat Rev Immunol,* 2(8), pp. 569–79.

Théry, C., Amigorena, S., Raposo, G. and Clayton, A. (2006) 'Isolation and characterization of exosomes from cell culture supernatants and biological fluids', *Curr Protoc Cell Biol,* Chapter 3, pp. Unit 3.22.

Théry, C., Ostrowski, M. and Segura, E. (2009) 'Membrane vesicles as conveyors of immune responses', *Nat Rev Immunol,* 9(8), pp. 581–93.

Théry, C. (2011) 'Exosomes: secreted vesicles and intercellular communications', *F1000 Biol Rep,* 3, pp. 15.

Todaro, G. J., Lazar, G. K. and Green, H. (1965) 'The initiation of cell division in a contact-inhibited mammalian cell line', *J Cell Physiol,* 66(3), pp. 325–33.

Torre, L. A., Bray, F., Siegel, R. L., Ferlay, J., Lortet-Tieulent, J. and Jemal, A. (2015) 'Global cancer statistics, 2012', *CA Cancer J Clin,* 65(2), pp. 87–108.

Trajkovic, K., Hsu, C., Chiantia, S., Rajendran, L., Wenzel, D., Wieland, F., Schwille, P., Brügger, B. and Simons, M. (2008) 'Ceramide triggers budding of exosome vesicles into multivesicular endosomes', *Science,* 319(5867), pp. 1244–7.

Trams, E. G., Lauter, C. J., Salem, N. and Heine, U. (1981) 'Exfoliation of membrane ecto-enzymes in the form of micro-vesicles', *Biochim Biophys Acta,* 645(1), pp. 63–70.

Tsai, J. H. and Yang, J. (2013) 'Epithelial-mesenchymal plasticity in carcinoma metastasis', *Genes Dev,* 27(20), pp. 2192–206.

Tumne, A., Prasad, V. S., Chen, Y., Stolz, D. B., Saha, K., Ratner, D. M., Ding, M., Watkins, S. C. and Gupta, P. (2009) 'Noncytotoxic suppression of human immunodeficiency virus type 1 transcription by exosomes secreted from CD8+ T cells', *J Virol,* 83(9), pp. 4354–64.

Turchinovich, A., Weiz, L., Langheinz, A. and Burwinkel, B. (2011) 'Characterization of extracellular circulating microRNA', *Nucleic Acids Res,* 39(16), pp. 7223–33.

Twarock, S., Röck, K., Sarbia, M., Weber, A. A., Jänicke, R. U. and Fischer, J. W. (2009) 'Synthesis of hyaluronan in oesophageal cancer cells is uncoupled from the prostaglandin-cAMP pathway', *Br J Pharmacol,* 157(2), pp. 234–43.

Vader, P., Breakefield, X. O. and Wood, M. J. (2014) 'Extracellular vesicles: emerging targets for cancer therapy', *Trends Mol Med,* 20(7), pp. 385–93.

Valadi, H., Ekström, K., Bossios, A., Sjöstrand, M., Lee, J. J. and Lötvall, J. O. (2007) 'Exosome-mediated transfer of mRNAs and microRNAs is a novel mechanism of genetic exchange between cells', *Nat Cell Biol,* 9(6), pp. 654–9.

Valencia, K., Luis-Ravelo, D., Bovy, N., Antón, I., Martínez-Canarias, S., Zandueta, C., Ormazábal, C., Struman, I., Tabruyn, S., Rebmann, V., De Las Rivas, J., Guruceaga, E., Bandrés, E. and Lecanda, F. (2014) 'miRNA cargo within exosome-like vesicle transfer influences metastatic bone colonization', *Mol Oncol,* 8(3), pp. 689–703.

Valerie, K. and Povirk, L. F. (2003) 'Regulation and mechanisms of mammalian double-strand break repair', *Oncogene,* 22(37), pp. 5792–812.

van der Vlist, E. J., Nolte-'t Hoen, E. N., Stoorvogel, W., Arkesteijn, G. J. and Wauben, M. H. (2012) 'Fluorescent labeling of nano-sized vesicles released by cells and subsequent quantitative and qualitative analysis by high-resolution flow cytometry', *Nat Protoc,* 7(7), pp. 1311–26.

van der Zee, J. (2002) 'Heating the patient: a promising approach?', *Ann Oncol,* 13(8), pp. 1173–84.

van Niel, G., Porto-Carreiro, I., Simoes, S. and Raposo, G. (2006) 'Exosomes: a common pathway for a specialized function', *J Biochem,* 140(1), pp. 13–21.

Verweij, F. J., van Eijndhoven, M. A., Hopmans, E. S., Vendrig, T., Wurdinger, T., Cahir-McFarland, E., Kieff, E., Geerts, D., van der Kant, R., Neefjes, J., Middeldorp, J. M. and Pegtel, D. M. (2011) 'LMP1 association with CD63 in endosomes and secretion via exosomes limits constitutive NF-κB activation', *EMBO J,* 30(11), pp. 2115–29.

Vlassov, A. V., Magdaleno, S., Setterquist, R. and Conrad, R. (2012) 'Exosomes: current knowledge of their composition, biological functions, and diagnostic and therapeutic potentials', *Biochim Biophys Acta,* 1820(7), pp. 940–8.

Volk, T., Geiger, B. and Raz, A. (1984) 'Motility and adhesive properties of high- and low-metastatic murine neoplastic cells', *Cancer Res,* 44(2), pp. 811–24.

von Schwedler, U. K., Stuchell, M., Müller, B., Ward, D. M., Chung, H. Y., Morita, E., Wang, H. E., Davis, T., He, G. P., Cimbora, D. M., Scott, A., Kräusslich, H. G., Kaplan, J., Morham, S. G. and Sundquist, W. I. (2003) 'The protein network of HIV budding', *Cell,* 114(6), pp. 701–13.

Wada, I., Rindress, D., Cameron, P. H., Ou, W. J., Doherty, J. J., Louvard, D., Bell, A. W., Dignard, D., Thomas, D. Y. and Bergeron, J. J. (1991) 'SSR alpha and associated calnexin are major calcium binding proteins of the endoplasmic reticulum membrane', *J Biol Chem,* 266(29), pp. 19599–610.

Wahlgren, J., De L Karlson, T., Brisslert, M., Vaziri Sani, F., Telemo, E., Sunnerhagen, P. and Valadi, H. (2012) 'Plasma exosomes can deliver exogenous short interfering RNA to monocytes and lymphocytes', *Nucleic Acids Res,* 40(17), pp. e130.

Wang, H. P., Hanlon, J. G., Rainbow, A. J., Espiritu, M. and Singh, G. (2002) 'Up-regulation of Hsp27 plays a role in the resistance of human colon carcinoma HT29 cells to photooxidative stress', *Photochem Photobiol,* 76(1), pp. 98–104.

Wang, J. H., Thampatty, B. P., Lin, J. S. and Im, H. J. (2007) 'Mechanoregulation of gene expression in fibroblasts', *Gene,* 391(1–2), pp. 1–15.

Wang, J., Yang, Y., Xu, J., Lin, X., Wu, K. and Yu, M. (2013) 'Pirfenidone inhibits migration, differentiation, and proliferation of human retinal pigment epithelial cells in vitro', *Mol Vis,* 19, pp. 2626–35.

Wang, T., Gilkes, D. M., Takano, N., Xiang, L., Luo, W., Bishop, C. J., Chaturvedi, P., Green, J. J. and Semenza, G. L. (2014) 'Hypoxia-inducible factors and RAB22A mediate formation of

microvesicles that stimulate breast cancer invasion and metastasis', *Proc Natl Acad Sci U S A,* 111(31), pp. E3234–42.

Webber, J., Steadman, R., Mason, M. D., Tabi, Z. and Clayton, A. (2010) 'Cancer exosomes trigger fibroblast to myofibroblast differentiation', *Cancer Res,* 70(23), pp. 9621–30.

Webber, J. and Clayton, A. (2013) 'How pure are your vesicles?', *J Extracell Vesicles,* 2, pp. 19861.

Weigelt, B., Peterse, J. L. and van 't Veer, L. J. (2005) 'Breast cancer metastasis: markers and models', *Nat Rev Cancer,* 5(8), pp. 591–602.

Weinberg, R. A. (1996) 'How cancer arises', *Sci Am,* 275(3), pp. 62–70.

Weston, C. R. and Davis, R. J. (2007) 'The JNK signal transduction pathway', *Curr Opin Cell Biol,* 19(2), pp. 142–9.

Whiteside, T. L. (2013) 'Immune modulation of T-cell and NK (natural killer) cell activities by TEXs (tumour-derived exosomes)', *Biochem Soc Trans,* 41(1), pp. 245–51.

Wiesen, J. and Werb, Z. (2000) 'Proteinases, cell cycle regulation, and apoptosis during mammary gland involution (minireview)', *Mol Reprod Dev,* 56(4), pp. 534–40.

Williams, R. L. and Urbé, S. (2007) 'The emerging shape of the ESCRT machinery', *Nat Rev Mol Cell Biol,* 8(5), pp. 355–68.

Willmore, E., Elliott, S. L., Mainou-Fowler, T., Summerfield, G. P., Jackson, G. H., O'Neill, F., Lowe, C., Carter, A., Harris, R., Pettitt, A. R., Cano-Soumillac, C., Griffin, R. J., Cowell, I. G., Austin, C. A. and Durkacz, B. W. (2008) 'DNA-dependent protein kinase is a therapeutic target and an indicator of poor prognosis in B-cell chronic lymphocytic leukemia', *Clin Cancer Res,* 14(12), pp. 3984–92.

Wolfers, J., Lozier, A., Raposo, G., Regnault, A., Théry, C., Masurier, C., Flament, C., Pouzieux, S., Faure, F., Tursz, T., Angevin, E., Amigorena, S. and Zitvogel, L. (2001) 'Tumor-derived exosomes are a source of shared tumor rejection antigens for CTL cross-priming', *Nat Med,* 7(3), pp. 297–303.

Wu, S., Loke, H. N. and Rehemtulla, A. (2002) 'Ultraviolet radiation-induced apoptosis is mediated by Daxx', *Neoplasia,* 4(6), pp. 486–92.

Wubbolts, R., Leckie, R. S., Veenhuizen, P. T., Schwarzmann, G., Möbius, W., Hoernschemeyer, J., Slot, J. W., Geuze, H. J. and Stoorvogel, W. (2003) 'Proteomic and biochemical analyses of human B cell-derived exosomes. Potential implications for their function and multivesicular body formation', *J Biol Chem,* 278(13), pp. 10963–72.

Wust, P., Hildebrandt, B., Sreenivasa, G., Rau, B., Gellermann, J., Riess, H., Felix, R. and Schlag, P. M. (2002) 'Hyperthermia in combined treatment of cancer', *Lancet Oncol,* 3(8), pp. 487–97.

Xiao, D., Ohlendorf, J., Chen, Y., Taylor, D. D., Rai, S. N., Waigel, S., Zacharias, W., Hao, H. and McMasters, K. M. (2012) 'Identifying mRNA, microRNA and protein profiles of melanoma exosomes', *PLoS One,* 7(10), pp. e46874.

Yáñez-Mó, M., Siljander, P. R., Andreu, Z., Zavec, A. B., Borràs, F. E., Buzas, E. I., Buzas, K., Casal, E., Cappello, F., Carvalho, J., Colás, E., Cordeiro-da Silva, A., Fais, S., Falcon-Perez, J. M., Ghobrial, I. M., Giebel, B., Gimona, M., Graner, M., Gursel, I., Gursel, M., Heegaard, N. H., Hendrix, A., Kierulf, P., Kokubun, K., Kosanovic, M., Kralj-Iglic, V., Krämer-Albers, E. M., Laitinen, S., Lässer, C., Lener, T., Ligeti, E., Linē, A., Lipps, G., Llorente, A., Lötvall, J., Manček-Keber, M., Marcilla, A., Mittelbrunn, M., Nazarenko, I., Nolte-'t Hoen, E. N.,

Nyman, T. A., O'Driscoll, L., Olivan, M., Oliveira, C., Pállinger, É., Del Portillo, H. A., Reventós, J., Rigau, M., Rohde, E., Sammar, M., Sánchez-Madrid, F., Santarém, N., Schallmoser, K., Ostenfeld, M. S., Stoorvogel, W., Stukelj, R., Van der Grein, S. G., Vasconcelos, M. H., Wauben, M. H. and De Wever, O. (2015) 'Biological properties of extracellular vesicles and their physiological functions', *J Extracell Vesicles,* 4, pp. 27066.

Yang, H. W., Menon, L. G., Black, P. M., Carroll, R. S. and Johnson, M. D. (2010) 'SNAI2/Slug promotes growth and invasion in human gliomas', *BMC Cancer,* 10, pp. 301.

Yang, M., Chen, J., Su, F., Yu, B., Lin, L., Liu, Y., Huang, J. D. and Song, E. (2011) 'Microvesicles secreted by macrophages shuttle invasion-potentiating microRNAs into breast cancer cells', *Mol Cancer,* 10, pp. 117.

Yoo, S. and Dynan, W. S. (1999) 'Geometry of a complex formed by double strand break repair proteins at a single DNA end: recruitment of DNA-PKcs induces inward translocation of Ku protein', *Nucleic Acids Res,* 27(24), pp. 4679–86.

Yoon, Y. J., Kim, D. K., Yoon, C. M., Park, J., Kim, Y. K., Roh, T. Y. and Gho, Y. S. (2014) 'Egr-1 activation by cancer-derived extracellular vesicles promotes endothelial cell migration via ERK1/2 and JNK signaling pathways', *PLoS One,* 9(12), pp. e115170.

Yu, H., Cook, T. J. and Sinko, P. J. (1997) 'Evidence for diminished functional expression of intestinal transporters in Caco-2 cell monolayers at high passages', *Pharm Res,* 14(6), pp. 757–62.

Yue, P., Zhang, X., Paladino, D., Sengupta, B., Ahmad, S., Holloway, R. W., Ingersoll, S. B. and Turkson, J. (2012) 'Hyperactive EGF receptor, Jaks and Stat3 signaling promote enhanced colony-forming ability, motility and migration of cisplatin-resistant ovarian cancer cells', *Oncogene,* 31(18), pp. 2309–22.

Zakharova, L., Svetlova, M. and Fomina, A. F. (2007) 'T cell exosomes induce cholesterol accumulation in human monocytes via phosphatidylserine receptor', *J Cell Physiol,* 212(1), pp. 174–81.

Zarubin, T. and Han, J. (2005) 'Activation and signaling of the p38 MAP kinase pathway', *Cell Res,* 15(1), pp. 11–8.

Zhang, L., Wu, X., Luo, C., Chen, X., Yang, L., Tao, J. and Shi, J. (2013) 'The 786-0 renal cancer cell-derived exosomes promote angiogenesis by downregulating the expression of hepatocyte cell adhesion molecule', *Mol Med Rep,* 8(1), pp. 272–6.

Zhang, H. G. and Grizzle, W. E. (2014) 'Exosomes: a novel pathway of local and distant intercellular communication that facilitates the growth and metastasis of neoplastic lesions', *Am J Pathol,* 184(1), pp. 28–41.

Zhang, Z., Wang, C., Li, T., Liu, Z. and Li, L. (2014) 'Comparison of ultracentrifugation and density gradient separation methods for isolating Tca8113 human tongue cancer cell line-derived exosomes', *Oncol Lett,* 8(4), pp. 1701–1706.

Zhang, W., Peng, P., Kuang, Y., Yang, J., Cao, D., You, Y. and Shen, K. (2015) 'Characterization of exosomes derived from ovarian cancer cells and normal ovarian epithelial cells by nanoparticle tracking analysis', *Tumour Biol*, In press.

Zhao, Y., Yan, Q., Long, X., Chen, X. and Wang, Y. (2008) 'Vimentin affects the mobility and invasiveness of prostate cancer cells', *Cell Biochem Funct,* 26(5), pp. 571–7.

Zhao, H., Yang, Z., Wang, X., Zhang, X., Wang, M., Wang, Y., Mei, Q. and Wang, Z. (2012) 'Triptolide inhibits ovarian cancer cell invasion by repression of matrix metalloproteinase 7 and 19 and upregulation of E-cadherin', *Exp Mol Med,* 44(11), pp. 633–41.

Zhou, H., Yuen, P. S., Pisitkun, T., Gonzales, P. A., Yasuda, H., Dear, J. W., Gross, P., Knepper, M. A. and Star, R. A. (2006) 'Collection, storage, preservation, and normalization of human urinary exosomes for biomarker discovery', *Kidney Int,* 69(8), pp. 1471–6.

Zhuang, X., Xiang, X., Grizzle, W., Sun, D., Zhang, S., Axtell, R. C., Ju, S., Mu, J., Zhang, L., Steinman, L., Miller, D. and Zhang, H. G. (2011) 'Treatment of brain inflammatory diseases by delivering exosome encapsulated anti-inflammatory drugs from the nasal region to the brain', *Mol Ther,* 19(10), pp. 1769–79.

Zhuang, G., Wu, X., Jiang, Z., Kasman, I., Yao, J., Guan, Y., Oeh, J., Modrusan, Z., Bais, C., Sampath, D. and Ferrara, N. (2012) 'Tumour-secreted miR-9 promotes endothelial cell migration and angiogenesis by activating the JAK-STAT pathway', *EMBO J,* 31(17), pp. 3513–23.

Zitvogel, L., Regnault, A., Lozier, A., Wolfers, J., Flament, C., Tenza, D., Ricciardi-Castagnoli, P., Raposo, G. and Amigorena, S. (1998) 'Eradication of established murine tumors using a novel cell-free vaccine: dendritic cell-derived exosomes', *Nat Med,* 4(5), pp. 594–600.

Zomer, A., Maynard, C., Verweij, F. J., Kamermans, A., Schäfer, R., Beerling, E., Schiffelers, R. M., de Wit, E., Berenguer, J., Ellenbroek, S. I., Wurdinger, T., Pegtel, D. M. and van Rheenen, J. (2015) '*In Vivo* imaging reveals extracellular vesicle-mediated phenocopying of metastatic behavior', *Cell,* 161(5), pp. 1046–57.

Appendices

8.   <u>Appendices</u>

8.1. Appendix A – Publications

<u>Mulcahy, L.A.</u>, Pink, R.C., Carter, D.R.F. (2014) 'Routes and mechanisms of extracellular vesicle uptake', *Journal of Extracellular Vesicles*, 3, pp. 24641.

Jacobs, L. A., Bewicke-Copley, F., Poolman, M. G., Pink, R. C., **<u>Mulcahy, L. A.</u>**, Baker, I., Beaman, E. M., Brooks, T., Caley, D. P., Cowling, W., Currie, J. M., Horsburgh, J., Kenehan, L., Keyes, E., Leite, D., Massa, D., McDermott-Rouse, A., Samuel, P., Wood, H., Kadhim, M. and Carter, D. R. (2013) 'Meta-analysis using a novel database, miRStress, reveals miRNAs that are frequently associated with the radiation and hypoxia stress-responses', *PLoS One*, 8(11), pp. e80844.

<u>Mulcahy, L.A.</u> and Carter, D. R. (2013) 'RNAi2013: RNAi at Oxford', *J RNAi Gene Silencing*, 9, pp. 486-489.

8.1.1. <u>**Mulcahy, L.A.**</u>**, Pink, R.C., Carter, D.R.F. (2014) Routes and mechanisms of extracellular vesicle uptake.** *Journal of Extracellular Vesicles***, 3:24641.**

REVIEW ARTICLE

Routes and mechanisms of extracellular vesicle uptake

Laura Ann Mulcahy*, Ryan Charles Pink and David Raul Francisco Carter

Department of Biological and Medical Science, Faculty of Health and Life Sciences,
Oxford Brookes University, Oxford, UK

Extracellular vesicles (EVs) are small vesicles released by donor cells that can be taken up by recipient cells. Despite their discovery decades ago, it has only recently become apparent that EVs play an important role in cell-to-cell communication. EVs can carry a range of nucleic acids and proteins which can have a significant impact on the phenotype of the recipient. For this phenotypic effect to occur, EVs need to fuse with target cell membranes, either directly with the plasma membrane or with the endosomal membrane after endocytic uptake. EVs are of therapeutic interest because they are deregulated in diseases such as cancer and they could be harnessed to deliver drugs to target cells. It is therefore important to understand the molecular mechanisms by which EVs are taken up into cells. This comprehensive review summarizes current knowledge of EV uptake mechanisms. Cells appear to take up EVs by a variety of endocytic pathways, including clathrin-dependent endocytosis, and clathrin-independent pathways such as caveolin-mediated uptake, macropinocytosis, phagocytosis, and lipid raft–mediated internalization. Indeed, it seems likely that a heterogeneous population of EVs may gain entry into a cell via more than one route. The uptake mechanism used by a given EV may depend on proteins and glycoproteins found on the surface of both the vesicle and the target cell. Further research is needed to understand the precise rules that underpin EV entry into cells.

Keywords: *extracellular vesicles*; *EV uptake*; *EV internalization*; *cell–EV interaction*; *endocytosis*; *cell communication*; *exosomes*

Extracellular vesicles (EVs) are small spherical packages that are released by cells into the extracellular environment (1). EVs consist of a lipid bilayer membrane that encases a small organelle-free cytosol. Suspended in the aqueous core, or associated with the lipid casing, are proteins and nucleic acids derived from the cell of origin (2,3). EVs can be categorized further depending upon where in the cell they originate; for example, vesicles that are derived from multi-vesicular bodies (MVBs) are referred to as exosomes and those from the plasma membrane as microvesicles (1). It has become evident that EVs are important factors involved in a range of physiological processes including intercellular exchange of proteins and RNA (4,5), induction of angiogenesis (6), bystander effect (7) and immune regulation (2,8,9).

EVs protect their cargo from enzymatic degradation during transit through the extracellular environment (10–12). Upon release of their functionally active mRNA and microRNA load inside the recipient cell, EV contents can regulate gene expression through de-novo translation and post-translational regulation of target mRNAs (3). Changes in miRNA levels are particularly important during development (13) and stress response (14), and EVs may play a role in their exchange between cells (7). EVs can also exert effects on cells by stimulating specific signalling pathways (15). The ability of EVs to alter the transcriptome and signalling activity within recipient cells allows them to induce specific phenotypic changes (16–18). Indeed, alterations in EV activity may be a feature of certain pathologies, including cancer (19). There is also interest in EVs as potential therapeutics. By harnessing the capability of EVs to transfer their contents into target cells it may be possible to convert these vesicles into vehicles for the delivery of therapeutic proteins, RNA molecules and drugs (20,21). Given their emerging roles in normal physiological processes and in disease, and their therapeutic potential, it is important to understand the molecular mechanisms of EV release by donor cells and the processes by which they are taken up

(page number not for citation purpose)

by recipient cells. In this review we will outline the ways in which EV uptake can be studied and review the current understanding of how EVs enter target cells.

Evidence for EV uptake

Both direct and indirect evidence exists to suggest that EVs are internalized into recipient cells. EVs have been shown to transfer functional mRNA and miRNA from mouse to human mast cells where mouse proteins were identified in the recipient human cells (3). EV-mediated siRNA delivery has been shown to knockdown target gene expression (20), and administration of EVs laden with luciferin substrate to luciferase expressing cells resulted in production of bioluminescence (22). These results imply that merging of the EV cytosol and the cytoplasmic compartment had occurred through membrane fusion at the plasma membrane or by uptake through other pathways followed by fusion with the endosomal membrane (22).

EV uptake can also be visualized directly. The most common method for detecting EV uptake involves the use of fluorescent lipid membrane dyes to stain EV membranes. Examples of such dyes include PKH67 (23–29), PKH26 (28,30–32), rhodamine B (also known as R18) (22,33–38), DiI (30,33,39) and DiD (40) which are lipophilic dyes. Membrane permeable chemical compounds are also used to stain EVs. These include carboxy-fluorescein succinimidyl ester (CFSE) (39–46) and 5(6)-carboxyfluorescein diacetate (CFDA) (46). These compounds become confined to the cytosolic lumen and fluoresce as a consequence of esterification. Subsequent entry of EVs into recipient cells can be measured using methods such as flow cytometry and confocal microscopy. To distinguish between internalized and surface-bound fluorescent EVs, the surface of the cell can be stripped by treatment with acid (27) or trypsin (32). Such experiments suggest that many cells do indeed internalize EVs.

One potential issue with membrane-binding dyes is that the presence of the fluorescent molecules could affect the normal behaviour of EVs. Uptake of EVs has been observed with many different lipid-binding dyes, suggesting that such molecules do not affect the coarse internalization of vesicles; nevertheless, further experimentation is needed to verify whether the precise biological behaviour of EVs is affected by dyes. Another consideration is that the distinct types of dyes may lead to different patterns of cellular staining following uptake. Lipophilic dyes associate with lipids, whereas molecules that become esterified in the lumen remain in solution; their fate is thus bound with membrane and cytosol, respectively. Another potential limitation of the use of such lipophilic dyes is the leaching of the fluorescent molecules from EV onto cellular membranes, leading to a pattern of internalization that is due to normal membrane recycling rather than EV uptake. However, this seems unlikely given the numerous reports of molecular inhibitors that appear to prevent EV uptake (Table I). Other control experiments, such as incubation of cells with excess unlabelled EVs and direct measurement of the rate of transfer of fluorescence between EVs also support the idea that the increased fluorescence in recipient cells is due to specific uptake of EVs rather than non-specific dye leaching (25).

It should also be appreciated, however, that almost all studies have relied on fluorescence microscopy, which has limited resolution because the wavelength of visible light is approximately 390–700 nm; therefore single EVs or clusters of vesicles that are less than 390 nm in diameter cannot be distinguished. This should not affect the assessment of EV uptake in general but may affect the visualization and dynamic localization analysis of individual EVs. EVs can be visualized in a potentially more specific way via the use of fluorescent proteins fused with vesicular proteins. For example, CD9 and CD63 are tetraspanin proteins found enriched in EVs which, when tagged with GFP, can be used to show uptake and processing of vesicles in cells (10,47,48). A caveat of such experiments is the assumption the fluorescent protein tag does not affect the normal function or trafficking of the tetraspanin protein, and does not therefore potentially alter the behaviour of the EV during uptake.

The evidence that EVs can enter cells and deliver their cargo is overwhelming. The mechanism responsible for EV internalization into cells, however, has raised great debate in the literature. Various mechanisms for EV uptake have been proposed (Fig. 1), including clathrin-mediated endocytosis (CME), phagocytosis, macropinocytosis and plasma or endosomal membrane fusion. The roles of lipid rafts and specific protein–protein interactions have also been studied. A range of techniques can be used in conjunction with EV uptake assays to tease out these molecular mechanisms. This includes the use of antibodies to test the role of specific ligands or receptors, and the use of chemical inhibitors to block specific uptake pathways. The results of such studies have shed much light on the routes by which EVs enter cells.

Protein interactions

The EV uptake mechanisms involve protein interactions that facilitate subsequent endocytosis (9,25,26,30,49). Proteinase K treatment of EVs was shown to significantly reduce their uptake by ovarian cancer cells which strongly supports the role of proteins in the EV uptake pathway (41). Many EV proteins have been shown to interact with membrane receptors on target cells (50,51). Hence, EV uptake is most likely dependent upon the signalling status of recipient cells and of the protein complement of the vesicle. In the literature there is a growing list of specific protein–protein interactions that mediate EV attachment and uptake into cells. Many of these interactions have been elucidated by the use of specific antibodies that

Table I. Compounds, chemicals and peptides used to inhibit EV uptake

Pathways blocked	Inhibitor	Target	Treatment recipient
Endocytosis	Heparin	Heparan sulphate proteoglycans	Glioblastoma multiforme primary tumour cells (25); SW-780 bladder cancer cells (32);
Endocytosis	α-difluoromethylornithine (DFMO)	Heparan sulphate proteoglycans	Glioblastoma multiforme primary tumour cells (25);
Endocytosis	Asialofetuin	Galectin-5	Macrophages (24);
Endocytosis	Human receptor–associated protein (RAP)	CD91	Dendritic cells (79);
Endocytosis	RGD (Arg-Gly-Asp) peptide	Fibronectin	Macrophages (23); Dendritic cells (30);
Endocytosis	Ethylenediaminetetra acetic acid (EDTA)	Calcium	Macrophages (24); Dendritic cells (30,44); bone marrow–derived dendritic cells (22);
Endocytosis	Cytochalasin D	Actin	Human macrophages (23); SKOV-3 ovarian cancer cells (41); RAW-264.7 macrophages (27); Microglia (28); Dendritic cells (30,44); Bone marrow–derived dendritic cells (22); human A549 alveolar epithelial cells (77); Human umbilical cord endothelial cells (26); HeLa cells (26);
Endocytosis	Cytochalasin B	Actin	Macrophages (24);
Endocytosis	Latrunculin A	Actin	Human umbilical cord endothelial cells (26); HeLa cells (26);
Endocytosis	Latrunculin B	Actin	RAW-264.7 macrophages (27);
Clathrin- and caveolin-dependent endocytosis	NSC23766	Dynamin	Microglia (28);
Clathrin- and caveolin-dependent endocytosis	Dynasore	Dynamin-2	Macrophages (24); Microglia (28);
Clathrin-dependent endocytosis	Chlorpromazine	Dopamine receptors, serotonin receptors, histamine receptors, α1- and α2-adrenergic receptors and M1 and M2 muscarinic acetylcholine receptors	SKOV-3 ovarian cancer cells (41); RAW-264.7 macrophages (27);
Macropinocytosis	5-(N-Ethyl-N-isopropyl)amiloride (EIPA)	Sodium/proton exchanger	SKOV-3 ovarian cancer cells (41); RAW-264.7 macrophages (27);
Macropinocytosis	Amiloride	Sodium/proton exchanger	Microglia (28);
Macropinocytosis	Bafilomycin A Monensin and Chloroquine	H(+)-ATPase activity (increase pH)	Microglia (28);
Phagocytosis and macropinocytosis	Annexin-V	Phosphatidylserine	Microglia (28,31); Ovarian cancer patient ascites-derived EVs (10); Neuro-2A mouse neuroblastoma cells (31);
Phagocytosis	Wortmannin	Phosphoinositide 3-kinases (Pl3Ks)	RAW-264.7 macrophages (27);
Phagocytosis	LY294002	Phosphoinositide 3-kinases (Pl3Ks)	RAW-264.7 macrophages (27);
Lipid raft–mediated endocytosis	Methyl-β-cyclodextrin (MβCD)	Cholesterol	SKOV-3 ovarian cancer cells (41); RAW-264.7 macrophages (27); BT-549 breast cancer cells (47); Human umbilical cord endothelial cells (26); U87-MG glioblastoma cells (26);
Lipid raft–mediated endocytosis	Filipin	Cholesterol	Bone marrow–derived dendritic cells (22); Melanoma cells (34); Human umbilical cord endothelial cells (26);
Lipid raft–mediated endocytosis	Simvastatin	Cholesterol	Human umbilical cord endothelial cells (26);

Table I (*Continued*)

Pathways blocked	Inhibitor	Target	Treatment recipient
Lipid raft–mediated endocytosis	Fumonisin B1 and N-butyldeoxynojirimycin hydrochloride	Glycosphingolipid	Pre-treatment of EV-producing Jurkat cells (80); HEK-293T kidney cells (80);
Lipid raft–mediated endocytosis	U0126	ERK1/2	Human umbilical cord endothelial cells (26), HeLa cells (26); Mouse embryonic fibroblasts (26);
Membrane fusion	Proton pump inhibitor (AstraZeneca)	Sodium reabsorption (decrease pH)	Melanoma cells (34);

recognize ligands or receptors, leading to a steric block that prevents their interaction. Here we review some of the proteins shown to participate in EV uptake. It should be noted that in some cases the phenotypic effects of EVs do not require internalization of the vesicle (see conclusions and future directions); therefore in our discussion we focus on examples where the involvement of specific protein–protein interactions is evidenced by the effect on direct EV uptake or binding, rather than by functional outputs.

Tetraspanins

Tetraspanins are membrane proteins which have numerous functions including cell adhesion, motility, activation and proliferation (reviewed in (52)). Tetraspanins are highly abundant on the EV surface which suggests they may have a role in EV function (53,54). CD63, CD9 and CD81 are well-established markers of EVs (2,54–58). CD9 and CD81 are tetraspanins involved in oocyte-spermatozoa and phagocyte fusion (56,57,59,60); in addition, numerous viruses and parasites require interaction with tetraspanins in order to enter the cell and replicate (61). Due to the high abundance of tetraspanins and their roles in cell adhesion it is possible that EV uptake could occur through similar processes (37). Tetraspanin-enriched microdomains (TEMs) are clusters of tetraspanins, adhesion molecules and transmembrane receptor proteins located in raft-like structures in the plasma membrane (52). TEMs have been shown to be involved in a number of processes, including vesicular and cellular fusion (52,62,63), leading to the hypothesis that they have a role in EV-cell binding (64–67).

Treatment of recipient cells with antibodies against the tetraspanins CD81 or CD9 can reduce uptake of EVs by dendritic cells (30). Tspan8 is a tetraspanin known to complex with integrins (35). Cells over-expressing Tspan8 released EVs bearing a Tspan8-CD49d complex, the presence of which contributed to EV uptake by rat aortic endothelial cells (35). Antagonistic antibody treatment suggests that CD106 strengthens this interaction (35). In addition, it was discovered that EVs that presented Tspan8-CD49d complex on their surface were readily internalized by endothelial cells and pancreatic cells where

intercellular adhesion molecule 1 (ICAM-1, also known as CD54) was the major ligand (37). These data point to a role for tetraspanins in the internalization of EVs.

Integrins and immunoglobulins

The observation that EVs play a role in the immune response has garnered much interest in the roles of integrins and immunoglobulins in the interaction between vesicles and cells. These proteins are involved in a range of functions, including cell-to-cell adhesion, cell signalling, leukocyte transendothelial transmigration and antigen presentation (68). Indeed, several reports in the literature suggest they may also be involved in EV uptake. Antibodies that mask the binding sites of CD11a or its ligand ICAM-1 can reduce dendritic cell uptake of EVs (30). Similar results were observed after blocking the integrins αv (CD51) and β3 (CD61) on the dendritic cell surface (30). CD11a is a subunit of the lymphocyte function-associated antigen 1 (LFA-1), which interacts with ICAM-1 to regulate critical pathways in the immune response (69). Inducing a high-affinity state of LFA-1 on resting T-cells using manganese chloride treatment was sufficient to increase EV binding in a dose-dependent manner (70). Antagonistic antibody treatment inhibited this process (44,45,70). Naïve T-cells have been shown to internalize EVs through a mechanism requiring the participation of T-cell receptor (TCR), CD28 and LFA-1 (71). It was also shown that dendritic cell–derived EVs were internalized via TCR-major histocompatibility complex (MHC) and LFA-1–ICAM-1 interactions in CD4+ cells (44). Similarly dendritic cells take up CD8+T-cell EVs in an endocytic pathway that requires pMHC I/TCR and LFA-1-ICAM-1 interactions (43). The protein milk fat globule-epidermal growth factor 8 (MFG-E8) is thought to enhance the phagocytic uptake of apoptotic cells by binding phosphatidylserine (PS) via 1 domain and with cell surface integrin proteins CD51 and CD61 via a second domain (72). Perturbation of MFG-E8 leads to alterations in the rate of EV uptake (30). These results highlight the emerging roles of protein–protein interactions in vesicle uptake, particularly in cells of the immune system.
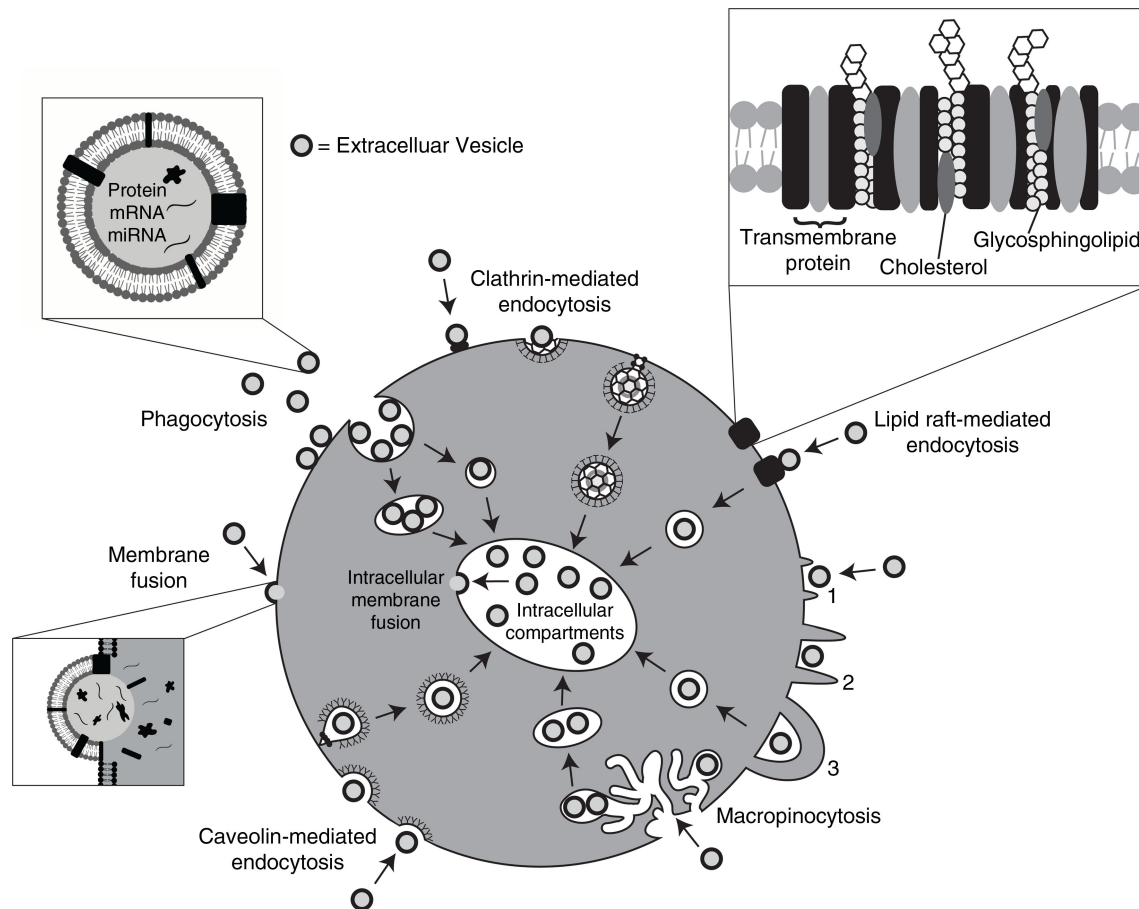
Fig. 1. Pathways shown to participate in EV uptake by target cells. EVs transport signals between cells. EVs have been shown to be internalized by cells through phagocytosis, clathrin- and caveolin-mediated endocytosis. There is also evidence to support their interaction with lipid rafts resulting in EV uptake. Lipid rafts are involved in both clathrin- and caveolin-mediated endocytosis. EVs can be internalized by macropinocytosis where membrane protrusions or blebs extend from the cell, fold backwards around the EVs and enclose them into the lumen of a macropinosome; alternatively EVs are macropinocytosed after becoming caught in membrane ruffles. EVs may also deliver their protein, mRNA and miRNA cargo by fusion with the plasma membrane. Alternatively, intraluminal EVs may fuse with the endosomal limiting membrane following endocytosis to enable their EV contents to elicit a phenotypic response.

A role for proteoglycans

Proteoglycans are proteins with significant carbohydrate components. For example, the heparin sulphate proteoglycans (HSPGs) are proteins with sulphated glycosaminoglycan polysaccharides attached. Various complexes, including viral particles and lipoproteins, use HSPGs to help gain entry into cells (73). Fluorescently labelled EVs co-localize with internal vesicles containing GFP-linked syndecan or glypican (the 2 main types of HSPG) inside recipient cells (25). Treatment of cells with a heparin sulphate mimetic reduced EV uptake in a dose-dependent manner (25,32). Cells whose ability to produce normal levels and structures of HSPGs, either because of genetic defects or chemical inhibition, showed a reduced ability to internalize EVs (25). These results are consistent with a role for proteoglycans in the uptake of EVs. Interestingly, treatment of EVs with heparinase to remove surface proteoglycans had no effect on uptake, suggesting that it is the presence of HSPGs on the cell surface that are important for mediating vesicular entry (25).

Lectins

DC-SIGN is a C-type lectin receptor (a receptor able to recognize and internalize glycoprotein ligands) that can trigger phagocytic entry for a range of molecules, including viruses and bacteria (74). One potential ligand is the MUC1 protein found on epithelial cells and on the surface of EVs derived from breast milk. The recruitment of these EVs by monocyte-derived dendritic cells was blocked by antibodies specific to DC-SIGN on the recipient cell surface (29). Another C-type lectin, DEC-205, also appears to mediate entry of EVs into dendritic cells; vesicle uptake was inhibited by treatment with DEC-205-specific antibodies or by incubation with excess mannose (a sugar recognized by DEC-205) (44). Chelation of calcium with ethylenediaminetetraacetic acid (EDTA)

significantly reduced EV uptake by dendritic cells (44), and also in macrophages (24); supporting the hypothesis that the EV uptake is facilitated by C-type lectin/C-type lectin receptor interactions. Interestingly, ovarian cancer–derived EVs were found to be enriched in specific mannose- and sialic acid containing glycoproteins (41). Sialic acid removal caused a small but non-significant increase in uptake (41). Galectin-5, a lectin with binding specificity towards certain glycoproteins, can be found associated with EVs (24). Incubating EVs with cells in the presence of excess galectin-5 significantly reduced vesicular internalization (24). When asialofetuin (a glycoprotein that can bind galectin-5) was included in the uptake assay the entry of EVs was abrogated (24). These results are all consistent with a role for glycoproteins and proteoglycans in the uptake of EVs.

Endocytosis

Most experimental evidence suggests that EVs are usually taken up into endosomal compartments via endocytosis (22,30,41). Uptake can be extremely rapid, with EVs being identified inside cells from as early as 15 minutes after initial introduction (27,48). A number of research groups have shown that when cells are incubated at 4°C their capacity to internalize EVs is dramatically reduced suggesting that uptake is an energy-requiring process (25,30,33,38,41,46). Further evidence that internalization is not a passive process is provided by observations that EVs are not taken up by cells fixed in paraformaldehyde (28,36). Cytochalasin D is a metabolite known to depolymerize the actin filament network resulting in inhibition of endocytic pathways (75,76). Cytochalasin D treatment has been shown, on several occasions in various cell types, to significantly reduce, but not completely prevent, EV uptake in a dose dependent manner (22,23,26–28, 30,41,44,77). Taken together these results suggest that EV uptake is an energy-dependent process that requires a functioning cytoskeleton, both of which are indicative of endocytic pathways. However, one implication of the frequent failure to completely abrogate internalization following treatment with any given inhibitor is that EV uptake occurs through more than one mechanism (24,27,30,40,41,44,77).

Endocytosis is an umbrella term for a range of molecular internalization pathways (78). By using a range of inhibitors to block specific pathways (Table I), antibodies to prevent receptor–ligand interactions (Table II) and other experimental techniques such as RNAi to knock-down certain genes the role of the endocytic processes responsible for EV uptake are being elucidated. Roles for many of these subdivisions have been shown, including macropinocytosis (28,41), phagocytosis (22,27,41,82) and CME (41) (Fig. 1).

Clathrin-mediated endocytosis

CME involves cellular internalization of molecules through progressive and sequential assembly of clathrin-coated vesicles that contain a range of transmembrane receptors and their ligands. The clathrin-coated vesicles strategically deform the membrane which collapses into a vesicular bud, matures and pinches off. The subsequent intracellular vesicle undergoes clathrin un-coating and then fuses with the endosome where it deposits its contents (83). Various studies implicate CME in the uptake of EVs. Chlorpromazine prevents formation of clathrin-coated pits at the plasma membrane (84). CME inhibition by chlorpromazine decreased uptake of EVs by ovarian cancer recipient cells (41) and phagocytic recipient cells (27). Dynamin2 is a GTPase required for the CME process (85,86). Dynamin2 is recruited to nascent clathrin-coated pits where it forms a collar-like structure at the neck of deeply invaginated clathrin-coated pits (87–89). GTP-hydrolysis mediated changes in dynamin2 conformation lead to membrane fission and clathrin-coated vesicle release (86,90–92). Dynamin2 also facilitates membrane binding (93–95) and membrane curvature (96) during CME. In phagocytic cells, inhibition of dynamin2 (85,86) prevented almost all EV internalization activity (24,27,28). A small percentage of EVs were also shown to co-localize with clathrin during uptake in macrophages (27). Epidermal growth factor receptor pathway substrate clone 15 (EPS15) is a component of clathrin-coated pits that is ubiquitously associated with AP-2 adaptor complex which is an integral component of the clathrin coat (97). Expression of a dominant-negative mutant of EPS15 inhibits CME and leads to a reduction in EV uptake (27). These results suggest that CME plays at least some part in EV uptake.

Caveolin-dependent endocytosis

CME has been extensively studied for many years, but it is becoming increasingly apparent that a plethora of clathrin-*independent* endocytotic pathways exist in eukaryotic cells (78). One such mechanism is caveolin-dependent endocytosis (CDE). Caveolae are small cave-like invaginations in the plasma membrane which, like clathrin-coated pits, can become internalized into the cell. Caveolae are sub-domains of glycolipid rafts of the plasma membrane that are rich in cholesterol, sphingolipids and caveolins; hence, CDE is sensitive to cholesterol depletion agents such as filipin, and methyl-β-cyclodextrin (MβCD) (98–100). Caveolin-1 is a protein that is required and sufficient for the formation of caveolae (78) and can be found clustered within such membrane invaginations. Oligomerization of caveolins (facilitated by caveolin oligomerization domains) mediates formation of caveolin-rich rafts in the plasma membrane. The increased levels of cholesterol accompanied by attachment of caveolin

Table II. Antibodies used to block EV uptake

Target	Treatment recipient
ICAM-1	Dendritic cells (30); lymph node cells and spleen cells (38);
LFA-1	Dendritic cells (43,44); CD8+ ConA T cells (45); T cells (70);
TIM-4	RAW-264.7 macrophages (27); BaF3 bone marrow pro-B cells (79);
MFG-E8	Dendritic cells (30);
DC-SIGN	Monocyte-derived dendritic cells (29);
DEC205	Dendritic cells (44);
H-2Kb	Dendritic cells (43);
Tspan8	Rat aortic endothelial cells (35);
CD9	Dendritic cells (30); Lung fibroblasts (35); rat pancreatic adenocarcinoma BSp73ASML (ASML) cell-derived EVs (38);
CD11a	Dendritic cells (30);
CD11b	Lymph node cells and spleen cells (38);
CD11c	Lymph node cells and spleen cells (38);
CD44	Lymph node cells and spleen cells (38);
CD49c	Lung fibroblasts (35);
CD49d	Rat aortic endothelial cells (35); lymph node cells and spleen cells (38);
αv (CD51)	Dendritic cells (30);
β3 (CD61)	Dendritic cells (30);
CD62L	Lymph node cells and spleen cells (38);
CD81	Dendritic cells (30); rat pancreatic adenocarcinoma BSp73ASML (ASML) cell-derived EVs (38);
CD91	Dendritic cells (79);
CD106	Rat aortic endothelial cells (35);
CD151	Lung fibroblasts (35);

scaffolding domains to the plasma membrane and dynamin2 (also required in CME) activity enable assembly and expansion of caveolar endocytic vesicles (78,100,101). Dynamin2, can be blocked by the specific inhibitor dynasore (102). Blocking dynamin2 leads to significantly reduced internalization of exosomes (103) or larger microvesicles (24,104), suggesting a role for caveolae-mediated endocytosis in vesicular uptake. However, because dynamin2 is also required for CME it is not possible to rule out a role for clathrin-coated vesicles in these experiments (105). Specific knockdown of the CAV1 gene leads to reduced caveolin-1 protein and significantly impaired uptake of EVs (103). Paradoxically, knockout of CAV1 in mouse embryonic fibroblast cells leads to increased EV uptake (26). CAV1 null mice show phenotypic changes in vasculature but are viable (106), suggesting that either CAV1 is not essential for full EV uptake or that the ability to internalize vesicles via CDE is not essential for viability. Nevertheless, taken together the

results described above imply some kind of function for caveolae-mediated endocytosis in EV uptake, though the precise role of this pathway may vary between cell and EV types.

Macropinocytosis

Macropinocytosis is an endocytic uptake pathway that involves the formation of invaginated membrane ruffles that then pinch off into the intracellular compartment. The vesicles carry extracellular fluid and components sampled from the region around the membrane ruffles (78). Ruffled extensions of the plasma membrane protrude from the cell surface and encompass an area of extracellular fluid, subsequently this area of extracellular fluid is internalized entirely as a result of fusion of the membrane protrusions with themselves or back with the plasma membrane (Fig. 1) (107). The mechanism is similar to that of phagocytosis, however, direct contact with the internalized material is not required. This mechanism is rac1-, actin- and cholesterol-dependent and requires $Na+/H+$ exchanger activity (108). Cholesterol is required for the recruitment of activated rac1 to sites of macropinocytosis (109). Phosphatidylinositol-3-kinase (PI3K), ras, and src activities have also been shown to stimulate macropinocytosis (78). Rac1 is a GTPase which not only has a major role in macropinocytosis (110), but also in regulation of cell growth, cytoskeletal reorganization, protein kinase activation (111) and epithelial-to-mesenchymal transition (EMT) in cancer (112). Abrogation of macropinocytosis by inhibiting the $Na+/H+$ exchanger results in significantly reduced oligodendrocyte-derived EV uptake by microglia (28). A small molecule inhibitor of rac1, NSC23766, also inhibited EV uptake by microglia (28). The alkalinizing drugs bafilomycin A, monensin and chloroquine all inhibited microglial internalization of EVs, consistent with a role for the acidification of vacuoles in macropincytosis (28). However, other studies using inhibitors do not find a role for macropinocytosis in the uptake of EVs (25,27,103). These findings suggest that macropinocytosis is either a minor pathway used by cells to internalize EVs, or a mechanism used in specific cell types.

Phagocytosis

The process of phagocytosis involves the internalization of opsonized particulate matter, including bacteria and fragments of apoptotic cells. This function is often performed by specialized cells such as macrophages (78). Phagocytosis is a receptor-mediated event that involves the progressive formation of invaginations surrounding the material destined for internalization, with or without the participation of enveloping membrane extensions (as required for macropinocytosis) (78,107). Generally, phagocytosis is employed to internalize larger particles.

However, it has been shown that particles as small as 85 nm in diameter have been internalized by phagocytosis; therefore it is possible that EVs could be internalized via this route (113). In one study the EVs released by leukaemia cells were shown to be taken up efficiently by macrophages but were not internalized by other cell types (27). PI3Ks play an important role in phagocytic processes, particularly in enabling membrane insertion into forming phagosomes (114). The PI3K inhibitors wortmannin and LY294002 were used to assess the necessity of functional PI3Ks in EV uptake. Both drugs inhibited EV uptake in a dose dependant manner (27). Furthermore, the EVs co-localized with fluorescent phagosome tracers (27). Dendritic cell–derived EVs were labelled with pHrodo, a dye that becomes fluorescent red at the phagosome pH. Acceptor dendritic cells treated with pHrodo-EVs emitted red fluorescence confirming that dendritic cells can phagocytose EVs (22). Taken together these results implicate phagocytosis in EV uptake.

Phosphatidylserine (PS) is essential in initiating the removal of apoptotic bodies by phagocytosis (115) and is used by some viruses to enter cells by macropinocytosis (116). PS is typically located on the inner leaflet of the plasma membrane; however, EVs are enriched for PS on their outer-membrane (117) which may facilitate entry into cells. Incubation of macrophages with an antibody that masks TIM4, a receptor involved in PS-dependent phagocytosis (27,81), leads to reduced uptake of EVs (27). Treatment of dendritic cells with a competitive soluble PS analogue also reduced EV uptake (30). Treatment of EVs with annexin-V (a protein that binds PS) reduces the uptake of EVs into macrophages (31) and natural killer cells (70). Phagocytic and macropinocytic uptake of EVs may therefore be, at least in part, triggered by the PS found on the outer leaflet of EV membranes.

Involvement of lipid rafts

Lipid rafts are microdomains within the plasma membrane with altered phospholipid compositions. They are rich in protein receptors and sphingolipids such as sphingomyelin. They act as organizing centres for the assembly of signalling molecules, they affect membrane fluidity and mediate membrane protein trafficking (100). Components of lipid rafts are highly ordered and more tightly packed than the surrounding bilayer, consequently they are less fluid but float freely in the plasma membrane (118). Endocytosis that is clathrin-independent largely requires cholesterol, which is found enriched in lipid rafts. Lipid rafts are known to contribute to viral particle uptake by mediating glycoprotein binding and adjusting the physicochemical and mechanical properties of the membrane (119). These rafts can be found in the invaginations formed by caveolin-1 or in planar regions of the plasma membrane marked by another family of proteins called flotillins (120). Flotillins associate with lipid rafts and mediate endocytosis independent of clathrin and caveolin (121–125). Flotillins have been found to bind to GPI-anchored proteins during their internalization (121,122,125). It is possible that EVs are internalized by cells through lipid raft domains.

To test the role of lipid rafts in EV uptake, a range of inhibitors have been employed. EV uptake was significantly reduced in dendritic cells when EV-producing cells were pre-treated with fumonisin B1 and N-butyldeoxynojirimycin hydrochloride (80), compounds which decrease glycosphingolipid composition in the plasma membrane by preventing its biosynthesis (126,127). This suggests that sphingolipids within the EV have an important role in binding and endocytosis, possibly through cholesterol-rich microdomains in dendritic cells (80). EV uptake was prevented following pre-treatment of recipient cells with the cholesterol reducing agents MβCD (26,27,41,47), filipin (22,26,34) and simvastatin (26). These treatments disrupt lipid raft–mediated endocytosis but may also affect EV membrane integrity, causing the reduced EV uptake effects observed. Co-localization can be observed between fluorescently labelled EVs and cholera toxin B (a protein known to be internalized via lipid rafts) in recipient cells (26,47). Poor co-localization was observed between caveolin-1 and labelled EVs, suggesting that the lipid rafts used by EVs may be caveolae-independent (26,41). The potential roles of some proteins involved in this process are also being identified. For example, annexin II may have a role in anchoring of EVs to lipid raft domains of the plasma membrane whilst annexin-VI may contribute to the trafficking of EVs to the late endosomal compartment (47). These findings support the hypothesis that lipid rafts are involved in the EV uptake mechanism; the scale and precise mechanisms of this route into cells remains to be elucidated.

Cell surface membrane fusion

Another possible entry mechanism is via direct fusion of the EV membrane with the cell plasma membrane (34). Fusion of lipid bilayers in an aqueous environment is a process whereby 2 initially distinct membranes merge. The lipid bilayers are brought into close proximity and the outer-leaflets come into direct contact which leads to formation of a hemi-fusion stalk with fused outer-leaflets. Following this, stalk expansion produces the hemi-fusion diaphragm bilayer from which a fusion pore opens (128–130). As a result, the two hydrophobic cores mix forming one consistent structure. Several protein families participate in this process including SNAREs, Rab proteins, and Sec1/Munc-18 related proteins (SM-proteins) (131).

Fusion of membranes can be observed in various ways, including via fluorescent lipid dequenching. This technique was applied to study the uptake of EVs from melanoma cells, the results suggested that at least some of the vesicles are able to fuse with the recipient cell

(34); this fusion was enhanced under acidic conditions. Similarly, when the dequenching method was used to demonstrate fusion of R18-labelled EVs with the plasma membrane of bone marrow-derived dendritic cells (22). The delivery of miRNAs and luciferin to the cytosol of the recipient cells provides further evidence of fusion of EVs with either the plasma or endosomal membrane (22). The lipid raft-like membrane composition of EVs may aid their fusion with recipient cell membranes (132). EV-cell fusion may be limited to acidic pH conditions which are present in endosomes, perhaps owing to differences in lipid content or overall ionic charge of the EV surface following release (34). The body of research supporting a primarily endocytic mechanism for EV uptake makes it unlikely that fusion is the main entry route, but a fusion-based pathway cannot be ruled out. Future work will be needed to ascertain the extent to which fusion-based EV entry occurs under physiological conditions.

Cell-specific EV uptake

One question currently vexing the EV field is whether or not EV uptake is a cell type–specific process. Results from some studies show that fluorescently labelled EVs can be taken up by virtually every cell type tested (26,38), whereas others suggest that vesicular uptake is a highly specific process which can only occur if cell and EV share the right combination of ligand and receptor. Heterogeneity in the donor/recipient cells, EVs, experimental setup and the context of experiments will all affect the outcome, and may thus account for the observed discrepancies. However, there are certainly examples of cell-type specific uptake. Pancreatic adenocarcinoma–derived EVs were shown to be internalized most efficiently by peritoneal exudate cells and less proficiently in granulocytes and T-cells (38). Tspan8 containing lymph node stroma–derived EVs were most effectively internalized by endothelial cells and pancreatic cells but to a lower degree by parental lymph node stroma cells (37). In some cases, the basis for a specific interaction may have been elucidated. For example, milk EVs can be taken up via monocyte-derived dendritic cells thanks to the interaction between DC-SIGN and MUC1, whereas EVs derived from other sources and lacking MUC1 were unable to enter these cells (29). Treatment with an RGD peptide (which can block integrin-mediated receptor internalization) reduced EV uptake in dendritic cells (30) and macrophages (23), but did not inhibit EV uptake by microglia (28). This indicates that multiple mechanisms are responsible for EV-cell communication and different combinations of EV communication strategies are used by different cell types.

Conclusions and future directions

A growing body of evidence suggests that EVs are involved in normal homeostasis (133) and are deregulated in disease (51). EVs, which are released in greater numbers by cancer cells (134), can promote tumour development and are involved in mediating intercellular communication within the tumour microenvironment (135). Further advancing our understanding of both the EV uptake mechanism and characterization of disease-promoting EVs will enable development of therapeutic strategies to inhibit interactions between such EVs and healthy recipient cells (136). EVs are also being explored as natural vectors for therapeutic delivery, with some early studies showing great potential (20,137,138). Improved understanding of the EV uptake mechanism will therefore benefit design of novel and sophisticated drug delivery systems.

To this end, we have reviewed here the mechanisms by which EVs are internalized by cells. Endocytosis, in its various guises, appears to be the primary method of entry by EVs. There appears to be little agreement in the literature as to which type of endocytic mechanisms are most important, with clathrin-dependent, caveolae-dependent, macropinocytosis, phagocytosis and lipid raft–mediated uptake variously described as being prevalent. These differences reflect the heterogeneity both in EV populations and in the cell types being used. It is possible that a population of EVs can simultaneously trigger a number of different gateways into a cell, with the primary entry points depending on the cell type and EV constituents (29,37,38). This would also explain why inhibition of any given pathway rarely leads to a complete abrogation of EV entry (23–25,27,34,38,40–42,44,45,81). There are also potential problems with the use of some inhibitors that have known (or potentially unknown) cross-reactivity with multiple pathways. For example, cytochalasin D inhibits actin polymerization and so the finding that it reduces EV uptake has been used to support an endocytic uptake pathway for vesicles (139). However, the global cellular effects of disrupting the actin cytoskeleton are profound. The reduced EV uptake caused by cytochalasin D could therefore be caused indirectly via perturbation of other cellular processes, such as cellular polarization (140), migration or cell cycle (141). Similarly, PI3K has a multitude of roles within various cell-signalling networks (142). PI3K signalling has been implicated in phagocytic uptake (143). The reduced EV uptake observed following treatment of recipient cells with the PI3K inhibitors wortmannin and LY294002 could be independent of any effects on phagocytosis, and instead caused indirectly by the deregulation of other processes such as migration, cell growth, or motility (144,145). There is also overlap in the pathways that such inhibitors can affect. For example, inhibiting PI3K can perturb both phagocytosis and macropinocytosis (146). Dynamin2 is involved in both CME and CDE, so its inhibition cannot easily distinguish between these 2 processes (147,148). MβCD causes depletion of cholesterol and can

cause a decrease in both lipid raft–mediated uptake as well as caveolin-dependent internalization. Furthermore, MβCD has substantial effects across a range of cellular functions, including effects that are independent of cholesterol chelation (149). The results of studies using small molecular inhibitors are important contributions towards understanding the EV uptake puzzle, but the pleiotropic nature of these compounds means that interpretation of such data must be tempered with extreme caution.

Large areas of plasma membrane are naturally recycled as part of normal cellular maintenance (150). Indeed, an area equivalent to the entire surface of the cell can be internalized and replenished every few hours (151). It could be expected that EVs bound at the cell surface would eventually be internalized as part of this normal membrane recycling. In such a scenario, it would stand to reason that inhibiting any of the processes that regulate membrane recycling would also reduce EV uptake. The results of the small molecule inhibitor experiments described above (28) could therefore be explained by their effects on membrane recycling rather than by their proposed ability to affect a direct EV uptake pathway. However, the rapidity of EV uptake would argue against this model of "passive endocytosis." The ability to inhibit uptake with antibodies that block specific protein–protein interactions also suggest that internalization is an active process. Nevertheless, these arguments all highlight the complexities in studying vesicular uptake. It is also worth mentioning that there are several other clathrin-independent endocytic pathways, such as the recently described CLIC/GLEEC pathway (78,152). The extent to which these other pathways may be involved remains to be determined.

Whilst EV uptake leads to the delivery of nucleic acids and protein, internalization is not always necessary to elicit a phenotypic response. Receptor–ligand interactions which take place on the cell surface may be sufficient; for example, interaction of soluble ligands (produced by proteolytic cleavage of EV membrane proteins) with cell receptors may successfully permit signal transduction and subsequent downstream signalling effects in the recipient cell (153–155). In another study, uptake of EVs by phagocytosis was not actually essential for the induction of cytokine IL-1β secretion suggesting that EV-associated fibronectin surface receptor interaction is sufficient to direct this activity (23). Interestingly, EVs may stimulate MAPK signalling leading to altered activity within the recipient cell (25,104). Indeed, pharmacological inhibition of ERK1/2 actually inhibited EV uptake, suggesting that these signalling pathways may also be involved in EV uptake (25).

In this review, we have focused on the mechanisms of exosomal uptake. However, there exists a range of types and sizes of EV. Many preparations of vesicles used in studies contain heterogeneous collections of such vesicles.

This heterogeneity probably contributes to the differences in apparent internalization mechanisms observed in various studies, as well as the lack of a single clear uptake route in any given study. Our ability to pinpoint the uptake route for different vesicles of similar sizes is still limited by a lack of biochemical markers to characterize and isolate them. As this knowledge increases the means by which they enter cells will be unravelled.

Understanding of EV internalization is a key goal of the fledgling EV field. Despite the EV research field still being in its infancy and the limited number of relevant studies performed to date, the discoveries concerning EV uptake made so far are promising for future research. The potential that EVs have shown as therapeutic agents means that it is imperative that the EV uptake mechanism is understood to aid prospective therapeutic design. Excitingly, EV research is continually expanding and developing, therefore greater understanding of the EV uptake pathway is certainly achievable in the foreseeable future.

Acknowledgements

Conflict of interest and funding

References

1. Raposo G, Stoorvogel W. Extracellular vesicles: exosomes, microvesicles, and friends. J Cell Biol. 2013;200:373–83.
2. Théry C, Regnault A, Garin J, Wolfers J, Zitvogel L, Ricciardi-Castagnoli P, et al. Molecular characterization of dendritic cell-derived exosomes. Selective accumulation of the heat shock protein hsc73. J Cell Biol. 1999;147:599–610.
3. Valadi H, Ekström K, Bossios A, Sjöstrand M, Lee JJ, Lötvall JO. Exosome-mediated transfer of mRNAs and microRNAs is a novel mechanism of genetic exchange between cells. Nat Cell Biol. 2007;9:654–9.
4. Jung T, Castellana D, Klingbeil P, Cuesta Hernández I, Vitacolonna M, Orlicky DJ, et al. CD44v6 dependence of premetastatic niche preparation by exosomes. Neoplasia. 2009;11:1093–105.
5. Qu JL, Qu XJ, Zhao MF, Teng YE, Zhang Y, Hou KZ, et al. Gastric cancer exosomes promote tumour cell proliferation through PI3K/Akt and MAPK/ERK activation. Dig Liver Dis. 2009;41:875–80.
6. Janowska-Wieczorek A, Wysoczynski M, Kijowski J, Marquez-Curtis L, Machalinski B, Ratajczak J, et al. Microvesicles derived from activated platelets induce metastasis and angiogenesis in lung cancer. Int J Cancer. 2005;113:752–60.
7. Al-Mayah AH, Irons SL, Pink RC, Carter DR, Kadhim MA. Possible role of exosomes containing RNA in mediating nontargeted effect of ionizing radiation. Radiat Res. 2012; 177:539–45.

8. Clayton A, Harris CL, Court J, Mason MD, Morgan BP. Antigen-presenting cell exosomes are protected from complement-mediated lysis by expression of CD55 and CD59. Eur J Immunol. 2003;33:522–31.

9. Raposo G, Nijman HW, Stoorvogel W, Liejendekker R, Harding CV, Melief CJ, et al. B lymphocytes secrete antigen-presenting vesicles. J Exp Med. 1996;183:1161–72.

10. Keller S, Ridinger J, Rupp AK, Janssen JW, Altevogt P. Body fluid derived exosomes as a novel template for clinical diagnostics. J Transl Med. 2011;9:86.

11. Silverman JM, Clos J, de'Oliveira CC, Shirvani O, Fang Y, Wang C, et al. An exosome-based secretion pathway is responsible for protein export from Leishmania and communication with macrophages. J Cell Sci. 2010;123:842–52.

12. Klibi J, Niki T, Riedel A, Pioche-Durieu C, Souquere S, Rubinstein E, et al. Blood diffusion and Th1-suppressive effects of galectin-9-containing exosomes released by Epstein-Barr virus-infected nasopharyngeal carcinoma cells. Blood. 2009;113:1957–66.

13. Tang F, Kaneda M, O'Carroll D, Hajkova P, Barton SC, Sun YA, et al. Maternal microRNAs are essential for mouse zygotic development. Genes Dev. 2007;21:644–8.

14. Jacobs LA, Bewicke-Copley F, Poolman MG, Pink RC, Mulcahy LA, Baker I, et al. Meta-analysis using a novel database, miRStress, reveals miRNAs that are frequently associated with the radiation and hypoxia stress-responses. PLoS One. 2013;8:e80844.

15. Mathivanan S, Ji H, Simpson RJ. Exosomes: extracellular organelles important in intercellular communication. J Proteomics. 2010;73:1907–20.

16. Camussi G, Deregibus MC, Bruno S, Cantaluppi V, Biancone L. Exosomes/microvesicles as a mechanism of cell-to-cell communication. Kidney Int. 2010;78:838–48.

17. Aliotta JM, Pereira M, Johnson KW, de Paz N, Dooner MS, Puente N, et al. Microvesicle entry into marrow cells mediates tissue-specific changes in mRNA by direct delivery of mRNA and induction of transcription. Exp Hematol. 2010;38: 233–45.

18. Luo SS, Ishibashi O, Ishikawa G, Ishikawa T, Katayama A, Mishima T, et al. Human villous trophoblasts express and secrete placenta-specific microRNAs into maternal circulation via exosomes. Biol Reprod. 2009;81:717–29.

19. Ogorevc E, Kralj-Iglic V, Veranic P. The role of extracellular vesicles in phenotypic cancer transformation. Radiol Oncol. 2013;47:197–205.

20. Alvarez-Erviti L, Seow Y, Yin H, Betts C, Lakhal S, Wood MJ. Delivery of siRNA to the mouse brain by systemic injection of targeted exosomes. Nat Biotechnol. 2011;29: 341–5.

21. Tang K, Zhang Y, Zhang H, Xu P, Liu J, Ma J, et al. Delivery of chemotherapeutic drugs in tumour cell-derived microparticles. Nat Commun. 2012;3:1282.

22. Montecalvo A, Larregina AT, Shufesky WJ, Stolz DB, Sullivan ML, Karlsson JM, et al. Mechanism of transfer of functional microRNAs between mouse dendritic cells via exosomes. Blood. 2012;119:756–66.

23. Atay S, Gercel-Taylor C, Taylor DD. Human trophoblast-derived exosomal fibronectin induces pro-inflammatory IL-1β production by macrophages. Am J Reprod Immunol. 2011; 66:259–69.

24. Barrès C, Blanc L, Bette-Bobillo P, André S, Mamoun R, Gabius HJ, et al. Galectin-5 is bound onto the surface of rat reticulocyte exosomes and modulates vesicle uptake by macrophages. Blood. 2010;115:696–705.

25. Christianson HC, Svensson KJ, van Kuppevelt TH, Li JP, Belting M. Cancer cell exosomes depend on cell-surface heparan sulfate proteoglycans for their internalization and functional activity. Proc Natl Acad Sci U S A. 2013;110: 17380–5.

26. Svensson KJ, Christianson HC, Wittrup A, Bourseau-Guilmain E, Lindqvist E, Svensson LM, et al. Exosome uptake depends on ERK1/2-heat shock protein 27 signalling and lipid raft-mediated endocytosis negatively regulated by caveolin-1. J Biol Chem. 2013;288:17713–24.

27. Feng D, Zhao WL, Ye YY, Bai XC, Liu RQ, Chang LF, et al. Cellular internalization of exosomes occurs through phago-cytosis. Traffic. 2010;11:675–87.

28. Fitzner D, Schnaars M, van Rossum D, Krishnamoorthy G, Dibaj P, Bakhti M, et al. Selective transfer of exosomes from oligodendrocytes to microglia by macropinocytosis. J Cell Sci. 2011;124:447–58.

29. Näslund TI, Paquin-Proulx D, Paredes PT, Vallhov H, Sandberg JK, Gabrielsson S. Exosomes from breast milk inhibit HIV-1 infection of dendritic cells and subsequent viral transfer to CD4 + T cells. AIDS. 2014;28:171–80.

30. Morelli AE, Larregina AT, Shufesky WJ, Sullivan ML, Stolz DB, Papworth GD, et al. Endocytosis, intracellular sorting, and processing of exosomes by dendritic cells. Blood. 2004;104:3257–66.

31. Yuyama K, Sun H, Mitsutake S, Igarashi Y. Sphingolipid-modulated exosome secretion promotes clearance of amyloid-β by microglia. J Biol Chem. 2012;287:10977–89.

32. Franzen CA, Simms PE, Van Huis AF, Foreman KE, Kuo PC, Gupta GN. Characterization of uptake and internalization of exosomes by bladder cancer cells. Biomed Res Int. 2014;2014:619829.

33. Tian T, Zhu YL, Hu FH, Wang YY, Huang NP, Xiao ZD. Dynamics of exosome internalization and trafficking. J Cell Physiol. 2012;228:1487–95.

34. Parolini I, Federici C, Raggi C, Lugini L, Palleschi S, De Milito A, et al. Microenvironmental pH is a key factor for exosome traffic in tumor cells. J Biol Chem. 2009;284: 34211–22.

35. Nazarenko I, Rana S, Baumann A, McAlear J, Hellwig A, Trendelenburg M, et al. Cell surface tetraspanin Tspan8 contributes to molecular pathways of exosome-induced endothelial cell activation. Cancer Res. 2010;70:1668–78.

36. Pan Q, Ramakrishnaiah V, Henry S, Fouraschen S, de Ruiter PE, Kwekkeboom J, et al. Hepatic cell-to-cell transmission of small silencing RNA can extend the therapeutic reach of RNA interference (RNAi). Gut. 2012;61:1330–9.

37. Rana S, Yue S, Stadel D, Zöller M. Toward tailored exosomes: the exosomal tetraspanin web contributes to target cell selection. Int J Biochem Cell Biol. 2012;44:1574–84.

38. Zech D, Rana S, Büchler MW, Zöller M. Tumor-exosomes and leukocyte activation: an ambivalent crosstalk. Cell Commun Signal. 2012;10:37.

39. Obregon C, Rothen-Rutishauser B, Gitahi SK, Gehr P, Nicod LP. Exovesicles from human activated dendritic cells fuse with resting dendritic cells, allowing them to present alloantigens. Am J Pathol. 2006;169:2127–36.

40. Tian T, Wang Y, Wang H, Zhu Z, Xiao Z. Visualizing of the cellular uptake and intracellular trafficking of exosomes by live-cell microscopy. J Cell Biochem. 2010;111:488–96.

41. Escrevente C, Keller S, Altevogt P, Costa J. Interaction and uptake of exosomes by ovarian cancer cells. BMC Cancer. 2011;11:108.

42. Keller S, König AK, Marmé F, Runz S, Wolterink S, Koensgen D, et al. Systemic presence and tumor-growth promoting effect of ovarian carcinoma released exosomes. Cancer Lett. 2009;278:73–81.

43. Xie Y, Zhang H, Li W, Deng Y, Munegowda MA, Chibbar R, et al. Dendritic cells recruit T cell exosomes via exosomal LFA-1 leading to inhibition of CD8+CTL responses through downregulation of peptide/MHC class I and Fas ligand-mediated cytotoxicity. J Immunol. 2010;185:5268–78.

44. Hao S, Bai O, Li F, Yuan J, Laferte S, Xiang J. Mature dendritic cells pulsed with exosomes stimulate efficient cytotoxic T-lymphocyte responses and antitumour immunity. Immunology. 2007;120:90–102.

45. Nanjundappa RH, Wang R, Xie Y, Umeshappa CS, Chibbar R, Wei Y, et al. GP120-specific exosome-targeted T cell-based vaccine capable of stimulating DC- and CD4(+) T-independent CTL responses. Vaccine. 2011;29:3538–47.

46. Temchura VV, Tenbusch M, Nchinda G, Nabi G, Tippler B, Zelenyuk M, et al. Enhancement of immunostimulatory properties of exosomal vaccines by incorporation of fusion-competent G protein of vesicular stomatitis virus. Vaccine. 2008;26:3662–72.

47. Koumangoye RB, Sakwe AM, Goodwin JS, Patel T, Ochieng J. Detachment of breast tumor cells induces rapid secretion of exosomes which subsequently mediate cellular adhesion and spreading. PLoS One. 2011;6:e24234.

48. Fabbri M, Paone A, Calore F, Galli R, Gaudio E, Santhanam R, et al. MicroRNAs bind to Toll-like receptors to induce prometastatic inflammatory response. Proc Natl Acad Sci U S A. 2012;109:E2110–6.

49. Tumne A, Prasad VS, Chen Y, Stolz DB, Saha K, Ratner DM, et al. Noncytotoxic suppression of human immunodeficiency virus type 1 transcription by exosomes secreted from CD8+ T cells. J Virol. 2009;83:4354–64.

50. Rana S, Zöller M. Exosome target cell selection and the importance of exosomal tetraspanins: a hypothesis. Biochem Soc Trans. 2011;39:559–62.

51. Record M, Carayon K, Poirot M, Silvente-Poirot S. Exosomes as new vesicular lipid transporters involved in cell-cell communication and various pathophysiologies. Biochim Biophys Acta. 2014;1841:108–20.

52. Hemler ME. Tetraspanin functions and associated microdomains. Nat Rev Mol Cell Biol. 2005;6:801–11.

53. Zöller M. Tetraspanins: push and pull in suppressing and promoting metastasis. Nat Rev Cancer. 2009;9:40–55.

54. Escola JM, Kleijmeer MJ, Stoorvogel W, Griffith JM, Yoshie O, Geuze HJ. Selective enrichment of tetraspan proteins on the internal vesicles of multivesicular endosomes and on exosomes secreted by human B-lymphocytes. J Biol Chem. 1998;273:20121–7.

55. Heijnen HF, Schiel AE, Fijnheer R, Geuze HJ, Sixma JJ. Activated platelets release two types of membrane vesicles: microvesicles by surface shedding and exosomes derived from exocytosis of multivesicular bodies and alpha-granules. Blood. 1999;94:3791–9.

56. Rubinstein E, Ziyyat A, Prenant M, Wrobel E, Wolf JP, Levy S, et al. Reduced fertility of female mice lacking CD81. Dev Biol. 2006;290:351–8.

57. Zhu GZ, Miller BJ, Boucheix C, Rubinstein E, Liu CC, Hynes RO, et al. Residues SFQ (173–175) in the large extracellular loop of CD9 are required for gamete fusion. Development. 2002;129:1995–2002.

58. Helming L, Gordon S. The molecular basis of macrophage fusion. Immunobiology. 2007;212:785–93.

59. Rubinstein E, Ziyyat A, Wolf JP, Le Naour F, Boucheix C. The molecular players of sperm-egg fusion in mammals. Semin Cell Dev Biol. 2006;17:254–63.

60. Takeda Y, Tachibana I, Miyado K, Kobayashi M, Miyazaki T, Funakoshi T, et al. Tetraspanins CD9 and CD81 function to prevent the fusion of mononuclear phagocytes. J Cell Biol. 2003;161:945–56.

61. Thali M. The roles of tetraspanins in HIV-1 replication. Curr Top Microbiol Immunol. 2009;339:85–102.

62. Levy S, Shoham T. The tetraspanin web modulates immune-signalling complexes. Nat Rev Immunol. 2005;5:136–48.

63. Vjugina U, Evans JP. New insights into the molecular basis of mammalian sperm-egg membrane interactions. Front Biosci. 2008;13:462–76.

64. Johnstone RM. Exosomes biological significance: a concise review. Blood Cells Mol Dis. 2006;36:315–21.

65. Lakkaraju A, Rodriguez-Boulan E. Itinerant exosomes: emerging roles in cell and tissue polarity. Trends Cell Biol. 2008;18:199–209.

66. Schorey JS, Bhatnagar S. Exosome function: from tumor immunology to pathogen biology. Traffic. 2008;9:871–81.

67. Lebreton A, Séraphin B. Exosome-mediated quality control: substrate recruitment and molecular activity. Biochim Biophys Acta. 2008;1779:558–65.

68. Aplin AE, Howe A, Alahari SK, Juliano RL. Signal transduction and signal modulation by cell adhesion receptors: the role of integrins, cadherins, immunoglobulin-cell adhesion molecules, and selectins. Pharmacol Rev. 1998;50:197–263.

69. Marlin SD, Springer TA. Purified intercellular adhesion molecule-1 (ICAM-1) is a ligand for lymphocyte function-associated antigen 1 (LFA-1). Cell. 1987;51:813–9.

70. Nolte-'t Hoen EN, Buschow SI, Anderton SM, Stoorvogel W, Wauben MH. Activated T cells recruit exosomes secreted by dendritic cells via LFA-1. Blood. 2009;113:1977–81.

71. Hwang I, Shen X, Sprent J. Direct stimulation of naive T cells by membrane vesicles from antigen-presenting cells: distinct roles for CD54 and B7 molecules. Proc Natl Acad Sci U S A. 2003;100:6670–5.

72. Hanayama R, Tanaka M, Miwa K, Shinohara A, Iwamatsu A, Nagata S. Identification of a factor that links apoptotic cells to phagocytes. Nature. 2002;417:182–7.

73. Shukla D, Liu J, Blaiklock P, Shworak NW, Bai X, Esko JD, et al. A novel role for 3-O-sulfated heparan sulfate in herpes simplex virus 1 entry. Cell. 1999;99:13–22.

74. Garcia-Vallejo JJ, van Kooyk Y. The physiological role of DC-SIGN: a tale of mice and men. Trends Immunol. 2013;34:482–6.

75. Flanagan MD, Lin S. Cytochalasins block actin filament elongation by binding to high affinity sites associated with F-actin. J Biol Chem. 1980;255:835–8.

76. Lamaze C, Fujimoto LM, Yin HL, Schmid SL. The actin cytoskeleton is required for receptor-mediated endocytosis in mammalian cells. J Biol Chem. 1997;272:20332–5.

77. Obregon C, Rothen-Rutishauser B, Gerber P, Gehr P, Nicod LP. Active uptake of dendritic cell-derived exovesicles by epithelial cells induces the release of inflammatory mediators through a TNF-alpha-mediated pathway. Am J Pathol. 2009;175:696–705.

78. Doherty GJ, McMahon HT. Mechanisms of endocytosis. Annu Rev Biochem. 2009;78:857–902.

79. Skokos D, Botros HG, Demeure C, Morin J, Peronet R, Birkenmeier G, et al. Mast cell-derived exosomes induce phenotypic and functional maturation of dendritic cells and elicit specific immune responses in vivo. J Immunol. 2003;170:3037–45.

80. Izquierdo-Useros N, Naranjo-Gómez M, Archer J, Hatch SC, Erkizia I, Blanco J, et al. Capture and transfer of HIV-1 particles by mature dendritic cells converges with the exosome-dissemination pathway. Blood. 2009;113:2732–41.

81. Miyanishi M, Tada K, Koike M, Uchiyama Y, Kitamura T, Nagata S. Identification of Tim4 as a phosphatidylserine receptor. Nature. 2007;450:435–9.

82. Pasquetto MV, Vecchia L, Covini D, Digilio R, Scotti C. Targeted drug delivery using immunoconjugates: principles and applications. J Immunother. 2011;34:611–28.

83. Kirchhausen T. Clathrin. Annu Rev Biochem. 2000;69: 699–727.

84. Wang LH, Rothberg KG, Anderson RG. Mis-assembly of clathrin lattices on endosomes reveals a regulatory switch for coated pit formation. J Cell Biol. 1993;123:1107–17.

85. Vallee RB, Herskovits JS, Aghajanian JG, Burgess CC, Shpetner HS. Dynamin, a GTPase involved in the initial stages of endocytosis. Ciba Found Symp. 1993;176:185–93; discussion 93–7.

86. Herskovits JS, Burgess CC, Obar RA, Vallee RB. Effects of mutant rat dynamin on endocytosis. J Cell Biol. 1993;122: 565–78.

87. Ehrlich M, Boll W, Van Oijen A, Hariharan R, Chandran K, Nibert ML, et al. Endocytosis by random initiation and stabilization of clathrin-coated pits. Cell. 2004;118:591–605.

88. Merrifield CJ, Feldman ME, Wan L, Almers W. Imaging actin and dynamin recruitment during invagination of single clathrin-coated pits. Nat Cell Biol. 2002;4:691–8.

89. Taylor MJ, Lampe M, Merrifield CJ. A feedback loop between dynamin and actin recruitment during clathrin-mediated endocytosis. PLoS Biol. 2012;10:e1001302.

90. Damke H, Baba T, Warnock DE, Schmid SL. Induction of mutant dynamin specifically blocks endocytic coated vesicle formation. J Cell Biol. 1994;127:915–34.

91. Marks B, Stowell MH, Vallis Y, Mills IG, Gibson A, Hopkins CR, et al. GTPase activity of dynamin and resulting conformation change are essential for endocytosis. Nature. 2001;410:231–5.

92. Chappie JS, Acharya S, Leonard M, Schmid SL, Dyda F. G domain dimerization controls dynamin's assembly-stimulated GTPase activity. Nature. 2010;465:435–40.

93. Achiriloaie M, Barylko B, Albanesi JP. Essential role of the dynamin pleckstrin homology domain in receptor-mediated endocytosis. Mol Cell Biol. 1999;19:1410–5.

94. Lee A, Frank DW, Marks MS, Lemmon MA. Dominant-negative inhibition of receptor-mediated endocytosis by a dynamin-1 mutant with a defective pleckstrin homology domain. Curr Biol. 1999;9:261–4.

95. Vallis Y, Wigge P, Marks B, Evans PR, McMahon HT. Importance of the pleckstrin homology domain of dynamin in clathrin-mediated endocytosis. Curr Biol. 1999;9:257–60.

96. Ramachandran R, Pucadyil TJ, Liu YW, Acharya S, Leonard M, Lukiyanchuk V, et al. Membrane insertion of the pleckstrin homology domain variable loop 1 is critical for dynamin-catalyzed vesicle scission. Mol Biol Cell. 2009; 20:4630–9.

97. Benmerah A, Bayrou M, Cerf-Bensussan N, Dautry-Varsat A. Inhibition of clathrin-coated pit assembly by an Eps15 mutant. J Cell Sci. 1999;112:1303–11.

98. Anderson RG. The caveolae membrane system. Annu Rev Biochem. 1998;67:199–225.

99. Kurzchalia TV, Parton RG. Membrane microdomains and caveolae. Curr Opin Cell Biol. 1999;11:424–31.

100. Nabi IR, Le PU. Caveolae/raft-dependent endocytosis. J Cell Biol. 2003;161:673–7.

101. Parton RG, Simons K. The multiple faces of caveolae. Nat Rev Mol Cell Biol. 2007;8:185–94.

102. Newton AJ, Kirchhausen T, Murthy VN. Inhibition of dynamin completely blocks compensatory synaptic vesicle endocytosis. Proc Natl Acad Sci U S A. 2006;103:17955–60.

103. Nanbo A, Kawanishi E, Yoshida R, Yoshiyama H. Exosomes derived from Epstein-Barr virus-infected cells are internalized via caveola-dependent endocytosis and promote phenotypic modulation in target cells. J Virol. 2013;87:10334–47.

104. Menck K, Klemm F, Gross JC, Pukrop T, Wenzel D, Binder C. Induction and transport of Wnt 5a during macrophage-induced malignant invasion is mediated by two types of extracellular vesicles. Oncotarget. 2013;4:2057–66.

105. Orth JD, Krueger EW, Cao H, McNiven MA. The large GTPase dynamin regulates actin comet formation and movement in living cells. Proc Natl Acad Sci U S A. 2002; 99:167–72.

106. Razani B, Engelman JA, Wang XB, Schubert W, Zhang XL, Marks CB, et al. Caveolin-1 null mice are viable but show evidence of hyperproliferative and vascular abnormalities. J Biol Chem. 2001;276:38121–38.

107. Swanson JA. Shaping cups into phagosomes and macropinosomes. Nat Rev Mol Cell Biol. 2008;9:639–49.

108. Kerr MC, Teasdale RD. Defining macropinocytosis. Traffic. 2009;10:364–71.

109. Grimmer S, van Deurs B, Sandvig K. Membrane ruffling and macropinocytosis in A431 cells require cholesterol. J Cell Sci. 2002;115:2953–62.

110. Ahram M, Sameni M, Qiu RG, Linebaugh B, Kirn D, Sloane BF. Rac1-induced endocytosis is associated with intracellular proteolysis during migration through a three-dimensional matrix. Exp Cell Res. 2000;260:292–303.

111. Ridley AJ. Rho GTPases and actin dynamics in membrane protrusions and vesicle trafficking. Trends Cell Biol. 2006;16: 522–9.

112. Sanz-Moreno V, Gadea G, Ahn J, Paterson H, Marra P, Pinner S, et al. Rac activation and inactivation control plasticity of tumor cell movement. Cell. 2008;135:510–23.

113. Rudt S, Müller RH. In vitro phagocytosis assay of nano- and microparticles by chemiluminescence. III. Uptake of differently sized surface-modified particles, and its correlation to particle properties and in vivo distribution. Eur J Pharm Sci. 1993;1:31–9.

114. Stephens L, Ellson C, Hawkins P. Roles of PI3Ks in leukocyte chemotaxis and phagocytosis. Curr Opin Cell Biol. 2002;14: 203–13.

115. Fadok VA, Voelker DR, Campbell PA, Cohen JJ, Bratton DL, Henson PM. Exposure of phosphatidylserine on the surface of apoptotic lymphocytes triggers specific recognition and removal by macrophages. J Immunol. 1992;148:2207–16.

116. Shiratsuchi A, Kaido M, Takizawa T, Nakanishi Y. Phosphatidylserine-mediated phagocytosis of influenza A virus-infected cells by mouse peritoneal macrophages. J Virol. 2000;74:9240–4.

117. Fomina AF, Deerinck TJ, Ellisman MH, Cahalan MD. Regulation of membrane trafficking and subcellular organization of endocytic compartments revealed with FM1-43 in resting and activated human T cells. Exp Cell Res. 2003;291: 150–66.

118. Simons K, Ehehalt R. Cholesterol, lipid rafts, and disease. J Clin Invest. 2002;110:597–603.

119. Teissier E, Pécheur EI. Lipids as modulators of membrane fusion mediated by viral fusion proteins. Eur Biophys J. 2007;36:887–99.

120. Palecek SP, Schmidt CE, Lauffenburger DA, Horwitz AF. Integrin dynamics on the tail region of migrating fibroblasts. J Cell Sci. 1996;109:941–52.

121. Glebov OO, Bright NA, Nichols BJ. Flotillin-1 defines a clathrin-independent endocytic pathway in mammalian cells. Nat Cell Biol. 2006;8:46–54.

122. Frick M, Bright NA, Riento K, Bray A, Merrified C, Nichols BJ. Coassembly of flotillins induces formation of membrane microdomains, membrane curvature, and vesicle budding. Curr Biol. 2007;17:1151–6.

123. Volonte D, Galbiati F, Li S, Nishiyama K, Okamoto T, Lisanti MP. Flotillins/cavatellins are differentially expressed in cells and tissues and form a hetero-oligomeric complex with caveolins in vivo. Characterization and epitope-mapping of a novel flotillin-1 monoclonal antibody probe. J Biol Chem. 1999;274:12702–9.

124. Bickel PE, Scherer PE, Schnitzer JE, Oh P, Lisanti MP, Lodish HF. Flotillin and epidermal surface antigen define a new family of caveolae-associated integral membrane proteins. J Biol Chem. 1997;272:13793–802.

125. Otto GP, Nichols BJ. The roles of flotillin microdomains – endocytosis and beyond. J Cell Sci. 2011;124:3933–40.

126. Wang E, Norred WP, Bacon CW, Riley RT, Merrill AH. Inhibition of sphingolipid biosynthesis by fumonisins. Implications for diseases associated with Fusarium moniliforme. J Biol Chem. 1991;266:14486–90.

127. Platt FM, Neises GR, Dwek RA, Butters TD. N-butyldeoxynojirimycin is a novel inhibitor of glycolipid biosynthesis. J Biol Chem. 1994;269:8362–5.

128. Jahn R, Lang T, Südhof TC. Membrane fusion. Cell. 2003;112:519–33.

129. Chernomordik LV, Melikyan GB, Chizmadzhev YA. Bio-membrane fusion: a new concept derived from model studies using two interacting planar lipid bilayers. Biochim Biophys Acta. 1987;906:309–52.

130. Chernomordik LV, Kozlov MM. Mechanics of membrane fusion. Nat Struct Mol Biol. 2008;15:675–83.

131. Jahn R, Südhof TC. Membrane fusion and exocytosis. Annu Rev Biochem. 1999;68:863–911.

132. Valapala M, Vishwanatha JK. Lipid raft endocytosis and exosomal transport facilitate extracellular trafficking of annexin A2. J Biol Chem. 2011;286:30911–25.

133. Yuana Y, Sturk A, Nieuwland R. Extracellular vesicles in physiological and pathological conditions. Blood Rev. 2013; 27:31–9.

134. Logozzi M, De Milito A, Lugini L, Borghi M, Calabrò L, Spada M, et al. High levels of exosomes expressing CD63 and caveolin-1 in plasma of melanoma patients. PLoS One. 2009;4:e5219.

135. Kharaziha P, Ceder S, Li Q, Panaretakis T. Tumor cell-derived exosomes: a message in a bottle. Biochim Biophys Acta. 2012;1826:103–11.

136. Marcus ME, Leonard JN. FedExosomes: engineering therapeutic biological nanoparticles that truly deliver. Pharmaceuticals (Basel). 2013;6:659–80.

137. Pegtel DM, Cosmopoulos K, Thorley-Lawson DA, van Eijndhoven MA, Hopmans ES, Lindenberg JL, et al. Functional delivery of viral miRNAs via exosomes. Proc Natl Acad Sci U S A. 2010;107:6328–33.

138. Zitvogel L, Regnault A, Lozier A, Wolfers J, Flament C, Tenza D, et al. Eradication of established murine tumors using a novel cell-free vaccine: dendritic cell-derived exosomes. Nat Med. 1998;4:594–600.

139. Casella JF, Flanagan MD, Lin S. Cytochalasin D inhibits actin polymerization and induces depolymerization of actin filaments formed during platelet shape change. Nature. 1981;293:302–5.

140. Brawley SH, Robinson KR. Cytochalasin treatment disrupts the endogenous currents associated with cell polarization in fucoid zygotes: studies of the role of F-actin in embryogenesis. J Cell Biol. 1985;100:1173–84.

141. Selden SC, Rabinovitch PS, Schwartz SM. Effects of cytoskeletal disrupting agents on replication of bovine endothelium. J Cell Physiol. 1981;108:195–211.

142. Cantley LC. The phosphoinositide 3-kinase pathway. Science. 2002;296:1655–7.

143. Greenberg S. Signal transduction of phagocytosis. Trends Cell Biol. 1995;5:93–9.

144. Hazeki O, Hazeki K, Katada T, Ui M. Inhibitory effect of wortmannin on phosphatidylinositol 3-kinase-mediated cellular events. J Lipid Mediat Cell Signal. 1996;14:259–61.

145. Knight ZA. Small molecule inhibitors of the PI3-kinase family. Curr Top Microbiol Immunol. 2010;347:263–78.

146. Araki N, Johnson MT, Swanson JA. A role for phosphoinositide 3-kinase in the completion of macropinocytosis and phagocytosis by macrophages. J Cell Biol. 1996;135:1249–60.

147. Prieto-Sánchez RM, Berenjeno IM, Bustelo XR. Involvement of the Rho/Rac family member RhoG in caveolar endocytosis. Oncogene. 2006;25:2961–73.

148. Rappoport JZ, Heyman KP, Kemal S, Simon SM. Dynamics of dynamin during clathrin mediated endocytosis in PC12 cells. PLoS One. 2008;3:e2416.

149. Ormerod KG, Rogasevskaia TP, Coorssen JR, Mercier AJ. Cholesterol-independent effects of methyl-β-cyclodextrin on chemical synapses. PLoS One. 2012;7:e36395.

150. Steinman RM, Mellman IS, Muller WA, Cohn ZA. Endocytosis and the recycling of plasma membrane. J Cell Biol. 1983;96:1–27.

151. McNeil PL, Steinhardt RA. Loss, restoration, and maintenance of plasma membrane integrity. J Cell Biol. 1997;137: 1–4.

152. Lundmark R, Doherty GJ, Howes MT, Cortese K, Vallis Y, Parton RG, et al. The GTPase-activating protein GRAF1 regulates the CLIC/GEEC endocytic pathway. Curr Biol. 2008;18:1802–8.

153. Stoeck A, Keller S, Riedle S, Sanderson MP, Runz S, Le Naour F, et al. A role for exosomes in the constitutive and stimulus-induced ectodomain cleavage of L1 and CD44. Biochem J. 2006;393:609–18.

154. Hakulinen J, Junnikkala S, Sorsa T, Meri S. Complement inhibitor membrane cofactor protein (MCP; CD46) is constitutively shed from cancer cell membranes in vesicles and converted by a metalloproteinase to a functionally active soluble form. Eur J Immunol. 2004;34:2620–9.

155. Hawari FI, Rouhani FN, Cui X, Yu ZX, Buckley C, Kaler M, et al. Release of full-length 55-kDa TNF receptor 1 in exosome-like vesicles: a mechanism for generation of soluble cytokine receptors. Proc Natl Acad Sci U S A. 2004;101: 1297–302.

8.1.2. Jacobs, L. A., Bewicke-Copley, F., Poolman, M. G., Pink, R. C., <u>Mulcahy, L. A.</u>, Baker, I., Beaman, E. M., Brooks, T., Caley, D. P., Cowling, W., Currie, J. M., Horsburgh, J., Kenehan, L., Keyes, E., Leite, D., Massa, D., McDermott-Rouse, A., Samuel, P., Wood, H., Kadhim, M. and Carter, D. R. (2013). Meta-analysis using a novel database, miRStress, reveals miRNAs that are frequently associated with the radiation and hypoxia stress-responses. *PLoS One*, 8(11):e80844.

Meta-Analysis Using a Novel Database, miRStress, Reveals miRNAs That Are Frequently Associated with the Radiation and Hypoxia Stress-Responses

Laura Ann Jacobs[1], Findlay Bewicke-Copley[1], Mark Graham Poolman[1], Ryan Charles Pink[1], Laura Ann Mulcahy[1], Isabel Baker[1], Ellie-May Beaman[1], Travis Brooks[1], Daniel Paul Caley[1,2], William Cowling[1], James Michael Stevenson Currie[1], Jessica Horsburgh[1], Lottie Kenehan[1], Emma Keyes[1], Daniel Leite[1], Davide Massa[1], Adam McDermott-Rouse[1], Priya Samuel[1], Hannah Wood[1], Munira Kadhim[1], David Raul Francisco Carter[1]*

1 Department of Biological and Medical Sciences, Oxford Brookes University, Oxford, United Kingdom, **2** Canada's Michael Smith Genome Sciences Centre, BC Cancer Agency, Vancouver, British Columbia, Canada

Abstract

Organisms are often exposed to environmental pressures that affect homeostasis, so it is important to understand the biological basis of stress-response. Various biological mechanisms have evolved to help cells cope with potentially cytotoxic changes in their environment. miRNAs are small non-coding RNAs which are able to regulate mRNA stability. It has been suggested that miRNAs may tip the balance between continued cytorepair and induction of apoptosis in response to stress. There is a wealth of data in the literature showing the effect of environmental stress on miRNAs, but it is scattered in a large number of disparate publications. Meta-analyses of this data would produce added insight into the molecular mechanisms of stress-response. To facilitate this we created and manually curated the miRStress database, which describes the changes in miRNA levels following an array of stress types in eukaryotic cells. Here we describe this database and validate the miRStress tool for analysing miRNAs that are regulated by stress. To validate the database we performed a cross-species analysis to identify miRNAs that respond to radiation. The analysis tool confirms miR-21 and miR-34a as frequently deregulated in response to radiation, but also identifies novel candidates as potentially important players in this stress response, including miR-15b, miR-19b, and miR-106a. Similarly, we used the miRStress tool to analyse hypoxia-responsive miRNAs. The most frequently deregulated miRNAs were miR-210 and miR-21, as expected. Several other miRNAs were also found to be associated with hypoxia, including miR-181b, miR-26a/b, miR-106a, miR-213 and miR-192. Therefore the miRStress tool has identified miRNAs with hitherto unknown or under-appreciated roles in the response to specific stress types. The miRStress tool, which can be used to uncover new insight into the biological roles of miRNAs, and also has the potential to unearth potential biomarkers for therapeutic response, is freely available at http://mudshark.brookes.ac.uk/MirStress.

Competing interests: The authors have declared that no competing interests exist.

* E-mail: dcarter@brookes.ac.uk

Introduction

When faced with an environmental stressor an organism can either extricate itself from the situation or adapt by other means. When individual cells encounter such stresses they are often unable to escape, and so a number of biological mechanisms have evolved to help cells cope with potentially cytotoxic changes in their environment. Stressful stimuli or 'stresses' may include extremes of temperature, chemical exposure, hypoxia, radiation or nutrient stress [1]. Cells within a multi-cellular organism employ mechanisms to adapt to the change, repair the damage caused by the stressor, or undergo apoptosis to protect the organism [2]. Organisms are often exposed to environmental pressures, such as radiation exposure, which affect homeostasis, and so it is important to understand the biological basis of stress-response.

Key survival mechanisms of cells include the heat shock response [3] or the unfolded protein response (UPR) [4]. In

reaction to most stresses there is a swift intervention to normal protein production within the cell. Though global translation is often reduced following stress-induction [5], translation of specific transcripts is up-regulated [6]. Cellular material that is deemed unnecessary, including various transcripts, are degraded [7]. Stress granules (SG) form inside cells, which appear to sequester specific transcripts along with ribosomal proteins; SGs are dispersed soon after the stimulus is removed [8]. Steady-state levels of different mRNAs can be affected by post-transcriptional mechanisms [9]. Post-transcriptional regulation, for example by interaction between mRNAs and binding proteins [7], affords a potentially more rapid response to stress [1].

Recent findings from genome analysis consortia have indicated that most organisms produce a myriad of non-coding RNAs. Whilst the role of the majority of this transcriptional output remains controversial, there are an increasing number of long [10,11] and short [12] non-coding RNAs with a demonstrated functional role in health or disease. miRNAs are short (approximately 22 nt) RNAs that can interact with the 3'UTRs of target mRNAs, resulting in translational repression and mRNA degradation [13]. Because the interaction between a miRNA and its target is based on a small region of ~7 nucleotides, which does not need to match perfectly, a single miRNA can affect the expression of many genes simultaneously [14]. Given the importance of regulating mRNA stability in response to stress it is unsurprising that miRNAs also show a dynamic response when cells encounter a perturbagen [15]. Indeed, it has been suggested that miRNAs may ultimately tip the balance between continued cytorepair and induction of apoptosis [1,16].

The importance of miRNAs in a cellular and organismal context remains controversial. Although miRNAs were first discovered through their phenotypic effect on *C. elegans* [17], deletion of various miRNAs has no apparent consequence [18,19]. This contradicts the functional importance of these miRNAs implied by their often high sequence conservation. This paradox has, at least in part, been resolved by studies looking at the effects of miRNAs in response to stress. Indeed, in some cases the phenotypic effects of the miRNA deletion only became apparent after the organism is exposed to environmental stress. For example, miR-214 was shown to be a marker of cardiac stress [20], yet knocking out miR-214 in mice had no effect on physiology under normal conditions [21]. However, when these mice were stressed by ischemia/ reperfusion injury they exhibited increased apoptosis of cardiac cells and decreased overall survival [21]. Similarly, miR-7 mutant flies have a wild-type phenotype under normal conditions, but when exposed to fluctuating temperature at the larval stage they exhibit aberrations in retinal development [22]. The role of some miRNAs may be to add biological robustness during development or homeostasis by modulating gene regulatory networks [23]. For these reasons it is particularly important to understand the roles of miRNAs in stress response.

Stress can originate biologically from within the organism (such as that caused by disease or abnormal cellular behaviour) or externally from non-biological sources (such as toxic agents or changes in the environment). In this study we have analysed the changes in miRNA levels that occur in response to the latter. Over the past decade a number of studies have been performed to profile changes in miRNA expression following insult with various environmental challenges. The results of such studies are often conflicting, and may be due to differences in the experimental setup. In order to make sense of this increasing pool of data a central resource is required which can be used to meta-analyse the results of these studies, confirm the identity of key miRNAs and infer novel biological roles for non-coding RNAs in stress. A database exists for miRNA responses following stress induction in plants [24]. However, a comprehensive database of such data with the functionality to perform useful meta-analyses has not been reported for other eukaryotes. Here we address this issue with a novel database and web tool which we call miRStress. This manually curated database contains more than 7,500 entries from over 300 publications. To validate the usefulness for biological discovery of this resource we used the database to meta-analyse the effects of various stress types, including hypoxia and radiation. The results confirm the identification of several miRNAs already known from functional studies to be directly involved in response to these stimuli. In addition, several other miRNAs are identified that have not previously been associated with these stresses. These results suggest the miRStress database is a useful new tool for understanding the biology of miRNAs.

Results and Discussion

The miRStress database

There is a wealth of data in the literature showing the effect of environmental stresses on miRNAs, but it is scattered in a large number of disparate publications. Meta-analyses of this data would produce added insight into the molecular mechanisms of stress-response. To facilitate this process we manually curated the miRStress database, which describes the changes in miRNA levels following a varied array of stress types in eukaryotic cells. As of June 2013 the database contained more than 7,500 entries, annotated from 315 publications spanning seven years. An initial analysis of all the entries in the database reveals the miRNAs that are most frequently deregulated in response to all stress types (table 1). The miRNAs that are affected most often are miR-21, miR-210 and miR-34a. This is consistent with previous reports of clear roles for these miRNAs in DNA damage-response and hypoxia [16].

Identification of miRNAs involved in radiation response

To demonstrate the potential of miRStress in identifying miRNAs with biological importance in stress response we analysed entries related to radiation. Several studies have attempted to measure the effects of radiation on miRNA levels. The degree of overlap between these studies is variable, due to the differences in radiation type, dose, cell type, miRNA measurement technique and other differences in experimental approach. Observing miRNAs that consistently change in response to radiation across many studies could imply they

Table 1. miRStress-generated list of the most frequently deregulated miRNAs across all stress types.

miRNA	Up	Down	NR	Sum	% up	% down
21	68	25	1	94	72.3	26.6
210	72	10	1	83	86.7	12.0
34a	49	14	0	63	77.8	22.2
17	24	37	1	62	38.7	59.7
16	35	23	1	59	59.3	39.0
125b	30	25	1	56	53.6	44.6
26a	25	27	1	53	47.2	50.9
20a	19	27	1	47	40.4	57.4
155	33	14	0	47	70.2	29.8
29a	25	20	1	46	54.3	43.5

Columns indicate the miRNA name, the number of incidences where the miRNA is stimulated (up) or repressed (down) by the stress. NR indicated that the direction of change was not reported in the publication.

doi: 10.1371/journal.pone.0080844.t001

Table 2. miRStress-generated list of the most frequently deregulated miRNAs following radiation treatment.

miRNA	Up	Down	NR	Sum	% up	% down
21	11	6	1	18	61.1	33.3
34a	11	6	0	17	64.7	35.3
16	10	5	1	16	62.5	31.3
17	8	6	1	15	53.3	40.0
let-7b	5	9	1	15	33.3	60.0
let-7g	9	5	0	14	64.3	35.7
let-7a	5	8	1	14	35.7	57.1
let-7f	6	7	0	13	46.2	53.8
19b	6	5	1	12	50.0	41.7
let-7d	4	6	2	12	33.3	50.0
let-7c	7	5	0	12	58.3	41.7
125b	5	6	1	12	41.7	50.0
143	4	5	2	11	36.4	45.5
24	8	3	0	11	72.7	27.3
20a	4	6	1	11	36.4	54.5
15b	4	5	2	11	36.4	45.5
106a	3	6	1	10	30.0	60.0
106b	4	5	1	10	40.0	50.0
let-7e	4	6	0	10	40.0	60.0
221	8	2	0	10	80.0	20.0

Columns indicate the miRNA name, the number of incidences where the miRNA is stimulated (up) or repressed (down) by the stress. NR indicated that the direction of change was not reported in the publication.

doi: 10.1371/journal.pone.0080844.t002

have greater functional importance. Some attempts have been made to collate and analyse these disparate publications [25,26], but a recent comprehensive meta-analysis of these studies has not been described.

To identify radiation-related miRNAs we selected the radiation treatment group on the miRStress database. The database returned a list of miRNAs along with the number of reports of a miRNA being significantly deregulated. Table 2 shows the list of miRNAs whose level changes in at least ten instances in the database. The most frequently deregulated miRNAs were miR-21 and miR-34a. This is consistent with previous work showing a role for these miRNAs in the response to genotoxic stress, including radiation [1,27,28]. Indeed, many of the miRNAs in table 2, which we term 'radiation-miRNAs' have been previously shown to play a role in either the response to radiation or in conferring differential sensitivity to radiation. There are other miRNAs in table 2, including miR-15b and miR-19b, which have not been overtly identified as being related to radiation, suggesting that these miRNAs represent novel candidates for further study by the radiobiology field. With some of these miRNAs there are clues to their potential involvement in radiation response from other studies. For instance, the let-7 family are known to regulate a number of oncogenes, so specific members of the family may tip the balance between cell cycle arrest and apoptosis following irradiation [29]. Evidence suggests that miR-15b can regulate cell cycle progression [30] and apoptosis [31]. Interestingly, miR-19a/b are able to increase resistance of gastric cancer cells to chemotherapy by affecting drug efflux pathways and inhibiting apoptosis [32]. The finding that exosomes associated with RNA mediate the radiation-induced bystander-effect also hints at a role for miRNAs in the intercellular response to ionizing radiation [33]. Whilst there is much left to elucidate in the miRNA-mediated responses to radiation, the results from this study provide some strong candidates worthy of further characterisation.

In order to gain further insight into the potential roles of miRNAs returned by miRStress we used bioinformatics tools to analyse the functions of their predicted targets. The online miRNA binding-site prediction tool miRWalk [34] was used to produce a list of predicted gene targets for each of the radiation-miRNAs in table 2. miRWalk reports the result of various miRNA target-prediction algorithms, thereby allowing the user to estimate whether predicted targets are low- or high-confidence interactions. For each radiation-miRNA we obtained a list of high-confidence predicted gene targets (at least six different algorithms within miRWalk predict an interaction). To analyse the potential role of these predicted genes we used the DAVID functional annotation [35,36]. For each radiation-miRNA we generated a list of high-confidence 'predicted' KEGG pathways that are enriched in the target mRNAs. The predicted-pathways most commonly targeted are shown in in text S1. Interestingly, the most commonly predicted pathway was MAPK signalling, which has been previously observed as playing a role in radiation response [37]. To assess whether the predicted-pathways targeted by radiation-miRNAs underpin a genuine biological phenomenon, rather than a non-specific quirk obtained when any set of miRNAs is analysed, we repeated the analysis with an equivalent number of control miRNAs. The control miRNAs were chosen on the basis that they appear only once on the list of radiation-affected miRNAs and are therefore unlikely to represent genuine radiation-miRNAs. The pattern of predicted-pathways for the control-miRNAs is different to those obtained with radiation-miRNAs (text S1). Indeed, many of the predicted pathways (such as the MAPK signalling pathway) appear much more often for the

radiation miRNAs than the control miRNAs, suggesting that they do represent a biological effect.

In addition to the studies measuring the levels of miRNAs there have also been a number of publications describing changes in mRNA levels in response to radiation. We downloaded 18 sets of microarray data from such studies and identified genes deregulated by at least two-fold from each dataset. These genes were then analysed using DAVID and the pathways enriched in the datasets were counted and compared to the predicted pathways (text S1). Interestingly, MAPK signalling was enriched in half of the 18 datasets, consistent with the identification of MAPK signalling in the radiation miRNA predicted-pathways. Radiation predicted-pathways appeared on average 4.2 times in the actual radiation pathways. This was significantly more (t test, p = 0.002) than the control predicted-pathways, which appeared on average 1.5 times in the list of pathways that are actually deregulated in radiation response (Figure 1A). In other words, the miRNAs which are most frequently affected by radiation are 'predicted' to target the pathways which are 'actually' affected following irradiation. This is consistent with a role for the radiation-miRNAs in influencing gene expression following irradiation of cells.

To further validate the biological relevance of the radiation miRNAs identified by miRStress we utilised previously published datasets featuring radiosensitivity and miRNA expression data across the NCI-60 panel. The NCI-60 panel is a collection of human cell lines derived from various cancer types. This panel has been well characterised at the molecular level [38], with data available on expression of miRNAs and mRNAs, as well as sensitivity to radiation and thousands of compounds. Specifically we used the SF5 (surviving fraction of cells after a 5 Gray dose of radiation) value for each cell line [39] and the levels of miRNA expression in the E-MTAB-327 dataset [40]. To test for relationships between miRNAs and radiation resistance we performed Pearson correlation analyses between miRNA levels and radiosensitivity across the panel. For each miRNA this yielded a Pearson correlation which is indicative of the strength of association between the level of that miRNA and the level of radioresistance. We then assessed whether the magnitude of the Pearson correlations for radiation miRNAs was, on average, significantly higher than those for the control miRNAs. Our results show that the magnitude of the average Pearson correlation for radiation miRNAs is indeed significantly higher (t test, p = 0.017) for the radiation miRNAs compared to control miRNAs (Figure 1B). A similar analysis using the coefficient of determination (R^2) for these correlations showed that the average R^2 value for radiation miRNAs was more than three times higher than that for control miRNAs (t test, p = 0.03). This suggests that the miRNAs identified by miRStress as being associated with radiation response are more likely to correlate with radiosensitivity than the control miRNAs.

In order to be more confident in the accuracy of miRStress in calling genuine radiation-related miRNAs we performed a receiver operating characteristic (ROC) curve analysis. This method can be used to determine how good a tool is at taking a variable input (in this case the number of times a miRNA is

Figure 1
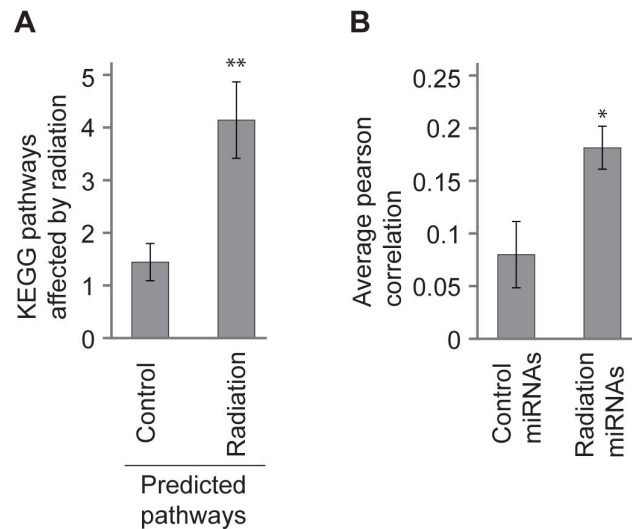
Figure 1. Radiation-responsive miRNAs predicted by miRStress are biologically relevant. A: The miRNAs which are most frequently deregulated following radiation stress, as reported by miRStress, were used to 'predict' radiation-responsive pathways, as described in the methods. Control pathways were selected by using a list of control miRNAs. These were then compared to a list of KEGG pathways which are observed (as opposed to predicted) to actually change following radiation (in a total of 18 datasets). The average frequency with which the predicted control or radiation pathways appears in the observed pathways is shown. On average the radiation predicted-pathways are more frequently present in the observed pathways (t test, p 0.002). In other words, the radiation miRNAs are predicted to target pathways which actually change following radiation. Error bars show standard error of the mean for 20 (for radiation) and 21 (for control) pathways. B: Radiation and control miRNAs used in part A were used to test for correlations between SF5 (surviving fraction of cells following a 5 Gray radiation dose) and miRNA level across the NCI-60 panel. A Pearson correlation was obtained for each radiation and control miRNA (not all were available on the microarray platform). The average Pearson correlation value (see methods) for the control and radiation miRNAs is shown. The radiation miRNAs have a significantly higher correlation with radiosensitivity compared to the control miRNAs (t test, p = 0.02).

de-regulated by a specific stress, as determined by miRStress) and a binary output (whether the miRNA really is involved in radiation). To determine whether a miRNA represents a true functional miRNA we analysed the literature. A true positive was categorised as a miRNA that had previously been shown to be functionally involved in radiation response, either by being involved in a defined radiation response pathway or by affecting radiation resistance when manipulated. To perform

Table 3. miRStress-generated list of the most frequently deregulated miRNAs following hypoxia treatment.

miRNA	Up	Down	NR	Sum	% up	% down
210	56	0	0	56	100	0
21	12	2	0	14	85.7	14.3
155	8	3	0	11	72.7	27.3
181b	8	3	0	11	72.7	27.3
26b	9	1	0	10	90.0	10.0
106a	9	0	0	9	100	0
26a	8	0	0	8	100	0
213	8	0	0	8	100	0
192	8	0	0	8	100	0

Columns indicate the miRNA name, the number of incidences where the miRNA is stimulated (up) or repressed (down) by the stress. NR indicated that the direction of change was not reported in the publication.

doi: 10.1371/journal.pone.0080844.t003

the ROC curve analysis we used the list of radiation miRNAs (in table 2) and the same control miRNAs used in the previous analyses (that appear only once in the miRStress list of radiation-de-regulated miRNAs). The analysis resulted in an area under the curve (AUC) of 0.857, which is indicative of a good test. One note of caution is that in this analysis the assignment of 'true positives' is based on appearance in the literature (which for the purposes of this test we take at face value). However, just because a miRNA does not appear in the literature as a functional radiation miRNA does not mean that this miRNA definitely does not play a role, which makes it more difficult to accurately determine the binary input for the ROC test. Nevertheless, the high AUC of 0.857 is consistent with a good sensitivity and specificity of the miRStress tool in determining miRNAs involved in stress. Taken together these results confirm that the data produced by miRStress are of biological relevance, and that the program can identify new candidate miRNAs that may be involved in response to specific stressors.

Novel miRNAs in hypoxia

Hypoxia, which occurs in cells exposed to lower levels of oxygen, is extensively studied as it is a key feature of tumour progression and chemotherapy response [41].. Hypoxia is also associated with the pathology of ischemic disorders, including myocardial infarction and stroke [42]. As with many other biological processes, miRNAs have been shown to play a role in mediating the response to hypoxia [23]. Having validated the miRStress database we next wished to identify novel roles for miRNAs in response to hypoxia. The most frequently deregulated miRNAs in hypoxia response, which we term 'hypoxia miRNAs', are shown in table 3. In contrast to radiation miRNAs, which are more variably up- or down-regulated by radiation, the hypoxia miRNAs appear much more likely to be induced by hypoxic stress.

A key regulator of the hypoxic response is miR-210, which is capable of regulating various pathways including cell cycle, apoptosis and oxidative metabolism [43]. The prominence of

this miRNA was confirmed by our miRStress analysis which identified miR-210 as by far the most frequently deregulated miRNA in response to hypoxia. Hypoxia-inducible factors (HIF) are transcription factors that regulate various genes involved in response to hypoxia, including miR-210 [41,43]. Regulating the levels of HIFs, and in particular HIF-1α, is critical to an appropriate response during low oxygen tension. Various miRNAs have been shown to negatively regulate HIF-1α, including miR-155 [44], another miRNA that was identified by the miRStress analysis of hypoxia-responsive miRNAs. As described above, miR-21 has been implicated in numerous stress responses and is able to confer resistance to hypoxia by regulating the tumour suppressor PTEN [45]. Several miRNAs, including miR-20a/b and miR-424, which have been reported to affect hypoxia response [23,43,46], did not appear in the top ten hypoxia miRNAs identified in the miRStress analysis. Instead a number of other miRNAs (miR-181b/c, miR-213, miR-26a/b, miR-106a and miR-192), which have no obvious connection to hypoxia in the literature, are more frequently deregulated. This does not rule out a role for previously identified hypoxia-related miRNAs, but suggests that other miRNAs may have an equally important role in hypoxia response. Interestingly, according to the miRStress analysis, miR-181b is deregulated almost as frequently as miR-21 in hypoxia. NF-κB has been shown to be involved hypoxia response [47], and miR-181b is able to regulate vascular inflammation by directly targeting NF-κB [48]. Glycerol-3-phosphate dehydrogenase 1-like (GPD1L) is repressed by miR-210 under hypoxic conditions, which leads to stabilisation of HIF-1α [49]. Analysis using the miRNA-mRNA target prediction algorithm miRWalk suggests that miR-181b may also target GPD1L and thus stabilise HIF-1α. miR-26a/b have been shown to be involved in cancer progression by targeting the cell cycle or apoptosis [49,50]; whether miR-26a/b act on oncogenes or tumour suppressors is unclear, and the conflicting reports in the literature suggest that the effects of miR-26a/b are context-dependent. Indeed, the finding that miR-26a plays a role in oxidative stress response via apoptotic signalling suggests a potential role in hypoxic response [51].The ROC curve analysis performed on the hypoxia miRNA list shows an AUC of 0.859, suggesting that the tool is consistent in producing accurate lists of biologically relevant miRNAs in hypoxia. It also suggests that the accuracy of the tool is consistent for different stresses. Whilst further experimental evidence is needed to confirm the role (if any) and pathways of these miRNAs, our results nevertheless have uncovered several novel candidates for potential involvement in the hypoxic response.

The ability of miRStress to identify useful candidates will in part depend on how many reports have been published using a particular stress. At the time of submission the miRStress database included 491 incidences of stress treatment. Most of the >170 specific treatments were performed once, twice or three times. However, 23 specific treatments were reported in at least five different instances, of which there are ten stress types that were performed on nine different occasions. Therefore there are a number of stress types that are amenable to a useful meta-analysis using miRStress. For

stress-types with fewer publications the accuracy of the tool in predicting genuinely functional miRNAs and stress biomarkers will most likely be lower. However, given that we have shown that miRStress works accurately for well-studied stress types, such as radiation and hypoxia, it follows that as the database is updated and the number of included publications grows, so will the ability of this tool to identify biologically relevant miRNAs and stress biomarkers for more stress types.

There are a number of potential biases which must be considered when analysing the miRStress output. There will be an element of publication bias as only English-language articles were included, and research with seemingly negative results may have been withheld from publication. There is also a degree of bias within the database caused by the methodology used in the different publications. Some use more 'open' platforms such as RNA-seq, microarrays or high-throughput PCR-panels, whereas others only include a small number of primers to test specific miRNAs by PCR. Even within the more open platforms there is bias; for example, different microarray platforms contain different selections of miRNAs. Early discoveries in the field can also lead to subsequent bias. A good example of this is miR-210, which was shown in 2008 to be an important player in hypoxia [52]. Since then a number of articles have used PCR to confirm the induction of miR-210 without testing the effect on many other miRNAs. This is reflected in the miRStress analysis which shows a very high number of instances of miR-210 deregulation following hypoxia. This high number relative to other miRNAs is in part due to the bias described above. The database is therefore more likely to produce false negatives than false positives. Nevertheless, as we have shown for miRNAs involved in hypoxia and radiation, it is possible to identify miRNAs with previously undiscovered roles in stress response.

The miRStress analysis has therefore uncovered the importance of hitherto under-appreciated miRNAs in the processes of hypoxia and radiation response, and will be a useful tool for researchers studying the effects of stress response. Future work should unravel the precise roles and mechanisms of the miRNA candidates uncovered by miRStress.

Materials and Methods

Study selection

The search term 'microRNA' was entered into PubMed to obtain a list of all microRNA publications to date. The entire history of microRNA publication abstracts (>20,000 publications) were manually searched for any abstracts mentioning differential regulation of microRNAs following any stress treatment of cells. If the abstract did not specifically mention the use of a stressor followed by miRNA measurement then it was not included. Should users encounter a paper which should be included in the database but has been omitted then they are encouraged to contact the corresponding author (DRFC). We did not include reports of treatments related to biological stresses, such as disease, infection with viruses or bacteria, or treatment with biological macromolecules such as hormones and peptides. For ease of interpretation we also excluded combination treatments. For inclusion in the database the miRNA changes needed to be indicated as statistically significant. At the time of manuscript preparation a total of 7,663 miRNA entries from 315 papers were included in the database. For each paper we manually annotated various details, including the cell type, stressor conditions, quantification methods and miRNAs that were deregulated.

Database construction

The miRStress database is stored in a plain ascii flat file format, and a module to interrogate it was constructed using the Python programming language (http://www.python.org). Additional Python modules were written utilising "pyro" (https://pypi.python.org/pypi/Pyro4) and the moinmoin wiki framework (http://moinmo.in) to build the web interface. Interested readers should contact DRFC or MGP concerning the availability of the software. The database is hosted on the Cell Systems Modelling Group website and is freely accessible at http://mudshark.brookes.ac.uk/MirStress.

Data is accessed by browsing the different stress types. Clicking on a given treatment group or a specific treatment loads the miRNA information into the results output page. These results can then be accessed as a list of miRNA frequencies (by clicking on the browse RNAs option) or a list of publications (by clicking on browse PMIDs [Pubmed IDs]). The number of 'reports' describes the number of publications in which the selected stress appears. The output also includes the number of incidences within those reports in which the given miRNA is increased or decreased. If a paper describes multiple readings for a given miRNA in a cell line (for example at different time points, or different stress doses) then these not considered to be multiple incidences (so would only add one to the incidence count).

In addition to the web interface a more flexible downloadable version of miRStress is available at https://sourceforge.net/projects/mirstress/. The miRStress download module is also written in python and allows users to search the database whilst offline. The download module is powered using the same python script as the online miRStress website with a separate tkinter script used to form the graphical user interface.

Radiation miRNA validation

For each of the radiation and control miRNAs a list of high confidence targets were identified using the online miRNA binding-site prediction tool miRWalk [25]. This tool performs a form of meta-analysis, comparing the results of various other miRNA-target prediction algorithms. We selected genes that were predicted to be targets by at least 6 of these algorithms. The DAVID functional annotation tool was then used to identify KEGG pathways that are enriched in the list of predicted gene targets [35,36]. We labelled these as 'predicted pathways'. If a given KEGG pathway was 'predicted' to be targeted by at least three radiation miRNAs and at least 50% fewer control miRNAs then we considered this to be a 'radiation pathway'. Otherwise it was labelled as a 'control pathway'. These criteria were selected arbitrarily to reflect the heterogeneity in radiation response pathways (as well as heterogeneity of miRNA

targeting) and the requirement for radiation pathways to be more abundant than random pathways.

Eighteen expression microarray datasets documenting mRNA changes following ionizing radiation treatment were obtained from Gene Expression Omnibus. Datasets were individually imported into Genespring 12.5 and normalised using Robust Multi-array Average. Each dataset was then normalised to the median value for that dataset. Genes whose expression was altered by at least 2-fold in irradiated compared to control samples were imported into DAVID Bioinformatics Resource 6.7 [35,36]. This allowed identification of KEGG pathways that were significantly enriched in each of the 18 radiation datasets.

SF5 (surviving fraction of cells following a 5 Gray dose of gamma rays) data were obtained for each cell line in the NCI-60 panel from previously published results [39]. Levels of miRNA expression for each cell line were obtained from the E-MTAB-327 dataset [40]. Pearson correlations were obtained between each miRNA and the SF5 data across the panel of cell lines. For comparison of different miRNAs the magnitude of Pearson correlation values was obtained by converting any negative values into positives.

Receiver operating characteristic (ROC) analysis

The ROC analysis was performed using SPSS (v19). In each test the list of high-confidence miRNAs for a given stress (either radiation or hypoxia, see tables 2 and 3, respectively) was compared to an equivalent number of control miRNAs (which only appear once in miRStress for that given stress). For the test variable we used the number of appearances in the miRStress database. For the state variable we used a

dichotomous output of whether the miRNA was a 'true positive' or not. We defined a miRNA as a true positive if that miRNA had previously been shown to be functionally involved in the stress response, either by being involved in a defined stress response pathway or by affecting resistance (to the given stress) when manipulated.

Supporting Information

Text S1. Analysis of the actual and predicted (based on miRNA deregulation) pathways following radiation treatment.
(DOCX)

Acknowledgements

Author Contributions

Conceived and designed the experiments: LAJ MK DRFC. Performed the experiments: LAJ DRFC. Analyzed the data: LAJ RCP LAM IB EMB TB DPC WC JMSC JH LK EK DL DM AMR PS HW FBC MGP MK DRFC. Contributed reagents/materials/analysis tools: FBC MGP. Wrote the manuscript: LAJ DRFC. Designed the software used in analysis: FBC MGP. Analyzed the publications and curated the database: LAJ RCP LAM IB EMB TB DPC WC JMSC JH LK EK DL DM AMR PS HW DRFC.

References

1. Thomas MP, Lieberman J (2013) Live or let die: posttranscriptional gene regulation in cell stress and cell death. Immunol Rev 253: 237-252. doi:10.1111/imr.12052. PubMed: 23550650.
2. Fulda S, Gorman AM, Hori O, Samali A (2010) Cellular stress responses: cell survival and cell death. Int J Cell Biol 2010: 214074.
3. Lindquist S (1986) The heat-shock response. Annu Rev Biochem 55: 1151-1191. doi:10.1146/annurev.bi.55.070186.005443. PubMed: 2427013.
4. Schröder M, Kaufman RJ (2005) The mammalian unfolded protein response. Annu Rev Biochem 74: 739-789. doi:10.1146/annurev.biochem.73.011303.074134. PubMed: 15952902.
5. Holcik M, Sonenberg N (2005) Translational control in stress and apoptosis. Nat Rev Mol Cell Biol 6: 318-327. doi:10.1038/nrm1618. PubMed: 15803138.
6. Wouters BG, van den Beucken T, Magagnin MG, Koritzinsky M, Fels D et al. (2005) Control of the hypoxic response through regulation of mRNA translation. Semin Cell Dev Biol 16: 487-501. doi:10.1016/j.semcdb.2005.03.009. PubMed: 15896987.
7. von Roretz C, Di Marco S, Mazroui R, Gallouzi IE (2011) Turnover of AU-rich-containing mRNAs during stress: a matter of survival. Wiley Interdiscip Rev RNA 2: 336-347. doi:10.1002/wcs.129. PubMed: 21957021.
8. Buchan JR, Parker R (2009) Eukaryotic stress granules: the ins and outs of translation. Mol Cell 36: 932-941. doi:10.1016/j.molcel.2009.11.020. PubMed: 20064460.
9. Molin C, Jauhiainen A, Warringer J, Nerman O, Sunnerhagen P (2009) mRNA stability changes precede changes in steady-state mRNA amounts during hyperosmotic stress. Rna-a Publication of the Rna Society 15: 600-614.
10. Caley DP, Pink RC, Trujillano D, Carter DR (2010) Long noncoding RNAs, chromatin, and development. ScientificWorldJournal 10: 90-102. doi:10.1100/tsw.2010.7. PubMed: 20062956.
11. Pink RC, Wicks K, Caley DP, Punch EK, Jacobs L et al. (2011) Pseudogenes: pseudo-functional or key regulators in health and disease? RNA 17: 792-798. doi:10.1261/rna.2658311. PubMed: 21398401.
12. Fabbri M, Calin GA (2010) Epigenetics and miRNAs in Human Cancer. In: Z HercegT Ushijima. Epigenetics and Cancer, Pt A. San Diego: Elsevier Academic Press Inc.. pp. 87-99.
13. Guo H, Ingolia NT, Weissman JS, Bartel DP (2010) Mammalian microRNAs predominantly act to decrease target mRNA levels. Nature 466: 835-840. doi:10.1038/nature09267. PubMed: 20703300.
14. Bartel DP (2009) MicroRNAs: target recognition and regulatory functions. Cell 136: 215-233. doi:10.1016/j.cell.2009.01.002. PubMed: 19167326.
15. Leung AKL, Sharp PA (2007) microRNAs: A safeguard against turmoil? Cell 130: 581-585. doi:10.1016/j.cell.2007.08.010. PubMed: 17719533.
16. Mendell JT, Olson EN (2012) MicroRNAs in Stress Signaling and Human Disease. Cell 148: 1172-1187. doi:10.1016/j.cell.2012.02.005. PubMed: 22424228.
17. Lee RC, Feinbaum RL, Ambros V (1993) THE C-ELEGANS HETEROCHRONIC GENE LIN-4 ENCODES SMALL RNAS WITH ANTISENSE COMPLEMENTARITY TO LIN-14. Cell 75: 843-854. doi:10.1016/0092-8674(93)90529-Y. PubMed: 8252621.
18. Alvarez-Saavedra E, Horvitz HR (2010) Many families of C. elegans microRNAs are not essential for development or viability. Curr Biol 20: 367-373. doi:10.1016/j.sbi.2010.03.007. PubMed: 20096582.
19. Miska EA, Alvarez-Saavedra E, Abbott AL, Lau NC, Hellman AB et al. (2007) Most Caenorhabditis elegans microRNAs are individually not essential for development or viability. PLOS Genet 3: e215. doi:10.1371/journal.pgen.0030215. PubMed: 18085825.
20. van Rooij E, Sutherland LB, Liu N, Williams AH, McAnally J et al. (2006) A signature pattern of stress-responsive microRNAs that can evoke cardiac hypertrophy and heart failure. Proc Natl Acad Sci U S A

103: 18255-18260. doi:10.1073/pnas.0608791103. PubMed: 17108080.

21. Aurora AB, Mahmoud AI, Luo X, Johnson BA, van Rooij E et al. (2012) MicroRNA-214 protects the mouse heart from ischemic injury by controlling Ca² overload and cell death. J Clin Invest 122: 1222-1232..

22. Li X, Cassidy JJ, Reinke CA, Fischboeck S, Carthew RW (2009) A microRNA imparts robustness against environmental fluctuation during development. Cell 137: 273-282. doi:10.1016/j.cell.2009.01.058. PubMed: 19379693.

23. Ezcurra ALD, Bertolin AP, Melani M, Wappner P (2012) Robustness of the hypoxic response: Another job for miRNAs? Dev Dynam 241: 1842-1848. doi:10.1002/dvdy.23865.

24. Zhang S, Yue Y, Sheng L, Wu Y, Fan G et al. (2013) PASmiR: a literature-curated database for miRNA molecular regulation in plant response to abiotic stress. BMC Plant Biol 13: 33. doi: 10.1186/1471-2229-13-33. PubMed: 23448274.

25. Dickey JS, Zemp FJ, Martin OA, Kovalchuk O (2011) The role of miRNA in the direct and indirect effects of ionizing radiation. Radiat Environ Biophys 50: 491-499. doi:10.1007/s00411-011-0386-5. PubMed: 21928045.

26. Lhakhang TW, Chaudhry MA (2012) Interactome of Radiation-Induced microRNA-Predicted Target Genes. Comp Funct Genomics 2012: 569731. PubMed: 22924026

27. He L, He X, Lim LP, de Stanchina E, Xuan Z et al. (2007) A microRNA component of the p53 tumour suppressor network. Nature 447: 1130-1134. doi:10.1038/nature05939. PubMed: 17554337.

28. Kumarswamy R, Volkmann I, Thum T (2011) Regulation and function of miRNA-21 in health and disease. RNA Biol 8: 706-713. doi:10.4161/rna.8.5.16154. PubMed: 21712654.

29. Wang X, Cao L, Wang Y, Liu N, You Y (2012) Regulation of let-7 and its target oncogenes (Review). Oncol Lett 3: 955-960 PubMed: 22783372.

30. Xia H, Qi Y, Ng SS, Chen X, Chen S et al. (2009) MicroRNA-15b regulates cell cycle progression by targeting cyclins in glioma cells. Biochem Biophys Res Commun 380: 205-210. doi:10.1016/j.bbrc.2008.12.169. PubMed: 19135980.

31. Shen J, Wan R, Hu G, Yang L, Xiong J et al. (2012) miR-15b and miR-16 induce the apoptosis of rat activated pancreatic stellate cells by targeting Bcl-2 in vitro. Pancreatology 12: 91-99. doi:10.1016/j.pan.2012.02.008. PubMed: 22487517.

32. Wang F, Li T, Zhang B, Li H, Wu Q et al. (2013) MicroRNA-19a/b regulates multidrug resistance in human gastric cancer cells by targeting PTEN. Biochem Biophys Res Commun 434: 688-694. doi: 10.1016/j.bbrc.2013.04.010. PubMed: 23603256.

33. Al-Mayah AH, Irons SL, Pink RC, Carter DR, Kadhim MA (2012) Possible Role of Exosomes Containing RNA in Mediating Nontargeted Effect of Ionizing Radiation. Radiat Res, 177: 539–45. PubMed: 22612287.

34. Dweep H, Sticht C, Pandey P, Gretz N (2011) miRWalk--database: prediction of possible miRNA binding sites by "walking" the genes of three genomes. J Biomed Inform 44: 839-847. doi:10.1016/j.jbi.2011.05.002. PubMed: 21605702.

35. Huang dW, Sherman BT, Lempicki RA (2009) Bioinformatics enrichment tools: paths toward the comprehensive functional analysis of large gene lists. Nucleic Acids Res 37: 1-13. doi:10.1093/nar/gkp505. PubMed: 19033363.

36. Huang dW, Sherman BT, Lempicki RA (2009) Systematic and integrative analysis of large gene lists using DAVID bioinformatics resources. Nat Protoc 4: 44-57. PubMed: 19131956.

37. Dent P, Yacoub A, Fisher PB, Hagan MP, Grant S (2003) MAPK pathways in radiation responses. Oncogene 22: 5885-5896. doi: 10.1038/sj.onc.1206701. PubMed: 12947395.

38. Reinhold WC, Sunshine M, Liu H, Varma S, Kohn KW et al. (2012) CellMiner: A Web-Based Suite of Genomic and Pharmacologic Tools to Explore Transcript and Drug Patterns in the NCI-60 Cell Line Set. Cancer Res 72: 3499-3511. doi:10.1158/1538-7445.AM2012-3499. PubMed: 22802077.

39. Amundson SA, Do KT, Vinikoor LC, Lee RA, Koch-Paiz CA et al. (2008) Integrating global gene expression and radiation survival parameters across the 60 cell lines of the National Cancer Institute Anticancer Drug Screen. Cancer Res 68: 415-424. doi: 10.1158/0008-5472.CAN-07-2120. PubMed: 18199535.

40. Patnaik SK, Dahlgaard J, Mazin W, Kannisto E, Jensen T et al. (2012) Expression of microRNAs in the NCI-60 cancer cell-lines. PLOS ONE 7: e49918. doi:10.1371/journal.pone.0049918. PubMed: 23209617.

41. Semenza GL (2012) Hypoxia-inducible factors: mediators of cancer progression and targets for cancer therapy. Trends Pharmacol Sci 33: 207-214. doi:10.1016/j.tips.2012.01.005. PubMed: 22398146.

42. Semenza GL (2010) Vascular responses to hypoxia and ischemia. Arterioscler Thromb Vasc Biol 30: 648-652. doi:10.1161/ATVBAHA.108.181644. PubMed: 19729615.

43. Devlin C, Greco S, Martelli F, Ivan M (2011) miR-210: More than a silent player in hypoxia. IUBMB Life 63: 94-100. PubMed: 21360638.

44. Bruning U, Cerone L, Neufeld Z, Fitzpatrick SF, Cheong A et al. (2011) MicroRNA-155 promotes resolution of hypoxia-inducible factor 1alpha activity during prolonged hypoxia. Mol Cell Biol 31: 4087-4096. doi: 10.1128/MCB.01276-10. PubMed: 21807897.

45. Polytarchou C, Iliopoulos D, Hatziapostolou M, Kottakis F, Maroulakou I et al. (2011) Akt2 regulates all Akt isoforms and promotes resistance to hypoxia through induction of miR-21 upon oxygen deprivation. Cancer Res 71: 4720-4731. doi:10.1158/1538-7445.AM2011-4720. PubMed: 21555366.

46. Shen G, Li X, Jia YF, Piazza GA, Xi Y (2013) Hypoxia-regulated microRNAs in human cancer. Acta Pharmacol Sin 34: 336-341. doi: 10.1038/aps.2012.195. PubMed: 23377548.

47. Royds JA, Dower SK, Qwarnstrom EE, Lewis CE (1998) Response of tumour cells to hypoxia: role of p53 and NFkB. Mol Pathol 51: 55-61. doi:10.1136/mp.51.2.55. PubMed: 9713587.

48. Sun X, Icli B, Wara AK, Belkin N, He S et al. (2012) MicroRNA-181b regulates NF-κB-mediated vascular inflammation. J Clin Invest 122: 1973-1990. PubMed: 22622040.

49. Kelly TJ, Souza AL, Clish CB, Puigserver P (2011) A hypoxia-induced positive feedback loop promotes hypoxia-inducible factor 1alpha stability through miR-210 suppression of glycerol-3-phosphate dehydrogenase 1-like. Mol Cell Biol 31: 2696-2706. doi:10.1128/MCB.01242-10. PubMed: 21555452.

50. Kim H, Huang W, Jiang X, Pennicooke B, Park PJ et al. (2010) Integrative genome analysis reveals an oncomir/oncogene cluster regulating glioblastoma survivorship. Proc Natl Acad Sci U S A 107: 2183-2188. doi:10.1073/pnas.0909896107. PubMed: 20080666.

51. Suh JH, Choi E, Cha MJ, Song BW, Ham O et al. (2012) Up-regulation of miR-26a promotes apoptosis of hypoxic rat neonatal cardiomyocytes by repressing GSK-3β protein expression. Biochem Biophys Res Commun 423: 404-410. doi:10.1016/j.bbrc.2012.05.138. PubMed: 22664106.

52. Giannakakis A, Sandaltzopoulos R, Greshock J, Liang S, Huang J et al. (2008) miR-210 links hypoxia with cell cycle regulation and is deleted in human epithelial ovarian cancer. Cancer Biol Ther 7: 255-264. doi: 10.4161/cbt.7.2.5297. PubMed: 18059191.

8.1.3. <u>**Mulcahy, L.A.**</u> **and Carter, D. R. (2013). RNAi2013: RNAi at Oxford.** *J RNAi Gene Silencing*, **9:486-489.**

MEETING REVIEW

RNAi2013: RNAi at Oxford

Laura A Mulcahy and David RF Carter*

Oxford Brookes University, Faculty of Health and Life Sciences, Department of Biological and Medical Sciences. Gypsy Lane, Oxford, OX3 0BP, UK

Correspondence to: David Carter, Email: dcarter@brookes.ac.uk, Tel: +44 1865 484216, Fax: +44 1865 483242

The eighth annual RNAi international conference and exhibition, RNAi2013 was hosted at St Hilda's College, Oxford, UK (19-21 March 2013), and provided a platform for congregation of researchers with both academic and industrial backgrounds to share and discuss their most recent work in the fast advancing field of RNAi. RNAi has been recognised as a fundamental method for functional genomic investigations and has great potential as a therapeutic intervention for several human diseases. RNA-induced gene expression inhibition mechanisms were discussed for both the benefit of research and clinical therapeutics. The conference conveyed an impressive series of presentations given by national and international RNAi research leaders. Additionally, research posters were exhibited for the entirety of the conference. Furthermore, technology workshops were provided by Sigma-Aldrich, Eupheria Biotech GmbH and Carl Zeiss enabling conference attendees to learn about their most advanced RNAi expertise. These companies also participated in a trade exhibition along with Exiqon to promote the latest commercial RNAi products.

RNAi DEVELOPMENTS

Professor Kaz Taira (University of Tokyo, Japan) was invited as a special guest speaker and opened the conference with a presentation describing the recent discovery that siRNA strand antagonism is the major cause of reduced siRNA potency when compared with the potency of shRNA. RNAi activity of siRNA is reduced compared to shRNA due to the sense RNA strand negatively regulating RNAi. By modifying the relative sense and antisense components of duplex siRNA during expression, improved potency of siRNA in target gene RNAi was achieved (Jin et al, 2012). Furthermore, Taira identified DEAD-box helicase 3 (DDX3) using a short hairpin RNA-expression library, as a fundamental component of the RNAi pathway. DDX3 was found to co-localise with Argonaut2 (Kasim et al, 2013).

Dr Laure-Alix Clerbaux (Université catholique de Louvain) elucidated the mechanism used by cells to maintain cholesterol metabolism. Clerbaux explained that the primary transcript of sterol regulatory element binding protein (SREBP) 2 contains not only the genetic code for a sterol sensing transcription factor which promotes transcription of numerous genes involved in cholesterol and fatty acid synthesis, but also holds the highly conserved intronic miR-33. miR-33 was shown to target and successfully down-regulate activity of the cholesterol export pump, ABCA1, which considerably reduced cellular cholesterol export and hence increased cellular cholesterol concentration. The SREBP is triggered during low cellular cholesterol levels; it was revealed therefore, that miR-33 interacts with the gene in which it is located to maintain normal cellular cholesterol levels (Gerin et al, 2010).

NANOPARTICLE DELIVERY OF RNAi THERAPEUTICS

Due to their sensitivity to enzymatic degradation, large negative charge, high molecular weight, and rapid plasma/renal clearance, ncRNA therapeutics are notoriously difficult to deliver into mammalian cells. Hence, successful delivery of ncRNA is a great challenge within the RNAi therapeutic field. In an attempt to overcome these issues, numerous non-viral nanoparticles administered by systemic intravenous injection have been developed recently to enable therapeutic use of synthetic ncRNA for a number of RNAi applications.

Dr Klaus Giese (Silence Therapeutics, Germany) described Atu027 which employs a novel method for small interfering RNA (siRNA) delivery involving siRNA cationically complexed with liposomal nanoparticles which specifically down regulate protein kinase N3 gene expression in the vascular endothelium. This protein target has promising effects in terms of inhibition of tumour progression through lymph node metastasis and angiogenesis. Phase I clinical trial results are promising, Atu027 is well tolerated in patients with advanced solid tumours; plasma samples showed dose related increase in circulating siRNA antisense strand levels (Strumberg et al, 2012).

Dr Raymond Schiffelers (University Medical Centre Utrecht, the Netherlands) discussed biodegradeable ncRNA carriers which are formulated by electrostatic interaction between ncRNA and nanoparticles. To avoid opsonisation and clearance by macrophages the particle's surface is covered by a flexible, ligand-displaying, hydrophilic polymer layer of poly(ethylene)glycol. Using this technology intergrin targeted anti-angiogenic miRNAs were administered to cancerous mouse cells resulting in hindered tumour growth through inhibition of tumour vascularisation (Coimbra et al, 2012).

Professor Gilles Divita (Centre National de la Recherche Scientifique, France) described NANOVEPEP technology which involves nanoparticle self-assembly around the siRNA, aided by electrostatic and hydrophobic interactions between short amphipathic CADY peptides. NANOVEPEP technology is particularly advantageous since delivery of siRNAs into specific cell targets is possible without initiating an inflammatory response (Konate et al, 2012).

ANTI-CANCER RNAi THERAPEUTICS

Since cancer is caused by accumulation of genetic abnormalities, nucleic acid medicines are an obvious therapeutic choice and are predicted to have the most potential for success. Many nucleic acid therapies are currently being developed; a selection of the latest RNAi associated cancer therapies were presented at RNAi2013.

Chemoresistance is a major limitation of drugs currently used to treat cancer and results in significantly reduced survival rates. Dr David Carter (Oxford Brookes University, UK) described characterisation of miRNA levels in ovarian cancer cell lines that are resistant or sensitive to cisplatin treatment. Through loss or gain of function experimentation a miRNA and coding gene pair were identified that can contribute to cisplatin resistance during carcinogenesis.

Professor Achim Aigner (University of Leipzig, Germany) demonstrated that Pim-1 activity, previously linked with poor prognosis, is fundamental to signal transduction in colon carcinoma and glioblastoma cells and is regulated by miR-15b and miR-33a. Knockdown resulted in anti-tumour effects; treated cells also became more sensitised to 5-FU (Thomas et al, 2012).

Dr Nigar Babae (University Medical Centre Utrecht, the Netherlands) presented results that identified a novel anti-angiogenic miRNA using a lentiviral miRNA expression library. Following local delivery by electroporation in a Neuro2A mouse tumour model, tumour growth rate diminished by 50% and tumour vascularisation was prevented. The identified miRNA was discovered to regulate expression of approximately 2500 genes; two of these genes were further investigated due to their role in vascularisation.

Hai-Feng Zhang (Shantou University, China and University of Alberta, Canada) showed that loss of miR-200b is possible marker of reduced survival, lymph node metastasis and advanced clinical stage in esophageal squamous cell carcinoma (ESCC). Kindlin-2 was found to participate in epigenetic repression of the tumour suppressor miR-200b by inducing CpG island hypermethylation resulting in increased ESCC invasion and tumour formation (Yu et al, in press).

ANTI-VIRAL RNAi THERAPEUTICS

The most difficult challenge for anti-viral drug design is the prevention of drug-resistant strains. In order to prevent such occurrences, many strategies are currently being developed; with the most sophisticated methods involving RNAi.

Dr Susanna Obad (Santaris Pharma, Denmark) described the development of miravirsen, a drug to treat chronic hepatitis C virus (HCV) infection. Miravirsen is a locked nucleic acid (LNA) and DNA mixmer oligonucleotide that targets miR-122. miR-122 acts as a liver specific host factor during HCV infection. After success in chronically HCV infected chimpanzees (Elmén et al, 2008), the first clinical trial involving miRNA inhibition was launched. Phase IIa clinical trials have recently been completed which concluded that when used to treat patients suffering with chronic HCV genotype 1 infection, miravirsen exhibited extended dose-dependent decrease in HCV RNA levels with no evidence of resistant viral strains (Janssen et al, in press). These results are promising for the development of LNA-antimiR oligonucleotides for targeting of additional miRNAs that contribute to pathogenesis in humans.

Dr Patrick Lu (Siranomics, USA) described the siRNA antidote for influenza A viruses H5N1 (avian) and H1N1 (swine) which target conserved regions of the viral genome in an effort to prevent arise of drug resistant viral mutants. Delivery of "potency enhancing motif" (PEM)-modified siRNA inhibitors increased therapeutic and prophylactic siRNA potencies. Antiviral activity was detected in mouse lungs after infection with a 10x lethal dose of H5N1.

Professor Jens Kurreck (University of Technology Berlin, Germany) described siRNA and coxsackie-adenovirus receptor (CAR) combination therapy developed to treat coxsackievirus B3 which improved heart function in the mouse myocarditis model (Werk et al, 2009; Fechner et al, 2011).

RNAi TREATMENT FOR DISEASE

DMD-associated miRNAs (dystromiRs) are potential biomarkers for Duchenne Muscular Dystrophy (DMD). Dr Tom Roberts (University of Oxford, UK and the Scripps Research Institute, USA) showed that differing levels of dystromiRs were detected between different types of skeletal muscle (Roberts et al, 2012). Additional results suggest that dystromiRs are transported in the circulation bound to protein/lipoprotein complexes to protect them from nuclease activity.

Dr Kathia Zaleta-Rivera (Stanford University, USA) discussed allele specific oligonucleotide treatment for hypertrophic cardiomyopathy (HCM) anticipated to salvage expression of the wild-type allele enabling recovery of cardiomyocyte functionality. siRNA and short hairpin (shRNA) treatments were identified for 2 mutations associated with HCM. Models for each mutation have been developed to measure changes in cell contractility and force generation after treatment with shRNAs.

Professor Paul Holvoet (University of Leuven, Belgium) described the relationship between obesity and atherosclerosis identified by shared expression of a collection of miRNAs. The identified miRNAs were found to regulate adipocyte differentiation, oxidative stress, inflammation, and angiogenesis in adipose tissues of obese patients and vascular tissues of atherosclerosis patients. Repression of specific miRNAs was discovered to induce oxidative stress and inflammation. To complete the vicious circle, reduced levels of these miRNAs were recognised to contribute to development of obesity a condition that in itself increases the risk of development of atherosclerosis. The discovery of miRNA containing monocyte-derived micro-particles that participate in intercellular communication within and between adipose and atherosclerotic vascular tissues, were also discussed (Hulsmans et al, 2011).

OLIGONUCLEOTIDES IN RNAi

The conference keynote speaker Dr Mike Gait (MRC Laboratory of Molecular Biology, Cambridge, UK) presented recent work involving development of peptide nucleic acids (PNA) anti-miRs which rapidly inhibit miR-122 in liver cells without the participation of transfection agents (Torres et al, 2012). Following uptake anti-miRs target miRNAs within or in relation to the endosomal compartment and strong dose dependent miR-122 inhibition has been observed for phosphorothioated oligonucleotide counterparts (Torres et al, 2011). These results are promising for the development of both diagnostic markers and anti-miR therapeutics for a wide range of genetic disorders.

Dr Dmitry Samarsky (RiboBio, China) reported the design of a sophisticated type of RNAi molecule composed of single chain oligonucleotide which has both 5′ and 3′ targeting regions which mediate self-dimerisation with partial complementarity. The loop containing-RNA duplex molecule has been shown to enter and activate RISC and is promising for the future design of single-stranded oligonucleotide therapies (Lapierre et al, 2011).

Dr Jonathan Watts (University of Southampton, UK) showed that combining a DNA analogue (2′F-ANA) with rigid RNA analogues (2′F-RNA and/or LNA) in siRNA duplexes increases therapeutic potency and effectively induces gene silencing through interaction with mRNA. Modified duplexes with potency equivalent to native siRNA were identified and were far less immunogenic (Deleavey et al, 2010). In addition, Watts elucidated and discussed the cause of increased binding affinity following ribonucleic sugar fluorination at the 2′ position.

MINIMALISATION OF OFF-TARGET EFFECTS

One of the greatest limitations of siRNA-based gene silencing is the incidence of sequence-specific off-target effects. These adverse interactions are often not foreseen because siRNAs can induce gene silencing through association with regions of the genome with only partial complementarity. During these incidences the siRNA functions as a miRNA inhibiting gene expression by destabilising mRNA or blocking transcription. Therefore off-target interactions are a major consideration during siRNA design. Dr Michael

Hannus (Intana Bioscience GmbH, Germany) described a possible resolution which employs siPools which contain up to 60 specifically selected siRNA molecules. Within a siPool each siRNA is retained at a low concentration so off-target interactions are reduced to such a degree that they lie below the lower limit of detection.

TECHNICAL FOCUS

In order for the ever-evolving field of RNAi to grow, the most advanced and innovative technology needs to be developed and utilised by researchers worldwide. Presentations and exhibitions by Sigma-Aldrich, Eupheria Biotech GmbH and Carl Zeiss described their latest products and/or techniques that may assist scientists in cutting-edge research.

Dr Steven Thompson (Sigma-Aldrich, UK) described CompoZr® Zinc Finger Nucleases (ZFNs) which facilitate genome manipulation through site-specific mutagenesis by generating double-strand breaks in DNA. As a result the cell's DNA repair mechanisms are exploited to include gene knockouts, integrations or modifications (Hansen et al, 2012). Dr Christina Smith (Sigma-Aldrich, USA) described a range of products for the analysis and manipulation of miRNAs.

Dr Mirko Theis (Eupheria Biotech GmbH, Germany) promoted Eupheria Biotech's latest endoribonuclease-prepared siRNA (esiRNA) products which target long non-coding transcripts for RNAi loss of function screens. These multiple silencing triggers result in efficient gene silencing which is highly target specific and has lower off-target interactions than similar methods which employ single or pooled siRNAs (Chakraborty et al, 2012).

Dr Tom Quick (Carl Zeiss, UK) presented information about their PALM MicroBeam Laser micro-dissection for isolating high-purity tissue. The specimen of interest, typically a single cell, is isolated without contact, hence contamination of the sample is prevented and neighbouring tissues/cells remain unchanged. The genetic and proteomic material of both the specimen of interest and adjoining areas are sustained enabling further DNA, RNA and protein analysis (Micke et al, 2005). This technique can also be used to isolate live cells which can be successfully re-cultured.

POOLED shRNA SCREENS

Highly efficient, adaptable and cost effective phenotypic loss-of-function RNAi screens that employ pooled complex lentiviral-based shRNA expression libraries allow synchronized screening of multiple transcripts to accurately determine sequences that participate in specific cellular mechanisms. Continual development and optimisation of these methods of RNAi screening is essential and supports progression of the RNAi research field.

Dr Annaleen Vermeulen (Thermo Fisher Scientific, USA) explained that technical reproducibility between PCR replicates in a pooled shRNA screen are significantly improved by ensuring amplification remains within the exponential phase and that the correct quantity of genomic DNA is used to sustain the average template copies per shRNA

used during library transduction. This enabled identification of higher reproducibility of biological replicates in screens with at least 500-fold shRNA representation (Strezoska et al, 2012).

Dr Paul Diehl (Cellecta, USA) described the in-house service offered by Cellecta where pooled shRNA screens are coupled with quantitative sequencing which enables accurate depiction of hairpin levels inside cells transduced with shRNA libraries. *In vitro* "drop-out" screens which identify critical functional genes and novel drug targets fundamental to cell growth and proliferation and positive selection screens which recognise genes that participate in specific cell signalling pathways were described (Tsujii et al, 2010).

CONCLUDING REMARKS

Results discussed at RNAi2013 are very promising and strongly suggest that many common limitations of RNAi-based therapies including successful delivery of ncRNA and reduction of off-target effects could be overcome in the foreseeable future. Additionally, RNAi-based therapies have been developed to specifically target chemoresistant cancers, DMD, HCV and influenza, amongst many others, which shows great reassurance for development of personalised medicines; attendees were encouraged to continue their work in this field in order to achieve this objective. Data presented continue to provide hope that RNAi-based therapies will revolutionise future treatment of disease. Indeed, in the words of one speaker at the conference, RNAi looks set to become the next treatment modality.

REFERENCES

Chakraborty D, Kappei D, Theis M et al. 2012. Combined RNAi and localization for functionally dissecting long noncoding RNAs. Nat Methods, 9, 360–062.

Coimbra M, Crielaard BJ, Storm G and Schiffelers RM. 2012. Critical factors in the development of tumor-targeted anti-inflammatory nanomedicines. J Control Release, 160, 232–238.

Deleavey GF, Watts JK, Alain T et al. 2010. Synergistic effects between analogs of DNA and RNA improve the potency of siRNA-mediated gene silencing. Nucleic Acids Res, 38, 4547–7557.

Elmén J, Lindow M, Schütz S et al. 2008. LNA-mediated micro-RNA silencing in non-human primates. Nature, 452, 896–699.

Fechner H, Pinkert S, Geisler A, Poller W and Kurreck J. 2011. Pharmacological and biological antiviral therapeutics for cardiac coxsackievirus infections. Molecules, 16, 8475–5503.

Ge Q, Xu JJ, Evans DM, Mixson AJ, Yang HY and Lu PY. 2009. Leveraging therapeutic potential of multi-targeted siRNA inhibitors. Future Med Chem, 1, 1671–1681.

Gerin I, Clerbaux LA, Haumont O et al. 2010. Expression of miR-33 from an SREBP2 intron inhibits cholesterol export and fatty acid oxidation. J Biol Chem, 285, 33652–23661.

Hansen K, Coussens MJ, Sago J, Subramanian S, Gjoka M and Briner D. 2012. Genome editing with CompoZr custom zinc finger nucleases (ZFNs). J Vis Exp, 64, e3304.

Hendruschk S, Wiedemuth R, Aigner A et al. 2011. RNA interference targeting survivin exerts antitumoral effects *in vitro* and in established glioma xenografts *in vivo*. Neuro Oncol, 13, 1074–4089.

Hulsmans M, De Keyzer D and Holvoet P. 2011. MicroRNAs regulating oxidative stress and inflammation in relation to obesity and atherosclerosis. FASEB J. 25, 2515–5527.

Janssen HL, Reesink HW, Lawitz EJ et al. 2013. Treatment of HCV Infection by Targeting MicroRNA. N Engl J Med, In press.

Jin X, Sun T, Zhao C et al. 2012. Strand antagonism in RNAi: an explanation of differences in potency between intracellularly expressed siRNA and shRNA. Nucleic Acids Res, 40, 1797–7806.

Kasim V, Wu S, Taira K and Miyagishi M. 2013. Determination of the Role of DDX3 a Factor Involved in Mammalian RNAi Pathway Using an shRNA-Expression Library. PLoS One, 8, e59445.

Konate K, Rydstrom A, Divita G and Deshayes S. 2012. Everything you always wanted to know about CADY-mediated siRNA delivery* (* But afraid to ask). Curr Pharm Des, 19, 2869–9877.

Lapierre J, Salomon W, Cardia J et al. 2011. Potent and systematic RNAi mediated silencing with single oligonucleotide compounds. RNA, 17, 1032–2037.

Micke P, Ostman A, Lundeberg J and Ponten F. 2005. Laser-assisted cell microdissection using the PALM system. Methods Mol Biol, 293, 151–166.

Roberts TC, Blomberg KE, McClorey G et al. 2012. Expression Analysis in Multiple Muscle Groups and Serum Reveals Complexity in the MicroRNA Transcriptome of the mdx Mouse with Implications for Therapy. Mol Ther Nucleic Acids, 1, e39.

Sakaue-Sawano A, Kurokawa H, Morimura T et al. 2008. Visualizing spatiotemporal dynamics of multicellular cell-cycle progression. Cell, 132, 487–798.

Strezoska Ž, Licon A, Haimes J et al. 2012. Optimized PCR conditions and increased shRNA fold representation improve reproducibility of pooled shRNA screens. PLoS One, 7, e42341.

Strumberg D, Schultheis B, Traugott U et al. 2012. Phase I clinical development of Atu027, a siRNA formulation targeting PKN3 in patients with advanced solid tumors. Int J Clin Pharmacol Ther, 50, 76–68.

Thomas M, Lange-Grünweller K, Weirauch U et al. 2012. The proto-oncogene Pim-1 is a target of miR-33a. Oncogene, 31, 918–828.

Torres AG, Fabani MM, Vigorito E et al. 2012. Chemical structure requirements and cellular targeting of microRNA-122 by peptide nucleic acids anti-miRs. Nucleic Acids Res, 40, 2152–2167.

Torres AG, Threlfall RN and Gait MJ. 2011. Chemical structure requirements and cellular targeting of microRNA-122 by peptide nucleic acids anti-miRs . Artif DNA PNA XNA, 2, 71–18.

Tsujii H, Eguchi Y, Chenchik A, Mizutani T, Yamada K and Tsujimoto Y. 2010. Screening of cell death genes with a mammalian genome-wide RNAi library. J Biochem, 148, 157–770.

Werk D, Pinkert S, Heim A et al. 2009. Combination of soluble coxsackievirus-adenovirus receptor and anti-coxsackievirus siRNAs exerts synergistic antiviral activity against coxsackievirus B3. Antiviral Res, 83, 298–806.

Xiao J, Yang B, Lin H, Lu Y, Luo X and Wang Z. 2007. Novel approaches for gene-specific interference via manipulating actions of microRNAs: examination on the pacemaker channel genes HCN2 and HCN4. J Cell Physiol, 212, 285–292.

Yu Y, Wu J, Guan L et al. 2013. Kindlin 2 promotes breast cancer invasion via epigenetic silencing of the microRNA200 gene family. Int J Cancer, In press.

8.2. Appendix B – Cancer cell line motility rate, proliferation rate, exosome secretion level, migration rate and invasion capacity data

8.2.1. Summary of cell line characteristics

Table 8.1: Summary of cell line characteristics: proliferation, exosome size, exosome secretion rate, motile capacity, migratory phenotype and invasiveness.

Cell line	Doubling time (hours)	Exosomes size (nm)	Exosome secretion (vesicles/cell)	Motility (% area reduction/hour)	Migration (no. invasive cells through uncoated membrane)	Invasion (no. invasive cells through Matrigel membrane)
A-2780	19.44	147.53	704.66	1.48	528.19	449.53
CP-70	21.69	139.14	572.29	1.95	2827.52	80.91
IGROV-1	48.18	136.93	3489.83	0.97	2724.88	894.56
MCF-7					303.04	527.28
MCP-1	17.51	134.37	385.57	1.33	2730.87	112.13
OVCAR-3	33.69	132.83	721.92	2.18	99.07	49.64
OVCAR-4	37.62			1.64	10615.56	67.17
OVCAR-5	27.10	131.70	924.52	3.65	32914.30	8525.26
OVCAR-8	27.69	127.67	740.32	5.26	6176.49	307.00
SKOV-3	30.03	127.10	736.39	6.93	70031.67	21271.57

8.2.2. Motility

Table 8.2: Normalised scratch percentage area for ovarian cancer cell lines.

Time (hours)	A-2780	CP-70	IGROV-1	MCP-1	OVCAR-3	OVCAR-4	OVCAR-5	OVCAR-8	SKOV-3
0	100.00	100.00	100.00	100.00	100.00	100.00	100.00	100.00	100.00
6	-	-	-	-	-	-	-	-	67.01
12	85.18	61.03	92.29	92.77	68.65	74.37	54.21	36.88	14.76
24	63.83	33.29	80.35	68.90	44.24	53.76	15.12	0.00	0.00
36	42.69	16.54	67.45	51.13	20.97	38.14	0.16	0.00	0.00
48	28.75	6.51	53.23	36.29	6.89	23.63	0.00	0.00	0.00

Table 8.3: Standard error of the mean for normalised scratch percentage area in Table 8.1.

Time (hours)	A-2780	CP-70	IGROV-1	MCP-1	OVCAR-3	OVCAR-4	OVCAR-5	OVCAR-8	SKOV-3
0	0.00	0.00	0.00	0.00	0.00	0.00	0.00	0.00	0.00
6	-	-	-	-	-	-	-	-	4.89
12	1.97	4.04	2.05	4.44	4.89	2.88	3.11	4.65	4.94
24	2.78	3.72	2.74	6.20	4.06	4.37	3.02	0.00	0.00
36	3.17	3.04	3.55	7.67	5.08	4.86	0.16	0.00	0.00
48	3.04	1.42	4.60	8.91	3.32	4.58	0.00	0.00	0.00

Table 8.4: Average scratch closure speed for ovarian cancer cell lines.

Cell line	Average scratch closure speed (% area reduction/hour)	Standard error of the mean
A-2780	1.48	0.06
CP-70	1.95	0.03
IGROV-1	0.97	0.10
MCP-1	1.33	0.19
OVCAR-3	2.18	0.20
OVCAR-4	1.64	0.13
OVCAR-5	3.65	0.27
OVCAR-8	5.26	0.39
SKOV-3	6.93	0.32

8.2.3. Proliferation

Table 8.5: Ovarian cancer cell concentration over 120 hours.

Cell Line	Time (hours)					
	0	24	48	72	96	120
A-2780	500000	840000	2677777.8	8422222.2	15337500	22088888.9
CP-70	500000	1213333.3	3500000	8088888.9	14466666.7	15622222.2
IGROV-1	500000	373333.33	1223333.3	1328889	4773333.33	1873333.33
MCP-1	500000	484444.44	1305555.6	3477777.8	11316666.7	16244444.4
OVCAR-3	500000	440000	646666.67	1233333.3	2622222.22	3383333.33
OVCAR-4	500000	982222.22	1120000	2500000	3057777.78	4033333.33
OVCAR-5	500000	500000	1280000	4662222.3	6723333.33	3086666.67
OVCAR-8	500000	741666.67	2253333.3	5022222.3	8743333.33	5400000
SKOV-3	500000	440000	555000	1988888.7	3136666.67	4573333.33

Table 8.6: Standard error of the mean for ovarian cancer cell concentration over 120 hours.

Cell Line	Time (hours)					
	0	24	48	72	96	120
A-2780	0	46825.13	137549.09	419140.80	673416.35	623411.56
CP-70	0	30061.67	212785.76	146986.18	771542.47	145720.86
IGROV-1	0	57324.61	231666.67	106272.37	2136510.65	373511.86
MCP-1	0	77872.96	29397.24	117588.95	116666.67	160246.72
OVCAR-3	0	53333.33	32829.53	91792.84	67586.25	116666.67
OVCAR-4	0	39643.47	106926.77	608522.80	669165.69	357589.67
OVCAR-5	0	108282.04	117721.42	452308.22	3404038.45	522632.23
OVCAR-8	0	418622.08	365995.60	278017.71	3868928.94	581062.25
SKOV-3	0	76865.68	68251.98	189827.52	231396.73	1371742.61

Table 8.7: Ovarian cancer average cell doubling time.

Cell line	Average doubling time	STEM
IGROV-1	48.18	27.18
MCP-1	17.51	0.06
A-2780	19.44	0.61
OVCAR-4	37.62	4.25
CP-70	21.69	0.75
OVCAR-3	33.69	0.75
OVCAR-5	27.10	5.17
OVCAR-8	27.69	6.20
SKOV-3	30.03	0.74

8.2.4. Exosome secretion

Table 8.8: Ovarian cancer cell line exosome secretion rates in terms of the number of vesicles released per cell.

Cell line	Average exosomes released per cell	Average Standard Error of the Mean
A-2780	704.66	359.18
CP-70	572.29	386.78
IGROV-1	3489.83	2692.26
MCP-1	385.57	165.92
OVCAR-3	721.92	426.55
OVCAR-5	924.52	500.85
OVCAR-8	740.32	440.56
SKOV-3	736.39	333.99
PBS	0.38	0.15

8.2.5. Exosome size

Table 8.9: Ovarian cancer cell line mode average exosome diameter.

Cell line	Average Size (nm)	Standard error of the mean
A-2780	147.53	8.71
CP-70	139.14	2.19
IGROV-1	136.93	6.98
MCP-1	134.37	2.27
OVCAR-3	132.83	5.29
OVCAR-5	131.70	14.56
OVCAR-8	127.67	6.30
SKOV-3	127.10	2.13
PBS	121.70	3.54

8.2.6. Migration

Table 8.10: Number of migratory cells in the trans-well assay for each ovarian cancer cell line.

Cell line	Uncoated membrane average no. invasive cells*	STEM
A-2780	528.19	448.37
CP-70	2827.52	231.88
IGROV-1	2724.88	1021.64
MCF-7	303.04	169.12
MCP-1	2730.87	863.50
OVCAR-3	99.07	48.34
OVCAR-4	10615.56	2708.00
OVCAR-5	32914.30	7045.72
OVCAR-8	6176.49	429.18
SKOV-3	70031.67	3131.81

* 100,000 cells were assigned to each trans-well insert at commencement of the assay

8.2.7. Invasion

Table 8.11: Number of invasive cells in the Matrigel trans-well assay for each ovarian cancer cell line.

Cell line	Matrigel membrane average no. invasive cells*	STEM
A-2780	449.53	132.67
CP-70	80.91	23.62
IGROV-1	894.56	331.60
MCF-7	527.28	303.61
MCP-1	112.13	53.30
OVCAR-3	49.64	12.55
OVCAR-4	67.17	41.98
OVCAR-5	8525.26	4143.56
OVCAR-8	307.00	146.76
SKOV-3	21271.57	4569.89

* 100,000 cells were assigned to each trans-well insert at commencement of the assay